A STUDY OF MODIFIED MESOPOROUS SILICA FOR THE ADSORPTION OF SELECTED ORGANIC POLLUTANTS

by

SAMSON OGHENEMAURO AKPOTU

Submitted in fulfilment of the academic requirements of

Doctor of Philosophy

in

Chemistry
School of Chemistry and Physics
College of Agriculture, Engineering and Science
University of KwaZulu-Natal
Westville
South Africa

(June, 2016)

PREFACE

The research contained in this thesis was completed by the candidate while based in the Discipline of Chemistry, School of Chemistry and Physics, of the College of Agriculture, Engineering and Science, University of KwaZulu-Natal, Westville Campus, South Africa. The research was financially supported by the Association of African Universities small grant.

The contents of this work have not been submitted in any form to another university and, except where the work of others is acknowledged in the text, the results reported are due to investigations by the candidate.

_____

Signed: Supervisor

Date:

DECLARATION 1: PLAGIARISM

I, Samson Oghenemauro Akpotu, declare that:

(i) the research reported in this thesis, except where otherwise indicated or acknowledged, is my original work;

(ii) this thesis has not been submitted in full or in part for any degree or examination to any other university;

(iii) this thesis does not contain other persons' data, pictures, graphs or other information, unless specifically acknowledged as being sourced from other persons;

(iv) this thesis does not contain other persons' writing, unless specifically acknowledged as being sourced from other researchers. Where other written sources have been quoted, then:

a) their words have been re-written but the general information attributed to them has been referenced;

b) where their exact words have been used, their writing has been placed inside quotation marks, and referenced;

(v) where I have used material for which publications followed, I have indicated in detail my role in the work;

(vi) this thesis is primarily a collection of material, prepared by myself, published as journal articles or presented as a poster and oral presentations at conferences. In some cases, additional material has been included;

(vii) this thesis does not contain text, graphics or tables copied and pasted from the Internet, unless specifically acknowledged, and the source being detailed in the dissertation and in the References sections.

_____

Signed: Samson Oghenemauro Akpotu

Date:

DECLARATION 2: PUBLICATIONS

My role in each paper and presentation is indicated. The * indicates corresponding author.

Paper 1

1. Akpotu, S.O., *Moodley, B. **Effect of synthesis conditions on the morphology of mesoporous silica from elephant grass *via* the *sol-gel* technique and its application in adsorption of cationic dyes (ready for submission).**

   My contribution: I synthesised, characterised and executed the experiments to investigate the activity of the adsorbent materials and drafted the article under the guidance of my supervisor.

Paper 2

2. Akpotu, S.O., *Moodley, B. **Encapsulation of silica nanotubes from elephant grass with graphene/graphene oxide and application in remediation of sulfamethoxazole from aqueous solution (ready for submission).**

   My contribution: I synthesised, characterised and executed the experiments to investigate the activity of the adsorbent materials drafted the article under the guidance of my supervisor**.**

Paper 3

3. Akpotu, S.O., *Moodley, B **Synthesis and characterisation of MCM-41 and citric grafted MCM-41 from millet straw and its application in adsorption of methylene blue (ready for submission).**

   My contribution: I synthesised, characterised and executed the experiments to investigate the activity of the adsorbent materials drafted the article under the guidance of my supervisor

Paper 4

4. Akpotu, S.O., *Moodley, B. 2016. **Synthesis and characterization of citric acid grafted MCM-41 and its adsorption of cationic dyes. *Journal of Environmental Chemical Engineering*** 4: 4503–4513. (Published)

   My contribution: I synthesised, characterised and executed the experiments to investigate the activity of the adsorbent materials and drafted the article under the guidance of my supervisor

Paper 5

5. Akpotu, S.O., *Moodley, B. **As-synthesised MCM-41 and encapsulation of MCM-41 with graphene/graphene oxide and their application in the remediation of pharmaceuticals from aqueous solution (ready for submission).**

My contribution: I synthesised, characterised and executed the experiments to investigate the activity of the adsorbent materials and drafted the article under the guidance of my supervisor

Paper 6

6. Akpotu, S.O., *Moodley, B. **As-synthesised MCM-48 and encapsulation of MCM-48 with graphene/graphene oxide and their application in the remediation of pharmaceuticals from aqueous solution (ready for submission).**

My contribution: I synthesised, characterised and executed the experiments to investigate the activity of the adsorbent materials and drafted the article under the guidance of my supervisor.

_____

Signed: Samson Oghenemauro Akpotu

Date:

CONFERENCE PARTICIPATION

1. Akpotu, S.O., *Moodley. B. **Synthesis and characterization of citric acid grafted MCM-41 and its adsorption of methylene blue** (Poster presentation at the 3rd Conference on Emerging Frontiers For Sustainable Water: A Trilateral Partnership Africa-India-UK, Johannesburg 3-5 August, 2015).

2. Akpotu, S.O., *Moodley. B. **Tuning the properties of silica with graphene oxide/graphene** (Oral presentation at the South Africa-UK Workshop: Materials-Based Hydrogen: Design, Synthesis and Characterisation of Porous Materials, 1st – 4th September, 2015, CSIR International Convention Centre, Pretoria).

3. Akpotu, S.O., *Moodley. B. **Synthesis, characterisation of MCM-41 from millet straw and its application in the adsorption of methylene blue** (Oral presentation at the College of Agriculture, Engineering and Science Research Day, 22nd September 2015, Pietermaritzburg Campus, UKZN).

4. Akpotu, S.O., *Moodley. B. **Effect of synthesis conditions on the morphology of mesoporous silica from elephant grass *via* the *sol-gel* technique and its application in adsorption of cationic dyes** (Best Poster presentation 5th International Conference on Nanotek & Expo, November 16th – 18th 2015, San Antonio, Texas, USA).

5. **Akpotu, S.O** and Brenda Moodley**. Encapsulation of silica nanotubes from elephant grass with graphene/graphene oxide and its application in remediation of sulfamethoxazole from aqueous solution.** Poster presentation at the "ChromSAAMS New Limits – New Applications" 11 – 14 September, 2016, Riverside Sun Hotel, Vanderbijlpark, Gauteng, South Africa

LIST OF ABBREVIATIONS

Full name	Abbreviations
3-aminopropyltriethoxysilane	APTES
Acetaminophen	Acet
Activated carbon	AC
Aspirin	Asp
Blue Lagoon	BLG
Barret-Joyner-Halenda	BJH
Biochemical oxygen demand	BOD
Brunauer-Emmett-Teller	BET
Caffeine	CAF
Carbon nanotubes	CNT
Cetyltrimethyl ammonium bromide	CTAB
Cetyltrimethyl ammonium chloride	CTACI
Chemical oxygen demand	COD
Chemical vapour deposition	CVD
Citric acid	CA
Cyclodextrin	CD
Dichlorodiphenyldichloroethylene	DDE
Dichlorodiphenyltrichloroethane	DDT
Double distilled water	DDW
Elemental analysis	EA
Elephant grass	EG
Elephant grass ash	EGA
Energy dispersive x-ray	EDX
Field emission scanning electron microscope	FESEM
Fourier transform infrared	FTIR
Graphene	G
Graphene oxide	GO
High pressure liquid chromatography	HPLC

High resolution transmission electron microscope	HRTEM
International union of pure and applied chemist	IUPAC
Liquid crystal templating	LCT
Mesoporous silica	MSi
Methylene blue	MB
Methylene red	MR
Mobil catalytic material (-41, -48)	MCM
Mobil catalytic material (-41, -48) graphene oxide	MCM-GO
Mobil catalyst of matter (-41, -48) graphene	MCM-G
Ordered mesoporous silica	OMSi
Organophosphorus pesticide	OPP
Phenacetin	PHE
Point of zero charge	PZC
Polycyclic aromatic hydrocarbon	PAH
Post synthetic grafting	PSG
Santa babara acid	SBA
Scanning electron microscopy	SEM
Silica citric acid	SCA
Silica nanoparticles	SNP
Silica nanotubes	SNT
Solid state nuclear magnetic resonance	SSNMR
Structure directing agent	SDA
Sulfamethoxazole	SMZ
Tetraethylorthosilicate	TEOS
Tetramethylorthosilicate	TMOS
Thermogravimetric analysis	TGA
Total dissolved solids	TDS
Transmission electron microscopy	TEM
Ultraviolet-Visible	UV-VIS
X-ray diffractometer	XRD
X-ray fluorescence	XRF

ABSTRACT

Water is an essential natural resource the world over. Only one-tenth of the world's water is pollution free and hence there is a need for remediating polluted water. These pollutants, some of which are organic (dyes and pharmaceuticals), are often difficult to remediate from wastewater. Of all the available remediation techniques, adsorption is a proven technique that combines ease of use and cost effectiveness in removal of these organic pollutants. This study is aimed at the synthesis and characterisation of mesoporous silica/ordered mesoporous silica from agrowastes and commercial precursors, and their utilization in adsorption of organic pollutants. Silica was modified with citric acid, graphene oxide and graphene because of silica's ready availability, low cost and its environmentally benign nature. The synthesized materials were charactersied by means of various standard analytical techniques. In the first study, silica nanoparticles (SNP) and silica nanotubes (SNT) were synthesized from elephant grass. Parameters such as surfactant concentration and temperature were investigated on the morphology of mesoporous silica which yielded SNTs and SNPs. These parameters, especially the surfactant concentration had a profound effect on the morphology of silica. SNT and SNP were applied in the adsorption of 2 dyes; methylene blue (MB) and methylene red (MR). The adsorption of MB and MR on SNT were 109.97 mg/g and 40.6 mg/g, respectively. For SNP, MB and MR adsorption was 104.85 mg/g and 40.98 mg/g, respectively. The adsorption of MB and MR increased with an increase in pH with pH 6 and 8 being the optimal pH for MR and MB, respectively. This slight difference in sorption capacities can be attributed to the surface area. Pseudo-second order and the Langmuir isotherm model best fitted the data obtained. In the second study, mobil catalytic material (MCM-41) was synthesised using tetraethylorthosilicate and elephant grass as precursors. Citric acid was used a modifier and applied in the adsorption of methylene blue. The citric acid had a significant effect on the adsorption capacity, which increased at basic pH. The mechanism for adsorption was electrostatic ion interaction. The maximum adsorption capacity of the modified material improved considerably with a q_m of 204.08 mg/g at pH 10 and a temperature of 25 °C. The adsorption kinetics favoured the pseudo-second-order model and the best fit model for the equilibrium data was the Freundlich model. In the third study, MCM-41 was synthesized from millet straw (agrowaste). A citric acid-MCM-41 (SCA-MCM-41) composite was prepared by grafting citric acid (CA) onto MCM-41 for improvement of its adsorptive capacity for methylene

blue (MB). The highest adsorption capacity was achieved at pH 8. The Temkin isotherm model was the best fit in analyzing the equilibrium data. Kinetics favoured the pseudo-second order and the optimum temperature for adsorption was 25 ^{o}C. In the fourth study, SNT was synthesized using elephant grass as a precursor and was encapsulated with graphene oxide and graphene and applied in the remediation of sulfamethoxazole from aqueous media. The highly hydrophobic materials had high adsorptive capacities for sulfamethoxazole. In this study, ordered mesoporous silica-graphene oxide (MCM-41-GO) and graphene (MCM-41-G) composites and as-synthesised MCM-41 were synthesized and applied in the adsorption of acetaminophen and aspirin from aqueous solution. Elemental analysis showed that the percentage carbon was MCM-41-G > MCM-41-GO > AS-MCM-41 > MCM-41. This conferred various degrees of hydrophobicity on these materials and hydrophobic interaction was the main mechanism of adsorption. The pseudo-second order model best fitted the adsorption kinetics and the Freundlich isotherm best described the equilibrium. These materials had higher sorption capacities as compared to unmodified MCM-41. In the last study, MCM-48 encapsulated with graphene and graphene oxide, and as-synthesised MCM-48 were synthesized and applied in the remediation of caffeine and phenacetin from wastewater. The results obtained were similar to that of the previous study and hydrophobic interaction was the main mechanism of adsorption. Overall the modification of mesoporous/ordered mesoporous materials proved very useful in the remediation of organic pollutants from aqueous media.

ACKNOWLEDGMENTS

My gratitude goes to the Almighty God, The Generator, Operator and Director of my life, for His mercies, blessings and guidance throughout the duration of this study.

I appreciate the effort of my supervisor, Dr. Brenda Moodley for the opportunity, for her patience and understanding and her role in making this study successful. Thanks for the words of encouragement and constructive criticism.

I also appreciate the School of Chemistry and Physics, College of Agriculture, Engineering and Science, University of KwaZulu-Natal for providing the right environment to carry out my research. I am also grateful to the Association of African Universities (AAU) for the provision of financial support *via* the AAU small grant.

I am eternally grateful to my dearest parents, Mr. And Mrs. R.U. Akpotu, for the unconditional, unequivocal and unwavering love and support shown to me. I lack better adjectives to contextualise what you really mean to me, but I simply say you my parents are the best. To my siblings Mr. L.O. Akpotu, Miss Elo and Omamuzo Akpotu, I love you all. My sincerest gratitude goes out to you guys for being my pillar and strength, and for being there physically, emotionally, spiritually and financially. I know even during the darkest days at my lowest ebb, I could always count on you guys. Once again, family, thank you.

I am grateful to the family of Professor J.S Oboreh for the academic and parental advice. I also want to appreciate the family of Dr. Shapi, my God's vessel in South Africa, an angel in human form. Words cannot express my deep debt of gratitude that I owe you, for financial, academic and career support.

To my friends, all of you I call my appendages, without you guys I probably would not have made it to the end, I salute. Afolabi Abayomi (my teacher), Dr. E.O. Oseghe, Dr. I.A. Lawal, Dr. O.A. Abafe, E.D. Akpan, O. Ebhuoma, Dr. A. Adebisi, Miss T. A. Nwabuebo, Mothusi, Mr. H. Nwaokoro, Miss N. Masombuka, Mr. G. Adeyinka, Mr. J.S. Oluleye, Dr. F.O. Agunbiade, Dr. S. Oyetade, you all should take a bow. Once more, thanks.

TABLE OF CONTENTS

Page

LIST OF TABLES

Table **Page**

LIST OF FIGURES

Figure Page

1.0 CHAPTER 1: INTRODUCTION

1.1 Background to Study

The earth's crust is constituted of approximately 75% silica, where approximately 28% of the earth's surface is quartz and 47% is covered by other minerals with silica in their matrix. Silica is the common name for inorganic ceramic material composed of silicon dioxide (SiO_2). Silica is a polymeric material which is crosslinked with silicic acid, and has a SiO_2 stoichiometry and a tetrahedral geometry. Silica is present in nature as quartz (found in sediments), hydrated disordered silica otherwise referred to as opaline silica and amorphous silica whose essential make up is pure SiO_2 in a mesomorphous state (Shen et al., 2014).

Amorphous silica can be found in agrowaste which are freely and cheaply available. Agrowaste materials, such as agricultural by-products, are mostly burnt and constitute a nuisance to the environment. However, these materials can be converted into valuable resources by the extraction of high purity silica from the agrowaste. The extraction process is fairly straight forward and cost effective. The amorphous silica from agrowaste can be used as a substitute/supplement for silica from commercial sources. Amorphous silica has low inorganic impurities and is obtained by a combination of thermal treatment, acid leaching and calcination of agrowaste (Adam et al., 2013, Thuc and Thuc, 2013). Amorphous silica from agrowaste (primarily from rice hulls/husks) has been used in the synthesis of mesoporous silica, (Adam et al., 2013, Jaroenworaluck et al., 2012, Thuc and Thuc, 2013) and ordered mesoporous silica, (Ghorbani et al., 2013, Bhagiyalakshmi et al., 2010) however, silica from commercial precursors can also be used. These silica precursors from commercial sources include tetramethyl orthosilicate (TMOS), tetraethyl orthosilicate (TEOS) and an alkoxide with a longer chain length such as sodium silicate. Ordered mesoporous silica material (OMS) have interesting properties such as ordered porosity, which is typical of a crystalline material such as zeolites but are in fact amorphous in nature. These materials have long ordered channels, a high specific surface area of 1000-2500 m^2/g, tunable pore volume, and controlled pore size of 2-10 nm and ordered geometry. Their long almost perfectly aligned mesochannels makes them an excellent candidate for adsorbent-adsorbate interactions (Gibson,

2014b) as well as suitable as supercapacitors, catalyst supports, fillers and adsorbents (Parida et al., 2012, Gibson, 2014b, Liou, 2011, Bai et al., 2015).

1.2 Adsorption of Organic Pollutants

Water is a scarce resource the world over and access to potable water remains a challenge. Industrialisation, however beneficial, has created many problems due to the release of large amounts of toxic chemicals (both inorganic and organic). Textile industries use chemicals such as methyl ethyl ketone, methanol, and dyes such as methyl red, methylene blue and malachite green and the excess or waste dyes often end up being dumped into rivers and water systems. The agricultural industry also contributes to water pollution with the use of harmful chemicals such as DDT, DDE, organophosphates and pesticides and herbicides. Pharmaceuticals and personal care products are currently classified as emerging contaminants in the environment. Pharmaceuticals are a global problem in water and wastewater treatment plants and has recently been receiving much attention from the scientific community (Nam et al., 2015).

The wastes generated by pharmaceutical industries can be detrimental to human and animal health and the environment. These pollutants can cause a lot of illness to humans such as cancer, respiratory infections, and heart diseases to name but a few (Cui et al., 2015, Kushwaha et al., 2014, Han et al., 2010). The presence of these contaminants in water systems cause an imbalance in the ecosystem creating large biochemical oxygen demand (BOD) and chemical oxygen demand (COD) which is not desirable as the aquatic organism becomes oxygen starved. Thus much research is now being carried out to develop technologies to remediate organic pollutants from water. Amongst the technologies that have been used for prerelease treatment are ozonation, biodegradation, photodegradation and adsorption. Adsorption is an extremely effective process because of its cost effectiveness and easy to use advantage over other conventional water treatment techniques (Adam et al., 2013).

1.3 Modification of Silica Surface

Carboxyl groups from carboxylic acid have been used in the modification of siliceous surfaces which showed improved adsorption for cationic dyes. The extensive network of –OH groups on the silica surface is utilized for functionalisation where carboxyl groups can be grafted on it. This causes increased adsorption of cationic dyes in aqueous medium at neutral to basic pH (Kushwaha et al., 2014, Kushwaha et al., 2010, Han et al., 2010, Sajab et al., 2011).

Graphene oxide and graphene are a new class of nanomaterials and have been acknowledged to possess interesting properties suitable to adsorption. Their structure is similar to that of carbon nanotubes but they are easily synthesised as compared to the former. They also theoretically possess a very high surface area of approximately 2500 m^2/g with an array of active functional groups on their surface. These functional groups include –COOH, -C=O and –OH, (Marcano et al., 2010) which can be exploited for improved adsorption of organic pollutants. Graphene oxide and graphene are less thermally stable than silica, and can be made into a composite with ordered mesoporous silica (OMS) resulting in improved hybrid properties of better surface area, improved functionality for adsorption in water treatment/environmental remediation, as well as improved thermal and mechanical properties.

1.4 Statement of Problem

Over the years, as a result of industrialization, there has been an increase in the impact of hazardous organic pollutants and their harmful effects on the environment. The consequence of these persistent organic pollutants has been felt in the environment and the ecosystem and has resulted in a decrease in water quality *vis*-à-*vis* life quality worldwide. Potable water is currently in short supply and therefore recirculation of surface water, water from agricultural runoff and industrial effluent including organic pollutants from medical/pharmaceutical wastes sent to water treatment plants needs to be cleaned-up and recycled into order to meet the demand for potable water. Conventional water treatment facilities are not equipped to remediate these organic pollutants (pharmaceuticals, pesticides, dyestuffs). In addition, the demand for potable water is expected to further increase. Currently, over 1 billion people across the world lack access to pota-

ble water with a projected increase of an estimated 1.8 billion people, and by 2025 it is estimated that two-thirds of the world's population will be living in water-stressed regions as a consequence of climate change (UNICEF., 2015). Hence, there is a need for the development of simple, efficient and cost effective water treatment/remediation technology. Adsorption is one such technology and this study will show that silica from commercial precursors and from agrowastes can be used in the synthesis of adsorbents. These agrowastes are regarded as materials with no economic value, but it can be made useful by converting them into sorbents to remediate organic pollutants from aqueous media *via* adsorption. In addition, silica modified with carboxylic acid, graphene oxide and graphene is shown to further increase organic pollutant adsorption.

1.5 Justification

Industrialisation and technological advancement, in the manufacturing of dyes and pharmaceutical drugs, however beneficial, has created diverse health issues for humans and animals and also poses environmental challenges. The remediation of polluted water in the world (South Africa inclusive) is of utmost importance particularly because South Africa is regarded as a water stressed country. The pressure on water resources and access to potable water will increase in the near future as the demand from an ever increasing population continues to grow. Therefore, the remediation of water polluted with organic contaminants is strategic in safeguarding the health of the people and presents an opportunity to make potable water more accessible and at the same time makes agrowastes a commodity of value. Also, an understanding of adsorbent-pollutant interaction provides insight into the mechanism of the pollutant uptake/remediation in water systems which is important in developing technology for water treatment.

1.6 Hypothesis

Mesoporous silica, ordered mesoporous silica, silica-graphene oxide and silica-graphene composites can be used in the remediation of organic contaminants in water due to their physical and chemical properties. These properties allow for the modification of surface functional groups that target pollutants, which in this study are dyes and pharmaceuticals in aqueous solution.

1.7 Aim and Objectives

The aim of this study was to utilise siliceous based materials from agrowaste and commercial sources to develope adsorbents for the remediation of organic pollutants such as dyes and pharmaceuticals from aqueous media.

Specific objectives:

i. To synthesise and characterize mesoporous silica (silica nanoparticles and silica nanotubes) from agricultural waste materials
ii. To synthesise and characterise MCM-41 and carboxylic acid grafted MCM-41, utilising millet straw and TEOS as precursors
iii. To synthesize and characterize MCM-48 from TEOS
iv. To synthesise and characterize graphene oxide and graphene and utilize them in the surface modification of MCM-41 and MCM-48
v. To determine the sorption capacity of the synthesised adsorbents and optimize the adsorption parameters such as pH, time and temperature in the adsorption of various organic pollutants from aqueous media
vi. To carry out kinetic studies on the synthesized/modified adsorbents and determine their mechanism of adsorption.

References

Adam, F., Appaturi, J. N., Khanam, Z., Thankappan, R. & Nawi, M. a. M. 2013. Utilization of tin and titanium incorporated rice husk silica nanocomposite as photocatalyst and adsorbent for the removal of methylene blue in aqueous medium. *Applied Surface Science,* 264**,** 718-726.

Bai, L., Li, Z., Zhang, Y., Wang, T., Lu, R., Zhou, W., Gao, H. & Zhang, S. 2015. Synthesis of water-dispersible graphene-modified magnetic polypyrrole nanocomposite and its ability to efficiently adsorb methylene blue from aqueous solution. *Chemical Engineering Journal*, 279, 757-766.

Bhagiyalakshmi, M., Yun, L. J., Anuradha, R. & Jang, H. T. 2010. Utilization of rice husk ash as silica source for the synthesis of mesoporous silicas and their application to CO_2 adsorption through TREN/TEPA grafting. *Journal of Hazardous Materials,* 175**,** 928-938.

Cui, L., Wang, Y., Gao, L., Hu, L., Wei, Q. & Du, B. 2015. Removal of Hg (II) from aqueous solution by resin loaded magnetic β-cyclodextrin bead and graphene oxide sheet: Synthesis, adsorption mechanism and separation properties. *Journal of Colloid and Interface Science,* 456**,** 42-49.

Ghorbani, F., Younesi, H., Mehraban, Z., Çelik, M. S., Ghoreyshi, A. A. & Anbia, M. 2013. Preparation and characterization of highly pure silica from sedge as agricultural waste and its utilization in the synthesis of mesoporous silica MCM-41. *Journal of the Taiwan Institute of Chemical Engineers,* 44**,** 821-828.

Gibson, L. 2014. Mesosilica materials and organic pollutant adsorption: part B removal from aqueous solution. *Chemical Society Reviews,* 43**,** 5173-5182.

Han, R., Zhang, L., Song, C., Zhang, M., Zhu, H. & Zhang, L. 2010. Characterization of modified wheat straw, kinetic and equilibrium study about copper ion and methylene blue adsorption in batch mode. *Carbohydrate Polymers,* 79**,** 1140-1149.

Jaroenworaluck, A., Pijarn, N., Kosachan, N. & Stevens, R. 2012. Nanocomposite TiO_2–SiO_2 gel for UV absorption. *Chemical Engineering Journal,* 181**,** 45-55.

Kushwaha, A. K., Gupta, N. & Chattopadhyaya, M. 2010. Enhanced adsorption of malachite green dye on chemically modified silica gel. *Journal of Chemical and Pharmaceutical Research,* 2**,** 34-45.

Kushwaha, A. K., Gupta, N. & Chattopadhyaya, M. 2014. Enhanced adsorption of methylene blue on modified silica gel: equilibrium, kinetic, and thermodynamic studies. *Desalination and Water Treatment,* 52**,** 4527-4537.

Liou, T.-H. 2011. A green route to preparation of MCM-41 silicas with well-ordered mesostructure controlled in acidic and alkaline environments. *Chemical Engineering Journal,* 171**,** 1458-1468.

Marcano, D. C., Kosynkin, D. V., Berlin, J. M., Sinitskii, A., Sun, Z., Slesarev, A., Alemany, L. B., Lu, W. & Tour, J. M. 2010. Improved synthesis of graphene oxide. *ACS Nano,* 4**,** 4806-4814.

Nam, S.-W., Jung, C., Li, H., Yu, M., Flora, J. R., Boateng, L. K., Her, N., Zoh, K.-D. & Yoon, Y. 2015. Adsorption characteristics of diclofenac and sulfamethoxazole to graphene oxide in aqueous solution. *Chemosphere,* 136**,** 20-26.

Parida, K., Mishra, K. G. & Dash, S. K. 2012. Adsorption of copper (II) on NH_2-MCM-41 and its application for epoxidation of styrene. *Industrial & Engineering Chemistry Research,* 51**,** 2235-2246.

Sajab, M. S., Chia, C. H., Zakaria, S., Jani, S. M., Ayob, M. K., Chee, K. L., Khiew, P. S. & Chiu, W. S. 2011. Citric acid modified kenaf core fibres for removal of methylene blue from aqueous solution. *Bioresource Technology,* 102**,** 7237-7243.

Shen, Y., Zhao, P. & Shao, Q. 2014. Porous silica and carbon derived materials from rice husk pyrolysis char. *Microporous and Mesoporous Materials,* 188**,** 46-76.

Thuc, C. N. H. & Thuc, H. H. 2013. Synthesis of silica nanoparticles from Vietnamese rice husk by sol–gel method. *Nanoscale Research Letters,* 8**,** 1-10.

Unicef. 2015. *Progress for children: a report card on water and sanitation,* UNICEF.

2.0 CHAPTER 2: LITERATURE REVIEW

2.1 Introduction

2.1.1 Silica

The earth's most abundant chemical compound is silica but despite this, silica is largely manufactured by synthetic means for technological applications. Naturally occurring silica has a lower surface area as compared to synthetically manufactured silica (up to 2500 m^2/g) (Qu and Gu, 2014). Synthetic silica has high purity and high surface area, and provides better surface when used as a catalyst support or adsorbent. Silica can exist in various forms, although its primary chemical formula is SiO_2. Silica is tetrahedral, SiO_4, with each silica atom double bonded to four oxygen atoms and those oxygen atoms in turn bonded to silica atoms.

Silica is a fundamental material and is valuable in the formation of inorganic compounds with a variety of applications. Naturally occurring silica is referred to as flint, sand or quartz. It exists as a gel, amorphous silica or crystalline silica. The manufacturing of silica is by extraction from sand or quartz. Sodium silicate, a precursor of silica, is obtained by smelting quartz sand with sodium carbonate at 1300 °C. Silica is applied in the manufacture of various products, such as ceramics, concrete, electronics, catalysts and as an adsorbent. However, since the manufacture of silica from sand is quite capital and energy intensive, alternative sources of silica production and generation are being explored.

The intrinsic properties of silica make it unique in the remediation of pollutants from water and wastewater. These pollutants may be inorganic (metals) or organic pollutants. The organic pollutants are known to be recalcitrant, have long range, are transboundary, lipophilic and are ubiquitous in the environment. These pollutants have adverse effects on human health and the environment. Hence, there is a need to purge the environment of these organic pollutants. This can be done using silica with agrowastes as a precursor and in the process turn waste, which is freely available, into wealth or using commercially available silica precursors such as tetraethyl orthosilicate (TEOS), tetramethyl orthosilicate (TMOS) and sodium silicate. Previous remediations of

organic pollutants in water by silica or silica-based substrates have been carried out with varying degrees of success. There are 2 ways in which silica is used in the remediation of organic pollutants from water; advanced oxidation technique and adsorption. In the advanced oxidation technique, silica is used as a catalyst support. This process breaks down the chromophoric group and decomposes organic molecules into a smaller fragment which is not as toxic as the parent material. Usually, silica is doped with a transition metal (mostly titania) to extend its absorption range from UV to visible region, reduce the energy band gap, retard or accelerate photo degradation of organic pollutants to give CO_2 and H_2O (Adam et al., 2013, Jaroenworaluck et al., 2012). Adsorption is the preferred method for the removal of organic pollutants. This is because of the ease of use, and no toxic by-products are generated in the process. Silica has also been used as adsorbents in its pure form or as a hybrid material in the removal of organic pollutants in water systems. Pure silica has limited use in the adsorption of organic molecules from aqueous solution because of its hydrophilic nature. Hence, a number of methods have been developed to increase its hydrophobicity and affinity for organic molecules. Different functional groups such as carboxylic acid, metals, carbonaceous materials, graphene oxide and graphene have been used to increase the adsorption of organic molecules by silica. .

2.2 Adsorption

Adsorption is the remediation technique of choice in the treatment of wastewater worldwide. This is due to its efficiency as compared to other known techniques for remediation. It possesses advantages such as low cost of operation, ease of use, flexibility and simplicity of design (Rasalingam et al., 2014). An added advantage of the adsorption process, is that there are no toxic by-products/substances produced. Adsorption has been employed in remediation of different pollutants from wastewater systems. These pollutants include dyes (Qu and Gu, 2014, Kushwaha et al., 2014, Gu et al., 2015, Khan et al., 2013), pharmaceutical wastes (Liu et al., 2014, Nam et al., 2015), heavy metals (Han et al., 2010, Parida et al., 2012), phenols (Anbia and Amirmahmoodi, 2011, Mangrulkar et al., 2008) and other harmful substances that may affect biota.

The removal of non-biodegradable waste pollutants from wastewater is possible with adsorption. Some of the most popular adsorbents are clay, clay-containing adsorbents, activated carbon (Song et al., 2012) and biomaterials (Reddy et al., 2012, Reddy et al., 2013), which have been applied in the remediation of industrial wastes. Nonetheless, the adsorptive performances by some of these adsorbents on some pollutants are not as effective because of poor adsorbent-adsorbate interaction. As a result, oxide materials are classified as a better form of adsorbent and have found usage in the adsorption of different pollutants. These oxides include silica gel (Kushwaha et al., 2014, Kushwaha et al., 2010), zeolitic materials (Sakadevan and Bavor, 1998, Bailey et al., 1999), titanium dioxide (Adam et al., 2013, Jaroenworaluck et al., 2012), aluminum oxide (Youngran et al., 2007, Harlick and Tezel, 2002) and a host of other materials.

2.2.1 Historical perspective of adsorption

Scheele, in 1773, and Fontana, in 1777, discovered adsorption independently, but it was not until 1881 that Kayser described the adsorption process based on gas condensing on free surfaces. Adsorption can be defined as the change in concentration of a given substance at the interface as compared with the neighbouring phases (Dąbrowski, 2001). The phases can be liquid-gas, liquid-liquid, solid-liquid and solid-gas. The term "adsorption" refers to a process where molecules accumulate in the interfacial layer and for desorption, the reverse occurs. When a material is present in the adsorbed state, it is referred to as the "adsorbate" but when present in the bulk gas or vapour phase before being released, it is termed the adsorptive. When the adsorbate molecules are retained inside the pores of the bulk solid, absorption is said to have occurred. An adsorbent can be described as the solid substance where adsorption takes place with the retained ions on its surface rather than locked inside its pores.

Table 2.1 History and application of adsorption (Dąbrowski, 2001)

Date	Scientist	Important discovery
1773	Scheele	Uptake of gases by charcoal and clay
1777	Fontana	Similar studies to Scheele
1786	Lowitz	Used charcoal to decolourise tartaric acid
1793	Kehl	Used coal to remove odour from gangrenous ulcer and also for removal of colour from sugar
1814	De Saussure	Studied adsorption of various gases from porous media and discovered the exothermic process
1881	Kayser	Coined the term adsorption
1901	Von Ostreyko	Started the development of activated carbon on commercial scale
1909	McBain	Proposed the term absorption
1918	Langmuir	Derived the concept for monolayer adsorption
1938	Brunauer, Emmet, Teller	Developed multilayer isotherm equation
1941	Martin and Synge	Introduced solid-liquid partition chromatography
1956	Barrer and Breck	Developed zeolite synthesis method

Adsorption can be influenced by a number of factors and the process may be a result of van der Waals interactions, physical adsorption otherwise termed physisorption (applicable to the adsorbate-adsorbent system if the temperature and pressure conditions are favourable), and chemical adsorption or chemisorption which involves the formation of chemical bonds during the adsorption process. If the conditions are favourable, both physisorption and chemisorption processes can take place simultaneously.

2.2.2 Physical adsorption

In physisorption, an equilibrium state is established between the molecules, adsorbate and adsorbent. The physisorption process is comparable to the condensation process of the adsorptive. A number of factors are responsible for physisorption such as the structural morphology of the adsorbent (porosity), and electrostatic ion interaction (London dispersion forces) between the adsorbent and the adsorbate. Physisorption is often a reversible process at temperatures slightly lower or near the critical temperature of the adsorbed substance (Dąbrowski, 2001).

In physisorption, the surface area of the adsorbent is critical because a high surface area often guarantees better adsorption. However, this is dependent on the nature of the adsorbent/adsorbate and size of the adsorbate. An adsorbent with high porosity achieves good adsorption because the adsorbate molecules are adsorbed on the walls of the adsorbent. Surface polarity is also a key factor that affects adsorption, where a polar substance such as water is attracted to polar surfaces. Zeolites, silica gel, and silica-alumina are hydrophilic in nature, whereas carbonaceous adsorbents are hydrophobic. A hybrid of these materials makes them better adsorbents in non-aqueous media (Sohn and Kim, 2005). In physisorption, adsorption does not depend on the surface chemistry of the adsorbent, but instead occurs on the heterogeneous surface at the sites of greatest potential of adsorption. In this process, there is a decrease in free energy and entropy of the adsorption system making the process exothermic (Dąbrowski, 2001).

The importance of pore size in physisorption cannot be over emphasized, and adsorption is largely dependent on pore sizes. If the size of the adsorbate is in the micropore region, for the adsorption process to be effective, the adsorbent must be of a mesoporous nature.

2.2.3 Chemical adsorption

In chemisorption, bonds are formed between the adsorbate and the adsorbent. It is often almost an irreversible process because of the bond formation. Consequently, regeneration of the adsorbent is extremely difficult (Cheremisinoff and Cheremisinoff, 1993). Some differences between chemisorption and physisorption are presented in the table below.

Table 2.2 Differences between physisorption and chemisorption

Physisorption	Chemisorption
The forces of attraction are van der Waals forces	Forces are similar to chemical bonds
Occurs at a temperature below the boiling point of the adsorbate	Occurs at all temperatures
Heat of adsorption is < 40 kJ/mol	Heat of adsorption maybe > 200 kJ/mol
No surface compounds occur	Surface compounds occur
It is a reversible process	The process is irreversible
Multilayer adsorption can occur	Only monolayer adsorption occurs
No activation energy is needed	Activation energy is required
Pressure is essential	Pressure is insignificant
Adsorption decreases with temperature increase	Adsorption remains unchanged at any temperature

2.3 Mesoporous Silica and Ordered Mesoporous Silica

Ordered mesoporous silica (OMS) combines the advantageous properties of silica and mesoporosity. These materials possess amorphous properties of gels, and are crystalline with ordered porosity found in materials such as zeolites (Gibson, 2014b). This class of material has various uses because of their inherent properties. These properties include high surface area, high pore volume making them suitable as catalyst supports and adsorbents. Silica can be mesoporous in nature but not ordered (Sivasubramanian et al., 2013, Jaroenworaluck et al., 2012) and may also be both (Qu and Gu, 2014). The difference between ordered mesoporous silica and mesoporous silica is that mesoporous silica has all the properties of mesoporous materials but lacks the channelization, orderliness and morphologies of the latter. Both types of mesoporous (ordered and non-ordered) siliceous materials can be synthesized using commercial precursors (TEOS, sodium silicate) or from agrowaste materials. Peng et al. (2011) and Parida et al. (2012) synthesized

(Mobil Catalytic Material-41) MCM-41 and MCM-48 from TEOS while Ghorbani et al. (2013) and Bhagiyalakshmi et al. (2010) synthesised OMS from agrowaste.

OMS was first discovered in the early 90's by Mobil Corporation scientists, and they soon synthesized MCM-41 and M-41 (Beck et al., 1992). M41S are classified according to their morphologies, MCM-41 (*p*6*mm*), MCM-48 (Ia3d) or MCM-50 (*p*2) which possess hexagonal, cubic and meso-lamellar phases, respectively (Figure 2.1).

This basic technique combines the surfactant template with siliceous materials. The surfactant acts as a structure directing agent (SDA), leading to formation of siliceous materials with different structural morphologies (Gibson, 2014a). The surfactant acts as building blocks, giving silica the choice of shape after manipulation of synthesis conditions, such as surfactant concentration, surfactant choice, synthesis temperature and speed of mechanical stirring/agitation. An interesting feature of this material was its pore size which was larger than that of zeolites making this class of materials more valuable as larger molecules could pass through them, making them better suited as adsorbents and catalyst support materials.

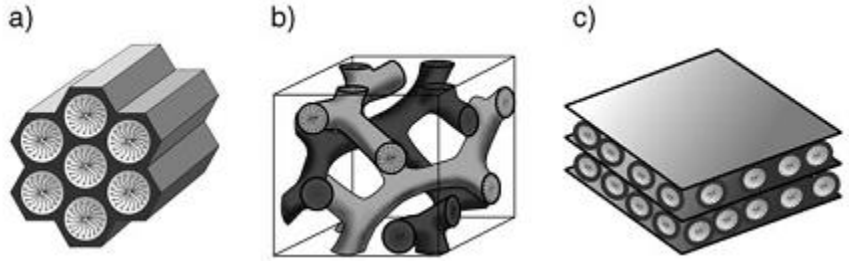

Figure 2.1 Structures of a) MCM-41 b) MCM-48 c) MCM-50 (Hoffmann et al., 2006)

Mesoporous silica has various applications, such as, in the medicine/pharmaceutical industry it is used for the controlled/measured delivery of drugs to target specific organs in the human system (Ciriminna et al., 2013), and is used to increase the available concentration of new drugs of active pharmaceutical ingredients (APIs) that are chemically unstable and cannot be administered orally (Barandeh et al., 2012). It is also used for the controlled release of aroma and fragrances (Berger, 2007). Mesoporous silica (MSi) are also used to deliver biocides for surface treatments and coatings to avoid contamination by microbes and bacteria in laboratories, operating rooms

and surgical instruments (Russell, 2003). MSi is extensively used as silica-based nanosols in the ink and coating industry. Ink made with the sol-gel technique from aqueous silica sol doped with various dyes for decorating glass with flatbed printers has recently been formulated (Pagliaro et al., 2009). Silica based sol-gel materials have been used extensively in the manufacturing industry as catalyst. MSi catalysts (consisting of entrapped metal complexes, metal nanoparticles and organic molecules) for the synthesis of fine and specialty chemicals have been rigourously researched since the late 1980s (Ciriminna et al., 2011). OMS has been used as a catalyst in the selective hydrogenation of edible fats and vegetable oils (Ciriminna et al., 2014). OMS industrially has been used in the heterogeneous catalysis of methanol (Tsvelikhovsky et al., 2009). OMS has also been used in the synthesis of different nanocomposites such as inorganic, organic, hybrid organic/inorganic materials. A class of ordered mesoporous silica nanocomposites known as ceramic matrix nanocomposites (CMnC) consisting of bulk ceramic with finely dispersed inorganic or organic nanofiller(s) have improved mechanical, optical, electrical, and/or magnetic properties, as well as corrosion-resistance and other protective capacities have been synthesised (Wang et al., 2003). OMS is also gaining attention in the field of energy storage and sorption (Wang et al., 2016).

2.4 Agriculture Waste as a Precursor for Mesoporous Silica

Agricultural waste can serve as a precursor for the production of mesoporous silica. These agrowastes are generated as by-products of the harvest season. Generally these wastes are gotten rid off by burning which releases huge amounts of nutrients. However, there are also toxic gases, H_2 and oxygen present in this waste which can be converted to gases such as carbon monoxide, methane and also ash which mainly consists of silica and carbon (Vaibhav et al., 2015). Presently, there is limited utilisation of this silica-rich ash from agrowastes. A large amount of these agrowastes are disposed off in landfill sites and may cause serious environmental pollution. In addition, as a result of burning of these wastes, some fine airborne particles are produced which can cause eye irritation and respiratory difficulties.

Recently, the extraction of silica from agrowastes is gaining more attention. This is because of the ease and cheap cost of extraction of pure silica. The most utilised material in the generation

of silica from agrowaste is rice husk, although other agrowaste materials have been used such as foxtail millet (Sivasubramanian et al., 2013) and sedge grass (Ghorbani et al., 2013). These burnt agrowastes, mostly rice husk, may contain between 10-20% of silica.

As a cheaper silica precursor to TEOS, these agrowaste materials have enormous potential. The silica is obtained by acid leaching which is the separation of a substance from a solid *via* a liquid medium. The fraction of interest diffuses into the solvent from its natural solid form. The acid serves a dual purpose, firstly, for the removal of elemental impurities thereby increasing the purity of the silica and secondly, the removal of the organic fraction of the waste (destruction of lignin) (Pang et al., 2011). Acids such as sulfuric (Jaroenworaluck et al., 2012) nitric (Adam et al., 2013) and hydrochloric acids (Thuc and Thuc, 2013) are used.

Silica is extracted through the use of a base such as caustic soda (NaOH) to form sodium silicate (Na_2SiO_3). At this stage, a structure directing agent is added to the silica to give it the mesoporous nature. The mechanism of formation can either be silicate anion initiated pathway or liquid crystal templating. The sodium is then treated with sulfuric acid to precipitate silica of high purity at an acidic pH between 3 and 4. The equations are as follows:

$$SiO_2 + 2\ NaOH \longrightarrow Na_2SiO_3 + H_2O$$

$$Na_2SiO_3 + H_2SO_4 \longrightarrow SiO_2 + Na_2SO_4 + H_2O$$

The gel obtained is thoroughly washed to a neutral pH and aged for a period of time. After ageing the gel is calcined normally at a temperature above 550 °C for a specific period of time. This is done to remove the template used in casting the mesoporous silica, leaving behind highly porous and pure silica. However, calcination at very high temperatures has been known to cause a reduction in the surface area and also a conversion to a more crystalline phase (Ghorbani et al., 2013). In a bid to obtain very high purity silica a combination of thermal and acid pretreatment steps was used (Thuc and Thuc, 2013).

Ordered mesoporous silica has also been produced using this method that was slightly modified. Modifications were made to the type and the concentration of SDA used in the synthesis.

Ghorbani et al. (2013) synthesised MCM-41 from sedge weed using CTAB as the SDA. Bhagiyalakshmi et al. (2010) synthesised MCM-41, MCM-48 and SBA-15 from rice husk. In the synthesis of the former two materials, CTAB was used as the SDA while in the latter, pluronic-123 which is a non-ionic triblock copolymer surfactant was used.

These materials have been used in the adsorption of dyes but have scarcely been used in the adsorption of other organic pollutants. Despite their large surface area and high pore volume, the major issue is their hydrophilic nature which makes them adsorb water molecules when present in aqueous solution. Hence, as a recent area of interest, scientists are beginning to devise ways of making this material more hydrophobic. This is done by modifying the surface of silica with amine or carbon functional groups, forming hybrid materials with more tendency to adsorb organic pollutants.

2.5 Formation Mechanism of Ordered Mesoporous Silica

The differentiating factor between MCM-41 and a single organic molecule or metal ion template is that the templates used are surfactants with alkyl chain lengths between 6-14 carbon atoms. Consequently, the mechanism responsible for the formation of MCM-41 from its precursors has gathered much attention. Beck et al. (1992), postulated 2 mechanisms for the formation of OMS. The first model is the liquid crystal templating method (LCT) and the second is the silicate anion method. Other authors such as Monnier et al. (1993), Inagaki et al. (1993) and Steel et al. (1994) proposed modified routes for the synthesis of MCM-41.

In the LCT model (Figure 2.2), silicate is added to preformed micelles using the structure directing agent (CTAB) and thereafter polymerisation of silicate occurs around preformed micelles. The SDA concentration is high, regardless of temperature and pH and the liquid crystalline phase is formed without the addition of the silica precursor (Hoffmann et al., 2006). In the silicate anion model, silicate material is added to a solution of the SDA (CTAB) to induce ordering of the silicate and surfactant micelles at the same time. After this, SDA is removed by one or a combination of the following processes of microwave digestion, solvent extraction and calcination. CTAB currently is the surfactant of choice in the synthesis of MCM-41 (Beck et al., 1992, Liou,

2011), however, another surfactant with a smaller hydrophobic tail has been used such as cetyltrimethyl ammonium chloride (CTACl) leading to the formation of smaller micelles (Qu and Gu, 2014).

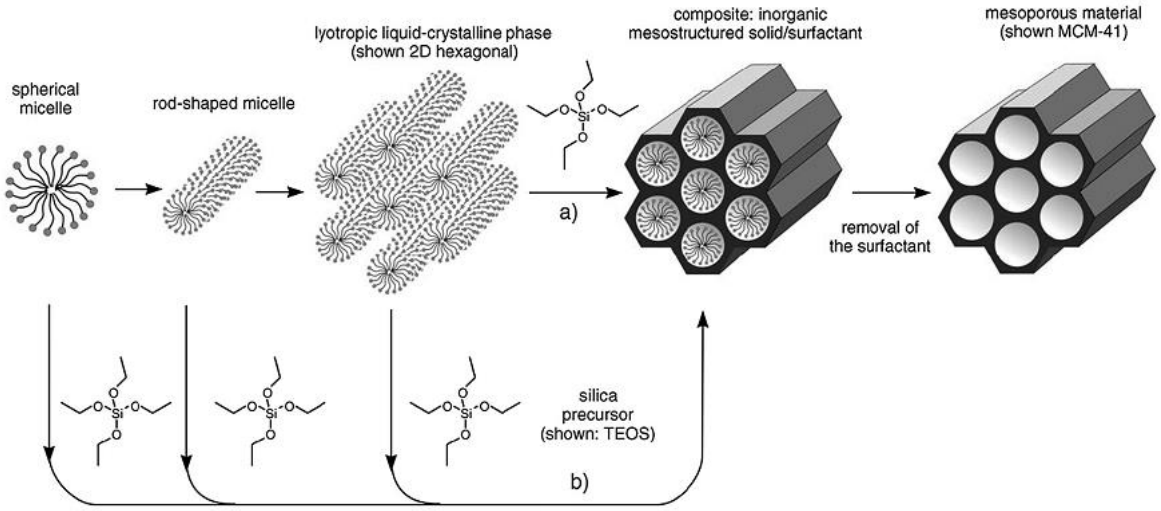

Figure 2.2 S Schematic diagram of MCM-41 synthesis (a) LCT mechanism (b) silicate anion initiated (Hoffmann et al., 2006)

In 1998 Stucky and co-workers (Zhao et al., 1998) developed another type of OMS after the M41S. This material was called SBA-15, where SBA meant Santa Barbara Amorphous. This material had excellent properties such as tailored particle morphology, variable pore sizes and thermal stability. A triblock copolymer template (non-ionic surfactant) was used under acidic conditions in this synthesis. This resulted in a material with a pore size of between 4-6 nm and a hexagonal 2-dimensional mesoporous silicate morphology. The silica network was composed of equally spaced mesoporous and microporous walls formed as a result of the liquid crystal micelle pattern. Poly(ethyleneoxide)-b-poly(propyleneoxide)-b-poly(ethyleneoxide) was the amphiphilic surfactant used providing a soft template for the hard inorganic porous material in solution. The micropore-mesopore structure gave an advantage of sorption over zeolitic materials because it exceeded the pore size of zeolites (Gibson, 2014a).

2.6 *Sol-gel* Chemistry

When colloidal sol particles are suspended in a solution, it is referred to as a sol. If the sol becomes aggregated in a solution and is present in a semi-rigid form (*gel*), it is called *sol-gel*. The gel obtained is calcined to expel the SDA and to produce the desired material. The *sol-gel* process basically entails the hydrolysis and condensation of organic salts or metal alkoxides with a base or an acid acting as a catalyst. Sol−gel materials are synthesized through hydrolytic polycondensation, at room temperature, of liquid precursors such as silicon alkoxides, under controlled conditions. This kind of synthesis is generally carried out in an organic cosolvent (alkoxysilanes are not water-soluble), through simultaneous or sequential reactions of hydrolysis (Ciriminna et al., 2013). This technique is very important in the synthesis of mesoporous silica materials with homogeneous properties. The sol-gel method is advantageous because of the ability to control various parameters in the reaction resulting in the production of materials with precise particle size, size distribution and morphology.

In the synthesis of mesoporous silica, different types of silica precursors are used. These precursors include TEOS, TMOS, sodium silicate and a less expensive silica precursor from agrowaste materials. These precursors can be used as alkoxides or can be used in combination with another alkoxide. TMOS use is limited by its toxicity. TEOS is the most used because of its low reactivity and slow hydrolysis. This allows the reaction to be controlled more easily and hydrolysis and condensation can take place in either acidic or basic environments simultaneously. Under conditions that are acidic, hydrolysis occurs more rapidly than condensation, leading to an increased number of siloxane linkages around the central silicon atom, thereby forming a fragile branched polymeric network. In a basic environment, the rate of condensation is proportional to hydrolysis, leading to the formation of more siloxane linkages. Hence, a highly branched polymeric network is formed extending throughout the volume of the sol as it thickens to a *gel* (Jal et al., 2004).

Hydrolysis induces a swop between the alkoxide group and the H ion and condensation results in siloxane bonding/linkages and products forming such as alcohol or water. This condensation

causes a growth in the silica network of particles in either an acidic or basic medium as shown in Figures 2.3 and 2.4 (Gibson, 2014b).

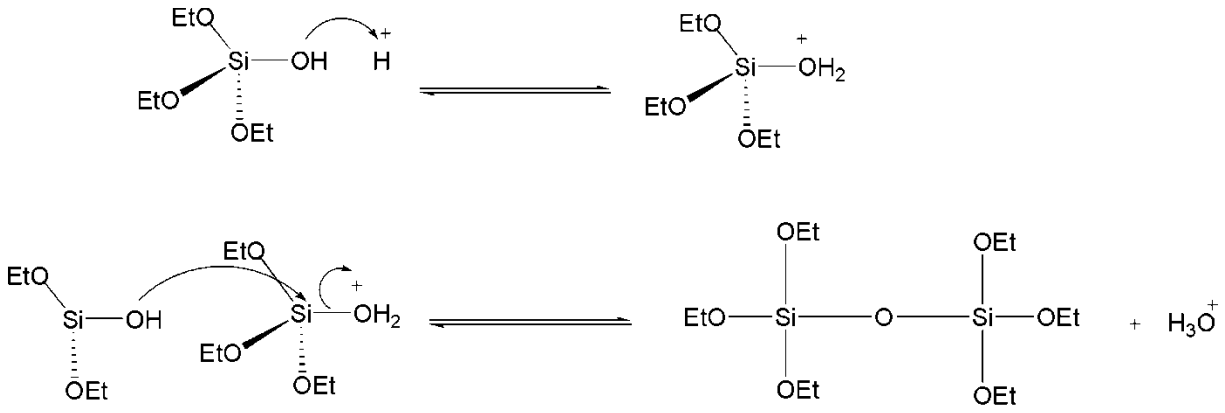

Figure 2.3 Hydrolysis and condensation of silica in acidic conditions (Gibson, 2014b)

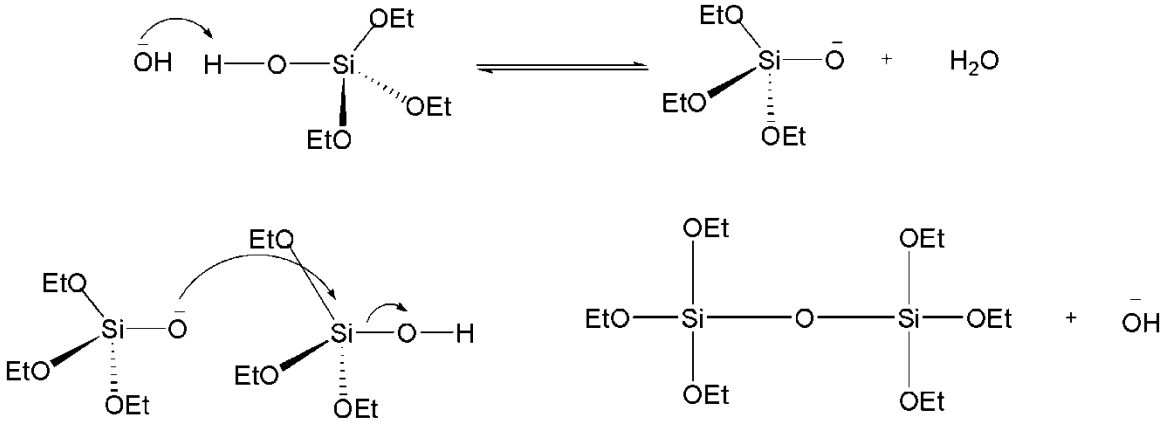

Figure 2.4 Hydrolysis and condensation of silica in basic conditions (Gibson, 2014b)

After the addition of the SDA, which is concentration and type dependent, the gel begins to thicken (ageing) by aggregation and assumes an orderly nature. At an advanced stage, the gel becomes very viscous and appears semi-rigid in nature. Silica framework is formed around pre-formed liquid crystal mesophases but the organized patterns are often obtained *via* self-assembly cooperative process taking place in situ between the templates and the silica network precursors (Wang et al., 2016). SDA pluronic-123 is used in the synthesis of SBA-15 while CTAB is used in the synthesis of MCM-41 and MCM-48 and the gel obtained is aged. The SDA enables terminal silanol groups to reorient themselves with each other, thereby forming further network link-

ages. The ageing process is very important because it determines particle size and the distribution of silica within the sol (Thuc and Thuc, 2013). The next process is drying the gel and the expulsion of the solvent from the gel pores. It is an important determinant of the pore size of the OMS synthesized. Silica gel can be classified into three types based on the solvent removal process. Xerogel is where the aqueous phase is removed by evaporation at ambient temperature and pressure below supercritical temperature, aerogel forms when the aqueous phase is removed by evaporation above its critical temperature and aquagel forms when the aqueous phase is removed by freezing and sublimation (Affandi et al., 2009).

The next step is drying which removes the SDA template leaving behind the hard inorganic gel. The gel is calcined in a muffle furnace at high temperature for several hours. Elevated temperatures above 700 ^{o}C have been known to transform amorphous silica to its crystalline form and also causes a reduction of its surface area (Ghorbani et al., 2013, Ying et al., 1993).

A key difference between sol-gel and mesoporous routes is that sol-gel entails the acidic or basic hydrolytic condensation of sols resulting in the formation of a gel of thicker proportion while in mesoporous route a surfactant is incorporated in the gel formed from the sol-gel process. The surfactant is ultimately expelled by calcination or refluxing, leaving behind gel with a mesoporous structure (Gibson, 2014b).

2.7 Surface Chemistry and Adsorption Characteristics of Silica

The surface of silica plays a vital role in adsorption. Materials with a large surface area are suitable as adsorbents and ion exchangers. Silica has 2 functional groups on its surface, siloxane (Si-O-Si) and silanol (Si-O-H). Of these 2 groups, the silanol groups are active and are responsible for activities taking place on the silica surface. In contrast siloxane is said to be unreactive (Dash et al., 2008, Jal et al., 2004). Silanol groups can be differentiated depending on their affinity for water (Parida et al., 2006). Three types of silanol groups are present on the silica surface. The first is the isolated silanol which has little affinity for water (the surface silica atom has a bond to the OH group and the other 3 bonds to the bulk structure) and absorbs at 3740-3750 cm^{-1}. The vicinal silanol (2 isolated silanol groups are attached to 2 different silicon atoms and are bridged

by a H-bond) absorbs at 3730-3740 cm^{-1} (Jal et al., 2004) and germinal silanol (made up of 2 hydroxyl groups attached to a silicon atom) absorbs at 3690-3730 cm^{-1} (Figure 2.5).

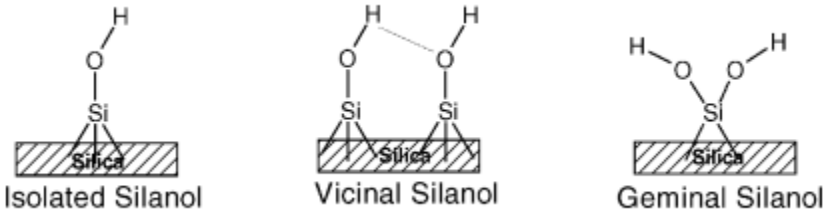

Figure 2.5 Types of silanol groups

The presence of these silanol groups plays a vital role in adsorption, with adsorption of adsorbates occuring mostly on the isolated silanols. According to Ong et al. (1992) there are 2 types of silanols at the silica/water interface, the first with a p*K*a value of 4.9 and a surface population density of 18%, and the second having a p*K*a value of 8.5 and a population density of 81%. Silanol with the lower p*K*a value of 4.9 are isolated silanols and the other type of silanol is connected to one another *via* H-bonding or a bridging water molecule.

Silanol groups are weakly acidic and the concentration on the surface of silica after activation at 150 °C is between 4.5-8.0 groups nm^{-2} (Jal et al., 2004). The number of silanols on the surface of silica differs from place to place as a function of temperature. At a temperature of 167 °C, physisorbed water is removed from silica. At temperatures higher than 167 °C, there is condensation of silanol groups and the liberation of water. When the temperature is further increased to 400 °C, almost half the silanols are removed and at 750 °C, only isolated silanols are present on the surface of the silica. At 450 °C, the removal of the OH group does not have serious implications on the morphology, density and specific surface area. This is because silica rehydroxylation makes it feasible to revert to its original state. There is a decrease in surface area at temperatures over 500 °C (Persello, 2000).

Pristine MCM-41 cannot hold up structurally if calcined at a temperature of 850 °C, and at a temperature of 1000 °C their surface area is reduced to nearly zero, leading to a constriction in pore size and a loss of mesostructure (Sangchoom and Mokaya, 2012). OMS are characterised by

small pores and a very large surface area which makes them suitable adsorbents. However, stearic hindrance may limit adsorption of large molecules.

Adsorption of pollutants by OMS is dependent on variables of size exclusion sieves effect, complexation, ionic exchange, electrostatic ion interaction, hydrogen bonding, hydrophobic interaction and molecular recognition based on imprinting (Wu and Lee, 2004). pH is very crucial in the adsorption of charged compounds by mesoporous silica. The PZC of silica is between 2 and 3, and at a pH less than PZC, the surface is positively charged due to the formation of $Si\text{-}OH^{2+}$. In contrast, when the pH is above the PZC, the silica surface becomes negatively charged as a result of deprotonation of silanol groups which gives $Si\text{-}O^{-}$. In the adsorption of non-ionic pollutants, adsorption by silanol groups is mostly by H-bonding or by van der Waals forces.

2.8 Modification of Mesoporous Silica (MS) Surface

To improve the performance of OMS, surface modification is necessary. The manipulation of the surface is possible due to their high surface area and high silanol density which makes modification possible of which much research has been carried out (Hoffmann et al., 2006). Modification of OMS surfaces considerably improves mechanical, chemical or optical properties, thus, making the materials more/less hydrophobic or corrosion resistant. Calcined OMS has a low adsorptive capacity for hydrophobic compounds in water because the high silanol density on the silica surface is favourably attracted to water molecules (Gibson, 2014b). OMS hydrophobicity can be increased by the addition of the alkyl group to the surface and pore walls of silica. This is achieved *via* two methods (a) post-synthetic grafting (PSG) and (b) co-condensation/in-situ method, with each method possessing advantages and disadvantages (Hoffmann et al., 2006).

2.8.1 Post synthesis grafting (PSG)

In this method, a pristine inorganic material is synthesised and the template is removed by calcination. This method is used in the modification of the inner surface of mesoporous surfaces by attaching organic functional groups to the surface. Eventually, the mesoporous silica is refluxed with a solution of functionalised silica species $(R'O)_3SiR$ or chlorosilanes $ClSiR_3$ or silazanes

$HN(SiR_3)_3$ that reacts with the silanol group of the pore wall (Figure 2.6) (Hoffmann et al., 2006). There are 3 main purposes for grafting which are (i) the removal of unreacted silanol groups (ii) to cause a change in the pore wall polarity and adsorption properties using organic functional groups and (iii) to introduce specific organic functionality. Advantages of PSG are synthesis conditions remain unchanged, the mesostructure is retained and calcination is possible. However, a major drawback of this process is an uneven distribution and formation of clusters of functional groups, on the pore surface which leads to blockage and reduced porosity.

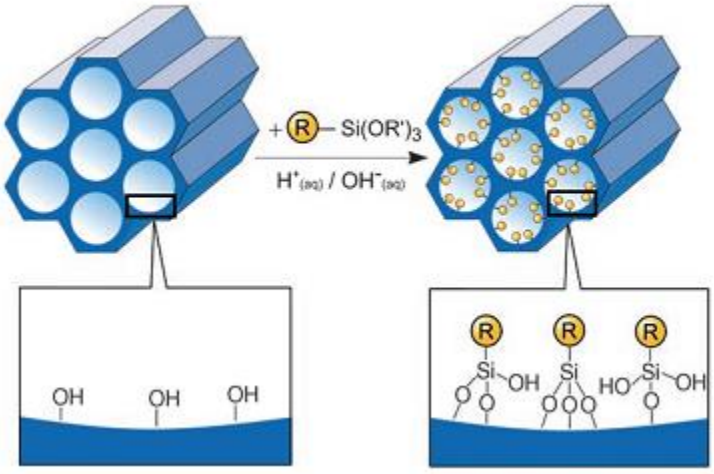

Figure 2.6 Post synthetic grafting process (Hoffmann et al., 2006)

2.8.2 Co-condensation method for surface functionalisation

The co-condensation or in-situ approach is a direct method of synthesis which involves tetralkoxylsilanes and trialkoxylorganosilanes with Si-C bonds in the presence of an SDA (Figure 2.7). Modification of the silica precursor influences the formation of the mesophase, consequently, the synthesis procedure may be tweaked to attain orderliness. Functional groups of an organic nature are hydrophobic and it is possible to intercalate them into the hydrophobic region of the SDA micelles thus resulting in the modification of pore walls by the incorporation of functional groups. Thus, some of the incorporated functional groups may be present inside the pore walls but not on the pore surface. SDA removal is carried out by extraction rather than calcination to prevent destruction of the functional groups present. Therefore, the blocking/shrinkage of pores is not much of an issue when co-condensation is used in the modification of OMS. Another

added advantage of this is that it is easier to control the final morphology of the mesoporous silica (Ozin, 2000, Yang et al., 1997). However, there are disadvantages associated with this method in that (i) addition of silane can drastically alter the properties of the reaction solute and maybe change the mesostructure of the final product leading to disorderliness, and (ii) an increase in the concentration of organosilane may lead to further loss in orderliness and porosity (Hoffmann et al., 2006, Gibson, 2014b).

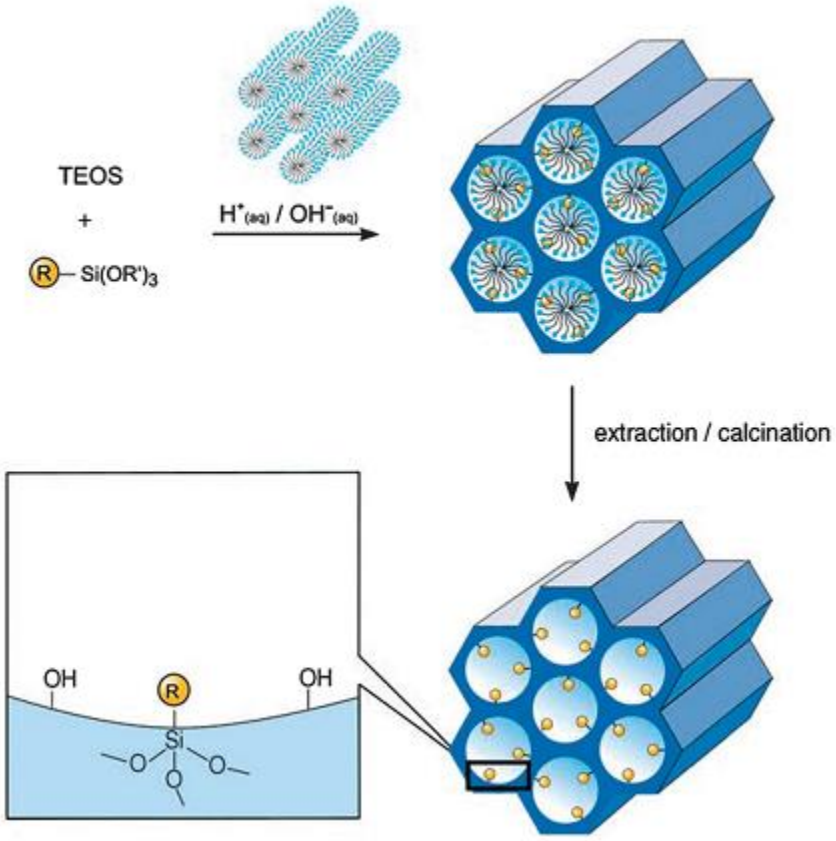

Figure 2.7 Co-condensation process (Hoffmann et al., 2006)

2.9 Use of MS for the Removal of Organic Pollutants from Aqueous Solution

Organic pollutants present in water sources are a major "grey area" in water treatment. This is because often conventional water treatment techniques are insufficient to remove these recalcitrant pollutants from the water system. Such pollutants include polycyclic aromatic hydrocarbons (PAHs), pesticides, phenolic compounds, chlorinated phenols, pharmaceuticals and personal care products as well as dyes. These organic pollutants are very harmful if present in water systems

even at trace concentrations. Therefore, the remediation of water systems contaminated with organic pollutants is of a high priority. Currently, there are many techniques for removing organic pollutants from wastewater, which include photocatalytic degradation, photo-Fenton process, ozone destruction and adsorption. Different kinds of adsorbents (mostly carbon/polymer based) have been utilized for the remediation of these pollutants from water systems. However, these materials when used as adsorbents have its short comings. For example, zeolitic materials are excellent adsorbers due to their large surface area and microporous nature but the microporous nature which makes it a good adsorber of gases does not make it a good adsorber of organic pollutants from aqueous systems. This is because the pores are constricted and access to the pores by these organic molecules is often repelled due to stearic hindrance. A promising class of adsorbents is carbonaceous materials, which have been successfully utilized in the adsorption of organic pollutants from aqueous systems. These carbonaceous-based adsorbents are activated carbon, carbon nanotubes, carbon biochar, graphite, graphene oxide and graphene. These sets of materials have been utilized in the adsorption of dyes (Song et al., 2012, Yu et al., 2015a), PAHs (Wang et al., 2014b, Zhang et al., 2013) and pharmaceuticals (Zhu et al., 2015, Nam et al., 2015, Liu et al., 2014). Despite being excellent adsorbents, the materials have a major drawback of not being selective and their regeneration is expensive (Gibson, 2014b). Also, they have a complicated adsorption mechanism and are not easily separated from aqueous solutions (Liu et al., 2013).

For the above-mentioned reasons, there is a need to further develop efficient sorbents. Hence, the extensive research involving mesoporous silica as adsorbents for organic pollutants in aqueous systems. The advantage of these materials is that they can be optimised to target specific molecules, and can be regenerated and reused with high adsorption capacity.

It is a documented fact that calcined mesoporous silica has low affinity for the remediation of hydrophobic compounds from aqueous solution because of its high silanol density and high attraction for water molecules. In order to improve the hydrophobicity of mesoporous silica, it has been used as as-synthesised and complexed with other compounds such as cyclodextrin, aluminium groups, as-synthesised mesosilica with encapsulated magnetic nanoparticles, graphene oxide and graphene (Gibson, 2014b, Liu et al., 2013).

2.9.1 MCM-41

MCM-41 should be a good adsorbent because of its properties such as large surface area and tailored porosity, but it is not. This is due to its silanol density which results in its high affinity for water molecules rather than organic pollutants. For it to be useful as an adsorbent, it has to be made more hydrophobic (Figure 2.8). To achieve this, it is used in the as-synthesised form, where the surfactant remains in the structure of the uncalcined silica.

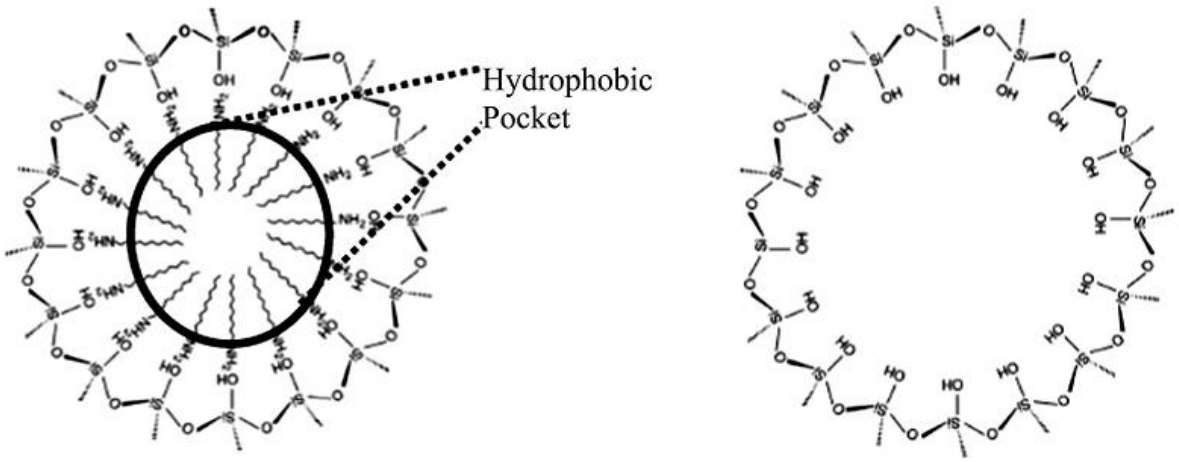

Figure 2.8 Hydrophobic pocket of as-synthesised MCM-41 (left) and calcined MCM-41 (right)

Denoyel and Sabio Rey (1998) developed as-synthesised MCM-41 for the removal of 3 chlorophenols from aqueous solution. In their studies, they utilized 3 different SDAs with increasing chain length, C12, C14 and C16 in the synthesis of as-synthesised MCM-41 and obtained an adsorption capacity of 0.91, 1.2 and 1.35 mmol/g, respectively for trichloroacetic acid. This was as a result of the chain length of the SDA as opposed to any other property of the adsorbent. The trichloroacetic acid anions were retained by the cationic surfactant group. Mangrulkar et al. (2008) used calcined and uncalcined MCM-41 in the adsorption of phenol and 3-chlorophenol. They discovered the uncalcined MCM-41 had a better sorption capacity which was approximately three times that of the calcined MCM-41. This was attributed to the hydrophobicity created by the surfactant template in the MCM-41. Also, pH and co-existing ions had a vital role to play in the removal of phenols from wastewater. There are several other studies that report the use of as-synthesised mesoporous silica in remediating organic pollutants, and in all cases, the as-

synthesised materials performed better. Of importance was that these materials were stable in water for a long time without a major loss of the SDA (Gibson, 2014b). SDAs with C12, C14, C16 and C18 chain length have been shown to increase adsorptive capacity with increased hydrophobicity of the target molecule (Denoyel and Sabio Rey, 1998).

2.9.2 Alkyl grafted mesosilica

PSG is the most widely used technique for modifying the chemical and physical properties of mesoporous silica. This is achieved by the introduction of an organic functional molecule on the surface of prefabricated mesoporous silica through grafting. PSG is done through the silylation reaction which involves the interaction of the free silanol groups with organosilane agents such as alkyl, aryl, amino and chlorosilanes on the surface of the silica material (Sánchez-Vicente et al., 2014). This is used to improve the hydrophobicity of mesoporous silica. Most researchers reported an increase in the sorption capacities of the surface modified materials. Alkyl grafted mesosilica has been utilized in the adsorption of polycyclic aromatic hydrocarbons (PAHs) (Vidal et al., 2011), nonylphenol (Inumaru et al., 2000), alkyl phenols and alkylaniline (Inumaru et al., 2006). These PSG materials are often specialized and selectively target specific organic pollutants. Vidal et al. (2011) showed that five polycyclic aromatic hydrocarbons (PAHs) were successfully removed from a simulated aqueous PAH solution. The adsorption rates were between 30-80% and were significantly higher than the values of the unmodified mesoporous silica.

2.9.3 SBA-15

SBA-15 is a very useful adsorbent in the adsorption of organic pollutants from aqueous solution. It is more useful in adsorption of organic pollutants from aqueous solution because of its larger pore size as compared to MCM-41 (better adsorber of gases). Another advantage SBA-15 has over MCM-41 in adsorption is based on greater pore wall thickness (Asgari et al., 2015) which enables it to capture larger molecules, form chemical complexes and is also very stable in aqueous solution. However, there are disadvantages regarding the use of SBA-15 as a sorbent, because it is made up of mesopores and micropores. The micropores may become blocked by alkyl

groups resulting in restricted access to the mesopores *via* micropores (Gibson, 2014b). SBA-15 has been used in the adsorption of dyes (Dong et al., 2011) and (di/tri) chlorophenols (Qin et al., 2012) with good sorption ability. Bifunctionalized SBA-15 has also been utilized for the removal of methylene blue from aqueous solution with good sorption capacity. Qiao and co-workers used oxygen-containing/amino-groups bifunctionalised SBA-15 for the adsorption of methylene blue from aqueous solution (Qiao et al., 2015). To further improve the adsorption capacity of SBA-15, combination agents' such as diamine-phenyl, diamine-cetyl and phenyl-cetyl groups were used in functionalizing SBA-15. This was applied for the removal of eison, 4-nonylphenol or di-n-butyl phthalate, respectively (Zhang et al., 2011c). Eison had a removal efficiency of 99% even at low concentration. The adsorption capacity of mixed amine and phenyl functionalized SBA-15 was quite low and there was no cooperative adsorption mechanism by both groups present on the surface of SBA-15.

2.9.4 Cyclodextrin (CD)

Cyclodextrins are obtained from starch and can form inclusion complexes in solution, or in solid state with organic molecules, through host-guest interaction (Landy et al., 2012). Cyclodextrin can be used as guest molecules in as-synthesised mesosilica because of their properties such as hydrophobic cavities, large pores and hydrophilic surface (Figure 2.9). When cyclodextrin molecules are incorporated into mesosilica, their hydrophobicity is increased. Organic pollutants are trapped in the hydrophobic cavity of cyclodextrin during the removal of toxic organic substances in aqueous solution. A setback associated with the use of cyclodextrin is its high water solublity and it must be grafted onto a stationary phase such as porous silica (Asouhidou et al., 2009). Cyclodextrin-mesosilica has the advantage of being able to rapidly adsorb organic molecules with improved selectivity, is environmentally inert and is easily synthesized (Sawicki and Mercier, 2006).

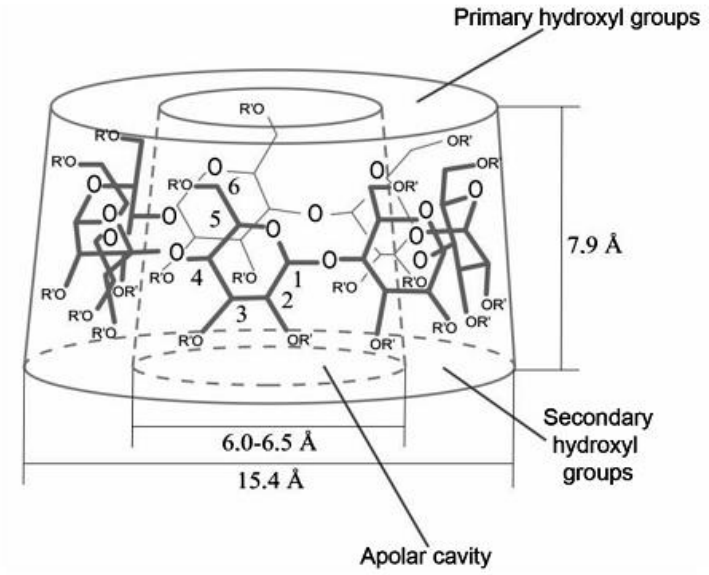

Figure 2.9 Hydrophobic cavity of cyclodextrin (Miranda et al., 2011)

Cyclodextrin-incorporated mesosilica has been used in the removal of phenols, phenolic compounds (Landy et al., 2012) and DDT (Sawicki and Mercier, 2006). An improved adsorption capacity was observed in mesoporous silica that was modified with cyclodextrin. Optimal adsorption was reported when cyclodextrin concentration was between 2-8 % with rapid analyte uptake, however, CD concentration > than 8 % caused a significant drop in the performance of the adsorbents. A lower concentration of CD often produces the best results when incorporated into mesosilica and used as an adsorbent. Cyclodextrin loading accessibility, molecular size, molecular structure and accessibility are important when cyclodextrin-silica are used as adsorbents (Gibson, 2014b).

2.9.5 Mesoporous silica coated iron magnetic nanoparticles

In this class of materials, mesoporous silica is coated with magnetic nanoparticles mostly iron oxide. In order to overcome the limited adsorption capacity of pristine mesoporous silica because of the lower number of surface functional groups, discrete nanocomposites with a magnetic core and porous shell structure have been developed to remove organic species from water (Mahto et al., 2015). This material combines the functionalities of the mesoporous structure of silica and sufficient magnetization of the magnetic nanoparticles. Their magnetic properties ensures that

separation is relatively easy in liquid phase by applying an external magnetic field (Tian et al., 2009). Tian et al. (2009) used as-synthesised mesosilica Fe_3O_4 to remove 1,1-bis(4-chlorophenyl)-2,2,2-trichloroethane (DDT) from aqueous solution. The material was highly effective in the removal of DDT and the magnetic core ensured good separation of the adsorbent from the aqueous solution. A similar but slightly complex material with iron oxide-improved mesoporous silica shell and a Fe_3O_4 /SiO_2 core was developed by Tian and co-workers, for the removal of DDT from aqueous solution. Firstly, they prepared magnetic Fe_3O_4 and wrapped it in a non-porous silica shell by the Stober process. Next CTAB was used to make a mesoporous silica shell around the outside and finally, another layer of Fe_3O_4 was coated on the mesoporous silica. The surfactant used was CTAB and it was removed *via* acidic extraction with ethanol. The adsorption process proceeded very quickly with adsorption equilibrium being reached before 60 minutes. The best adsorption occurred at an optimum iron concentration of ten percent weight content. The hybrid material performed significantly better as compared to mesoporous silica on its own. Interestingly ease of separation of the adsorbent from the aqueous solution after adsorption was easy because of its magnetic properties.

2.9.6 Graphene oxide

Graphene oxide (GO) is graphite which has been severely oxidized to give a C/O atomic ratio of approximately 2. GO is a two dimensional atomic carbon that has some specific advantages over other carbon nanomaterials. Its chemical and electrical properties have been found to be useful in various applications, including sensors, computer memories, hydrogen storage, generation of solar energy and as adsorbents. GO is unique because it has a high surface area, good physisorption, good biocompatibility, excellent water dispersion and is also laden with a variety of functional groups. These functional groups include phenol hydroxyl and epoxide groups at the basal plane, carboxylic acid at the edge and C=C sp^2 domain (Fakhri, 2013). A large number of oxygen containing functional groups have been introduced to the single layer of graphite sheet (graphene). These oxygens are implanted into the carbon sheet and enlargens the interlayer spacing. The GO sheet becomes expanded and can be pulled open by mechanical agitation or sonication. This results in the expansion and exfoliation of graphite into single or multi-layer sheets. As a consequence of oxidation, multiple defects can be seen on the surface of the GO and the level of

such defects is dependent on the type of oxidants and the oxidising time (Sun and Fugetsu, 2013).

GO is produced by oxidising graphite by any of the following techniques developed by Brodie (Poh et al., 2012), Hummers (Shahriary and Athawale, 2014), Staudenmeir (Poh et al., 2012) and Tour (Marcano et al., 2010). However, the Hummers method is the most popular used in the synthesis of GO. All the methods are quite similar with only a variation in synthesis conditions and chemicals. During the oxidation of graphite, oxygen reacts with different sites on the graphite sheet resulting in graphene oxide.

In 1859, Brodie oxidized graphite flakes with a mixture of potassium chlorate and nitric acid. He obtained a substance that was easily dispersed in water but not in acid which he named "graphic acid" (Dreyer et al., 2010).

Staudenmaier made an improvement of Brodie's procedure, by adding small aliquots of $KMnO_4$ and introducing the $KClO_3$-HNO_3 mixture over the course of the reaction and introduced H_2SO_4 to increase the acidity. This change resulted in better overall oxidation in a single reaction vessel.

Hummers and Offerman developed a method for the oxidation of graphite by reacting it with a mixture of potassium permanganate, sulfuric acid and sodium nitrate. Very good oxidation was achieved.

The Tour method (Marcano et al., 2010) recently developed in 2010, gave the best result in terms of oxidation, with a conversion of 96-98% of graphite to graphene and the non generation of toxic fumes. They used a mixture of 9:1 sulfuric to phosphoric acid.

2.9.7 Graphene

Graphene is a new class of carbon nanomaterials. It is composed of 2-dimensional single sheets of carbon atoms that have a hexagonal arrangement. Because of its unique properties, its discovery has led to increased environmental and chemical application. It was discovered through the

scotch tape peeling method by Novoselov et al. (2004). It is highly ordered, has a high surface area of approximately 2630 m^2/g, high thermal conductivity, high electrical conductivity, high chemical durability and high electron mobility. The large theoretical surface area, electron rich π system and hydrophobic surface makes graphene the most sought after material for remediation of organic pollutants in the environment. The adsorption sites on graphene are mainly from hydrophobic carbon conjunction for surface π-π interaction. The scotch tape peeling method is labour intensive and currently, there are five methods for the production/synthesis of graphene.

These methods are chemical vapour deposition, mechanical graphite exfoliation, epitaxal growth on an electrical insulating surface, solvothermal synthesis and the reduction of GO (Singh et al., 2014, Lee and Park, 2012). In most cases GO is the precursor in the synthesis of graphene, except in the scotch tape peeling method, where graphite is used. The GO is produced by acidic oxidation of graphite, causing acidity of the different functional groups on its surface. The graphite oxide from that process is ultrasonicated to give a single layer of GO.

Chemical vapour deposition (CVD) is used in large scale graphene synthesis. In this method, graphene is deposited on a (transition) metal surface and can form single to multi-layer graphene sheets. This process is usually associated with small crystal surface defects on the graphene and the graphene produced is semitransparent to transparent.

Mechanical exfoliation was used in the production of the first graphene sheet. This was a top-down method. Novoselov et al. (2004) isolated 2-dimensional crystals from 3-dimensional graphite using this method. Overcoming van der Waals forces between the first and second layer without distorting subsequent layers, is key in generating a single layer of graphene with this technique. However, this technique is plagued with several issues of reproducibility, is time consuming and the results are often unreliable (Lee and Park, 2012).

2.9.7.1 Chemical reduction

This method makes use of chemical reducing agents such as hydrazine (Marcano et al., 2010), dimethyl hydrazine, hydroquinone, hexylamine, sulfur containing compounds, and sodium boro-

hydride (Lee and Park, 2012) to synthesise graphene from GO. It is very effective for large scale production of reduced graphene oxide. Reduced GO is dispersed easily in aqueous solution because of trace amounts of oxygen present in it. This method allows for easy transfer and manipulation of graphene on a substrate.

2.9.7.2 Thermal exfoliation

Thermal exfoliation is achieved by GO placement in a muffle furnace at a high temperature under an inert environment for a period of time. The merit of thermal reduction of GO is that it is eco-friendly, ensures production of high quality graphene and no toxic chemical reducing agents are used.

2.10 Remediation of Organic Pollutants with OMS, OMS Composites, OMS-GO and OMS-G

2.10.1 Mesoporous silica graphene oxide/graphene removal of persistent organic pollutants from aqueous media

Graphene oxide and graphene are excellent adsorbents of organic pollutants from aqueous media, however, they suffer certain drawbacks. Graphene oxide is highly dispersive in water, making it difficult to separate from solution after adsorption. Reduced graphene oxide, (graphene) has defects/wrinkle areas which are regarded as high surface energy adsorption sites and are occupied by external molecules. Graphene sheets aggregate in water due to their π-π interactions and strong van der Waals interactions between the layers of the sheets. This stacking/aggregation restricts interaction between those in-between adsorption sites in the graphene sheet layers and the adsorbates. Thus, graphene does not fulfill its maximum adsorption potential. In a bid to improve the adsorption capacity, graphene oxide and graphene can be loaded onto a mesoporous silica frame work. This serves to stabilize high energy areas, and improve separation of adsorbent from aqueous solution allowing it to achieve its true potential as an adsorbent (Liu et al., 2013, Yang et al., 2015a).

Liu et al. (2013) used fumed silica graphene composites in the adsorption of 12 organophosphorus pesticides (OPP) from aqueous solution. The silica graphene composite was a better adsorbent when compared to other conventional adsorbents such as silica gel, C-18 silica, activated carbon, graphite and graphene. It was discovered that the composite had over 95% adsorption efficiency for all 12 OPPs. The pH of the solution played no part in the adsorption process as adsorption capacity was uniform throughout the full pH range. The isotherm data best fitted the Langmuir model.

Yang et al. (2015a) synthesised silica graphene composite for the removal of phenanthrene from aqueous solution. Fumed silica nanoparticles were used to form a composite with graphene using hydrazine for the reduction of graphene in the composite. The results were very interesting, as the composite had an adsorption capacity of 100 fold when compared to pristine graphene at the same level. Interestingly, they also found the adsorption capacity of the composite increased with an increased loading of graphene on silica and reduced significantly with the introduction of an oxygen containing group in the graphene nanosheets. The high adsorption capacity was attributed to hydrophobic effects and strong π-π stacking interactions of the exposed graphene nanosheets.

2.10.2 Use of mesosilica to remove organic dyes from aqueous solution

Dyes sometimes known as colourants have been used since time immemorial. Dyes absorb visible light between 400-700 nm making them appear coloured to human eyes. Annually, it is estimated that approximately 3.5×10^6 kg of dyes are discharged into water bodies. These dyes generate coloured wastewater and pollute the environment. The major culprit of this pollution type is the textile industry, and other industries such as food, tanneries, and electroplating industries also discharge coloured effluent. Coloured effluent is recalcitrant in nature and is highly persistent in an aqueous system. The resultant colours from dyes are aesthetically unpleasant, causes a decrease in light penetration in water bodies, thereby causing retardation in photosynthetic activities, inhibiting the growth of aquatic biota and utilising dissolved oxygen. In addition to these detrimental behaviours of dyes and its degradation products in water systems, dyes have been implicated in causing dermatitis, skin irritation, cancer and mutation in mammals. Consequently,

various techniques have been developed to remediate dyes from wastewater which includes floatation, coagulation, photo degradation, hyperfiltration, oxidation, biological treatment, and adsorption. However, some of these techniques do not effectively remove the dyes and sometimes harmful by-products are generated. Therefore, adsorption is often the preferred method for dye remediation due to ease of use, cost-effectiveness and no by-products. The materials most used in the adsorption of dyes are alumina, metal hydroxides and activated carbon. However, a major disadvantage of these materials is the cost of production. Other materials, such as sawdust, coir pith, olive stone have also been used for the removal of dyes from aqueous solution (Patil et al., 2011).

Mesoporous silica adsorbents have also been used as an adsorbent for the removal of organic dyes from aqueous solution. This is because it has a high surface area, high pore volume and is easily regenerated. Dyes can be neutral, acidic or basic. Therefore, the mechanism of adsorption of mesosilica for the different dye classes differs. Often, mesoporous silica are functionalized with different groups to achieve tailored adsorption based on the adsorbate involved. In the adsorption of cationic dyes, the adsorbate-adsorbent interaction is mostly controlled by electrostatic attraction and is strongly dependent on the pH of the solution, where an increase in pH causes an increase in adsorption efficiency. In contrast, for acidic dyes, a decrease in solution pH causes an increase in adsorption. The PZC of silica is between 2 and 3, therefore, adsorption of both cationic and anionic dyes can be favourable if the solution pH of adsorption is manipulated. At pH values of 4-10, which is above the PZC of silica, the silica surface has a net negative charge thereby electrostatically increasing its interaction with cationic dyes. At a pH below 2, the silica surface has a net positive charge and can electrostatically attract anionic dyes. If the adsorbate being adsorbed is not ionic, adsorption is by van der Waals interactions which are due to the extensive network of H-bonds on the surface of silica.

2.10.3 Basic/cationic dye remediation

Both modified and unmodified mesoporous silica has been used in the adsorption of cationic dyes from aqueous solution. Unmodified mesoporous silica has been applied in the adsorption of methylene blue (MB) by Monash and Pugazhenthi (2010), Wang and Li (2006), Dong et al.

(2011), Anbia and Hariri (2010) and Qu and Gu (2014). Researchers, such as Shao et al. (2014) and Xiao et al. (2015) used metal oxides to modify mesoporous silica in the adsorption of MB with improved adsorptive capacities. Others have modified MS with amine functional groups and reported improved adsorptive capacities for cationic dyes (Ho et al., 2003, Karim et al., 2012). Other cationic dyes such as basic violet, basic green 5, rhodamine B, crystal violet, and janus green have been adsorbed with pristine and modified mesoporous silica (Huang et al., 2011, Juang et al., 2006, Eftekhari et al., 2010). In all cases, where MCM-41 and MCM-48 were used in the adsorption of dyes, unless modified, they were plagued by 2 main issues; firstly, low adsorption capacities despite their large surface area and secondly, the inability to retain adsorbed dyes for a long period. This may be due to the destruction of pore structure (Gibson, 2014b). However MCM-50 with its lamellar structure SBA-3 and SBA-15 performed better with respect to the mentioned above problems.

2.10.4 Acidic/anionic dye remediation

Mesoporous silica is used in the adsorption of anionic dyes. The mesosilica with the best performance was the modified/functionalized form. The mechanism of adsorption is electrostatic ion interaction because the PZC of silica is between 2-3, and at low pH below the PZC, the surface of the silica has a net positive charge. Hence, the attraction of anionic dyes becomes feasible. These anionic dyes possess sulfonated functional groups making interaction at low pH possible. The conventional carbon based adsorbent is not useful in the removal of acid blue, but, in contrast, amine-functionalised MCM-41 performed considerably better in the adsorption of the dye (Ho et al., 2003). Anbia et al. (2010) used mesoporous SBA-3 to remove anionic dyes such as methyl orange (MO), orange G (OG) and brilliant red X-3B from aqueous solution. They compared the results of as-synthesised MCM-41 to synthesized ones and found the as-synthesised material had a better adsorption capacity than the calcined one. The Freundlich isotherm was the most appropriate model to describe the experimental data while the adsorption kinetics best fitted the pseudo-second order model.

Qin et al. (2009) used ammonium-functionalised MCM-41 in adsorbing 4 anionic dyes from aqueous solution. The dyes were methyl orange (MO), orange IV (OIV), reactive brilliant red X-

3B (X-3B) and acid fuchsine (AF). The modified MCM-41 performed considerably better than the unmodified MCM-41. The intraparticle diffusion model best described the adsorption kinetics and the adsorption fitted into the Langmuir model. Electrostatic ion interaction was the main mechanism for the adsorption of the dyes.

Mahmoodi et al. (2011) used amine-functionalised mesoporous silica for the adsorption of anionic dyes. The adsorbed dyes were acid red 14 (AR 14), acid black 1 (AB1) and acid blue 25 (AB25). The modified amine-functionalised MCM-41 performed over 200 times better as compared to the unmodified MCM-41. The Langmuir and Freundlich isotherms were the best fit models. Adsorption kinetics were found to conform to the pseudo-second-order kinetic model.

2.10.5 Adsorption of pharmaceuticals

Recently, attention is being given to the presence of pharmaceuticals in aquatic systems because of their toxic effects. These pharmaceuticals are described as emerging contaminants. They are ubiquitously present in low concentrations in water systems and soil, and at approximately 100 μg/L in the effluent of pharmaceutical manufacturers. They are known to cause chronic toxic effects if aquatic life are exposed to them over a long period of time. Conventional water treatment facilities have a very low capability for the removal of these pharmaceuticals because of their resistance effects and old technologies used in wastewater treatment plants hence, making these pharmaceuticals ubiquitous and persistent in the environment (Bui and Choi, 2009, Bui et al., 2011, Bui et al., 2013). Conventional water treatment systems often have less than 50% removal efficiency for these pharmaceuticals in aqueous systems.

To safeguard the health of people, it is imperative to develop new technologies with improved efficiency for the removal of pharmaceuticals from aqueous systems. Adsorption is invaluable in water treatment for the removal of organic pollutants from water. However, due to the size and structure of these pollutants (pharmaceuticals), adsorption with mesoporous materials may be better suited for their remediation. Amongst mesoporous materials, mesoporous silica has been applied in the adsorption of pharmaceuticals from aqueous systems with varying degrees of success achieved.

Bui and Choi (2009) utilised mesoporous SBA-15 in the adsorption of 5 pharmaceuticals (carbamazepine, clofibric acid, diclofenac, ibuprofen and ketoprofen) from water. It was found that adsorption kinetics were rapid, less than 5 minutes as compared to several hours for activated carbons that are primarily used in the adsorption of pharmaceuticals. The percentage removal recorded was quite high in acidic media (pH 3-5) and was 85.2%, 88.3%, 93.0%, 94.3% and 49.0% for carbamazepine, diclofenac, ibuprofen, ketoprofen and clofibric acid, respectively. There was high adsorption by SBA-15, even when a mixture of the five pharmaceuticals was prepared, with efficiencies between 75.2 to 89.3%. The adsorption model was found to be pseudo-second-order and the adsorption isotherm best fitted the Freundlich model. Interestingly, they discovered the mechanism of adsorption was hydrophilic in nature suggesting that SBA-15 can be further modified/tailored for specific adsorption of pharmaceuticals. This could be achieved by tweaking or introducing certain functional groups to the surface of SBA.

Bui et al. (2011) developed a modified mesoporous silica SBA-15. SBA-15 was functionalised with hydroxymethyl, aminopropyl and trimethylsilyl. The optimal pH for the study was 5.5-7.6. These materials were used in the removal of 12 pharmaceuticals from aqueous systems. SBA demonstrated considerable affinity for amino-containing (atenolol, trimethoprim) and hydrophobic pharmaceuticals, but it showed minimal adsorption for hydrophilic compounds. Hydroxymethyl had a similar adsorption pattern/efficiency as SBA-15 towards the adsorption of the pharmaceuticals. In contrast, aminopropyl SBA-15 showed increased adsorption of 2 acidic pharmaceuticals (clofibric acid and diclofenac) but a decrease in the adsorption of 2 amino-containing compounds and estrone. The material with the highest adsorption capacity was trimethylsilyl SBA-15. It performed significantly better and had a higher adsorption capacity for 9 of the adsorbed pharmaceuticals than pristine SBA-15. The percentage removal recorded was between 70.6-98.9% for 7 of the 9 pharmaceuticals.

Bui et al. (2013) utilised trimethylsilylated mesoporous SBA-15 in the adsorption of 12 pharmaceuticals from an aqueous medium. Adsorption was found out to be mainly dependent on the solution pH and pharmaceutical properties (i.e hydrophobicity (log K_{ow}) and acidity (p*K*a)). For efficient adsorption, the existing log-linear relationship between pH-dependent octanol-water coefficients(K_{ow}^{pH}) and adsorption (*K*d) must be good. Based on this relationship, the pharmaceuticals were separated into neutral, anionic and cationic compounds, thus implying that hydropho-

bic interaction was the driving force in the adsorption. The adsorption kinetics fitted into the pseudo-first-order (for five pharmaceuticals) and pseudo-second-order models (for seven pharmaceuticals). The adsorption rate was fast, and equilibrium was reached before an hour in most cases, however, some pharmaceuticals exceeded the one hour mark.

In the continued endeavor to develop better adsorbents, this study focused on developing a number of modified silica based materials to adsorb organic pollutants (dyes and pharmaceuticals). Silica nanotubes and silica nanoparticles were synthesized for the first time from elephant grass and were applied in the adsorption of methylene blue and methylene red. MCM-41 was synthesized from elephant grass and was modified with citric acid and used in the adsorption of methylene blue. Also, MCM-41 was synthesized from TEOS and modified with citric acid by a new method and was extensively characterized. This material was applied in the adsorption of a cationic dye, methylene blue. As-sythensised MCM-41, MCM-41, GO encapsulated MCM-41, and G encapsulated MCM-41 were synthesized and extensively characterized. These materials were applied in the adsorption of 2 pharmaceuticals (phenacetin and ampicilin) from aqueous solutions. Three real aqueous systems were utilized in this experiment, tap water sample, Umgeni River water sample and Blue Lagoon sample (part of the Indian Ocean) to show their application to real water samples. As-synthesised MCM-48, MCM-48, GO encapsulated MCM-48 and G encapsulated MCM-48 were synthesized and also extensively characterized. These materials were used in adsorbing caffeine and acetaminophen from aqueous systems. Lastly, silica nanotubes synthesised from elephant grass was encapsulated with GO and G and characterised. The coated materials were also used as adsorbents for pharmaceuticals from simulated water and real water samples. The materials prepared and the adsorption studies carried out with these materials on organic pollutants is the first reported study and thus contributes to original research and new knowledge in this field of research.

References

Adam, F., Appaturi, J. N., Khanam, Z., Thankappan, R. & Nawi, M. a. M. 2013. Utilization of tin and titanium incorporated rice husk silica nanocomposite as photocatalyst and adsorbent for the removal of methylene blue in aqueous medium. *Applied Surface Science,* 264**,** 718-726.

Affandi, S., Setyawan, H., Winardi, S., Purwanto, A. & Balgis, R. 2009. A facile method for production of high-purity silica xerogels from bagasse ash. *Advanced Powder Technology,* 20**,** 468-472.

Anbia, M. & Amirmahmoodi, S. 2011. Adsorption of phenolic compounds from aqueous solutions using functionalized SBA-15 as a nano-sorbent. *Scientia Iranica,* 18**,** 446-452.

Anbia, M. & Hariri, S. A. 2010. Removal of methylene blue from aqueous solution using nanoporous SBA-3. *Desalination,* 261**,** 61-66.

Anbia, M., Hariri, S. A. & Ashrafizadeh, S. 2010. Adsorptive removal of anionic dyes by modified nanoporous silica SBA-3. *Applied Surface Science,* 256**,** 3228-3233.

Asgari, M. S., Zonouzi, A., Rahimi, R. & Rabbani, M. 2015. Application of porphyrin modified SBA-15 in adsorption of lead ions from aqueous media. *Oriental Journal of Chemistry,* 31**,** 1537-1544.

Asouhidou, D. D., Triantafyllidis, K. S., Lazaridis, N. K. & Matis, K. A. 2009. Adsorption of Remazol Red 3BS from aqueous solutions using APTES-and cyclodextrin-modified HMS-type mesoporous silicas. *Colloids and Surfaces A: Physicochemical and Engineering Aspects,* 346**,** 83-90.

Bailey, S. E., Olin, T. J., Bricka, R. M. & Adrian, D. D. 1999. A review of potentially low-cost sorbents for heavy metals. *Water Research,* 33**,** 2469-2479.

Beck, J., Vartuli, J., Roth, W., Leonowicz, M., Kresge, C., Schmitt, K., Chu, C., Olson, D. H. & Sheppard, E. 1992. A new family of mesoporous molecular sieves prepared with liquid crystal templates. *Journal of the American Chemical Society,* 114**,** 10834-10843.

Bhagiyalakshmi, M., Yun, L. J., Anuradha, R. & Jang, H. T. 2010. Utilization of rice husk ash as silica source for the synthesis of mesoporous silicas and their application to CO_2 adsorption through TREN/TEPA grafting. *Journal of Hazardous Materials,* 175**,** 928-938.

Bui, T. X. & Choi, H. 2009. Adsorptive removal of selected pharmaceuticals by mesoporous silica SBA-15. *Journal of Hazardous Materials,* 168**,** 602-608.

Bui, T. X., Kang, S.-Y., Lee, S.-H. & Choi, H. 2011. Organically functionalized mesoporous SBA-15 as sorbents for removal of selected pharmaceuticals from water. *Journal of Hazardous Materials,* 193**,** 156-163.

Bui, T. X., Pham, V. H., Le, S. T. & Choi, H. 2013. Adsorption of pharmaceuticals onto trimethylsilylated mesoporous SBA-15. *Journal of Hazardous Materials,* 254**,** 345-353.

Cheremisinoff, N. P. & Cheremisinoff, P. N. 1993. Carbon adsorption for pollution control.

Dąbrowski, A. 2001. Adsorption—from theory to practice. *Advances in Colloid and Interface Science,* 93**,** 135-224.

Dash, S., Mishra, S., Patel, S. & Mishra, B. K. 2008. Organically modified silica: synthesis and applications due to its surface interaction with organic molecules. *Advances in Colloid and Interface Science,* 140**,** 77-94.

Denoyel, R. & Sabio Rey, E. 1998. Solubilization in confined surfactant mesophases. *Langmuir,* 14**,** 7321-7323.

Dong, Y., Lu, B., Zang, S., Zhao, J., Wang, X. & Cai, Q. 2011. Removal of methylene blue from coloured effluents by adsorption onto SBA-15. *Journal of Chemical Technology and Biotechnology,* 86**,** 616-619.

Dreyer, D. R., Park, S., Bielawski, C. W. & Ruoff, R. S. 2010. The chemistry of graphene oxide. *Chemical Society Reviews,* 39**,** 228-240.

Eftekhari, S., Habibi-Yangjeh, A. & Sohrabnezhad, S. 2010. Application of AlMCM-41 for competitive adsorption of methylene blue and rhodamine B: thermodynamic and kinetic studies. *Journal of Hazardous Materials,* 178**,** 349-355.

Fakhri, A. 2013. Adsorption characteristics of graphene oxide as a solid adsorbent for aniline removal from aqueous solutions: Kinetics, thermodynamics and mechanism studies. *Journal of Saudi Chemical Society*. *doi:10.1016/j.jscs.2013.10.002*.

Ghorbani, F., Younesi, H., Mehraban, Z., Çelik, M. S., Ghoreyshi, A. A. & Anbia, M. 2013. Preparation and characterization of highly pure silica from sedge as agricultural waste and its utilization in the synthesis of mesoporous silica MCM-41. *Journal of the Taiwan Institute of Chemical Engineers,* 44**,** 821-828.

Gibson, L. 2014a. Mesosilica materials and organic pollutant adsorption: part A removal from air. *Chemical Society Reviews,* 43**,** 5163-5172.

Gibson, L. 2014b. Mesosilica materials and organic pollutant adsorption: part B removal from aqueous solution. *Chemical Society Reviews,* 43**,** 5173-5182.

Gu, F., Liang, M., Han, D. & Wang, Z. 2015. Multifunctional sandwich-like mesoporous silica–Fe_3O_4–graphene oxide nanocomposites for removal of methylene blue from water. *RSC Advances,* 5**,** 39964-39972.

Han, R., Zhang, L., Song, C., Zhang, M., Zhu, H. & Zhang, L. 2010. Characterization of modified wheat straw, kinetic and equilibrium study about copper ion and methylene blue adsorption in batch mode. *Carbohydrate Polymers,* 79**,** 1140-1149.

Harlick, P. & Tezel, F. 2002. Adsorption of carbon dioxide, methane, and nitrogen: pure and binary mixture adsorption by ZSM-5 with SiO_2/Al_2O_3 ratio of 30. *Separation Science and Technology,* 37**,** 33-60.

Ho, K. Y., Mckay, G. & Yeung, K. L. 2003. Selective adsorbents from ordered mesoporous silica. *Langmuir,* 19**,** 3019-3024.

Hoffmann, F., Cornelius, M., Morell, J. & Fröba, M. 2006. Silica-based mesoporous organic–inorganic hybrid materials. *Angewandte Chemie International Edition,* 45**,** 3216-3251.

Huang, C.-H., Chang, K.-P., Ou, H.-D., Chiang, Y.-C. & Wang, C.-F. 2011. Adsorption of cationic dyes onto mesoporous silica. *Microporous and Mesoporous Materials,* 141**,** 102-109.

Inagaki, S., Fukushima, Y. & Kuroda, K. 1993. Synthesis of highly ordered mesoporous materials from a layered polysilicate. *Journal of the Chemical Society, Chemical Communications***,** 8, 680-682.

Inumaru, K., Kiyoto, J. & Yamanaka, S. 2000. Molecular selective adsorption of nonylphenol in aqueous solution by organo-functionalized mesoporous silica. *Chemical Communications***,** 15, 903-904.

Inumaru, K., Nakano, T. & Yamanaka, S. 2006. Molecular selective adsorption of alkylphenols and alkylanilines from water by alkyl-grafted mesoporous alumina: A comparative study to alkyl-grafted mesoporous silica. *Microporous and Mesoporous Materials,* 95**,** 279-285.

Jal, P., Patel, S. & Mishra, B. 2004. Chemical modification of silica surface by immobilization of functional groups for extractive concentration of metal ions. *Talanta,* 62**,** 1005-1028.

Jaroenworaluck, A., Pijarn, N., Kosachan, N. & Stevens, R. 2012. Nanocomposite TiO_2–SiO_2 gel for UV absorption. *Chemical Engineering Journal,* 181**,** 45-55.

Juang, L.-C., Wang, C.-C. & Lee, C.-K. 2006. Adsorption of basic dyes onto MCM-41. *Chemosphere,* 64**,** 1920-1928.

Karim, A., Jalil, A., Triwahyono, S., Sidik, S., Kamarudin, N., Jusoh, R., Jusoh, N. & Hameed, B. 2012. Amino modified mesostructured silica nanoparticles for efficient adsorption of methylene blue. *Journal of Colloid and Interface Science,* 386**,** 307-314.

Khan, T. A., Nazir, M. & Khan, E. A. 2013. Adsorptive removal of rhodamine B from textile wastewater using water chestnut (*Trapa natans L.*) peel: adsorption dynamics and kinetic studies. *Toxicological & Environmental Chemistry,* 95**,** 919-931.

Kushwaha, A. K., Gupta, N. & Chattopadhyaya, M. 2010. Enhanced adsorption of malachite green dye on chemically modified silica gel. *Journal of Chemical and Pharmaceutical Research,* 2**,** 34-45.

Kushwaha, A. K., Gupta, N. & Chattopadhyaya, M. 2014. Enhanced adsorption of methylene blue on modified silica gel: equilibrium, kinetic, and thermodynamic studies. *Desalination and Water Treatment,* 52**,** 4527-4537.

Landy, D., Mallard, I., Ponchel, A., Monflier, E. & Fourmentin, S. 2012. Remediation technologies using cyclodextrins: an overview. *Environmental Chemistry Letters,* 10**,** 225-237.

Lee, S.-Y. & Park, S.-J. 2012. Comprehensive review on synthesis and adsorption behaviors of graphene-based materials. *Carbon Letters,* 13**,** 73-87.

Liou, T.-H. 2011. A green route to preparation of MCM-41 silicas with well-ordered mesostructure controlled in acidic and alkaline environments. *Chemical Engineering Journal,* 171**,** 1458-1468.

Liu, F.-F., Zhao, J., Wang, S., Du, P. & Xing, B. 2014. Effects of Solution Chemistry on Adsorption of Selected Pharmaceuticals and Personal Care Products (PPCPs) by Graphenes and Carbon Nanotubes. *Environmental Science & Technology,* 48**,** 13197-13206.

Liu, X., Zhang, H., Ma, Y., Wu, X., Meng, L., Guo, Y., Yu, G. & Liu, Y. 2013. Graphene-coated silica as a highly efficient sorbent for residual organophosphorus pesticides in water. *Journal of Materials Chemistry A,* 1**,** 1875-1884.

Mahmoodi, N. M., Khorramfar, S. & Najafi, F. 2011. Amine-functionalized silica nanoparticle: Preparation, characterization and anionic dye removal ability. *Desalination,* 279**,** 61-68.

Mahto, T. K., Chandra, S., Haldar, C. & Sahu, S. K. 2015. Kinetic and thermodynamic study of polyaniline functionalized magnetic mesoporous silica for magnetic field guided dye adsorption. *RSC Advances,* 5**,** 47909-47919.

Mangrulkar, P. A., Kamble, S. P., Meshram, J. & Rayalu, S. S. 2008. Adsorption of phenol and o-chlorophenol by mesoporous MCM-41. *Journal of Hazardous Materials,* 160**,** 414-421.

Marcano, D. C., Kosynkin, D. V., Berlin, J. M., Sinitskii, A., Sun, Z., Slesarev, A., Alemany, L. B., Lu, W. & Tour, J. M. 2010. Improved synthesis of graphene oxide. *ACS Nano,* 4**,** 4806-4814.

Miranda, J. C. D., Martins, T. E. A., Veiga, F. & Ferraz, H. G. 2011. Cyclodextrins and ternary complexes: technology to improve solubility of poorly soluble drugs. *Brazilian Journal of Pharmaceutical Sciences,* 47**,** 665-681.

Monash, P. & Pugazhenthi, G. 2010. Investigation of equilibrium and kinetic parameters of methylene blue adsorption onto MCM-41. *Korean Journal of Chemical Engineering,* 27**,** 1184-1191.

Monnier, A., Schüth, F., Huo, Q., Kumar, D., Margolese, D., Maxwell, R., Stucky, G., Krishnamurty, M., Petroff, P. & Firouzi, A. 1993. Cooperative formation of inorganic-organic interfaces in the synthesis of silicate mesostructures. *Science,* 261**,** 1299-1303.

Nam, S.-W., Jung, C., Li, H., Yu, M., Flora, J. R., Boateng, L. K., Her, N., Zoh, K.-D. & Yoon, Y. 2015. Adsorption characteristics of diclofenac and sulfamethoxazole to graphene oxide in aqueous solution. *Chemosphere,* 136**,** 20-26.

Novoselov, K. S., Geim, A. K., Morozov, S., Jiang, D., Zhang, Y., Dubonos, S. A., Grigorieva, I. & Firsov, A. 2004. Electric field effect in atomically thin carbon films. *Science,* 306**,** 666-669.

Ong, S., Zhao, X. & Eisenthal, K. B. 1992. Polarization of water molecules at a charged interface: second harmonic studies of the silica/water interface. *Chemical Physics Letters,* 191**,** 327-335.

Ozin, G. A. 2000. Panoscopic materials: synthesis over 'all'length scales. *Chemical Communications,* 25, 419-432.

Pang, S. C., Chin, S. F. & Yih, V. 2011. Conversion of cellulosic waste materials into nanostructured ceramics and nanocomposites. *Advanced Materials Letters,* 2, 118-124.

Parida, K., Mishra, K. G. & Dash, S. K. 2012. Adsorption of copper (II) on NH_2-MCM-41 and its application for epoxidation of styrene. *Industrial & Engineering Chemistry Research,* 51**,** 2235-2246.

Parida, S. K., Dash, S., Patel, S. & Mishra, B. K. 2006. Adsorption of organic molecules on silica surface. *Advances in Colloid and Interface Science,* 121**,** 77-110.

Patil, S., Renukdas, S. & Patel, N. 2011. Removal of methylene blue, a basic dye from aqueous solutions by adsorption using teak tree (Tectona grandis) bark powder. *International Journal of Environmental Sciences,* 1**,** 711-726.

Peng, R., Zhao, D., Dimitrijevic, N. M., Rajh, T. & Koodali, R. T. 2011. Room temperature synthesis of Ti–MCM-48 and Ti–MCM-41 mesoporous materials and their performance on photocatalytic splitting of water. *The Journal of Physical Chemistry C,* 116**,** 1605-1613.

Persello, J. 2000. Surface and interface structure of silicas. *Surfactant Science Series***,** 5, 297-342.

Poh, H. L., Šaněk, F., Ambrosi, A., Zhao, G., Sofer, Z. & Pumera, M. 2012. Graphenes prepared by Staudenmaier, Hofmann and Hummers methods with consequent thermal exfoliation exhibit very different electrochemical properties. *Nanoscale,* 4**,** 3515-3522.

Qiao, W.-J., Wang, Z.-Z., Zhai, S.-R., Xiao, Z.-Y., Zhang, F. & An, Q.-D. 2015. Oxygen-containing/amino groups bifunctionalized SBA-15 toward efficient removal of methylene blue: kinetics, isotherm and mechanism analysis. *Journal of Sol-Gel Science and Technology,* 76**,** 320-331.

Qin, Q., Liu, K., Fu, D. & Gao, H. 2012. Effect of chlorine content of chlorophenols on their adsorption by mesoporous SBA-15. *Journal of Environmental Sciences,* 24**,** 1411-1417.

Qin, Q., Ma, J. & Liu, K. 2009. Adsorption of anionic dyes on ammonium-functionalized MCM-41. *Journal of Hazardous Materials,* 162**,** 133-139.

Qu, Q. & Gu, Z. 2014. Facile synthesis of hierarchical MCM-41 spheres with an ultrahigh surface area and their application for removal of methylene blue from aqueous solutions. *Analytical Methods,* 6**,** 1397-1403.

Rasalingam, S., Peng, R. & Koodali, R. T. 2014. Removal of hazardous pollutants from wastewaters: applications of TiO_2-SiO_2 mixed oxide materials. *Journal of Nanomaterials,* 2014**,** 10.

Reddy, M. S., Sivaramakrishna, L. & Reddy, A. V. 2012. The use of an agricultural waste material, Jujuba seeds for the removal of anionic dye (Congo red) from aqueous medium. *Journal of Hazardous Materials,* 203**,** 118-127.

Reddy, P. M. K., Mahammadunnisa, S., Ramaraju, B., Sreedhar, B. & Subrahmanyam, C. 2013. Low-cost adsorbents from bio-waste for the removal of dyes from aqueous solution. *Environmental Science and Pollution Research,* 20**,** 4111-4124.

Sakadevan, K. & Bavor, H. 1998. Phosphate adsorption characteristics of soils, slags and zeolite to be used as substrates in constructed wetland systems. *Water Research,* 32**,** 393-399.

Sánchez-Vicente, Y., Pando, C., Cortijo, M. & Cabañas, A. 2014. Chemical surface modification of mesoporous silica SBA-15 with a tertiary aminosilane using supercritical carbon dioxide. *Microporous and Mesoporous Materials,* 193**,** 145-153.

Sangchoom, W. & Mokaya, R. 2012. High temperature synthesis of exceptionally stable pure silica MCM-41 and stabilisation of calcined mesoporous silicas via refluxing in water. *Journal of Materials Chemistry,* 22**,** 18872-18878.

Sawicki, R. & Mercier, L. 2006. Evaluation of mesoporous cyclodextrin-silica nanocomposites for the removal of pesticides from aqueous media. *Environmental Science & Technology,* 40**,** 1978-1983.

Shahriary, L. & Athawale, A. A. 2014. Graphene oxide synthesized by using modified hummers approach. *IJREEE,* 2**,** 58-63.

Shao, Y., Wang, X., Kang, Y., Shu, Y., Sun, Q. & Li, L. 2014. Application of Mn/MCM-41 as an adsorbent to remove methyl blue from aqueous solution. *Journal of Colloid and Interface Science,* 429**,** 25-33.

Singh, V. K., Cura, M. E., Liu, X., Johansson, L. S., Ge, Y. & Hannula, S. P. 2014. Tuning the Mechanical and Adsorption Properties of Silica with Graphene Oxide. *ChemPlusChem,* 79**,** 1512-1522.

Sivasubramanian, G., Shanmugam, C. & Parameswaran, V. 2013. Copper (II) immobilized on silica extracted from foxtail millet husk: a heterogeneous catalyst for the oxidation of tertiary amines under ambient conditions. *Journal of Porous Materials,* 20**,** 417-430.

Sohn, S. & Kim, D. 2005. Modification of Langmuir isotherm in solution systems—definition and utilization of concentration dependent factor. *Chemosphere,* 58**,** 115-123.

Song, X., Zhang, Y. & Chang, C. 2012. Novel method for preparing activated carbons with high specific surface area from rice husk. *Industrial & Engineering Chemistry Research,* 51**,** 15075-15081.

Steel, A., Carr, S. W. & Anderson, M. W. 1994. 14 N NMR study of surfactant mesophases in the synthesis of mesoporous silicates. *Journal of the Chemical Society, Chemical Communications***,** 10, 1571-1572.

Sun, L. & Fugetsu, B. 2013. Massive production of graphene oxide from expanded graphite. *arXiv preprint arXiv:1301.3253*.

Thuc, C. N. H. & Thuc, H. H. 2013. Synthesis of silica nanoparticles from Vietnamese rice husk by sol–gel method. *Nanoscale Research Letters,* 8**,** 1-10.

Tian, H., Li, J., Shen, Q., Wang, H., Hao, Z., Zou, L. & Hu, Q. 2009. Using shell-tunable mesoporous Fe_3O_4@ HMS and magnetic separation to remove DDT from aqueous media. *Journal of Hazardous Materials,* 171**,** 459-464.

Vaibhav, V., Vijayalakshmi, U. & Roopan, S. M. 2015. Agricultural waste as a source for the production of silica nanoparticles. *Spectrochimica Acta Part A: Molecular and Biomolecular Spectroscopy,* 139**,** 515-520.

Vidal, C. B., Barros, A. L., Moura, C. P., De Lima, A. C., Dias, F. S., Vasconcellos, L. C., Fechine, P. B. & Nascimento, R. F. 2011. Adsorption of polycyclic aromatic hydrocarbons from aqueous solutions by modified periodic mesoporous organosilica. *Journal of Colloid and Interface Science,* 357**,** 466-473.

Wang, J., Chen, Z. & Chen, B. 2014. Adsorption of polycyclic aromatic hydrocarbons by graphene and graphene oxide nanosheets. *Environmental Science & Technology,* 48**,** 4817-4825.

Wang, S. & Li, H. 2006. Structure directed reversible adsorption of organic dye on mesoporous silica in aqueous solution. *Microporous and Mesoporous Materials,* 97**,** 21-26.

Wu, Z.-J. & Lee, K. 2004. Adsorption mechanisms of mesoporous adsorbents in solutions. *Chemical Research in Chinese Universities,* 20**,** 185-187.

Xiao, X., Zhang, F., Feng, Z., Deng, S. & Wang, Y. 2015. Adsorptive removal and kinetics of methylene blue from aqueous solution using NiO/MCM-41 composite. *Physica E: Low-dimensional Systems and Nanostructures,* 65**,** 4-12.

Yang, H., Coombs, N. & Ozin, G. A. 1997. Morphogenesis of shapes and surface patterns in mesoporous silica. *Nature,* 386**,** 692-695.

Yang, K., Chen, B. & Zhu, L. 2015. Graphene-coated materials using silica particles as a framework for highly efficient removal of aromatic pollutants in water. *Scientific Reports,* 5**,** 11641-11653.

Ying, J. Y., Benziger, J. B. & Navrotsky, A. 1993. Structural evolution of alkoxide silica gels to glass: effect of catalyst pH. *Journal of the American Ceramic Society,* 76**,** 2571-2582.

Youngran, J., Maohong, F., Van Leeuwen, J. & Belczyk, J. F. 2007. Effect of competing solutes on arsenic (V) adsorption using iron and aluminum oxides. *Journal of Environmental Sciences,* 19**,** 910-919.

Yu, B., Zhang, X., Xie, J., Wu, R., Liu, X., Li, H., Chen, F., Yang, H., Ming, Z. & Yang, S.-T. 2015. Magnetic graphene sponge for the removal of methylene blue. *Applied Surface Science,* 351**,** 765-771.

Zhang, C., Wu, L., Cai, D., Zhang, C., Wang, N., Zhang, J. & Wu, Z. 2013. Adsorption of polycyclic aromatic hydrocarbons (fluoranthene and anthracenemethanol) by functional graphene oxide and

removal by pH and temperature-sensitive coagulation. *ACS Applied Materials & Interfaces,* 5**,** 4783-4790.

Zhang, Y., Qiao, Z.-A., Li, Y., Liu, Y. & Huo, Q. 2011. Cooperative adsorbent based on mesoporous SiO_2 for organic pollutants in water. *Journal of Materials Chemistry,* 21**,** 17283-17289.

Zhao, D., Feng, J., Huo, Q., Melosh, N., Fredrickson, G. H., Chmelka, B. F. & Stucky, G. D. 1998. Triblock copolymer syntheses of mesoporous silica with periodic 50 to 300 angstrom pores. *Science,* 279**,** 548-552.

Zhu, X., Tsang, D. C., Chen, F., Li, S. & Yang, X. 2015. Ciprofloxacin adsorption on graphene and granular activated carbon: kinetics, isotherms, and effects of solution chemistry. *Environmental Technology***,** 36, 1-9.

3.0 CHAPTER 3: MATERIALS, METHODS AND INSTRUMENTATION

3.1 Reagents

Tetraethylorthosilicate (TEOS) 98% (Aldrich), cetyltrimethylammonium bromide (CTAB) 99+% (Calbiochem), ammonium hydroxide 25% (BDH chemicals), absolute ethanol (Merck), HPLC grade methanol (Sigma Aldrich), methylene blue and methyl red (Sigma Aldrich), HCl 37%, H_3PO_4 80% (Sigma Aldrich), H_2SO_4 (Promark) 98%, H_2O_2 (Promark) 60%, 3-aminopropyltriethoxysilane (APTES) 99% (Sigma Aldrich) and citric acid (CA) monohydrate (Thomas Baker), acetaminophen, aspirin, phenacetin, caffeine, sulfamethoxazole (R and D grade) from (Sigma Aldrich), hydrazine monohydrate 80% (Sigma Aldrich) and natural graphite powder obtained from Sigma Aldrich were used in the experimental work.

Double-distilled water was used in the preparation of reagent solutions and solutions for dye adsorption studies. Mobile phase, stock and standard solution used for HPLC analysis of pharmaceuticals were prepared with ultrapure water from a Milli-Q system (Millipore, 18.2 MΩ.cm).

3.2 Water Samples

Water samples were obtained from the Blue Lagoon (BLG) (mouth of the Umgeni River into the Indian Ocean) with co-ordinates of 29° 48’ 41” S and 31° 02’ 12” E, and the Northern Wastewater Treatment plant (WWTP) with co-ordinates of 29° 48’ 27” S and 30° 59’ 51” E in Durban, South Africa. The samples were stored at 4 °C prior to analysis. The samples obtained were only filtered using a 0.45 µm just before analysis in order to imitate environmentally relevant conditions. The average physical parameters of these samples are presented in (Table 3.1).

Table 3.1 Physical properties of water samples

Parameter	WWTP	BLG
pH	4.94	3.39
TDS (mg/L)	670	3100.2
Conductivity (µS)	1000.12	5200.3
Res (Ω)	729	150.67
Redox (mV)	93.5	181.3
Temp (°C)	22.0	22.5

3.3 Synthesis of Adsorbents

In this study, six different adsorbent materials were synthesized, with each requiring a different synthesis technique. The adsorbents were either made up entirely of silica or were silica-carbon based composites. The synthesis procedure for all adsorbents required firstly, the synthesis of a siliceous framework and the loading of a carbon based modifier on it.

3.3.1 Synthesis of silica nanotubes (SNT) and nanoparticles (SNP) from elephant grass

Elephant grass (*Pennisetum Purpureum*) was acid washed and calcined. The ash was stirred with 1 M NaOH. SNT and SNP were obtained by the addition of 55% and 2% of CTAB, respectively, to the ash-silicate solution, thus yielding structures with different morphologies. The materials were characterized by different techniques which include fourier transform infrared spectroscopy (FTIR), thermogravimetric (TGA), scanning electron microscope (SEM), transmission electron microscope (TEM), high resolution transmission electron microscope (HRTEM), x-ray diffraction (XRD), x-ray fluorescence (XRF), as well as textural and surface area analysis. Detailed experimental are provided in chapter 4. The SNT and SNP were applied in the adsorption of methylene blue and methyl red from an aqueous solution.

3.3.2 Synthesis of MCM-41 and citric acid grafted MCM-41 from millet straw

Millet straw was subjected to a similar pretreatment step to SNT and SNP (section 3.3.1). Millet silica ash, obtained after calcining at 600 °C, was dispersed in 1 M NaOH. CTAB dissolved in double distilled water was added to the mixture while stirring and the pH was adjusted to 11 with acetic acid. The gel obtained was heated in a polypropylene bottle for 3 days and calcined at 550 °C to remove the organic template. The MCM-41 obtained was activated by stirring with 6 M HCl for 4 hrs. Furthermore, the activated MCM-41 was coated with (APTES), using ethanol as a medium. The product was dried in an oven and introduced into a 0.6 M citric acid solution. Carboxylic acid was grafted on it, giving it a –COOH functionality. Details of the experimental are provided in chapters 6 and 7. The adsorbents were characterized and applied in the adsorption of MB.

3.3.3 Synthesis of MCM-41 (from TEOS) and CA grafting on synthesised MCM-41

Briefly, CTAB was dissolved in water, and NH_4OH and ethanol added to it with stirring. After a while, TEOS was added to the mixture and left to stir for a further 4 hrs. The product was filtered and calcined at an elevated temperature to remove the CTAB template. The MCM-41 obtained was activated by stirring with 6 M HCl for 4 hrs. Furthermore, the activated MCM-41 was coated with (APTES), using ethanol as a medium. The product was dried in an oven and 0.6 M citric acid in solution was grafted on it with stirring to give it a –COOH functionality. The concentration of citric acid used varied from 0.6 – 1.4 M. The details of the experimental are provided in chapter 7. The adsorbents were characterized and applied in the adsorption of MB.

3.3.4 Synthesis of MCM-41 encapsulated with graphene oxide and MCM-41 encapsulated with graphene

Graphene oxide was firstly synthesized by a modified Tours method (Marcano et al., 2010). A 9:1 mixture of H_2SO_4/H_3PO_4 was added to graphite powder and $KMnO_4$ mixed mechanically. It was stirred for 12 hrs and ice was poured into it with a little H_2O_2 to stop the reaction. The product was sieved to remove the graphite powder that was not oxidized, the filtrate was centrifuged

and the supernatant decanted. The remaining solid was washed with water, HCl and ethanol (twice) and filtered through a 0.45 µm filter. The solid product was transferred to a dialysis tube and kept there for a month to discharge acid, with the water in the dialysis tube holder constantly changed. The brown solid graphene oxide was finally dried under vacuum.

Already activated APTES coated MCM-41 was firstly synthesized (section 3.3.3) and sonicated/dispersed in water. Sonicated GO was added to the suspension, the pH was brought to 7 by the addition of NH_4OH and the solution was stirred for a while and then left to settle. The final product was filtered with water and dried in a vacuum oven at 50 °C for 6 hrs to give MCM-41 encapsulated with GO. In the synthesis of MCM-41 encapsulated with graphene, the steps were similar to MCM-41 encapsulated with GO, but the temperature for synthesis was 80 °C and hydrazine hydrate was added to the mixture to reduce GO to G. The mixture was stirred for 12 hrs, left to settle for 2 hrs, washed with water and dried under vacuum. The black solid product was dried in a vacuum oven at 80 °C for 6 hrs. The adsorbents were characterized and applied in the adsorption of acetaminophen and aspirin. The details of the experimental are provided in chapter 8.

3.3.5 Synthesis of MCM-48 coated graphene oxide and MCM-48 coated graphene

Graphene oxide was firstly synthesized by a modified Tours method as described in section 3.3.4 (Marcano et al., 2010). MCM-48 was synthesized using a modified procedure by Peng et al. (2011). The MCM-48 was activated and coated with APTES (section 3.3.4). Already activated APTES coated MCM-48 was sonicated/dispersed in water. Sonicated GO was added to the suspension and the pH was brought to 7 using NH_4OH. It was stirred for a while and left to settle. The final product was filtered with water and oven dried in a vacuum at 50 °C for 6 hrs and this was denoted as MCM-41 encapsulated with GO. . In the synthesis of MCM-41 encapsulated with G, the steps were similar to MCM-48 encapsulated with GO, but the temperature for synthesis was 80 °C and hydrazine hydrate was added to the mixture to reduce the graphene oxide to graphene. The mixture was stirred for 12 hrs, left to settle for 2 hrs, then washed with water and dried under vacuum. It was then oven dried at 80 °C for 6 hrs. The adsorbents were characterized

and applied in the adsorption of caffeine and phenacetin. Detailed experimental are provided in chapter 9.

3.3.6 Synthesis of silica nanotubes encapsulated with graphene oxide and graphene

Already synthesized SNT (section 3.3.1) was activated with acid and coated with APTES. It was sonicated in water for an hour. The synthesis was similar to that described in sections 3.3.4 and 3.3.5, but MCM-41 and MCM-48 was replaced with SNT. The adsorbents were characterized and applied in the adsorption of sulfamethoxazole.

3.4 Analysis of Pharmaceuticals by HPLC with a UV Detector

3.4.1 Preparation of calibration standards for quantification of specific analytes

The stability of all analytes and matrix effects with respect to analyte detection was determined before adsorption experiments were carried out. Calibration curves were prepared for each analyte for each experiment. The analytes were run individually and the retention times were noted before they were run in a binary system. All standard solutions were stored at 4 °C and the vials containing the samples and standards for HPLC analysis were wrapped in aluminium foil to minimize degradation. Quantification was carried out using external standards with at least 6 data points. Blank samples were also analysed to account for errors that may occur.

A stock solution of 1000 mg/L was prepared by weighing 25 mg of each analyte into a 250 mL volumetric flask and dissolved in 1% methanol and 99% water, except for sulfamethoxazole where 40% methanol and 60% water was used. The choice of solvent was based on minimizing co-solvent effects. Standard solutions of caffeine and phenatecin were prepared in a binary system, aspirin and acetaminophen were prepared in a binary system, and sulfamethoxazole was prepared singularly to determine the efficiency of the adsorbents. The binary systems were based on the properties of the drugs, that is, one being neutral and the other acidic to show that the adsorbent could function over a wide pH range. Working solutions were prepared by serial dilution with Milli-Q water to obtain the required range of standards (0.1 - 100 mg/L).

3.4.2 HPLC-UV method

3.4.2.1 HPLC method for analysis of caffeine and phenacetin mixture

A high pressure liquid chromatography (HPLC) system consisting of an Agilent 1200 SL (Agilent Technology, USA) with a pressure gradient pump equipped with a UV-Vis detector was used in the separation of caffeine and phenacetin. This was carried out at room temperature (25 °C) using an Agilent Eclipse XDB-C18 4.6 x 150 mm analytical column (5 µm particle size) at a flow rate of 0.6 mL/min. Resolution of peaks and sensitivity were key factors in the determination of wavelength selection. Wavelengths of 210 nm and 254 nm, which were the λ-max for caffeine and phenacetin, respectively were chosen. The injection volume was 5 µL and a combination of 60/40 (v/v) MeOH/H_2O adjusted to a pH of 2.3 with 0.01 M H_3PO_4 was used as the mobile phase. Figures 3.1 and 3.2 are the chromatograms that were obtained for the standards at the 2 wavelengths. Figures 3.3 (a) and (b) are the calibration curves with R^2 values of 0.9999 and 0.9996 for caffeine and phenacetin, respectively.

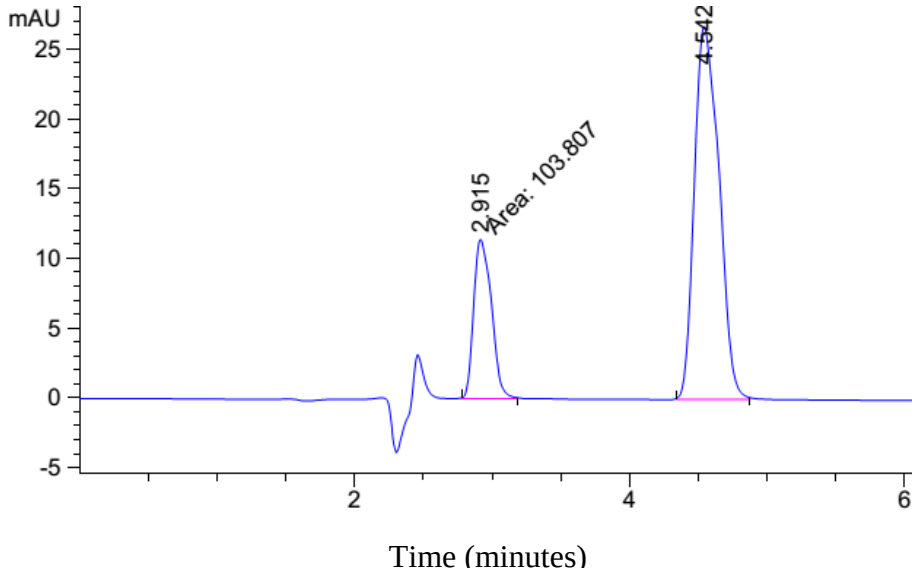

Figure 3.1 HPLC chromatogram of caffeine and phenacetin mixture with 60/40 (v/v) MeOH/H_2O at pH 2.3 (5 µL; λ = 210 nm, column: Agilent Eclipse XDB-C18 4.6 x 150 mm, 5 µm)

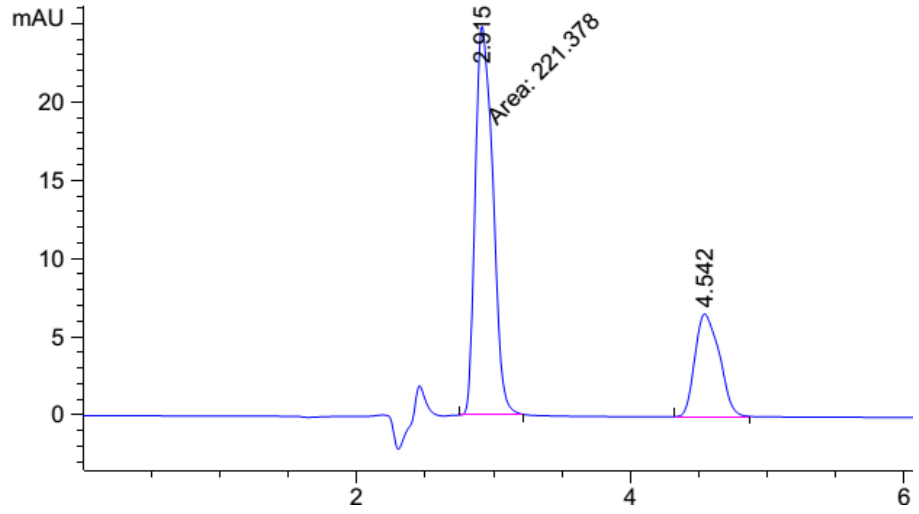

Figure 3.2 HPLC chromatogram of caffeine and phenacetin mixture with 60/40 (v/v) MeOH/H_2O at pH 2.3 (5 µL; λ = 254 nm, column: Agilent Eclipse XDB-C18 4.6 x 150 mm, 5 µm)

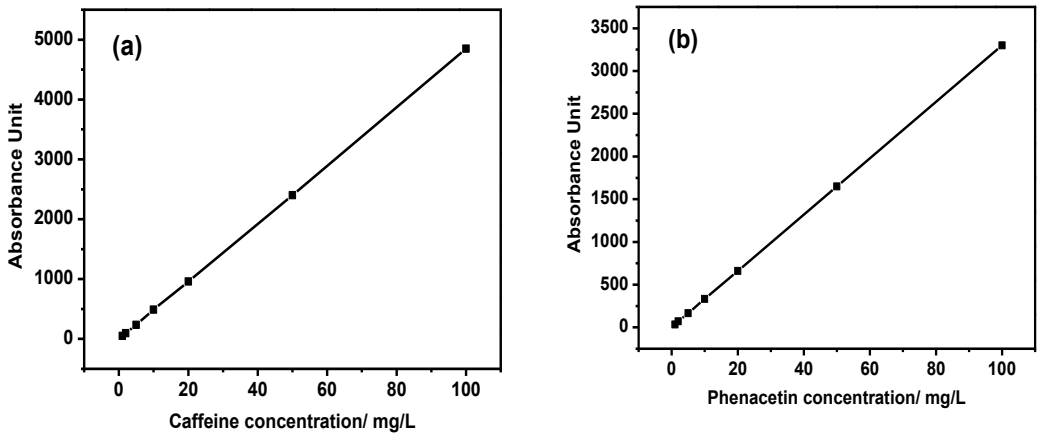

Figures 3.3 Calibration curves of (a) caffeine (λ = 210 nm) and and (b) phenacetin (λ = 254 nm) in a 1:1 mixture (caffeine: phenacetin)

3.4.3.2 HPLC method for analysis of acetaminophen and aspirin mixture

The same instrument and conditions as described in section 3.4.3.1. was used for the analysis of aceteaminophen and aspirin. Wavelengths of 254 nm and 210 nm, were the λ max for aspirin and

acetaminophen, respectively. These wavelengths were chosen due to sensitivity for both analytes. A combination of 60/40 (v/v) MeOH/H_2O adjusted to a pH of 2.3 with 0.01 M H_3PO_4 with an injection volume of 5 µL was used as the mobile phase. The method for acetaminophen and aspirin was isocratic and it was preferred because of its simplicity and good separation.

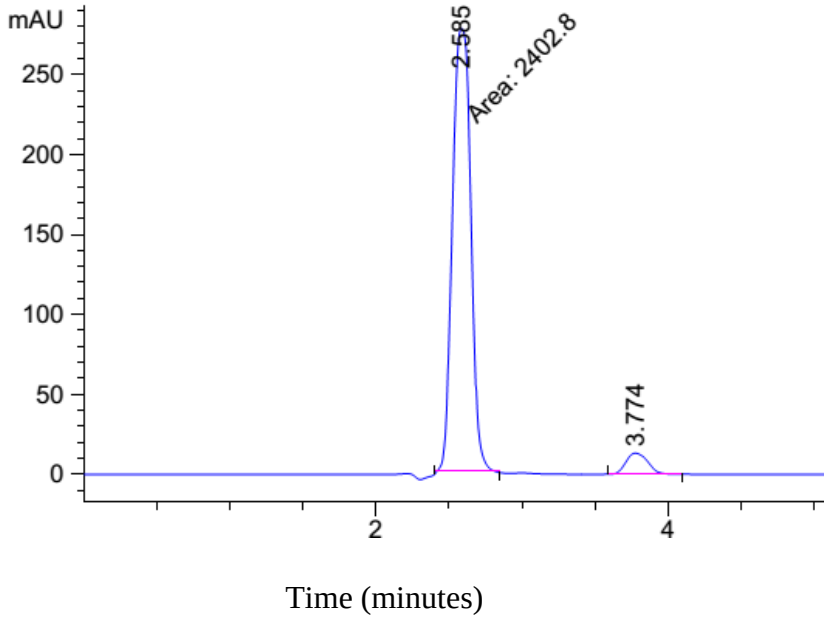

Figure 3.4 HPLC chromatogram of acetaminophen and aspirin mixture with 60/40 (v/v) MeOH/H_2O at pH 2.3 (5 µL; λ = 210 nm, column: Agilent Eclipse XDB-C18 4.6 x 150 mm, 5 µm)

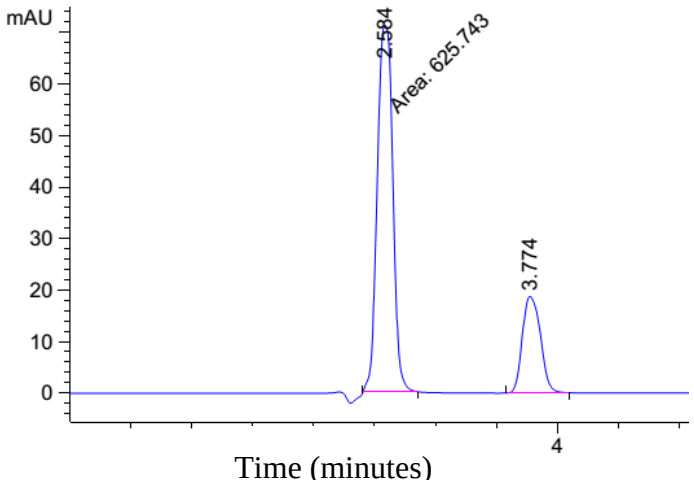

Figure 3.5 HPLC chromatogram of acetaminophen and aspirin mixture with 60/40 (v/v) MeOH/H_2O at pH 2.3 (5 µL; λ = 254 nm, column: Agilent Eclipse XDB-C18 4.6 x 150 mm, 5 µm)

The acetaminophen and aspirin peaks eluted at t_R 2.58 min and 3.79 min (Figs 3.4 and 3.5), respectively. The calibration curve was between 2-100 mg/L. The calculated correlation coefficient was $R^2 > 0.9996$ and $R^2 > 0.9991$ for acetaminophen and aspirin, respectively (Figures 3.6a and 3.6b)

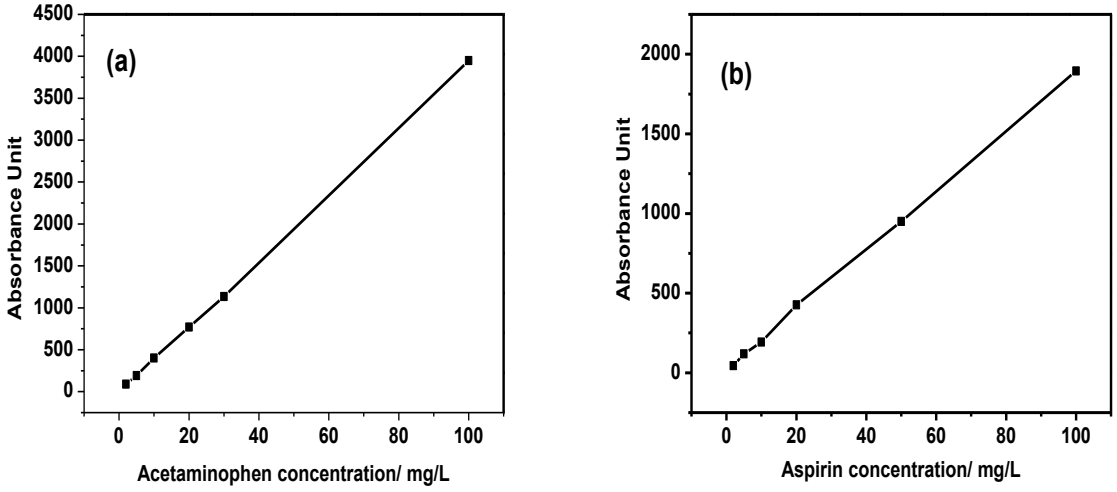

Figures 3.6 Calibration curves of (a) acetaminophen (λ = 210 nm) and and (b) aspirin (λ = 254 nm) in a 1:1 mixture (acetaminophen: aspirin)

3.4.3.3 HPLC method for sulfamethoxazole determination

The same instrument and instrument conditions that was used for the analysis of the previously described pharmaceuticals were used for the analysis of sulfmethoxazole. A wavelength of 270 nm was selected as the λ-max for sulfamethoxazole. This wavelength was chosen due to sensitivity of the analyte at this wavelength resulting in an intense peak. A combination of 60/40 (v/v) MeOH/H_2O adjusted to a pH of 2.3 with 0.01 M H_3PO_4 with an injection volume of 5 µL was chosen as the mobile phase. The sulfamethoxazole peak eluted at t_R 2.82 min (Fig 3.7). The range of the calibration curve was between 2-100 mg/L and the calculated correlation coefficient was $R^2 > 0.9999$ (Fig 3.8).

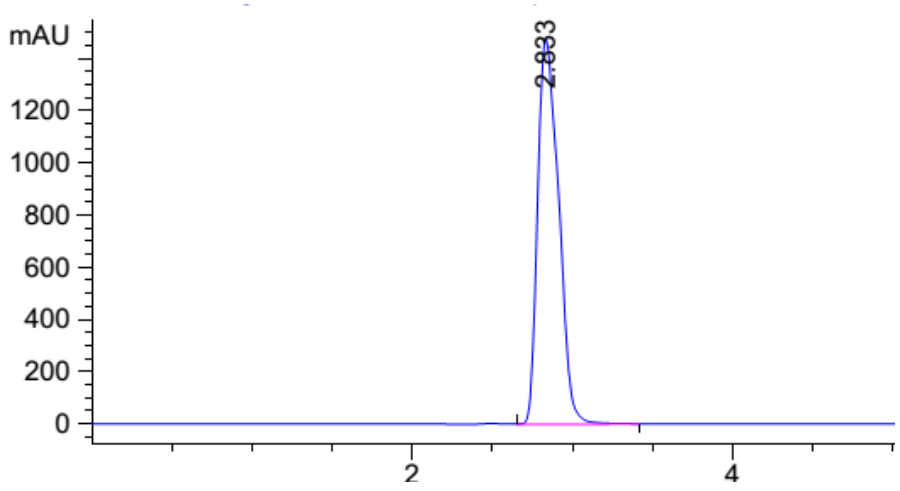

Figure 3.7 HPLC chromatogram of sulfamethoxazole with 60/40 (v/v) MeOH/H_2O at pH 2.3 (5 µL; λ = 270 nm, column: Agilent Eclipse XDB-C18 4.6 x 150 mm, 5 µm)

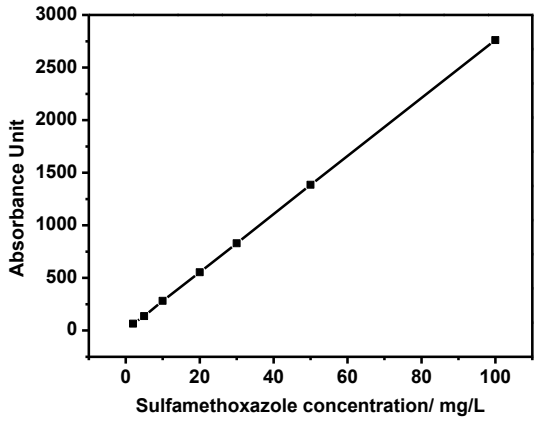

Figure 3.8 Calibration curve of sulfamethoxazole (λ = 270 nm)

3.5 UV Analysis for the Determination of Dyes

Methylene blue and methyl red were selected for adsorption studies. The adsorbances of the dyes were determined by a UV-3600-Shimadzu UV-VIS spectrophotometer at a wavelength of 663 nm and 540 nm, respectively. Three stock solutions, of each binary and the individual analyte, having concentrations of 1000 mg/L each were prepared by weighing 25 mg of each analyte into three 250 mL volumetric flasks and dissolved in double distilled water. Working solutions were prepared by serial dilution with water to prepare the required range of standards. Calibration curves (Figures 3.9 (a) and (b)) were prepared for each of the dyes with at least 6 data points and blank samples were also analysed. All standards were stored in vials at 4 °C which were wrapped in aluminium foil to prevent photo degradation. The obtained R^2 values were 0.9977 and 0.9942 for MB and MR, respectively.

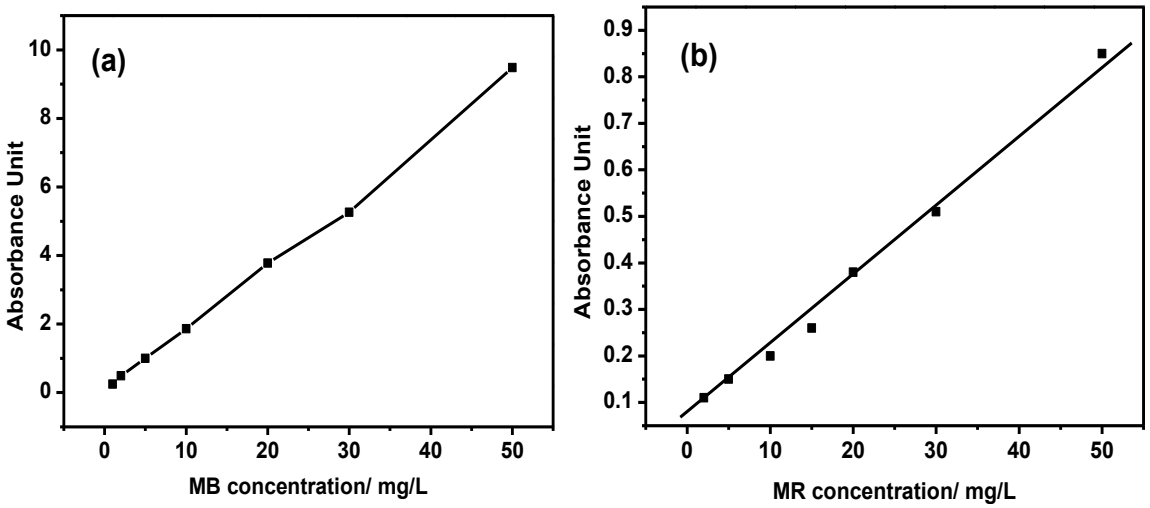

Figures 3.9 (a) Calibration curves for MB and and (b) MR

3.6 Sorption Studies

3.6.1 General procedure used in adsorption studies

For adsorption studies, a specific amount of adsorbent was placed in the adsorbate solution in a borosilicate glass flask, sealed and shaken at 150 rpm in the dark at 25 °C. Stock solutions (1000 mg/L) of dyes and pharmaceuticals were prepared by dissolving the appropriate amount of each analyte in Milli-Q and double distilled water and ultrasonicated for a period of time. The pH of the solution was monitored and adjusted with a pH meter between a range of 2-10. The studies were carried out in duplicate and blanks as control samples were also analysed using the same method.

For adsorption kinetic studies, approximately 1.5 mL of the samples were collected (adsorbent free) at regular intervals with a syringe. For the pharmaceuticals, the drawn solution was filtered through a 0.45 µm nylon syringe filter (Simplepure) to remove any adsorbent before analysis. Filtered samples (dyes and pharmaceuticals) were analysed using a UV-spectrophotometer and HPLC, respectively.

The quantity adsorbed, q (mg/g) denotes the substrate adsorbed and is calculated from the difference in adsorbate concentration (aqueous phase) before and after adsorption from the following equation:

$$q = \frac{V(C_i - C_f)}{W} \quad (3.1)$$

Where W is the mass of the adsorbent (g), q is quantity adsorbed (mg/g), V is the volume the adsorbate solution (L), Ci and C_f are the initial and final concentrations of the adsorbate solution before and after adsorption in mg/L, respectively.

3.6.2 Effect of initial pH

The details of the method are described in chapters 4-9. Briefly, all solutions of dyes and pharmaceuticals were adjusted with 0.1 M HCl and 0.1 NaOH solutions to a pH range 2–10. The acid/base solutions were added dropwise until the desired pH was achieved and measured with a pH meter (Hanna pH 211 microprocessor). When the required pH was reached, the adsorbent was added to the adsorbate solutions.

3.6.3 Effect of temperature

The effect of temperature on adsorption of dyes and pharmaceutical was determined. The details of the method are described in chapters 4-9. A certain mass of adsorbent was placed in an adsorbate solution and was agitated in a thermostatic shaker at varying temperatures of 25, 35 and 45 °C for a period of time. The solution was filtered and the concentration of the filtrate was determined with HPLC or a UV-Vis spectrophotometer. The data obtained was used in the determination of thermodynamic parameters such as Gibbs free energy ($\Delta G°$), change in enthalpy ($\Delta H°$) and change in entropy ($\Delta S°$).

3.6.4 The model used for adsorption analysis

3.6.4.1 Intraparticle diffusion model

The intraparticle diffusion model is expressed by the equation below:

$$Q_t = K_i\, t^{0.5} + C \qquad (3.2)$$

Where Q_t is the amount adsorbed (mg/g), K_i is the intraparticle rate diffusion constant (mg/g min-$^{0.5}$), t is time in min and C is the intercept depicting intra-boundary layer effect.

3.6.5 Models used in isotherm studies

3.6.5.1 Langmuir model

The Langmuir model can be expressed as:

$$\frac{C_e}{q_e} = \frac{1}{bQ_m} + \frac{C_e}{Q_m} \qquad (3.3)$$

Where q_e is the adsorption capacity (mg/g), Q_{m} is the maximum amount of adsorbate per unit weight of the adsorbent (mg/g), b is the Langmuir constant related to the free energy of adsorption (L/mg) and C_e is the equilibrium concentration (mg/L).

3.6.5.2 Freundlich model

This Freundlich model is expressed as:

$$ln\, q_e = ln\, K_F + \left(\frac{1}{n}\right) ln\, C_e \qquad (3.4)$$

Where q_e is the adsorption capacity (mg/g), C_e is the equilibrium concentration (mg/L), K_F and n are Freundlich constants related to adsorption capacity and *1/n* is the adsorption intensity of the adsorbent.

3.6.5.3 Temkin model

The Temkin model is expressed as:

$$ln\, q_e = B\, ln\, A + B\, ln\, C_e \quad (3.5)$$

Where q_e is the adsorption capacity (mg/g), C_e is the equilibrium concentration (mg/L), $B = RT/b$, B is the Temkin energy constant (J mol^{-1}), R is the universal gas constant (J mol^{-1} K^{-1}), T is the absolute temperature (K), b is the variation in adsorption energy (J mol^{-1}) and A is the equilibrium binding constant (L/mg) which corresponds to the maximum binding energy. B and A are calculated from the slope (B) and intercept (B ln A) of the plot q_e *vs* ln C_e.

3.6.5.4 Dubinin-Radushkevich isotherm (D-R)

The D-R isotherm is applied to determine if the adsorption mechanism with a Gaussian energy distribution is on a heterogeneous surface

$$\ln q_e = ln\, q_{max} - \beta\varepsilon^2 \quad (3.6)$$

Where ε is the D-R isotherm constant, β is D-R isotherm constant (mol^2/kj^2) and q_e is the amount of adsorbate at equilibrium (mg/g). The D-R model is used to determine if adsorption is chemical or physical. The slope is β, and intercept of ln q_{max} gives information about mean free energy E (kJ/mol/L) of adsorption per molecule of adsorbate and can be calculated using equation (3.7 below):

$$\varepsilon = RT\, ln(1 + \frac{1}{C_e}) \quad (3.7)$$

Where C_e is the adsorbate equilibrium constant (mg/L), *T* is absolute temperature (K), *R* is the gas constant (8.314 J/mol K). The adsorption data at various points are plotted as ln q_e *vs* ε^2 .

$$E = \frac{1}{\sqrt{-2\beta}} \tag{3.8}$$

3.7 Characterisation of Adsorbents

3.7.1 Field emission scanning electron microscopy (FESEM)

In FESEM (Zeiss 10 kV field), a narrow probing beam at low and high electron energy are provided by a field emission cathode in the electron gun of a scanning electron microscope, thus, resulting in improved spatial resolution and minimized sample charging and destruction. The samples were placed on a copper stub and gold coated to minimize charging and to obtain clearer images. Energy dispersive x-ray (EDX) images were obtained which gave quantitative elemental information about the samples. The image analyses of samples were carried out to determine the structural morphology of samples.

3.7.2 Transmission electron microscopy (TEM) and high resolution transmission electron microscopy (HRTEM)

In TEM (JEOL TEM) analysis of samples, electron beams in the electron microscope are used to illuminate the sample, thereby creating an image. The images are of very high resolution because the wavelengths of electrons are 100000 times shorter than that of visible light. The samples were placed in absolute ethanol and sonicated for 10 mins and placed on a copper grid. Samples were left to dry under a beam of light and dipped in chloroform before introduction into the HRTEM instrument. This image analysis of the samples was carried out to determine structural morphology of the samples.

3.7.3 X-ray diffraction

X-ray diffraction analyses of the samples were carried out to determine the phase and the crystallinity of the materials. In x-ray analysis, an atom produces a beam of incident x-rays to diffract into specific directions. The angles and the intensities of this beam are measured, and based on its intensity a crystal phase is formed or not. The samples analysed were placed on a borosilicate glass stub and exposed to x-rays from a Cu-Kα radiation source (Bruker D6). The diffraction angle (2-theta) was set in the range of 0.4-2 and 10-80 nm for low angle and full scan, respectively.

3.7.4 Fourier transform infrared spectroscopy

FTIR spectra were obtained with Perkin Elmer Series 100 spectrum. This was done to determine the functional groups present in all synthesized materials. Here molecules absorb light in the infrared region of the electromagnetic spectrum. The absorbed light corresponds to the organic functional group(s)/bond present in the molecules. The frequency range typically measured for samples are between wave numbers 4000 cm^{-1} - 400 cm^{-1}. The sample and the background emit characteristic emissions and the ratio of the sample spectrum to background spectrum is directly related to the sample absorption spectrum. About 2 mg of samples were placed in the (attenuated total reflection) ATR crystal sample holder and before inserting into the instrument.

3.7.5 X-ray fluorescence (XRF)

In this technique, the sample is irradiated with x-rays within the instrument. When an x-ray photon gets absorbed by adequate amounts of energy, this causes an electron to be emitted through photoelectric phenomenon causing an electron hole in the atom. Hence, an inner shell goes into the hole thereby discharging electromagnetic energy with a frequency characteristic of elements present in the sample. This is typically used in quantitative analysis of samples. The x-ray source was Cu-Kα. Here the sample was made into a compacted bead on a borosilicate glass before being examined on the XRF (PAnalytical Axios Max) instrument.

3.7.6 UV-Visible spectrophotometer

Dye samples for adsorption were quantitatively determined using a UV-Visible spectrophotometer (UV-3600-Shimadzu UV-VIS-NIR). This is because dyes contain species that absorb light in the visible and UV region of the electromagnetic spectrum. The absorption is brought about by a difference in electron energy levels in the molecules which is characteristic of the molecular structure.

3.7.7 High performance liquid chromatography (HPLC)

An Agilent 1200 connected to a UV detector was used in adsorption studies involving pharmaceuticals. It was used both in qualitative and quantitative determination of pharmaceuticals. This technique utilizes chemical interactions of the analyte between a mobile and a stationary phase. Analytes of differing polarity interact more with one phase than the other which allows selective separation of a mixture of analytes. Other important parameters in HPLC are the column and detector. In this study, the mobile phase used was methanol and water in a 60:40 ratio, respectively which gave good elution times and properly resolved peaks.

3.7.8 Thermal gravimetric analysis (TGA)

This technique uses heat and stoichiometric ratio to determine percentage mass of a substance. A sample is analysed by increasing temperature gradually in a program whilst plotting the reduction of the mass of the sample. The sample can be seen to degrade across the thermal profile/plot of the sample. The increase in sample temperature can either be done in air or in an inert environment. The samples in this study were heated in air and N_2 up to a temperature of 900 °C at a ramp rate of 5 °C /min using TGA SDT Q 600 V 209 Build 20.

3.7.9 Brunauer, Emmet and Teller (BET) analysis

BET analysis (Micromeritics 3000) on the samples was carried out to determine their specific surface areas and textural characteristics. The specific surface area of a powder is often deter-

mined by physical adsorption of a gas on the surface of a solid and also by calculating the amount of adsorbate gas corresponding to the monomolecular layer on the surface. Determination of surface and textural properties is usually carried out at the temperature of liquid nitrogen. The corresponding amount of N_2 gas adsorbed is measured by volumetric continuous flow procedure. In this study, samples were firstly degassed with nitrogen gas at a temperature of 90 °C for 1 hr and 200 °C for 12 hrs.

References

Marcano, D. C., Kosynkin, D. V., Berlin, J. M., Sinitskii, A., Sun, Z., Slesarev, A., Alemany, L. B., Lu, W. & Tour, J. M. 2010. Improved synthesis of graphene oxide. *ACS Nano,* 4**,** 4806-4814.

Peng, R., Zhao, D., Dimitrijevic, N. M., Rajh, T. & Koodali, R. T. 2011. Room temperature synthesis of Ti–MCM-48 and Ti–MCM-41 mesoporous materials and their performance on photocatalytic splitting of water. *The Journal of Physical Chemistry C,* 116**,** 1605-1613.

4.0 CHAPTER 4: EFFECT OF SYNTHESIS CONDITIONS ON THE MORPHOLOGY OF MESOPOROUS SILICA FROM ELEPHANT GRASS AND ITS APPLICATION IN THE ADSORPTION OF DYES

Samson O. Akpotu and Brenda Moodley*

School of Chemistry and Physics, University of KwaZulu-Natal, Westville Campus, Durban, 4000, South Africa.

***** corresponding author email: moodleyb3@ukzn.ac.za

Telephone: +27 31 2602796

Fax: +27 31 2603091

4.1 Abstract

In this study, different types of mesoporous silica (MS) were synthesised from elephant grass *via* the *sol-gel* technique, with varying synthesis conditions. This low cost, locally available, highly efficient adsorbent was applied in the adsorption of dyes. Characterisation of the adsorbent was carried out using scanning electron microscopy (SEM), high resolution transmission electron microscopy (HRTEM), x-ray fluorescence analysis (XRF), x-ray diffraction analysis (XRD), textural analysis, thermo-gravimetric analysis (TGA), and fourier transform infrared analysis (FTIR). The effect of surfactant concentration and temperature on the morphology of MS was also investigated, yielding silica nanotubes (SNT) and silica nanoparticles (SNP). Methylene blue (MB) and methyl red (MR) adsorption studies were carried out on SNT and SNP, varying parameters such as initial dye concentration, pH, adsorbent dose, contact time and temperature. Adsorption was affected by the molecular structure of the dyes and also the pores of mesoporous silica. Langmuir, Freundlich, intraparticle diffusion and Temkin models were used in analyzing equilibrium data. The adsorption of MB and MR on SNT were 40.6 mg/g and 109.97 mg/g, respectively. For SNP, MB and MR adsorption was 40.98 mg/g and 104.85 mg/g, respectively. The adsorption of MB and MR increased with an increase in pH with pH 10 being the optimal. The adsorption capacity of MB and MR for SNP and SNT were kinetically favoured and the adsorption data best fitted to pseudo-second-order and three stage intraparticle diffusion models.

Thermodynamic parameters were also evaluated for MB and MR adsorption onto SNP and SNT, and were found to be spontaneous and exothermic. The results are indicative that SNP and SNT could be considered as effective adsorbents for the removal of dyes from wastewater.

***Keywords**: Mesoporous silica, SNP, SNT, adsorption, methyl red, methylene blue*

4.2 Introduction

Amorphous and crystalline silica is found in 75% of the earth's crust and has been used to remediate organic and inorganic pollutants from aqueous solutions. Silica has been as bed filters in potable water treatment plants in the remediation of pollutants (Rasalingham et al., 2014**).** Amorphous silica has been produced from agricultural waste such as rice and millet husks *via* the sol-gel technique (Adam et al., 2013, Jaroenworaluck et al., 2012, Thuc and Thuc, 2013, Sivasubramanian et al., 2013). Grasses also have high silica content ranging between 1-13%, before combustion to ash (Matthews-Amune and Kakulu, 2012). Elephant grass (*Pennisetum purpureum*) presents an alternate economic source of silica (silica composition of elephant grass is between 5.5 – 6.1% producing good quality silica), because it contains abundant phytolith (microscopic units of silica) as reported by Sivasubramanian et al., (2013) for millet straw which is in the same family as elephant grass). Elephant grass grows rapidly as a weed (with no known uses) and clearing up to 4-6 times a year produces 50-150 tonnes green matter per hectare (Matthews-Amune and Kakulu, 2012).

Silica is a polymer of silicic acid with crosslinked SiO_4 in a tetrahedral shape, having a SiO_2 stoichiometry. Crystalline silica occurs naturally in contrast to synthesised amorphous silica (Thuc and Thuc, 2013). Silica-gel is a porous granular form of silica, synthetically manufactured from silicon tetrachloride, substituted chlorosilane/orthosilicate or sodium silicate solution. Mesoporous silica are synthesized through various techniquess; *sol-gel*, peptisation, precipitation and flame synthesis (Jal et al., 2004).

Mesostructural surfactant-silica nanocomposites are assumed to spontaneously assemble *via* self interaction of a pair of inorganic and organic components. In the formation of mesoporous silica

(silica with pore size between 2 -50 nm), thermodyammics of the surfactant silica assembly, and the shapes of the constituent materials are strongly reliant on the kinetics of sol-gel chemistry. *Sol-gel* technique can result in the formation of nano-sized mesoporous silica with desirable physical properties if the rate of condensation and self assembly are monitored carefully (Wu et al., 2013).

Therefore, *sol-gel* represents a versatile method of synthesis, involving hydrolysis of sodium silicate or alkoxysilane in the presence of acid or base. This produces $Si(OH)_4$ units and on controlled condensation, results in simultaneous solution hydrolysis and condensation. In acidic medium, hydrolysis is faster than condensation leading to an increasing number of siloxane linkages around the central silica atom. In contrast, in basic medium, condensation accelerates relative to hydrolysis and more siloxane linkages are formed. This causes a highly branched network extending through the entire volume and so the sol thickens to gel (Jal et al., 2004). Ultrafine silica powder, due to its small-diameter particles, large surface and extensive –OH network, is utilized in technological applications, such as thermal insulators, composite fillers, electronics, ceramics, pharmaceuticals, detergents, adhesives and polymer materials (Ghorbani et al., 2013). Its functionality is further improved at the nano scale (Thuc and Thuc, 2013).

These improved nanometric functionalities make MSi suitable as an adsorbent for different classes of pollutants due to its large specific surface area and extensive –OH network. Adsorption by silica is a surface phenomenon due to ion hydrogen bonding and the silanol group on the surface. The PZC of silica is between 2-3 and p*K*a of silica is 1.5, (Qu and Gu, 2014) therefore at a pH less than its PZC, the surface is positively charged due to the formation of $SiOH^{2+}$ and at pH above PZC the silica surface is negatively charged. As neutral pH is reached, the silanol sites react with the cations in solution, increasing its adsorptive property. These properties make MSi suitable for sorption of cationic dyes because in solution at pH above 2, the surface charge of silica is negative making it possible to electrostatically attract cationic dyes, as well as physically trap the dye molecules in its pores.

Dyes are pigments with widespread industrial use and are often discharged indiscriminately in water systems causing reduction of light penetration in aqueous environments, depletion of oxy-

gen in water bodies, dispersion in the atmosphere as aerosols and non-degradability (Leme et al., 2015). They can also be harmful to organisms if ingested, as some dyes are known carcinogenic agents. Methylene blue has been used in medicine as an antimalaria agent, in treatment of Alzheimer disease, cardiac surgery and cancer treatment (Ginimuge and Jyothi, 2010). (MB) (Figure 4.1(a)). MB has been implicated as one of the most notorious and broadly used dyes and has caused various illnesses in humans such as damaged nervous systems, heart defects, urinary tract infection (Vutskits et al., 2008). Methyl red (MR) (Figure 4.1(b)) is a cationic dye and causes allergies, cancer, skin irritation and dermatitis (Vidhyadevi et al., 2014). Hence, there is a need for an efficient and cheap method of remediating textile polluted wastewater *via* adsorption with adsorbents produced from agricultural by-products such as elephant grass (Yagub et al., 2014).

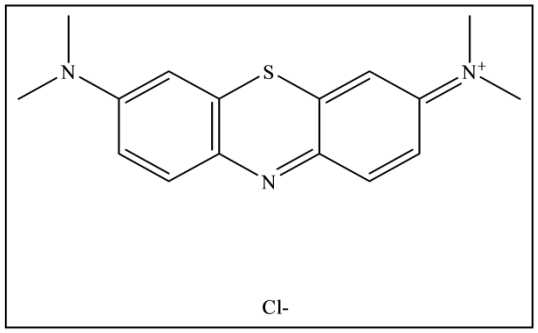

Figure 4.1 (a) Chemical structure of MB

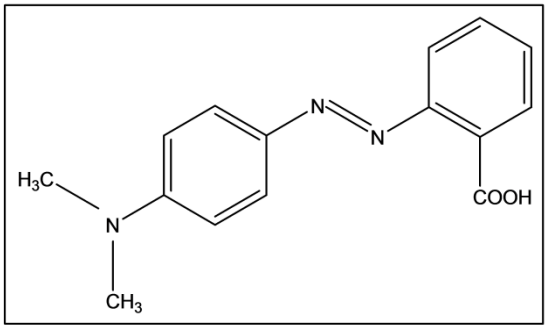

Figure 4.1 (b) Chemical structure of MR

In this study, we focused on the synthesis of mesoporous silica from elephant grass *via* the *sol-gel* technique. The effect of temperature and surfactant concentration on the morphology of mesoporous silica was also investigated. Surfactant concentration of 2, 10, 20, 40, and 55 wt% to silica were used. A 2-step treatment process was adopted, including chemical acid washing and heat treatment. The synthesized materials were characterized extensively using different instrumental techniques. Silica nanoparticles (SNP) and silica nanotubes (SNT) were applied in adsorption of two dyes, MB and MR.

4.3 Experimental

4.3.1 Materials and chemicals

Elephant grass (*Pennisetum Purpureum*) was obtained from Varsity Drive, Durban ($29^{o}48'20.49"$ S and $30^{o}57'53.26"$ E), South Africa. Sodium hydroxide (99.99 %), nitric acid (65 %), acetone ($\geq$99.8 %), MB and MR were all obtained from Sigma, cetyltrimethyl ammonium bromide (99.0+ %) used as a structure directing agent was obtained from Calbiochem and butan-1-ol (99.0 %) was obtained from Merck. All chemicals were used without further purification.

4.3.2 Adsorbent synthesis

4.3.2.1 Sample pre-treatment

This incorporated both acid and thermal treatments. EG was cut with a small stainless steel knife and copiously washed with distilled water and air dried and thereafter ball milled. Approximately 40 g of a clean and ground elephant grass (EG) sample was stirred with 1000 mL of 1.0 M HNO_3 at room temperature for 24 hs in a plastic beaker with a magnetic stirrer at a speed of 300 rpm. Acid treated EG was washed with double-distilled water to a constant pH, dried in an oven at 100 °C for 24 hours and calcined in a crucible placed in a muffle furnace (Kittec Squardo) at 600 °C for 6 h at a ramp rate of 2 °C/min to remove organics and form elephant grass ash (EGA) (Adam et al., 2013). Nitric acid was used to remove small quantities of soluble minerals (metal oxides) and complete delignification of EG. About 1 g EGA was stirred with 20 mL 1.0 M HNO_3 at 60 ^{o}C for 24 h. This was filtered with Whatman No. 5 filter paper and washed with double-distilled water until a neutral pH was reached and dried at 100 ^{o}C for 24 h.

4.3.2.2 Synthesis of mesoporous silica (MSi)

MSi was synthesized by using a modified method of (Thuc and Thuc, 2013). Approximately 2, 10, 20, 40, 55 wt % CTAB to EGA was added to a mixture of butanol and water in a ratio of 1:1 and allowed to completely dissolve with constant stirring at 60 °C. This was denoted as SNP, SNP10, SNP20, SNP40 and SNT, respectively. Sodium silicate was made by dissolving an ap-

propriate amount (1 g) of EGA in 20 mL of 1 M NaOH and was stirred with a magnetic stirrer at 60 ^{o}C for 24 h. This sodium silicate solution was added to the CTAB/EGA/butanol/water solution; thereafter 3.0 M nitric acid was also added dropwise until a pH of 3 was reached, signifying the removal of NaOH from the gel. The resultant gel was aged for 8 h at 60 ^{o}C, and thereafter gently broken up and centrifuged (DuPont Instrument Sorvall Centrifuge SS04) for 5 minutes at 6000 rpm. It was vacuum filtered and washed with boiling distilled water and acetone until a pH 7 was reached and a pure gel was obtained. The gel was dried at 100 ^{o}C for 24 hand calcined in a muffle furnace at 600 ^{o}C at a ramp rate of 2 ^{o}C/min for 5 h to remove the surfactant (CTAB). The products were ball milled and kept in a dessicator until further characterization. SNP 700, SNP 800 and SNP 900 were also synthesized and calcined at 700, 800 and 900 ^{o}C, respectively. This was done to determine the effect of temperature on the synthesis of mesoporous silica.

4.4 Characterisation of Adsorbents

N_2 adsorption-desorption analysis included measurements for specific surface area, pore size and pore volume of MS of samples which were determined using the Brunauer-Emmett-Teller (BET) method and the Barret-Joyner-Halenda (BJH) method on a Micromeritics 3000. About 0.2 g of sample was degassed using a Micromeretic vacprep 061 degasser for an hour at 90 ^{o}C and the temperature then raised to 200 ^{o}C for 12 h before analysis and porosity measurements were carried out in liquid nitrogen at – 196 ^{o}C.

Powder x-ray diffraction analysis (Rigaku 600 miniflex) was used to determine the crystallinity of all samples, employing a Co Kα1 and Kα2 radiation (λ = 1.78901 Å and 1.7920 Å, respectively) at a scan step time of 0.02/S to obtain a more accurate measurement. The accelerating voltage and applied current used was 40 kV and 45 mA, respectively. The diffraction angle was scanned in the 2Θ range at 10-80^{o}. X-ray fluorescence (PAnalytical Axios Max) was used to quantify the chemical components and also determine the purity of the samples. Samples were prepared by making a pellet where about 1.0 g of the silica sample was pressed with a boric acid binder (20 mg) using an applied force of 20 Psi on a Windsor bench press.

FT-IR spectra (Perkin Elmer Series 100 spectrum with ATR accessory with a scan rate of 40 spectra per second) in the range of 4000 – 400 cm^{-1} was obtained showing the presence of silanol and siloxane functional groups. For TGA and DSC analysis, approximately 5 mg of sample in an aluminium pan was placed in a furnace (SDT Q 600 V 209 Build 20) at a temperature of 25 °C with a ramping rate of 2 °C/min with constant air flow to a 1000 ^{o}C. This was carried out to determine the thermal stability of the material.

Silica microstructure and surface morphology was analysed using field emission scanning electron microscopy (FESEM) with an operating voltage of 10 kV and EDX on the SEM (Zeiss) instrument was used in determining purity of samples. The samples were coated with gold on copper stubs with a Zeiss coating instrument to minimize charging effects. The transmission electron microscope (TEM) and higher resolution TEM (JEOL) were also used in determining the surface morphology of the synthesized materials. Samples for SEM and EDX analyses were attached on a copper stub with carbon glue and coated with gold before examination. Samples for TEM and HRTEM analysis were placed in vials containing absolute ethanol and ultrasonicated for 10 mins. Holey lacey carbon grids with 10 µm mesh size were dipped into the vials containing the ultrasonicated samples and dried before microstructural determination.

4.5 Point of Zero Charge (pH_{PZC})

The PZC of samples were determined using the solid addition method (Reddy et al., 2012). An initial concentration of 25 mL of 0.1 M KNO_3 was adjusted to pH values between 2 - 12, with the addition of 0.1 M HCl or NaOH. About 50 mg of SNT and SNP were added to the solution and shaken at room temperature for 24 h with a shaker (Scientific Engineering) at 300 rpm and thereafter left to stand for 30 mins at room temperature. From the supernatant the final pH was obtained. A graph of the initial values of (*i*) *versus* the difference between the initial and final pH values (pH_f) was plotted.

4.6 Adsorption Studies

Approximately 0.02 g of the SNP and SNT samples were added to 20 mL of MB and MR solutions (prepared individually) in 50 mL amber bottles with varying concentrations. These were shaken on a mechanical shaker for a specific time at room temperature. The effect of adsorbent dosage, initial dye concentration, pH value, contact time and temperature were monitored varying one parameter at a time. The initial pH of the solution was adjusted using 0.1 M HCl or 0.1 M NaOH solutions and the supernatant was filtered using Whatman No. 5 filter paper. The concentration of MB and MR in the supernatant solution were determined before and after adsorption spectrophotometrically using a UV-3600-Shimadzu UV-VIS-NIR spectrophotometer at a wavelength of 663 nm and 540 nm, respectively. These studies were conducted in duplicates.

The adsorption capacity q_e (mg/g) of SNP and SNT at equilibrium time for MB and MR was calculated from the equation:

$$q_e = \frac{(C_o - C_e)V}{W} \quad (4.1)$$

Where C_o and C_e are initial and equilibrium concentrations of MB and MR in mg/L, V is the volume of the solution (L), and W is the mass of adsorbent used (g) in the experiment. The percentage MB removal at equilibrium time was calculated using the equation:

$$\%\ dye\ removal = 100\ x\ (\frac{C_o - C_e}{C_o}) \quad (4.2)$$

4.7 Results and Discussion

4.7.1 Characterisation of adsorbents

This section discusses the characterisation of adsorbents such as XRF, TGA, XRD, textural, FTIR, SEM and TEM analysis.

4.7.1.1 X-ray fluorescence analysis

Elemental composition of silica determined by x-ray fluorescence (Table 4.1) showed that a very high purity silica was obtained from EGA. Metal oxide impurities in silica were significantly reduced due to the acid treatment. The percentage purity of silica obtained was 99.2% and may be attributed to the combined acid and thermal treatments. Oxides of Ni, Ti, Ca, P, Fe and Al comprised a total of 0.80% of the sample, which are negligible impurities (Liou, 2011). The 2-step treatment had better efficiency as shown by Thuc and Thuc (2013) of 99.08%, however, that study utilised HCl and H_2SO_4 acid as compared to HNO_3 used for pretreatment in this study. Adam et al (2013) obtained silica of 98.5% purity. The higher percentage purity obtained may also be because nitrates of all elements are more soluble in nitric acid, thus causing a reduction in impurities. Acid leaching significantly eliminated the impurities, and synthesis at acidic pH values (pH 3) resulted in a high purity silica (Liou, 2011). It should be noted that XRF result presented is that of EGA after calcination. This shows the purity of the samples after the acid wash pretreatment process. EGA was also the precursor for all the silica samples synthesized and the changes in the temperature did not change the purity of silica thus only the XRF for EGA was shown.

Table 4.1 Percentage composition of EGA using XRF

Components (oxides)	% composition
SiO_2	99.20
TiO_2	0.113
Al_2O_3	0.418
Fe_2O_3	0.088
CaO	0.033
K_2O	0.030
P_2O_5	0.005
SO_3	0.008
V_2O_5	0.004
ZrO_2	0.020

4.7.1.2 Thermogravimetric decomposition analysis

Figure 4.2 shows the TGA profile of EG, SNP and SNT, respectively. The TGA analysis was carried out using the method employed by Zhang et al. (2011a). The thermal decomposition profile of EG showed 4 steps. Firstly, removal of adsorbed moisture on the silica surface between 100 -120 ^{o}C, (Liou, 2011, Zhuravlev, 2000) which was accompanied by a small change in mass. The second stage was characterized by maximum degradation of hemicelluloses between 120 - 305 ^{o}C. The third stage occurred between 305 - 400 ^{o}C. The combined losses in stage 2 and 3 were as a result of decomposition of volatile organic materials, residual carbon decomposition, cellulose, and lignin of EG and dehydroxylation and water loss associated with condensation of silanol groups (Liou, 2011). After 400 ^{o}C, the ash from EG became thermally stable even when heated to 900 ^{o}C and no further loss was recorded. Approximately 7 % of the sample remained consisting of amorphous silica and metal oxides.

The SNP degradation profile showed it to be a 2-step process. Firstly, the removal of physically adsorbed water which occurred at a temperature of about 120 ^{o}C and resulted in a significant weight loss. Secondly, a maximum degradation loss occurred in the range of 100-450 ^{o}C. This resulted in significant weight loss as residual carbon from the surfactant decomposed, and dehydroxylation and removal of the CTAB template occurred, which is mostly organic. SNP became thermally stable at 450 ^{o}C, as no change in mass occurred thereafter.

SNT thermogram, showed 2 stages of decomposition. The first stage was removal of physisorbed water below 120 ^{o}C and the second was removal of organics from the surfactant present, which was the silanol group condensation between 120-450 ^{o}C. After 450 ^{o}C, all samples became thermally stable. A 17.8 % mass loss was observed in SNT.

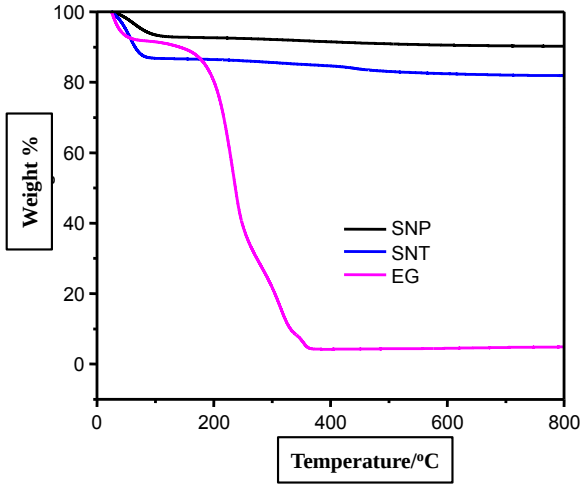

Figure 4.2 TGA profiles of SNP, SNT and EG samples

4.7.1.3 X-ray diffraction analysis

The powder XRD patterns of all samples are shown in Figure 4.3. SNP and SNT both had a very broad prominent peak at 23-29 2(Θ) due to the amorphous nature of synthesized silica calcined at temperatures below 600 °C (Figure 4.3 (a)) (Sivasubramanian et al., 2013). The amorphous nature of silica had a marked effect on the base lines of XRD profiles making it difficult to determine the crystalline sizes of silica (Adam et al., 2013). XRD profiles of SNP 700, SNP 800 and SNP-900 calcined at high temperature were of a crystalline nature and had very sharp peaks at 24 and 30.2*(Θ)* which were cristobalite and trydimite, respectively. Crystalline silica is not a good adsorbent and is of a much reduced surface area as confirmed by BET measurements. Crystallization is disadvantageous in silicon based materials, due to silica inactivity in its crystalline form (Ghorbani et al., 2013). Hence, amorphous silica SNT and SNP may likely be better adsorbents as compared to SNP 700, SNP 800 and SNP 900.

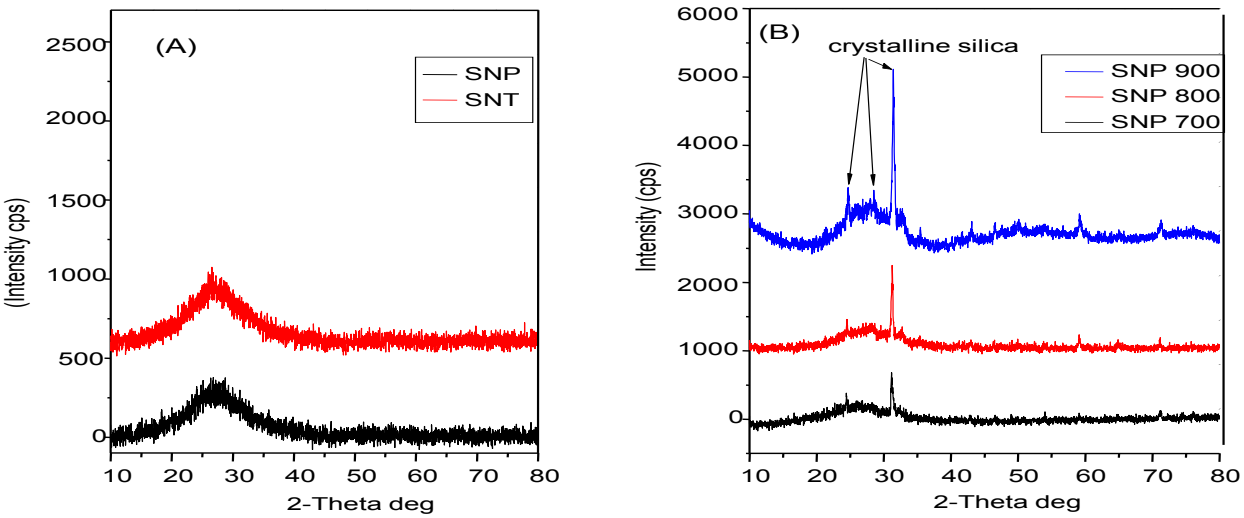

Figure 4.3 XRD profiles of (a) SNP and SNTand (b) SNP 700, SNP 800 and SNP 900

4.7.1.4 N_2 Adsorption-desorption analysis and isotherms

The N_2 adsorption-desorption isotherm of SNP and SNT is presented in Figure 4.4 (a). All samples exhibited a type IV isotherm and based on IUPAC classification, these are mesoporous materials having pore diameters between 2-50 nm. They are characterized by complete pore filling, monolayer-multilayer adsorption and capillary condensation (Sing, 1985). This is characteristic of materials that are non-rigid aggregates of plate like particles, having "ink bottle" or slit shaped pores (Adam et al., 2013). SNP and SNT had a H_3 hysterisis loop which is typical of materials with porous packing and having agglomerates that have non-uniform size and irregular shape (Adam et al., 2013). The sharp inflection at 0.9 is also indicative of the irregularly shaped pores (Jaroniec et al., 1999). Pore size distribution (Figure 4.4 (b)) of SNT and SNP showed it was made of a unimodal pore system with a sharp peak at 40 nm, though in SNPs, pore distribution was multi-modal with varied pore distribution.

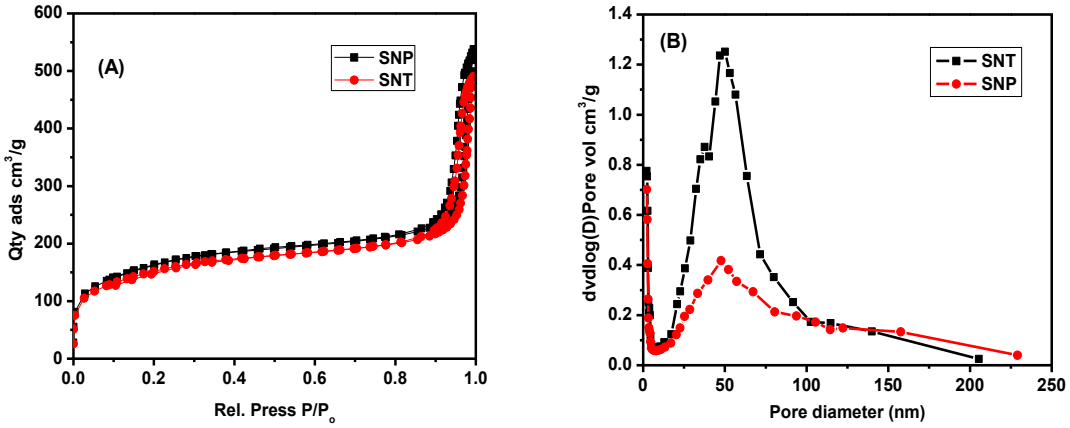

Figure 4.4: (a) N_2 adsorption-desorption isotherm (b) Pore size distribution of SNT and SNP

The BET specific surface area analysis of samples is presented in Table 4.2. It can be deduced from the data that an increase in temperature caused a reduction in BET surface area and pore volume. This is seen in the reduction of the surface area as temperature increased with SNP 900 having the lowest surface area. This indicated that higher temperature above 600 ^{o}C was not favourable for synthesis of silica. Dash et al. (2008) confirmed that mesoporous silica are thermally stable up to 873 K under air and removal of physiosorbed water molecules is at 440 K. Silanol groups are activated at 423 K with the number of silanol groups varying depending on the temperature. Each silanol group has a surface area of 4.5-8 nm and at temperatures above 423 K, silanol groups start condensing, thus liberating water molecules, and at 673 K almost half of the silanol groups are removed (Jal et al., 2004). For silica with high surface area, the surface population of silanol would be 39 %, thus there is a reduction in surface area at temperatures exceeding 823 K which was further confirmed by the TGA analysis showing the decomposition of the silanol groups at temperatures greater than 873 K °C. This describes why SNP 900 had the lowest surface area as there was severe constriction of adjacent silanol group which led to a severe reduction of surface area. However, at this temperature the ash was not white and had traces of organic matter and other impurities. In contrast, calcination at 600 °C gave satisfactory surface area, with an amorphous phase (Figure 4.3 (a)) andvery low impurity, thus it was chosen as the optimal temperature of synthesis. It is known that a larger surface area leads to larger pore diameter and pore volume, thus increasing the capacity of the material as an adsorbent in adsorption/trapping of pollutants.

Table 4.2 BET surface area and pore volumes of all samples and other studies

Sample	SBET (m^2/g)	Pore volume (cm^3/g)	References
SNP	437	0.75	This study
SNT	402	0.67	This study
SNP 700	287	0.39	This study
SNP 800	141	0.33	This study
SNP 900	101	0.19	This study
Silica nanoparticles	353	0.67	(Jaroenworaluck et al., 2012)
Silica nanotubes	315	0.36	(Adam et al., 2013)
Silica nanoparticles	340	NA	(Thuc and Thuc, 2013)

4.7.1.5 FTIR spectral analysis

FTIR analysis was used to determine the major functional groups present. The FTIR spectra of EG, EGA, SNP and SNT are presented in Figure 4.5 and FTIR spectra for SNP 700, SNP 800 and SNP 900 can be found in Appendix A 1.1. In EG and acid treated EG, there were major peaks that characterized the presence of lignin between 1600-1000 cm^{-1}. Peaks around 1423 cm^{-1} and 1027 cm^{-1} are attributed to C=C stretching and =C-H, respectively (Hu and Hsieh, 2014). The absorption band at 2855.41 and 2926.62 cm^{-1} on the EG spectrum is due to CH-CH_2 stretching. Acid treated EG had characteristics of silica, lignin, cellulose and hemicellulose present. Four major peaks define silica and are centered around 3400, 1600, 1100 and 470 cm^{-1}, which were present in the FTIR spectra of all samples. The absorption peak at 1100 cm^{-1} is attributed to asymmetric stretching of Si-O-Si, indicating a dense silica network (Pang et al., 2011). This was seen as being more pronounced in the calcined silica samples compared to the EG sample which still had lignin and hemicellulose present which may have masked the Si-O-Si peak. The absorption peak at 800 cm^{-1} represents symmetric stretching vibration of the Si-O-Si network, and at 470 cm^{-1} is the symmetric bending vibration of Si-O. The absorption band around 3400 cm^{-1}, is due to the OH stretch of water vibration coming from the remaining absorbed water molecules present in the material as well as the OH of the silanol group (Jaroenworaluck et al., 2012). The peak at approximately 1600 cm^{-1} was due to the OH bend of the silanol group. Calcining silica at 600 ^oC may be the ideal temperature for synthesis as there was no deformation, confirming the

results obtained by SEM, TEM, TGA and BET analysis. SNP calcined at 700, 800 and 900 ^{o}C had a shoulder between 950-960 cm^{-1} which may be as a result of high temperature calcinations which was not observed at 600 °C.

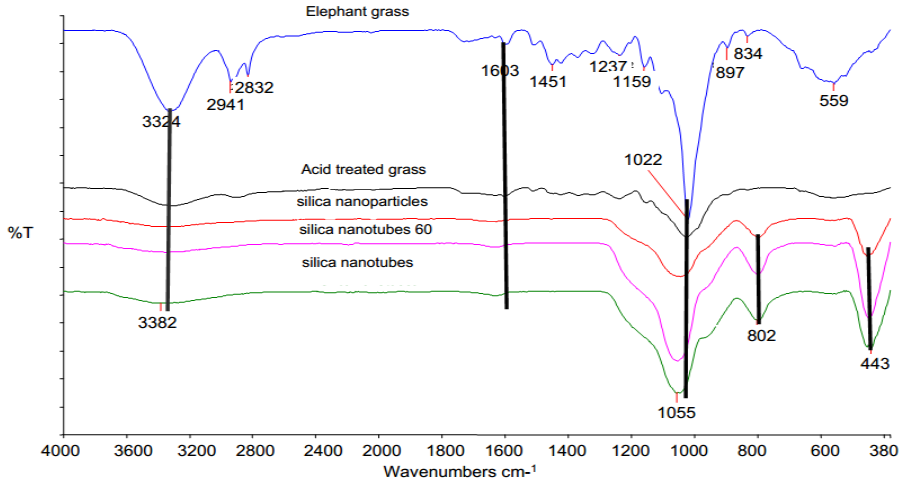

Figure 4.5 FTIR spectra of EG, EGA, SNP, SNT samples

Table 4.3 EDX percentage composition of samples

Sample	**Percentage composition**			
	% Si	% O	% C	% Fe
EG	0.1	33.64	61.99	4.27
EGA	60.00	40.00	-	-
SNP	55.66	44.34	-	-
SNT	41.48	58.52	-	-

EDX analysis was carried out on EG before and after acid leaching, as well as on SNP and SNT. The results from FTIR and EDX indicated that fairly pure silica was obtained when the structure directing agent was removed *via* calcination. Acid treatment also aided the removal of metal impurities. EDX results for elephant grass before any treatment showed it is mostly composed of carbon and oxygen with very small quantities of inorganics present. Therefore no further elemental analysis was carried out on elephant grass.

4.7.1.6 Surface morphology

4.7.1.6.1 SEM image analysis

The micrographs of EG, EGA, SNP, SNP10, SNP20, SNP40 and SNT are shown in Figure 4.6. Comparing SEM images of untreated and acid treated grass, there was a marked difference in surface morphology, evidenced by destruction of the microstructure. The surface appeared rough, showing it was leached and the lignin, which gives intracellular structure and acts as glue to bond and give grass hardness, was removed (Pang et al., 2011). After calcination of acid treated EG (Fig. 4.6 (b)), a different morphology was observed indicating deposition of hydrated silica intercellularly or intracellularly in plant tissues (Zhang et al., 2011a). From the SEM images, it can be clearly seen that, that SNP nanoparticles were formed at (2 wt%) CTAB, and as the concentration of CTAB increased, there is the aggregation of particles to give tubes. These tubes were completely visible in (55% wt CTAB) SNT. SNP nanoparticles had regular, spherical and non-agglomerated morphologies. SNT had a uniform web-like structure of tubes possessing a network of more or less even pores.

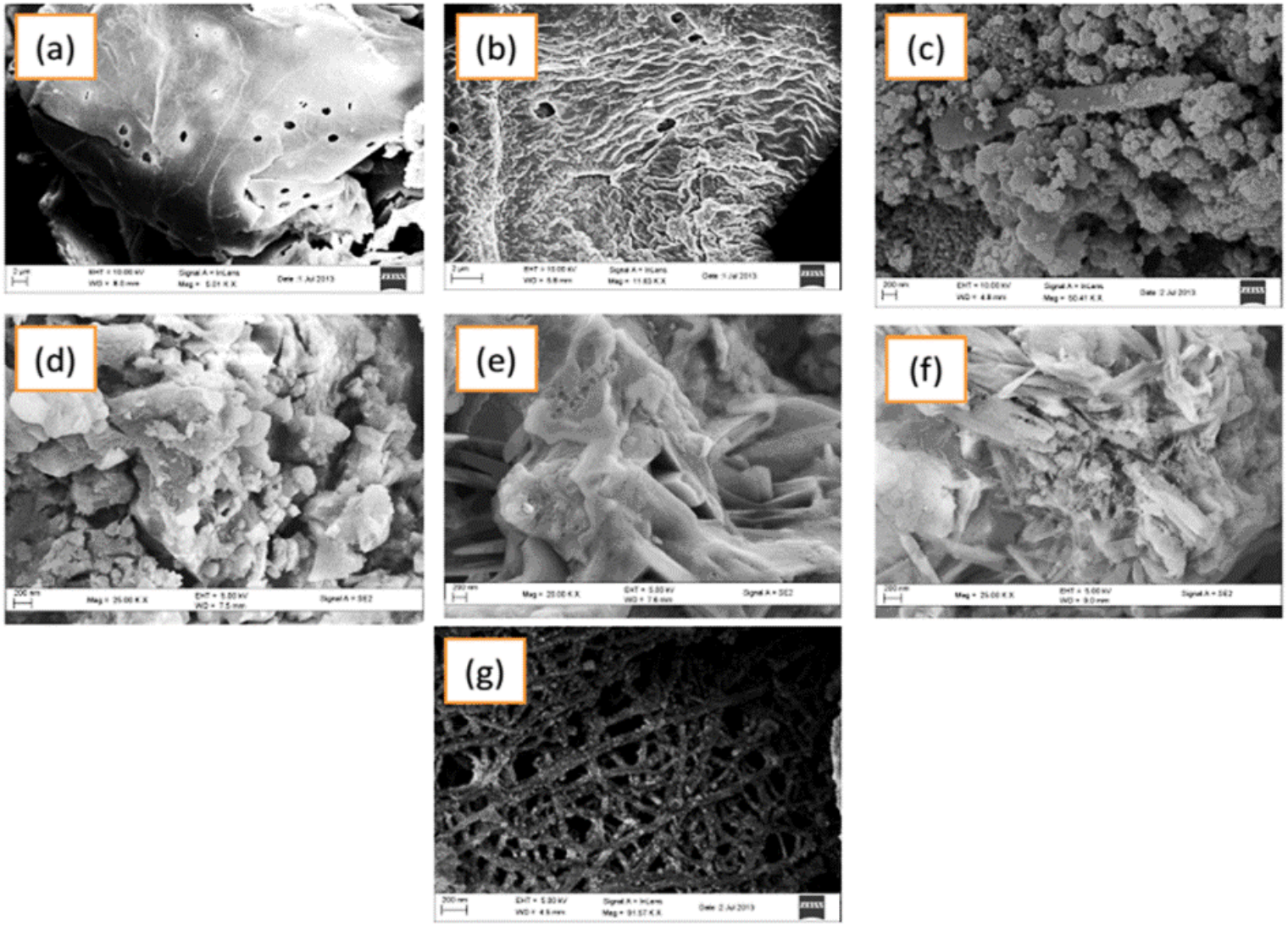

Figure 4.6 SEM micrographs of (a) EG and (b) acid treated EG obtained at 2 µm (c) SNP (d) SNP10 (e) SNP20 (f) SNP40 and (g) SNT55 obtained at 200 nm

4.7.1.6.2 TEM analysis

The micrographs of SNP, SNP10, SNP20, SNP40 and SNT are shown in Figure 4.7. The micrograph of SNP showed it to be well rounded with a non-agglomerated morphology. On the other hand, SNT had a twisted tubular morphology with clear porosity. However, as seen in SNP10, SNP20 and SNP40, as the concentration of CTAB increased, the tubular structure of silica became more visible. This clearly showed the impact of CTAB on the morphology of mesoporous silica. These images clearly corroborate with the images obtained from SEM analysis. Furthermore, no porosity was observed for these mesoporous silica samples even though an H_3 hystersis loop was observed in the BET analysis. The lack of porosity in the TEM images was due to this material being a mesoporous material unlike ordered mesoporous silica which shows clear porosity in TEM images. The TEM images for SNP 700, SNP 800 and SNP 900 are shown in Appendix A 1.3 and show no visible changes due to changes in calcination temperature.

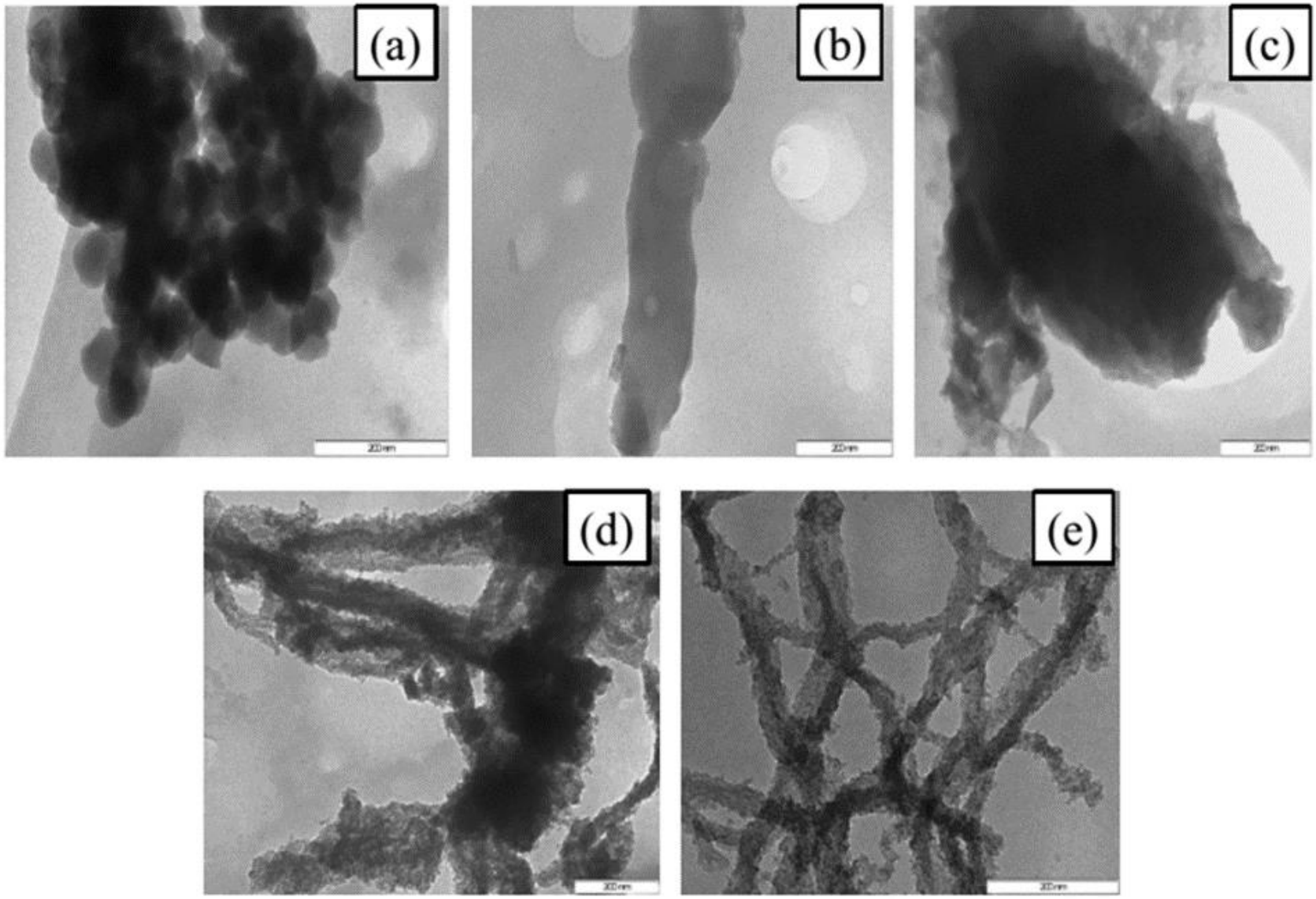

Figure 4.7 TEM images of (a) SNP (b) SNP10 (c) SNP20 (d) SNP40 and (e) SNT55

4.7.1.6.3 Effect of surfactant concentration

The surfactant used in the synthesis is cationic in nature and the self assembly mechanism is such that there is a head to tail arrangement between the surfactant head group and the silica. In synthesizing silica nanotubes, experimental evidence from this study indicated the most important variable was concentration of surfactant. Addition of 2 wt % CTAB to EGA resulted in formation of silica nanoparticles with spherical morphology which was in agreement with Thuc and Thuc (2013). As the concentration of surfactant increased the particles become morphed into tubes and it became visible at 55 wt% CTAB. This is the concentration at which silica nanotube was formed.

In the formation of SNTs, a study by Zhang et al. (2011a) showed that SNTs did not form when low concentrations of a combination of CTAB/SDBS were used. Instead irregularly shaped structures formed, resulting from shear stress of mechanical stirring, decreasing the ability to form nanotubes. Zhang et al. (2011) suggested temperature was the most important parameter in synthesizing SNTs in a typical hydrothermal synthesis at 100 °C. However, this may be for surfactants of a specific nature (SDBS/CTAB) because, when a 55 wt% concentration of CTAB to sodium silicate solution was used at room temperature and at 60 ^{o}C, SNT was obtained, irrespective of synthesis temperature as observed by Adam et al. (2013). SNPs with higher surface area were also obtained using hydrothermal synthesis conditions of 60 ^{o}C. Thus lower temperatures can also be used when using other surfactants.

In this study, when the concentration of CTAB was increased to 55 wt% (Figures 4.6 (g) and 4.7 (e) the surfactant molecule organizes itself independently and a siliceous framework polymerises around the preformed surfactant aggregates. Since, the surfactant preforms independently, a higher concentration of CTAB resulted in the formation of SNT, and CTAB was expelled by heating at 600 ^{o}C for 5 hours leaving behind hollow nanotubes. This was confirmed by the observation of silica nanoparticles when 2 wt% of CTAB was used as shown in Figure 4.6 (c) and Figure 4.7 (a) which then lead to the formation of nanoparticle aggregates as the CTAB concentation increased and finally formed nanotubes when a 55 wt% CTAB concentration was used (Figure 4.6 (g) and Figure 4.7 (e)).”

Thuc and Thuc (2013) showed that, 2 wt% CTAB to mass of sample represented the critical micelle concentration in synthesizing silica nanoparticles. CTAB concentration had a profound effect on microstructure determination, surface area, and average nanoparticle size, pore volume and pore diameter (Table 4.2). During synthesis, there was a marked difference in the gel formation process. On addition of 55% CTAB to 45% EGA, the gel was quick to form and reaction time was relatively short. Furthermore, a low pH of 3 was important for the formation of the gel and at pH values lower than 3, the gel tended towards a liquid state.

Qu and Gu (2014) found that high concentrations of surfactant and silica caused strong interaction and the silica/surfactant mixture grew rapidly, having aggregation tendency and also a reduced surface area. This study found similar results where the surface area was found to decrease from 437 to 402 m^2/g and a corresponding decrease in pore volume 0.75 to 0.67 cm^3/g (Table 4.3). In contrast, on addition of 2 wt% CTAB to EGA, the gel was slow to form and there was more interaction between CTAB, silica and the mother liquor. Consequently, uniformity was ensured, CTAB was well dispersed and coated on the surface of individual nanoparticles resulting in less agglomeration of nanoparticles (Figure 4.6 (c) and Figure 4.7 (a)(Thuc and Thuc, 2013). The addition of 55 wt% to 45 wt% CTAB to EGA resulted in formation of silica nanotubes which were not ordered while addition of 2 wt% CTAB to EGA gave high surface area silica nanoparticles. Hence, the concentration of surfactant effectively determined the type of nanostructure formed.

4.8 Adsorption Studies

The choice of adsorbent selected was informed by the surface properties obtained from textural, FTIR and XRD analysis. Two of the synthesised samples, SNP and SNT, were chosen for adsorption studies to determine their respective adsorptive capacities.

4.8.1 Effect of adsorbent dosage

The effect of adsorbent dose on uptake of MB and MR on SNP and SNT was studied (Figures 4.8 (a) and (b)). The morphology of the adsorbent played an important role in the sorption of the

dyes, as SNP with a slightly larger surface area and pore size had a better sorption capacity than SNT. The MB and MR solutions were not a mixture. For MB an increase in adsorbent dose caused an initial increase in adsorption but the incremental increase in adsorption was not as great after 20 mg which was selected for further experiments. Maximum % MB removal by SNT and SNP at 20 mg, was 49.6% and 61.4%, respectively. Initially there was some physical adsorption occurring that accounted for the initial percentage removal of MB. The MB structure (Figure 4.1) shows that it dissociates in solution to form cationic species (Kushwaha et al., 2014). When the adsorbent was added to the adsorbate solution, the adsorbent took on a negative charge which resulted in electrostatic attraction leading to removal of MB. When higher doses of adsorbent were used, the adsorbent aggregated, however due to the availability of a greater amount of active sites on the adsorbent there was still some interaction between the MB cation and the negative charge on the adsorbent and thus overall there was an increase in removal of adsorbate. In addition, the increase in adsorbate removal may also be due to the very low equilibrium concentration of the solute yet with a high number of adsorption sites leading to increased adsorption at high adsorbent dose, i.e. driving force responsible for adsorption increased but thereafter leveled off and became negligible as observed by Mangrulkar et al., (2008).

A mass between 5-25 mg of adsorbent was used with optimal dose being 5 mg for MR adsorption. It was observed that percentage removal of pollutants decreased with an increase in adsorbent dose for MR on SNP and SNT, while the q_e value decreased gradually from 46.6 to 3.49 and 54.4 to 6.21 mg/g, respectively. Percentage maximum adsorption capacity of MR on SNT and SNP were 38.9% and 33.3%, respectively. Further addition of adsorbents resulted in a decrease in sorption capacity. MR is neutral in solution (Tobey, 1958) and there was only the physical adsorption that occurred initially at low adsorbent dose. As the adsorbent dose increased, aggregation and particle interaction occurred which together with no interaction between the neutral MR and the adsorbent resulted in an overall decrease in MR removal. Hence, 5 mg was selected as the optimal dose for experiments.

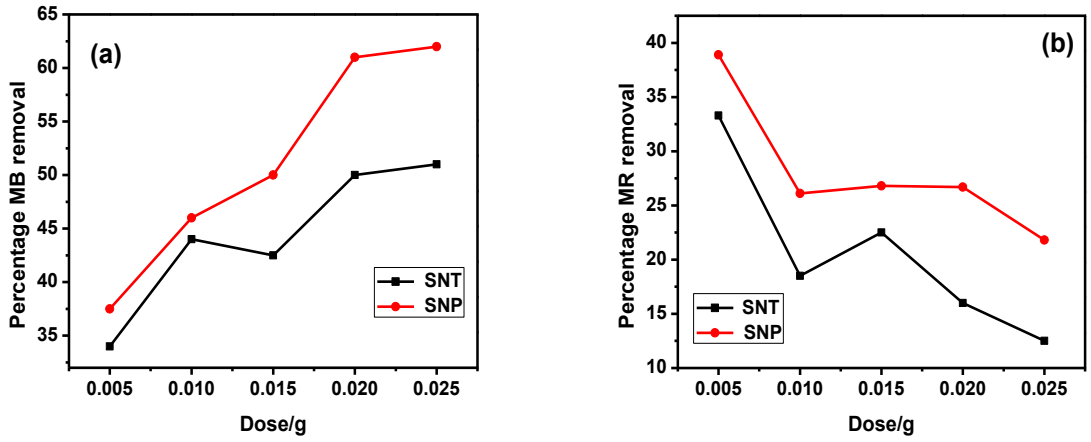

Figure 4.8 Effect of adsorbent dose on (a) MB adsorption and (b) MR adsorption as separate solutions

4.8.3 Effect of pH

The effect of solution pH on the removal of both dyes on SNT and SNP is shown in Figures 4.9 (a) and 4.9 (b). The percentage removal of MB and MR dyes was studied in the pH range 2-10 with pH 6 and 10 as the optimum for MR and MB, respectively. MR removal efficiency was higher under acidic condition (pH 6) for both SNT and SNP at 72.2 % and 75 %, respectively. MR underwent 4 interesting colour changes; at pH below 2 it changed from its original red colour to an intense pink colour which changed to a slightly lighter intensity of pink after adsorption, at pH 4 the solution changed to light pink and changed to an even lighter shade of pink after adsorption, at pH 6 it changed to orange and a lighter shade of orange after adsorption, at 8 it changed to yellow and at pH 10 it changed to an intense yellow colour which were also lighter in colour after adsorption. The change in colour was as a result of both a change in pH and also the adsorption by the adsorbent. MB removal efficiency at pH 10 was 95.6 % and 96.6 % for SNT and SNP, respectively.

The pH_{PZC} determines when the net total particle charge is zero. The pH_{PZC} of SNP was 2.01 and SNT was 2.04 (Table 1 Appendix B1). This resulted from the adsorbent surfaces being positively charged when the pH of the solution is less than pH_{PZC}. The adsorbents are of a cationic nature; therefore an increase in solution pH above PZC resulted in a higher percentage of dyes being

removed. Adsorption of dyes onto the adsorbent is affected by surface charge on the adsorbent surface determined by the pH of the solution. When pH is lower than the pH_{PZC} value, the acidic solution produces more H^+ than OH^- ions making the adsorbent surface positively charged. The silanol group is responsible for adsorption. At lower pH the silanol group is present as $SiOH^{2+}$ and at higher pH SiO^- dominate. At higher pH values, electrostatic interactions dominate the adsorption process. MB is cationic in nature and therefore in aqueous solution exist as positively charged ions. The pK_a of silica is about 1.5 (Qu and Gu, 2014) and the cationic group on silica increases with increasing pH value. An increase in pH causes the competition of H^+ with MB cations to decrease while in contrast, an increase in pH causes the competition of OH^- with MR anions to increase. Thus an increase in pH value from 6-10 causes an increase in adsorption capacity of MB and a reduction of MR, and at pH 11 both silica and MB dye were fully ionized resulting in a constant adsorption capacity. The optimal pH of adsorption chosen for was 8 because real wastewater samples do not generally have high pH values up to pH 10.

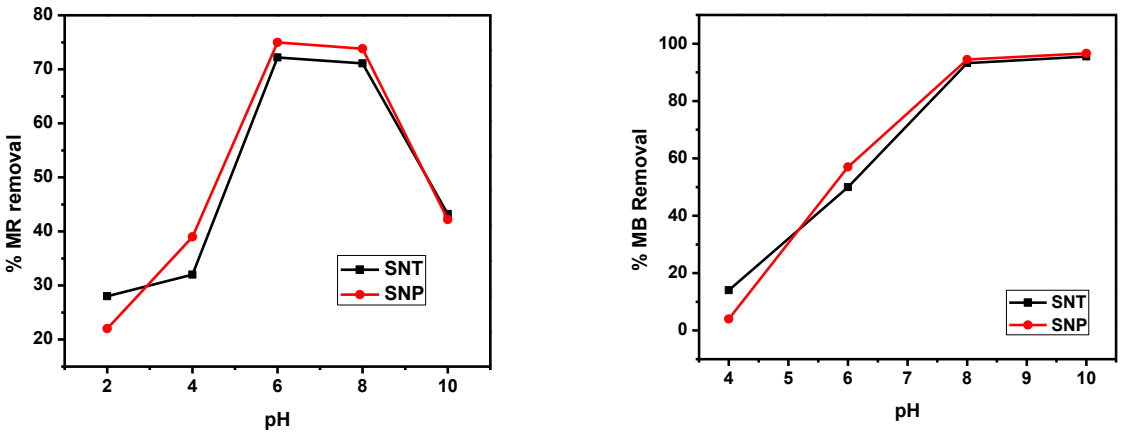

Figure 4.9: (a) Effect of pH on MR removal and (b) Effect on MB removal

4.8.4 Kinetic studies

4.8.4.1 Effect of initial concentration and contact time

The adsorption of MB and MR on SNT and SNP was studied at different concentrations of 30, 60 and 90 mg/L. MB and MR uptake was fast in the first hour and thereafter slowed down (Fig-

ures 4.10 and 4.11). An increase in initial concentration of MB and MR resulted in an increased adsorption of dyes on the adsorbent. At high concentrations, the initial increase in concentration of MB and MR led to a high concentration gradient which was the driving force for more MB and MR molecules to transfer to the adsorbent interface. This together with the availability of the vacant sites on the adsorbent led to the initial increase in adsorption. The q_e value increased from 44.42 to 115.80 mg/g with an increase in MB concentration from 30 to 90 mg/L for SNT and from 44.50 to 118.11 mg/g with the same increase in concentration for SNP. At further increases in MB concentrations, the concentration gradient is no longer as high as the initial concentration gradient which leads to a slower transfer of MB molecules to the adsorbent. This together with fewer available sites on the adsorbent, leads to a reduced % MB removal from 95.6 to 82.0 % for SNT and from 96.6 to 84.2 % for SNP because the adsorption sites are now saturated and minimal dye is adsorbed. For MR, an increase in initial dye concentration from 30 to 90 mg/L resulted in an increase in the q_e value from 109.9 to 205.2 mg/g for SNT, and 104.9 to 220.2 mg/g for SNP. At increased MR concentrations % MR removal reduced from 72.2 to 56.9 % for SNT and from 75.0 to 61.1 % for SNP as observed by (Sajab et al., 2011, Han et al., 2010, Kushwaha et al., 2014). After 2 hours, adsorption equilibrium was reached for all concentrations of dyes. It was also observed that for both SNT and SNP, adsorption of MR was higher compared to MB which may be due to the smaller molar mass and particle size of MR.

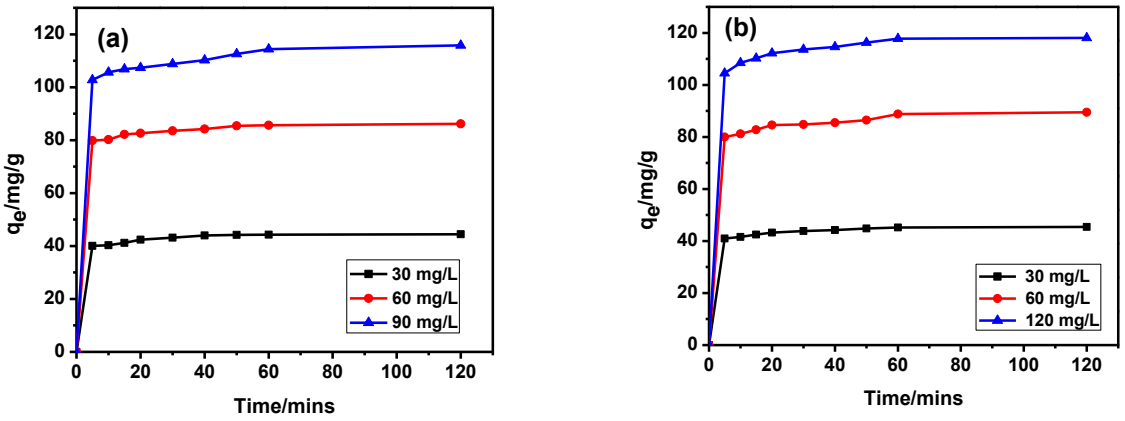

Figure 4.10: Effect of contact time and MR concentration on adsorption using (a) SNT (b) SNP (n=2)

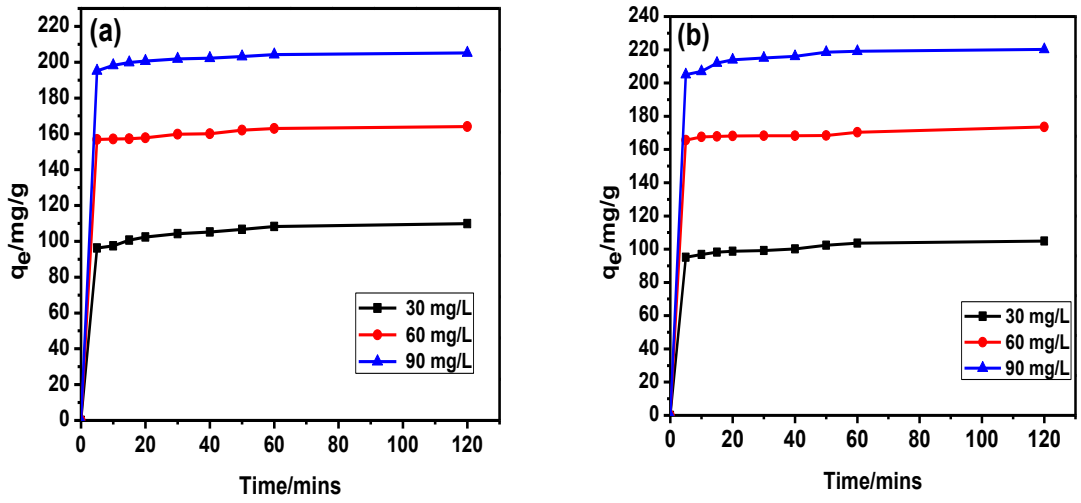

Figure 4.11: Effect of contact time and MB concentration on adsorption using (a) SNT (b) SNP (n=2)

4.8.4.2 Adsorption kinetics

This was to establish the rate controlling step and adsorption mechanism of MB and MR, using pseudo-first-order (equation 4.3), pseudo-second-order (equation 4.4), intraparticle diffusion model (equation 4.5) and the Elovich model (equation 4.6) in fitting experimental data.

$$ln\ (q_e - q_t) = ln\ q_e\ - ln\ K_{ad} t \quad \text{.....(4.3)}$$

$$\frac{t}{qt} = \frac{1}{K_2\ q_e^2} + \frac{t}{qe} \quad \text{.....(4.4)}$$

$$q_t = K_i t^{0.5} + C \quad \text{..... (4.5)}$$

$$q_t = a\ ln\ t + b \quad \text{.....(4.6)}$$

Where q_e, q_t and k_{ad} (min^{-1}) are amounts of MB and MR adsorbed at equilibrium and at time t (mg/g), and the rate constant of adsorption, respectively. The values of the k_{ad} and q_e^{cal} were calculated from the slopes ($-k_{ad}$) and the intercepts (ln q_e) of the plots of ln (q_e–q_t) *vs* t. k_i is the in-

traparticle rate diffusion constant (mg/g $min^{-1/2}$), *C* is the intercept depicting intra-boundary layer effect, k_2 is the rate constant of adsorption (g/mg min) and q_t value is the amount of MB adsorbed at time t (mg/g). The Elovich coefficient is obtained from the plot q_t *versus* ln t. The initial adsorption rate, *a,* and the desorption constant, *b,* were calculated from the intercept and slope, *x* is the initial adsorption rate (mg/g min).

The calculated kinetic parameters for adsorption of MB and MR on SNT and SNP with corresponding correlation coefficients are presented in Tables 4.4 and 4.5

Table 4.4 Kinetic parameters for adsorption of MR on SNP and SNT

Initial dye conc	Temp (K)	q_e^{exp}	Pseudo-first-order			Pseudo-second-order			Intraparticle diffusion			Elovich			
			q_e^{cal}	k_{ad}	R^2	q_e^{cal}	k_2	R^2	k_i	C	R^2	A	B	R^2	x
SNP	298		(mg/g)			(mg/g)			(mg/g/min$^{-1/2}$)						
30 mg/L		45.50	0.4082	0.0166	0.7546	44.5	0.0026	0.9999	0.0677	43.7	0.7565	0.2227	43.4	0.8902	194.8
60 mg/L		87.14	0.0188	1.4317	0.7382	86.4	0.0045	0.9998	0.3574	82.3	0.4506				
90 mg/L		118.11	0.0277	2.2085	0.6028	117.6	0.0060	0.9997	2.0783	100.2	0.5535				
30 mg/L	308	42.56	21.7	0.046	0.9599	42.5	0.0038	0.9999	0.0969	41.6	0.8808	0.269	41.3	0.9243	153.6
30 mg/L	318	42.01	16.4	0.0609	0.9044	42.0	0.0031	0.9999	0.1118	41.0	0.6355	0.3415	40.6	0.8078	118.8
SNT	298														
30 mg/L			0.92	0.0344	0.7096	44.4	0.001	0.9999	0.0285	44.2	0.6727	7.90	81.5	0.8906	10.3
60 mg/L			1.91	0.0395	0.8903	86.2	0.0045	0.9998	0.3584	82.4	0.4506				
90 mg/L			3.28	0.0538	0.9648	116.3	0.0106	0.9998	2.60 9	2.50	0.7064				
30 mg/L	308		1.06	0.0483	0.9601	42.1	0.0009	0.9999	0.2427	39.9	0.8811	0.6899	38.9	0.9695	56.5
30 mg/L	318		0.881	0.0451	0.8816	40.6	0.0008	0.9999	0.2042	38.2	0.8171	0.5833	37.5	0.9999	64.3

Table 4.5 Kinetic parameters for adsorption of MB on SNP and SNT

Initial dye conc	Temp (K)	q_e^{exp}	Pseudo-first-order			Pseudo-second-order			Intraparticle diffusion			Elovich			
			q_e^{cal}	k_{ad}	R^2	q_e^{cal}	k_2	R^2	k_i	C	R^2	A	B	R^2	x
SNP	298		(mg/g)			(mg/g)			(mg/gmin$^{-1/2}$)						
30 mg/L		104.9	4.70	0.0221	0.8854	106.4	0.0562	0.9999	4.52	54.4	0.6728	16.3	27.2	0.8669	1.67
60 mg/L		173.6	3.72	0.0213	0.9558	175.4	0.0174	0.9999	3.78	129.3	0.78				
90 mg/L		220.2	4.35	0.0191	0.8261	217.4	0.0216	0.9959	9.04	178.2	0.6116				
30 mg/L	308	99.4	4.12	0.0287	0.9548	104.2	0.0914	0.9942	5.28	39.6	0.8017	18.0	11.2	0.9338	0.6224
30 mg/L	318	95.0	4.04	0.031	0.9399	99.0	0.086	0.9954	5.35	39.3	0.7627	17.6	10.9	0.9235	0.620
SNT	298														
30 mg/L		100.9	3.81	0.0230	0.9186	103.1	0.0658	0.9974	4.54	49.6	0.7861	15.7	24.3	0.9436	1.54
60 mg/L		164.8	3.86	0.0241	0.8726	166.6	0.0118	0.9998	5.22	129.5	0.6625				
90 mg/L		205.2	4.58	0.0331	0.9141	212.5	0.283	0.9975	9.54	103.0	0.6544				
30 mg/L	308	94.8	3.77	0.0311	0.886	98.0	0.0596	0.9981	4.32	47.5	0.7354	15.6	21.9	0.926	1.40
30 mg/L	318	91.2	3.64	0.0248	0.8655	93.5	0.0646	0.9982	4.24	44.9	0.7122	15.2	19.6	0.9136	1.29

High correlation coefficients ($R^2 > 0.99$) were obtained for the pseudo second order model and the rate constant (k_2) and q_e values were determined from the plot. As the temperature increased, the q_e value decreased. Experimental and theoretical q_e values were very similar, hence, this model was best adsorption of MB and MR on SNT and SNP as compared to the pseudo-first-order model as observed by Kushwaha et al. (2014) and Shao et al. (2014). The intraparticle diffusion model was obtained from a plot of q_t *vs* $t^{0.5}$. A large *C* intercept for intraparticle diffusion plot (proportional to boundary thickness) value is indicative of surface adsorption and intraparticle diffusion is the rate limiting step (Han et al., 2010, Kushwaha et al., 2014). The term *k*i is obtained from the slope. The values of *k*i and *C* are shown in Tables 4.4 and 4.5, where the *C* intercept values were not zero and the lines did not pass through the origin. The plots revealed 3 regions depicting boundary layer diffusion which are followed by intraparticle diffusion in macro, meso and micro pores (Han et al., 2010, Reddy et al., 2012). It was observed that as concentration C_o increased, there was an increase in *k*i and *C* values as also observed by Reddy et al. (2012). Adsorption may therefore be a combination of surface adsorption and intra-particle diffusion (Han et al., 2010).

4.8.5 Effect of temperature

This was carried out to determine the effect of temperature on the adsorption efficiency of SNT and SNP on MR and MB as shown in Table 4.6. Adsorption temperature ranged between 25 - 45 °C. It was observed that the removal efficiency and q_e decreased slightly with an increase in temperature with the process being exothermic. An increase in temperature caused desorption resulting in a decrease in adsorption capacity (Gu et al., 2015).

4.8.5.1 Thermodynamic effects

The 3 thermodynamic parameters, Gibbs free energy (ΔG^o), change in enthalpy (ΔH^o) and change in entropy (ΔS^o) were calculated using equations 4.7 and 4.8 and the results are shown in Table 4.6:

$$ln\, K_d = \frac{\Delta S^\circ}{R} - \frac{\Delta H^\circ}{RT} \qquad (4.7)$$

$$\Delta G^0 = -RT\ lnK_d \tag{4.8}$$

Where T is temperature (K), R ideal gas constant and K_d is the distribution coefficient obtained from experimental data using equation 4.5:

$$K_d = \frac{Equilibrium\ concentration\ of\ MB\ adsorbed\ on\ 0.6SCA-MCM-41}{Equilibrium\ concentration\ of\ MB\ in\ solution} = \frac{(Co-Ce)}{Ce} v/m \tag{4.9}$$

Where v is the volume (mL) of solution and m is mass of sorbent (g).

ΔH^o and ΔS^o values were calculated from the slope and intercept of Van't Hoff plots and are presented in Table 4.6.

A positive ΔS^o which is the change in entropy value was indicative of disorderliness of the solid at the solution interface during the adsorption process (Sajab et al., 2011). The low value for ΔS^o confirmed that no remarkable entropy change occurred (Han et al., 2010). This means that adsorption of MB and MR on SNT and SNP are favoured and are spontaneous at lower temperature. The negative values of ΔH^o at all temperatures became more negative with an increasing temperature, indicating adsorption was better at lower temperatures and the adsorption process was spontaneous.

Table 4.6 Thermodynamic parameters for MB and MR adsorption on SNP and SNT

		MB		
Samples	**T (^{o}C)**	**ΔG^{o} (kJ/mol)**	**ΔH^{o} (kJ/mol)**	**ΔS^{o} (kJ/mol/K)**
SNP	25	-8.353	-9.451	28.0
	35	-8.633		
	45	-8.913		
SNT	25	-8.622	-9.675	28.9
	35	-8.910		
	45	-9.199		
		MR		
SNP	25	-1.705	-1.615	5.71
	35	-1.761		
	45	-1.818		
SNT	25	-1.685	-1.549	5.65
	35	-1.741		
	45	-1.797		

4.8.6 Equilibrium modelling

The models applied in this study on the adsorption of MR and MB on SNT and SNP are Langmuir which is applicable to a homogeneous adsorption system, Freundlich which is suitable for heterogenous adsorption, and Temkin predicts adsorbate-adsorbent interaction and heat of adsorption in equations 4.10, 4.11 and 4.12, respectively. These models were well suited for the experimental data of MB and MR on SNT and SNP, because high correlation coefficients were obtained.

$$\frac{Ce}{qe} = \frac{1}{bQm} + \frac{Ce}{Qm} \quad \text{(4.10)}$$

$$\ln qe = ln\, K_F + \left(\frac{1}{n}\right) ln\, C_e \quad \text{(4.11)}$$

$$ln\ q_e = B\ ln\ A + B\ ln\ C_e \quad \text{.....(4.12)}$$

For the Langmuir model, q_e is the adsorption density (mg/g) at equilibrium, Q_m is the monolayer adsorption capacity (mg/g), b is the Langmuir constant related to the free energy of adsorption (L/mg) and C_e is the equilibrium concentration (mg/L) of the dye in solution. The values of Q_m and b were calculated from slope ($1/Q_m$) and intercepts ($1/bQ_m$) of the linear plots of C_e/q_e *vs* C_e. For the Freundlich isotherm K_F and n are Freundlich constants related to adsorption capacity (mg/g), 1/n is adsorption intensity of adsorbents. K_F and n were calculated from intercept ($ln\ K_F$) and slope (1/n) of the plots of ln q_e *vs* ln C_e.

For the Temkin isotherm B = RT/b, where b is the Temkin constant (J/mol) related to adsorption heat, T = absolute temperature (K), R = gas constant (8.314 J/mol K), and A is the Temkin isotherm constant (L/g). B and A are calculated from slope (B) and intercept (B *ln* A) of the plot of q_e *vs ln* C_e.

In the Langmuir isotherm, it was observed that the values of q_e increased with increasing initial concentration as seen in Tables 4.4 and 4.5. An increased C_o enhanced interaction between the dyes and adsorbents. However, there was a marginal decline in adsorptive capacity of the adsorbents as temperature was increased and C_e values had the same trend as C_o. Values of Q_{max}, b and R^2 are shown in Table 4.7. A higher Q_{max} value for SNP was observed which indicated a higher monolayer adsorption capacity for MR and MB than for SNT (Table 4.6) and both adsorbents had high R^2 values. Hence, because of the high R^2 value and Q_m values obtained, the data obtained fitted into the Langmuir model.

In Table 4.7, for the Freundlich isotherm, the values of 1 indicate that adsorption is favourable (Kushwaha et al., 2014). N > 1 was obtained for all SNT and SNP. The higher K_F value indicated a higher uptake of MB and MR on SNP to SNT. The coefficient of correlation was very high which indicated that the data fitted well into this model as well.

Table 4.7 Isotherm values for the removal of MB and MR at different concentrations on SNP and SNT

	MR		MB	
Isotherm parameter	SNP	SNT	SNP	SNT
Langmuir				
Q_{max} (mg/g)	123.5	121.9	344.9	312.5
b (L/mg)	0.0064	0.0073	0.05	0.06
R^2	0.9999	0.9999	0.9888	0.9908
Freundlich				
K_F (mg/g(mg/L)$^{-1/n}$	61.5	59.1	34.3	32.7
N	4.11	3.74	1.84	1.97
R^2	0.9126	0.9158	0.9614	0.9611
Temkin				
B	37.6	39.4	83.1	75.4
b (J/mol)	66.0	62.9	34.5	32.9
A (L/g)	20.5	20.1	71.8	67.1
R^2	0.9682	0.9694	0.9893	0.9878

The Temkin isotherm values are shown in Table 4.7. Due to adsorbate/adsorbate interaction, the Temkin model indicated that the heat of adsorption of all molecules in the layer would decrease linearly.

From Table 4.8 in comparison to other adsorbents used in the adsorption of MB and MR, SNP and SNT had a higher q_m (mg/g). This indicates that these materials are favourable as adsorbents.

Table 4.8 Comparison of the maximum adsorbent capacity with other adsorbents

	MB	
Adsorbent	Langmuir (mg/g)	References
Magnetic coated SiO_2	49.5	Shariati-Rad et al., 2014
Banana peel	88.5	Harris et al., 2009
Amorphous resin	313-345	Vidhyadevi et al., 2014
SNT	312.5	This study
SNP	344.9	This study
	MR	
Chitin nanoparticles	6.9	Dhananasekaran et al., 2016
Functionalised aerogel & alcogel	43.4-68.2	Saad et al., 2015
Citric acid functionalised silica gel	75-125	Kushwaha et al., 2014
SNT	121.9	This study
SNP	123.5	This study

4.9 Conclusion

In this study elephant grass, regarded as a weed in most countries, was utilized in the synthesis of mesoporous silica. It was found out that 2 wt% of the surfactant to the silica gave silica nanoparticles but as the concentration of the surfactant increased, the morphology of SNP changed dramatically and at 55 wt% surfactant, silica nanotubes was obtained. Relative higher temperatures of above 600 °C may not be ideal for the synthesis of mesoporous silica because it morphs into the crystalline form of silica and becomes relatively inactive as adsorbents. Optimum adsorption of MR and MB onto SNT and SNP occurred at optimum conditions of pH 6 and 10, respectively and a dose of 5 mg for MR and 20 mg for MB at room temperature. SNP performed marginally better as compared to SNT, in the adsorption of MR and MB from aqueous solutions. This may be because of a slightly better surface area. It was established that the Langmuir adsorption isotherm provided the best fit to the experimental data for both dyes onto both adsorbents. The adsorption kinetics best fitted the pseudo-second-order kinetics. This study proved that mesoporous silica from elephant grass is a good adsorbent for the removal of MR and MB from aqueous solution.

4.10 Acknowledgements

The authors are grateful to the School of Chemistry and Physics for the facilities used in this research and also to the AAU small grant for financial assistance.

References

Adam, F., Appaturi, J. N., Khanam, Z., Thankappan, R. & Nawi, M. a. M. 2013. Utilization of tin and titanium incorporated rice husk silica nanocomposite as photocatalyst and adsorbent for the removal of methylene blue in aqueous medium. *Applied Surface Science,* 264**,** 718-726.

Dash, S., Mishra, S., Patel, S. & Mishra, B. K. 2008. Organically modified silica: synthesis and applications due to its surface interaction with organic molecules. *Advances in Colloid and Interface science,* 140**,** 77-94.

Dhananasekaran, S., Palanivel, R. & Pappu, S., 2016. Adsorption of methylene blue, bromophenol blue, and coomassie brilliant blue by α-chitin nanoparticles. *Journal of Advanced Research,* 7, 113-124.

Ghorbani, F., Younesi, H., Mehraban, Z., Çelik, M. S., Ghoreyshi, A. A. & Anbia, M. 2013. Preparation and characterization of highly pure silica from sedge as agricultural waste and its utilization in the synthesis of mesoporous silica MCM-41. *Journal of the Taiwan Institute of Chemical Engineers,* 44**,** 821-828.

Ginimuge, P.R. & Jyothi, S.D., 2010. Methylene blue: revisited. *Journal of Anaesthesiology, Clinical Pharmacology*, *26*(4), 517-520.

Gu, F., Liang, M., Han, D. & Wang, Z. 2015. Multifunctional sandwich-like mesoporous silica–Fe_3O_4–graphene oxide nanocomposites for removal of methylene blue from water. *RSC Advances,* 5**,** 39964-39972.

Han, R., Zhang, L., Song, C., Zhang, M., Zhu, H. & Zhang, L. 2010. Characterization of modified wheat straw, kinetic and equilibrium study about copper ion and methylene blue adsorption in batch mode. *Carbohydrate Polymers,* 79**,** 1140-1149.

Haris, M.R. & Sathasivam, K., 2009. The removal of methyl red from aqueous solutions using banana pseudostem fibers. *American Journal of Applied Sciences*, *6*(9),1690-1670.

Hu, S. & Hsieh, Y.-L. 2014. Preparation of activated carbon and silica particles from rice straw. *ACS Sustainable Chemistry & Engineering,* 2**,** 726-734.

Jal, P., Patel, S. & Mishra, B. 2004. Chemical modification of silica surface by immobilization of functional groups for extractive concentration of metal ions. *Talanta,* 62**,** 1005-1028.

Jaroenworaluck, A., Pijarn, N., Kosachan, N. & Stevens, R. 2012. Nanocomposite TiO_2–SiO_2 gel for UV absorption. *Chemical Engineering Journal,* 181**,** 45-55.

Kushwaha, A. K., Gupta, N. & Chattopadhyaya, M. 2014. Enhanced adsorption of methylene blue on modified silica gel: equilibrium, kinetic, and thermodynamic studies. *Desalination and Water Treatment,* 52**,** 4527-4537.

Liou, T.-H. 2011. A green route to preparation of MCM-41 silicas with well-ordered mesostructure controlled in acidic and alkaline environments. *Chemical Engineering Journal,* 171**,** 1458-1468.

Lowell, S., Shields, J. E., Thomas, M. A. & Thommes, M. 2012. *Characterization of porous solids and powders: surface area, pore size and density*, Springer Science & Business Media.

Mangrulkar, P. A., Kamble, S. P., Meshram, J. & Rayalu, S. S. 2008. Adsorption of phenol and o-chlorophenol by mesoporous MCM-41. *Journal of Hazardous Materials,* 160**,** 414-421.

Matthews-Amune, O. C. & Kakulu, S. 2012. Determination of heavy metals in forage grasses (carpet grass (Axonopus ompressus), guinea grass (Panicum maximum) and elephant grass (Pennisetum purpureum)) in the vicinity of Itakpe Iron Ore Mine, Nigeria. *International Journal of Pure and Applied Science Technology,* 13**,** 16-25.

Pang, S. C., Chin, S. F. & Yih, V. 2011. Conversion of cellulosic waste materials into nanostructured ceramics and nanocomposites. *Advanced Materials Letters,* 2, 118-124.

Qu, Q. & Gu, Z. 2014. Facile synthesis of hierarchical MCM-41 spheres with an ultrahigh surface area and their application for removal of methylene blue from aqueous solutions. *Analytical Methods,* 6**,** 1397-1403.

Rasalingam, S., Peng, R. & Koodali, R.T., 2014. Removal of hazardous pollutants from wastewaters: applications of TiO_2-SiO_2 mixed oxide materials. *Journal of Nanomaterials*, *2014*, p.10.

Reddy, M. S., Sivaramakrishna, L. & Reddy, A. V. 2012. The use of an agricultural waste material, Jujuba seeds for the removal of anionic dye (Congo red) from aqueous medium. *Journal of Hazardous Materials,* 203**,** 118-127.

Saad, N., Al-Mawla, M., Moubarak, E., Al-Ghoul, M. & El-Rassy, H., 2015. Surface-functionalized silica aerogels and alcogels for methylene blue adsorption. *RSC Advances*, *5*(8): 6111-6122.

Sajab, M. S., Chia, C. H., Zakaria, S., Jani, S. M., Ayob, M. K., Chee, K. L., Khiew, P. S. & Chiu, W. S. 2011. Citric acid modified kenaf core fibres for removal of methylene blue from aqueous solution. *Bioresource Technology,* 102**,** 7237-7243.

Shariati-Rad, M., Irandoust, M., Amri, S., Feyzi, M. & Ja'fari, F., 2014. Removal, preconcentration and determination of methyl red in water samples using silica coated magnetic nanoparticles. *Journal of Applied Research in Water and Wastewater, 1*(1),6-12.

Shao, Y., Wang, X., Kang, Y., Shu, Y., Sun, Q. & Li, L. 2014. Application of Mn/MCM-41 as an adsorbent to remove methyl blue from aqueous solution. *Journal of Colloid and Interface Science,* 429**,** 25-33.

Sivasubramanian, G., Shanmugam, C. & Parameswaran, V. 2013. Copper (II) immobilized on silica extracted from foxtail millet husk: a heterogeneous catalyst for the oxidation of tertiary amines under ambient conditions. *Journal of Porous Materials,* 20**,** 417-430.

Thuc, C. N. H. & Thuc, H. H. 2013. Synthesis of silica nanoparticles from Vietnamese rice husk by sol–gel method. *Nanoscale Research Letters,* 8**,** 1-10.

Vidhyadevi, T., Murugesan, A., Kalaivani, S., Premkumar, M., Vinoth Kumar, V., Ravikumar, L. & Sivanesan, S. 2014. Evaluation of equilibrium, kinetic, and thermodynamic parameters for adsorption of Cd^{2+} ion and methyl red dye onto amorphous poly (azomethinethioamide) resin. *Desalination and Water Treatment,* 52**,** 3477-3488.

Vutskits, Laszlo,Briner, Adrian Klauser, Paul, Gascon, Eduardo, Dayer, Alexandre G Kiss, Jozsef Z Muller, Dominique Licker, Marc J Morel, Denis R. 2008. Adverse effects of methylene blue on the central nervous system. *The Journal of the American Society of Anesthesiologists*, *108***,** 684-692.

Yagub, M.T., Sen, T.K., Afroze, S. and Ang, H.M., 2014. Dye and its removal from aqueous solution by adsorption: a review. *Advances in Colloid and Interface Science*, *209*,172-184.

Zhang, C., Kang, H., Lv, K., Chen, H. & Yuan, S. 2011. Maize phytoliths and photoluminescent silica nanotubes prepared from a natural silica resource. *Industrial & Engineering Chemistry Research,* 50**,** 12521-12526.

Zhuravlev, L. 2000. The surface chemistry of amorphous silica. Zhuravlev model. *Colloids and Surfaces A: Physicochemical and Engineering Aspects,* 173**,** 1-38.

5.0 CHAPTER 5: ENCAPSULATION OF SILICA NANOTUBES FROM ELEPHANT GRASS WITH GRAPHENE/GRAPHENE OXIDE AND ITS APPLICATION IN REMEDIATION OF SULFAMETHOXAZOLE FROM AQUEOUS SOLUTION

Samson O. Akpotu and Brenda Moodley*

School of Chemistry and Physics, University of KwaZulu-Natal, Westville Campus, Durban, 4000, South Africa.

***** corresponding author email: moodleyb3@ukzn.ac.za
Telephone: +27 31 2602796
Fax: +27 31 2603091

5.1 Abstract

In this study silica nanotubes (SNT) that were previously synthesised from elephant grass was now encapsulated with graphene oxide and graphene, to obtain silica nanotubes graphene oxide (SNTGO) and silica nanotubes graphene (SNTG), respectively. This was done to maximally exploit the potential of graphene oxide and graphene as adsorbents. The adsorbents were characterized and applied in the removal of sulfamethoxazole (SMZ) from polluted water. SNTGO was reduced to SNTG and elemental analysis of SNTG revealed it had higher carbon content when compared to SNTGO, thus confirming its more hydrophobic nature. SNTGO had an adsorption capacity of 125 mg/g which increased to 248 mg/g when it was reduced to SNTG. The pseudo-second order model best described the adsorption kinetics and the Freundlich isotherm was the best fit for the equilibrium data. The thermodynamic studies showed that the adsorption process was spontaneous and exothermic. The desorption studies carried out revealed that the adsorbent could be regenerated and reused in the adsorption of SMZ. SNTG was a better adsorbent when compared to SNTGO because of its better adsorption capacity and therefore showed better properties for wastewater remediation as compared to SNTGO.

Keywords: *Silica nanotubes, graphene oxide, graphene, sulfamethoxazole, adsorption*

5.2 Introduction

Pharmaceuticals have recently been classified as emerging organic pollutants in aquatic systems (Wan et al., 2014, Jones et al., 2005, Ziylan and Ince, 2011). Antibiotics have been widely used by humans for over a century to treat and prevent diseases (Zhang et al., 2010b). Sulfamethoxazole (SMZ) is part of a class of antibiotics that has found use in livestock production, treatment of human ailments such as urinary tract infection (White, 2011) and aquaculture (Thiele-Bruhn, 2003). The ImpactX database puts its use as a physcholeptic drug at 5 x 10^3 µg/L as a mixture of SMZ and trimethoprim in South Africa. Due to its widespread use, disposal is a major problem and as a result it often gets discharged into the environment (soil and water) (Kemper, 2008, Zhang et al., 2011b) with concentrations of 2, 27.2 and 0.016 µg/L of SMZ found in municipal sewage treatment plants, hospital waste and surface water, respectively (Trovó et al., 2009, Martins et al., 2011, Loos et al., 2010). In wastewater treatment plant in South Africa, Matongo et al (2015) found SMZ contration between the range of 7.93 -35.4 µg/L. SMZ, like most antibiotics has environmental risks associated with its usage. SMZ has p*K*a values of 1.7 and 5.7 and therefore can exist as cations, anions or zwitterions (Nam et al., 2015). This together with its slow metabolism and poor degradation, makes it persistent in the environment and results in an undesirable impact on microbial communities posing a great risk to non-target species in the ecosystem (Bouki et al., 2013). Therefore research has now focused on the removal of pharmaceuticals from wastewater. These pharmaceuticals are not easily removed by conventional water treatment systems (Zhang et al., 2010b, Wan et al., 2014).

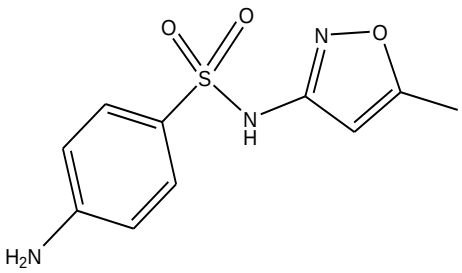

Figure 5.1 Structure of sulfamethoxazole

Adsorption is the preferred method of choice for the removal of SMZ and studies have investigated its removal from aqueous media by adsorption with manganese ferrite (Wan et al., 2014),

biochar (Lian et al., 2014), sediment (Zhang et al., 2012), soil (Ji et al., 2011), and activated carbon (Wang et al., 2014a, Nielsen et al., 2014). Thus far activated carbon (AC) has proven to be most effective as a sorbent for SMZ because of its large surface area, surface functional groups and delocalised π-electrons making it a fairly efficient asorbent for pharmaceuticals. However, the major drawback of adsorbing organic pollutants with AC is the complexity of the separation process of adsorbate from adsorbent due to the fine powdered nature of AC (Liu et al., 2013). Consequently, there is a need to develop a sorbent with a simpler separation mechanism. Carbon based nanomaterials are materials that are promising as sorbents because of their large surface area and pore volumes and these include carbon nanotubes (CNTs), graphene oxide and graphene. To improve the separation of these carbon based sorbents in aqueous solution, it is best anchored on a substrate such as silica, thus giving it a wider reach when interacting with pollutants. This process is referred to as encapsulation of the substrate by carbonaceous materials.

Graphene gained prominence, after it was isolated and characterised in 2004 by Novoselov et al. (2004). It is a 2-dimensional nanomaterial that is one carbon atom thick, arranged in a honey comb lattice structure. It has found various uses due to its high theoretical surface area (approximately 2630 m^2/g), electron rich π-system, and excellent mechanical, thermal and electrical properties (Meng et al., 2015, Al-Khateeb et al., 2014, Dreyer et al., 2010). Despite graphene's highly hydrophobic nature and ability to bind to organic pollutants through $\pi - \pi$ interactions, the potential maximum adsorption capacity is not always achieved. This is because graphene nanosheets form aggregates in aqueous solution due to van der Waals forces and a very strong $\pi - \pi$ interaction between the carbon layers. On the other hand, graphene oxide is made up of a single layer of graphite oxide and present on its surface is an abundance of oxygen functional groups making it easily dispersed in water. The numerous oxygen functional groups make it an excellent precursor in the synthesis of GO based adsorbents. Nonetheless, GO has a low affinity for organic pollutants because of its weak $\pi -$ electron structure and the influence of oxygen on van der Waals interactions, thereby rendering the GO surface strongly hydrophilic (Shi et al., 2015).

A potential way to make graphene/graphene oxide highly efficient as an adsorbent of organic pollutants is by loading G/GO on a low cost support (Yang et al., 2015b) which enables maxi-

mum utilization of the carbonaceous material as an adsorbent. Hence, the fabrication of a silica-graphene oxide/graphene hybrid adsorbent which has been utilized as liquid chromatographic packing material (Liang et al., 2012), solid-phase extraction sorbent (Luo et al., 2013, Shi et al., 2015), and a sorbent for uranium in water (Meng et al., 2015). Silica nanotubes from elephant grass agrowaste represent an excellent support for GO/G. This is because it is obtained from agrowaste of which thousands of tons are burnt yearly, is non-toxic which is important as an application in water treatment, and also because of the ease of production of the GO/G encapsulated silica nanotubes.

Silica, despite having the qualities of a good adsorbent such as a high surface area, is not as useful as an adsorbent for the adsorption of organic pollutants in aqueous media. This is because of its highly hydrophilic nature, which means it becomes attracted to water molecules in solution when used as a sorbent (Gibson, 2014b). In a bid to make silica hydrophobic, it is encapsulated with a highly hydrophobic material such as carbonaceous graphene oxide or graphene. This encapsulation is important as it serves 2 purposes: (i) it helps with an improved dispersion of graphene/graphene oxide because of their hydrophobic nature and (ii) it creates a better separation of the adsorbent and adsorbate when in solution. In a bid to surmount these challenges, silica nanotubes were synthesized from elephant grass and were encapsulated with graphene oxide and graphene.

In this study we report for the first time the encapsulation of previously synthesised silica nanotubes (SNT) from elephant grass with graphene/graphene oxide and its application as a highly efficient adsorbent for the remediation of sulfamethoxazole from wastewater. The adsorbents were characterized using elemental analysis (EA), FT-IR spectroscopy, thermogravimetric analysis (TGA), x-ray diffraction (XRD) studies, textural analysis, scanning electron microscopy (SEM) and transmission electron microscopy (TEM). Sulfamethoxazole was selected as a model pharmaceutical pollutant to determine the efficiency of the developed adsorbents and in understanding the adsorption mechanism. The relative low cost and green technique for the production of SNT from agrowaste, coupled with the simple procedure of encapsulation and its high efficiency makes it a potential adsorbent for the removal of pharmaceutical pollutants in wastewater.

5.3 Materials and Methods

5.3.1 Materials

Natural graphite powder, methanol (HPLC grade), hydrazine monohydrate (80%), 3-aminopropyl triethoxysilane (APTES, 99%), HCl (37%), $KMnO_4$ and the pharmaceutical sulfamethoxazole were obtained from Sigma-Aldrich. Absolute ethanol (Merck), cetyltrimethyl ammoniumbromide (CTAB 99%+) (Cabiochem), H_2SO_4 (98%), H_2O_2 (35%) and H_3PO_4 (80%) were obtained from Promark. All the reagents were analytically pure and were used without further purification. MilliQ water was used in the preparation of standard solutions and the mobile phase used for chromatography analysis. Elephant grass was obtained from the area around the University of KwaZulu-Natal, Westville Campus in Durban, South Africa.

5.3.2 Synthesis of silica nanotubes

The synthesis of SNT is described in detail in section 4.3.3**.**

5.3.3 Activation of SNT

This was done using a modified procedure from Kushwaha et al. (2014). Approximately 40 mL of 6 M HCl was added to SNT (1 g) and the mixture refluxed at 100 °C with continuous mechanical stirring for 4 h and thereafter cooled to room temperature. The material was vacuum filtered and washed until neutral pH and dried in an oven at 150 °C for 5 h. This was assigned as A-SNT.

5.3.4 Synthesis of NH_2-SNT

The surface of the SNT obtained was modified by an aqueous easy one-step synthesis. Approximately 1 g of SNT was dispersed in 30 mL of ethanol, which was sonicated for an hour and stirred for another hour. Approximately 500 µL of APTES was added to bind $–NH_2$ to SNT. The reaction was stirred at 50 °C for 8 hrs to obtain a monolayer and a positively charged SNT. The product was collected by filtration and vacuum dried at 60 °C.

5.3.5 Synthesis of GO

GO was synthesized using a modified Tour method (Marcano et al., 2010). Briefly, a 9:1 mixture of concentrated H_2SO_4:H_3PO_4 (360 mL : 40 mL) was added to a mixture of 3 g of graphite powder and 18 g of $KMnO_4$ and manually stirred in a beaker. It was then mechanically stirred on a hotplate at a temperature of 50 °C for 12 h, 400 mL of ice was then added into the mixture and 4 mL H_2O_2 was added to stop the reaction. The product was filtered to remove the unoxidised graphite powder, the filtrate was centrifuged and the supernatant decanted. The remaining solid was washed with water, HCl and ethanol (twice) and filtered through a 0.45 µm filter. The solid product was transferred to a dialysis tube and kept there for a month to discharge acid, with the water in the dialysis tube holder constantly changed. The brown solid graphene oxide was finally dried under vacuum.

5.3.6 Synthesis of SNT-GO and SNT-G

In this encapsulation process, SNT-NH_2 was dispersed and sonicated in water. GO (10 mg/L) previously sonicated for 2 hrs was added to the suspension and the pH was adjusted to 7 by adding NH_4OH whilst stirring. It was stirred continuously for 8 hrs and left to settle for an hour. The product was filtered, washed with water and dried in a vacuum oven for 6 hrs at 50 °C. This was labelled as SNTGO. In the synthesis of SNTG, a similar procedure as that for SNTGO was adopted but the temperature of synthesis was 80 °C and hydrazine monohydrate was added to the mixture to reduce GO to G. The mixture was stirred for 8 hrs, left to settle for an hour, filtered, washed with water and dried under vacuum. The solid black product was oven dried in a vacuum at 80 °C for 6 hrs. This was labelled SNTG.

5.3.7 Adsorption studies

Several 15.0 mL working solutions of 12.5 mg/L SMZ were prepared. The natural pH of the solution was used or otherwise stated adjusted using 0.1 M NaOH or 0.1 M HCl to the desired pH. An amount (0.05 g) of the adsorbent was added to the solution and it was shaken with a mechanical shaker (Scientific Engineering) for a period of time. Thereafter, the solution was centrifuged

at 5000 rpm for a minute to collect the supernatant. The supernatant was filtered with a 0.45 µm (cellulose acetate) filter disc and the concentration of SMZ in the solution was determined. The percentage adsorption was calculated using the equation below:

$$\%\, adsorption = \frac{(C_o - C_e)}{C_0}\, x\, 100 \qquad (5.1)$$

Where C_0 is the initial concentration (mg/L), C_e is the equilibrium concentration after a set time in mg/L. Kinetic studies were carried out using 150 mg of adsorbents with 200 mL of 25, 50, 75 and 100 mg/L of SMZ solution and the pH was adjusted to 2, using 0.1 M NaOH/0.1 M HCl solutions. Aliquots of the solution were withdrawn periodically (2 – 1440 mins), filtered, and the concentration of SMZ adsorbed was determined. The experimental data obtained were applied to the pseudo-first order, pseudo-second order, intraparticle diffusion and Elovich kinetic models. The equations for these models are shown in Table 5.1. The adsorption capacity was calculated from equation 5.2:

$$q = \frac{(C_o - C_e)V}{m} \qquad (5.2)$$

Where q is the amount of SMZ adsorbed by the adsorbents in mg/g, V is the initial volume of solution in L and m is the adsorbent mass in g.

Table 5.1 Kinetic models

Models	Equations	References
Pseudo first-order	$ln\,(q_e - q_t) = \ln q_e - ln\ k_i t$	(Ho and McKay, 1998)
Pseudo second-order	$\frac{t}{q_t} = \frac{1}{K_2\, q_e^2} + \frac{t}{q_e}$	(Ho and McKay, 1998)
Intraparticle diffusion	$q_t = K_i t^{0.5} + C$	(Kushwaha et al., 2014)
Elovich	$q_t = a\ ln\ t + b$	(Han et al., 2010)

Where q_e and q_t are the amount of SMZ adsorbed (mg/g) at equilibrium and time t (mins), respectively; k_i is the rate constant of the pseudo first-order kinetic model (min^{-1}). K_2 is the rate constant (g/mg/min) of pseudo second-order kinetic model for adsorption. For intraparticle diffusion model, C (mg/g) is the intercept and K_i is the intraparticle diffusion rate constant (g/mg $min^{/0.5}$) for adsorption. The Elovich coefficient is obtained from the plot of q_t *versus* $ln\ t$. The initial adsorption rate, a, and the desorption constant, *b*, were calculated from the intercept and slope, *x* is the initial adsorption rate (mg/g min) and is calculated by a division of a over *b*.

For thermodynamic studies, 0.05 g of the adsorbent was placed in the SMZ solution and adjusted to pH 2. The mixture was agitated in a thermostatic shaker bath at varying temperatures of 293, 303 and 313 K for 24 hrs. The solutions were centrifuged at 4000 rpm for 1 min and filtered with a 0.45 µm filter disc before the concentration of the filtrate was determined using HPLC. The equilibrium data obtained were analysed with the following isotherm models; Langmuir, Freundlich, Temkin and Dubinin-Radushkevich models. The equations for these models are presented in Table 5.2. Thermodynamic parameters such as change in enthalpy (ΔH°), change in Gibbs energy (ΔG°) and change in entropy (ΔS°), were also calculated. Experiments were carried out in duplicate and blanks were also carried out to ensure the integrity of the analytical procedure.

Table 5.2 Adsorption isotherm models

Models	Equations	References
Langmuir	$\frac{C_e}{q_e} = \frac{1}{bq_m} + \frac{C_e}{q_m}$	Kushwaha et al. (2014)
Freundlich	$ln\, q_e = ln\, K_F + \left(\frac{1}{n}\right) \ln C_e$	Kushwaha et al. (2014)
Temkin	$ln\, q_e = B \ln A + B\ lnC_e$	Kushwaha et al. (2014)
D-R	$ln\, q_e = lnq_m - \beta\varepsilon^2$	Shao et al. (2014)

In the D-R model, β is a constant related to the mean free energy (mol^2/kJ^2), q_m is the theoretical capacity and ε is the Polanyi potential defined as:

$$\varepsilon = RTln\ (1 + \frac{1}{Ce}) \quad (5.3)$$

Where R is the gas constant in J/mol/K) and T is temperature K. The B value is the mean energy of adsorption. E is calculated using the equation:

$$E = \frac{1}{\sqrt{-2\beta}} \quad (5.4)$$

E is the mean free energy E (kJ/mol/L) of the adsorption per molecule of the adsorbate, C_e is the equilibrium concentration of SMZ in solution (mg/L), b is the Langmuir constant related to the free energy of adsorption (L/mg), q_m is the theoretical limit of adsorption capacity when the monolayer surface is fully covered with molecules (mg/g), K_F and N are Freundlich constants, in the Temkin isotherm, B = RT/b where b is Temkin constant in J/mol, A is Temkin isotherm constant (L/g). R is gas constant, T is temperature in K.

5.3.8 Real water samples

Water samples were obtained from the Blue Lagoon (BLG) (mouth of the Umgeni River into the Indian Ocean) with co-ordinates of 29° 48’ 41” S and 31° 02’ 12” E, and the Northern Wastewater Treatment plant (WWTP) (inlet point) with co-ordinates of 29° 48’ 27” S and 30° 59’ 51” E, in Durban, South Africa. Samples were filtered using a 0.45 µm filter disc and were kept in amber bottles, wrapped in aluminium foil and stored at 4 °C. The physical properties of the water samples are shown Table 5.3. The concentration of SMZ in samples was determined initially and was found to be below the detection limit of the HPLC. A 10 mL aliquot of the real water samples were spiked with 0.125 mL (1000 mg/L) SMZ to obtain a concentration of 12.5 mg/L. The samples were equilibrated overnight and 0.05 g of the adsorbents were added to the spiked samples and shaken for 60 mins. The suspension was centrifuged and filtered and the removal efficiency and adsorption capacity for SMZ was evaluated with equation 5.1 and equation 5.2, respectively.

Table 5.3 Physical parameters of the water samples

Parameter	WWTP	BLG
pH	4.04	3.39
TDS (mg/L)	670	3100
Conductivity (mS)	1000.1	5200.3
Res (Ω)	729	150.7
Redox (mV)	93.5	181.3
Temp (°C)	22.0	22.5

5.4 Adsorbent Regeneration

In order to regenerate the adsorbents used, the adsorbents were washed with acidic ethanol at a pH of 2. It was then dried in a vacuum oven at a temperature of 60 °C and the adsorption capacity was calculated. The washing and recycling was carried out twice on the same adsorbent material.

5.5 Results and Discussion

The materials synthesized were characterized with various techniques to determine the suitability of its properties for the removal of SMZ from solution. The efficiency of SNTGO and SNTG in the adsorption of SMZ was determined using a batch adsorption process.

5.5.1 Synthesis of SNT

Silica nanotubes were synthesized using elephant grass as a precursor for the generation of mesoporous silica. The use of an agrowaste material, elephant grass, resulted in a high purity silica with moderate yield. After calcination the white powder obtained was analysed using XRF and FTIR. The XRF analysis showed a high purity silica (99.7%) was obtained. The FTIR spectrum showed the appearance of sharp peaks at 3340 cm^{-1} (-OH stretching), 1630 cm^{-1} (-OH bending), 1047 cm^{-1} (Si-O-Si asymmetric stretching) and 780 cm^{-1} (Si-O-Si symmetric bending) vibrations, respectively (Figure 5.4). This confirmed that silica was synthesized.

5.5.2 Characterisation of adsorbents

5.5.2.1 Thermogravimetric analysis

TGA was carried out to determine the thermal stability, purity and volatile portion of SNT, GO, SNTGO and SNTG with a temperature range from 25 °C to 900 °C, using a mass of 5 mg placed on an aluminium pan in the presence of nitrogen gas at a ramp rate of 10 °C/min. Their profiles are shown in Figure 5.2. The weight loss below 100 - 130 °C was attributed to the evaporation of physisorbed water in all samples. In SNT, there was a further weight loss of 10% between 350 – 450 °C which was due to the decomposition of the residual carbon and condensation of the adjacent silanol. Thereafter, no mass loss was observed. In GO, there was a remarkable weight loss between 200 °C to 250 °C attributed to the removal of the oxygen containing functional group (epoxy, carbonyl and carboxyl) which was also observed by Liu et al. (2013). In SNTGO and SNTG, there was a lower weight loss when compared to GO which can be attributed to the presence of graphene oxide and graphene on SNT, respectively. SNT had a higher thermal stability than GO and G on their own, hence, the possible encapsulation on silica helped in increasing GO and G thermal stabilities present on SNT. The weight loss before 250 °C SNTGO and SNTG was insignificant and this is indicative of the stability of both materials. However, at 250 °C to 550 °C, SNTGO and SNTG lost 15% and 25% amount of its weight, respectively. This loss in weight is due to the thermal degradation of (carbon) graphene oxide and graphene on SNTGO and SNTG, respectively.

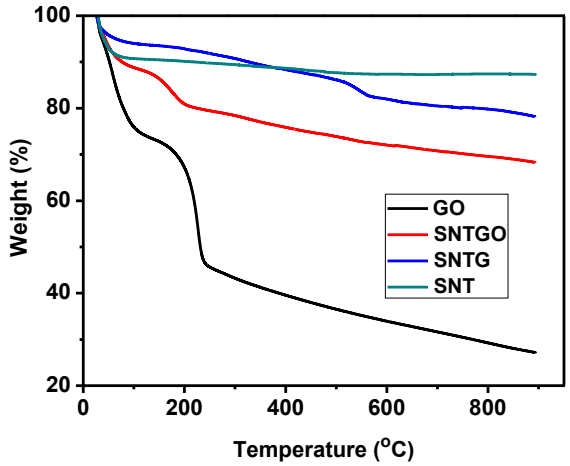

Figure 5.2 TGA profiles of GO, SNT, SNTGO and SNTG

5.5.2.2 Elemental analysis (EA)

The elemental compositions of the samples are presented in Table 5.4. GO had a carbon content of 47.6%. Comparing SNT to SNTGO and SNTG, the carbon content increased by 0, 17 and 21.4%, respectively. The lower H/C ratio of SNTG to SNTGO shows that SNTG was more aromatic, whereas the lower O/C ratio shows that SNTG was less hydrophilic than SNTGO as was also observed by Wang et al. (2014b), (Gao et al., 2009). There is still the presence of oxygen from the silica, however, SNGT and SNTGO now have a higher C/O ratio due to the presence of the carbon which gives SNTG and SNTGO their hydrophobicity.

Table 5.4 Elemental composition and atomic ratios, and surface areas (SA) of SNT, GO, SNTGO and SNTG

Sample	SNT	GO	SNTGO	SNTG
C/%	<0.6	37.6	17	21.4
H/%	<0.6	2.23	1.76	1.39
O/%	60	49.5	79.9	75
N/%	0	0.58	1.4	3.00
H/C	NA	0.71	1.24	0.78
O/C	NA	1.75	6.25	4.66
SA/m^2/g	402	38	152	100
Pore volume/cm^3/g	0.67	0.017	0.47	0.52
Pore diameter/nm	50	38.2	23.8	39

NA-Not applicable

5.5.2.3 Textural analysis

The nitrogen sorption isotherm results of GO, SNT, SNTGO and SNTG are shown in Table 5.4. All materials exhibited a distinctive type IV isotherm typical of mesoporous materials (Sing, 1985) as seen in Figure 5.3. GO had a H_3 hysteresis loop over a relative pressure of P/P_o 0.4-1.0. This type of loop is characteristic of materials having agglomerate particles with slit shape pores of irregular size and shape. However, SNT, SNTG and SNTGO had a H_2 hysteresis loop which typifies porous materials (Meynen et al, 2009). The materials were regular and uniformly packed agglomerates (Adam et al., 2013). The textural properties from the N_2 adsorption-desorption analysis are shown in (Table 5.4). The decreasing surface area in SNTGO and SNTG can be ascribed to their surface coverage by graphene oxide and graphene, respectively, causing the mate-

rials to have smaller surface area and porosity than SNT. This is in agreement with the elemental analysis which suggests that as more carbon is loaded on silica, its surface area decreases. The pore size distribution for GO showed it was made up of irregular shaped pores whereas SNT, SNTG and SNTGO had a monomodal pore system.

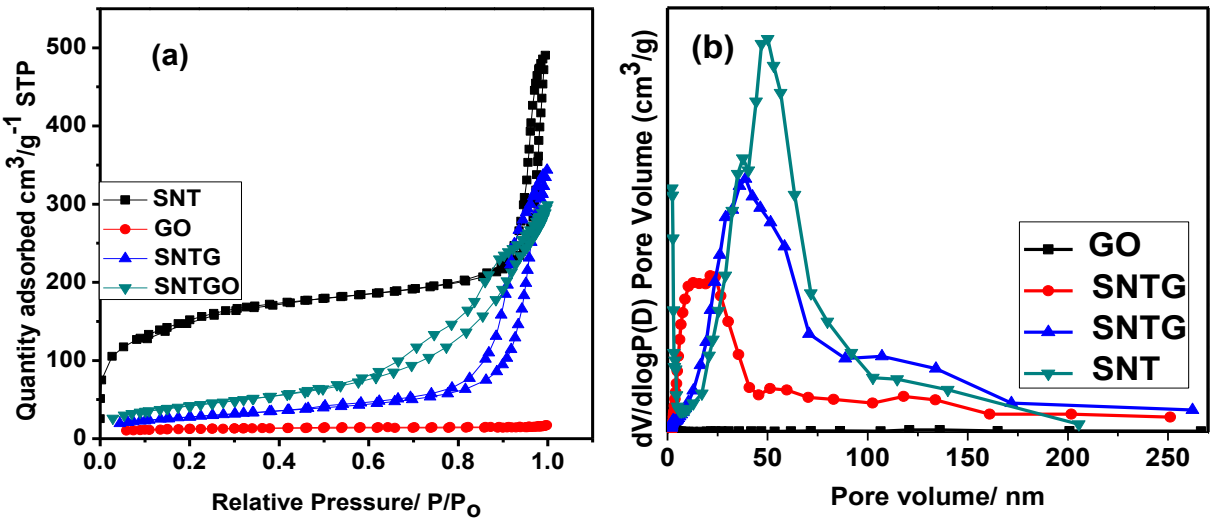

Figures 5.3 (a) N_2 adsorption desorption isotherm and (b) Pore size distribution of GO, SNT, SNTG and SNTG

5.5.2.4 FTIR analysis

The FTIR spectra of SNT, GO, SNTG and SNTGO is shown in (Figure 5.4). The peak around 3380 cm^{-1}, 3250 cm^{-1} and 3420 cm^{-1} are due to -OH stretching vibration in GO, SNTGO and SNT, respectively. In GO, the carbonyl vibration is seen at 1364 cm^{-1}, the vibrations present at 1727 cm^{-1} and 1632 cm^{-1} are attributed to C=O stretching of the carboxylic acid substituent, the vibration at 1226 cm^{-1} is attributed to the C-O (epoxy) and the peak at 1065 cm^{-1} is attributed to C-O alkoxyl vibration. This is consistent with the findings from Marcano et al. (2010) and Liu et al. (2013). When compared to GO, SNTGO and SNTG had peaks which are distinctive for silica. This implied that SNT was successfully coated with GO and G. In SNTGO, there was a shift of the peak to 1619 cm^{-1} from 1637 cm^{-1} which is seen in SNT and also there was the formation of a new peak at 1415 cm^{-1} which corresponded to -C=O stretching vibration. SNTGO had a similar profile to GO, which indicated the successful encapsulation of GO on SNT. In SNTG, there were

no peaks due to the carbonyl, C-O-C and epoxy groups. The band at 1040 cm^{-1} in SNTG which shifted from 1047 cm^{-1} in SNT was attributed to the Si-O-Si/Si-O-C asymmetric vibration and Si-O-C was linked by covalent bonds, which was also observed by Liu et al. (2013). There was also a reduction in the peak intensity of SNTG. This indicated that the carboxylic group was converted to a Si-O-C bond as was also observed by Meng et al. (2015). The peaks at 780 and 430 cm^{-1} were assigned as Si-O-Si symmetric and bending vibrations, respectively. In SNT, the peak at 1637 $cm^{-1}$for Si-OH bending vibration shifted to 1555 cm^{-1} which is Si-O-C in SNTG. In pure graphene, the peak at 1555 cm^{-1} is a -C=C- which is assigned as an amide group stretching vibration signifying the vinyl group was successfully introduced into SNTG (Meng et al., 2015). The results were clearly in agreement with the results from the elemental analysis.

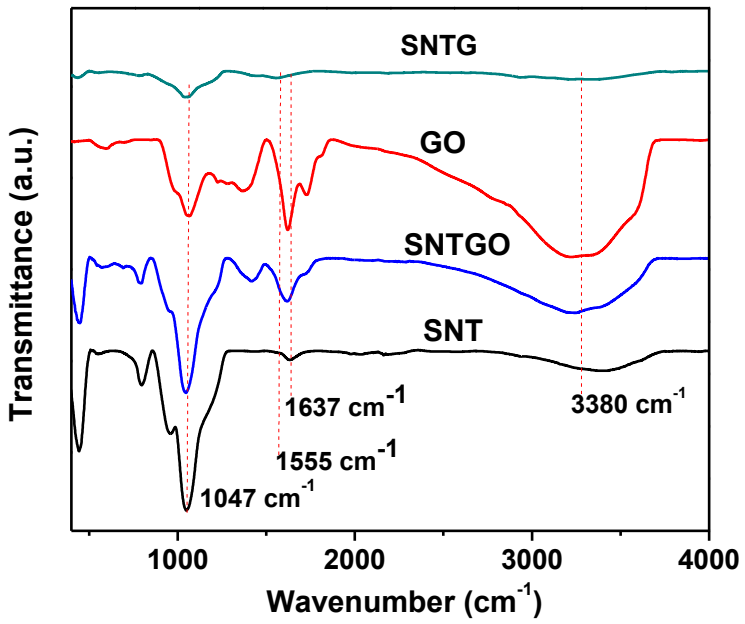

Figure 5.4 FTIR spectra of SNT, SNTGO, SNTG and GO

5.5.2.5 X-ray diffraction analysis

The XRD patterns for GO, SNT, SNTGO and SNTG are shown in Figure 5.5. An intense peak (001) at 2(Θ) = 9.74 which is GO peak and is typical for amorphous carbon was observed which fits the inter-planar spacing of 0.87 nm, which was also observed by Liu et al. (2013). The XRD profiles of SNT, SNTGO and SNTG had the amorphous nature of silica with a broad peak cen-

tred at 2(Θ) = 23 (Adam et al., 2013). This showed that the silica matrix was encapsulated by graphene and graphene oxide as seen in SNTG and SNTGO, respectively. In SNTG, the peak around 25.4 is typically the peak for graphene as also observed by Luo et al. (2013). The diffraction peak of SNTGO 2(Θ) = 26.20 is typically that of graphite (002) and this is because GO containing oxygen functional groups on the surface on SNTGO has been partially transformed to a certain degree as result of the interaction between SNT and GO as also observed by Li et al. (2015).

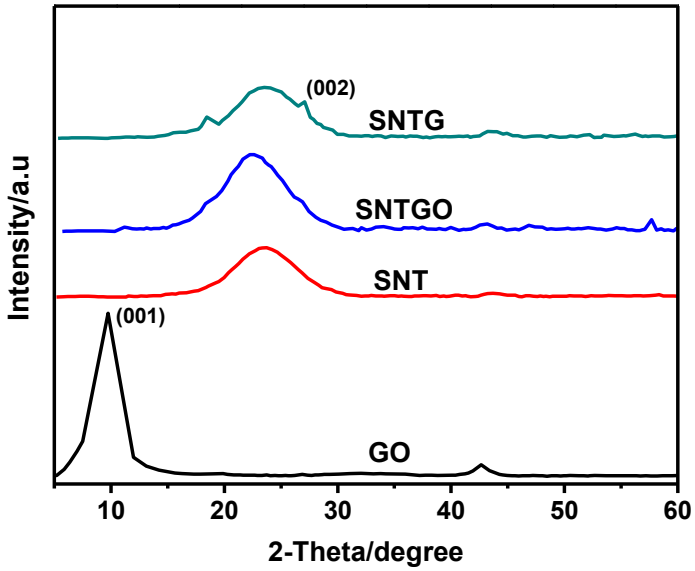

Figure 5.5 XRD profiles of GO, SNT, SNTGO and SNTG

5.5.2.6 FEGSEM and TEM analysis

The surface morphology of GO, SNT, SNTG and SNTGO was studied by SEM and TEM imaging techniques (Figure 5.6). The surface of the GO sheets obtained was smooth but also had pores and was a little transparent as seen on the TEM image (Figure 5.6 (e)) (Marcano et al., 2010). The SNT appeared as long webbed like tubes, with very visible large pores (SEM Figure 5.6 (b) and TEM 5.6 (f)). When SNTGO and SNTG were compared with SNT, there was a visible change in the structure. In SNTGO, the silica matrix was encapsulated under thin layers of homogeneous graphene oxide sheets which appeared transparent and the GO sheet was well layered and bonded on the SNT. The SNT pores can be seen under the graphene oxide coating (Fig-

ures 5.6 (c) (SEM) and 5.6 (g) (TEM)). In SNTG, the graphene layers appear as a thick stack on top of the silica matrix. It can be seen that total encapsulation occurs as the transparency was lost (Figure 5.6 (h)) and with no appearance of graphene as free standing. This can be attributed to the increase in percentage carbon by the chemical reduction of graphene oxide to graphene by hydrazine monohydrate. This is in agreement with results obtained from the elemental analysis, and the decrease in specific surface area from textural analysis and FTIR analysis. The SEM and TEM images suggest that the morphology of the synthesized SNTGO and SNTG depended more on the morphology of SNT rather than GO. It is also observed that there was no aggregation from the graphene sheets.

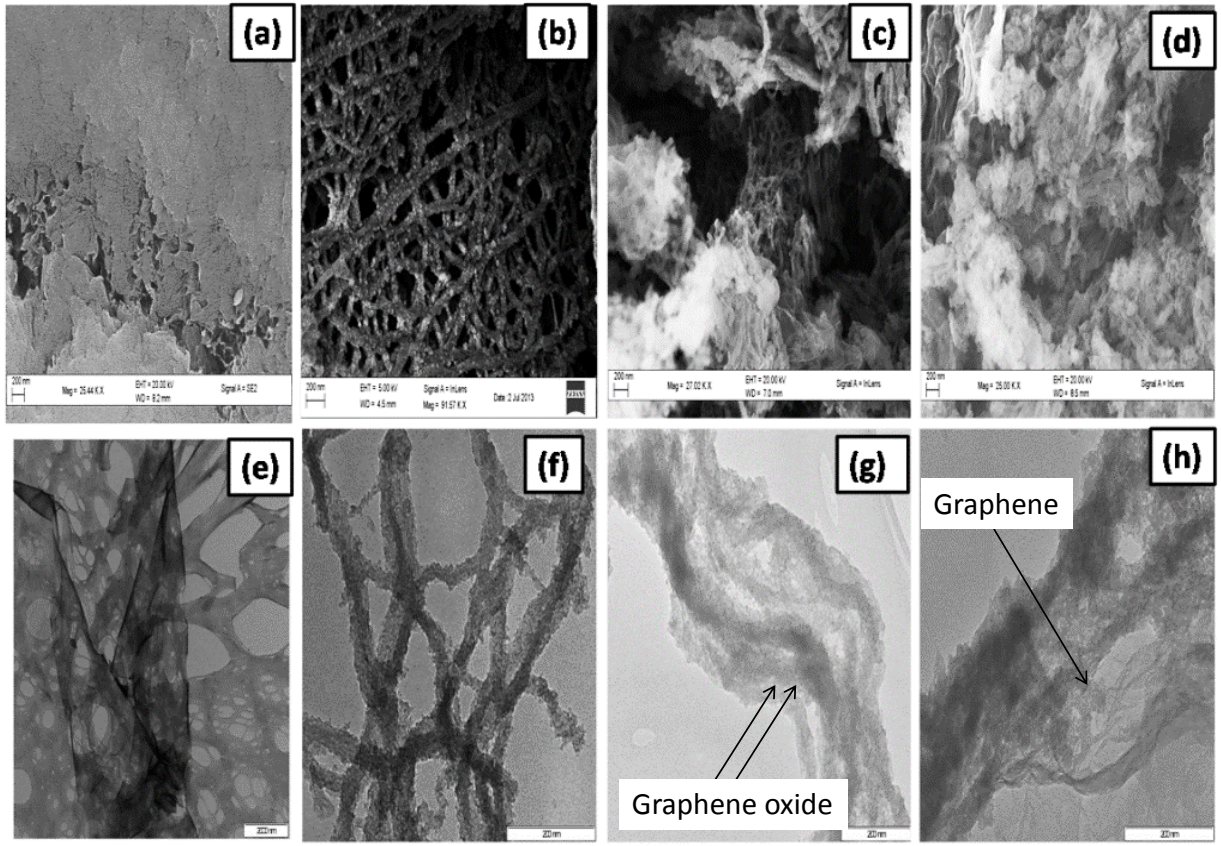

Figures 5.6 SEM of (a) GO (b) SNT (c) SNTGO (d) SNTG and TEM of (e) GO (f) SNT (g) SNTGO and (h) SNTG

5.6 Batch Adsorption Studies

Adsorption experiments were carried out to determine the efficiency of SNTGO and SNTG on the removal of SMZ from a simulated model water solution. The role of pH, ionic strength, adsorbent dose, contact time and temperature were carried out to determine the most suitable conditions for the removal of SMZ. Thermodynamics, kinetics and isotherm studies were also carried out.

5.6.1 The effect of pH on adsorption of SMZ on SNTGO and SNTG

Figure 5.7 shows the effect of pH on the adsorption of SMZ on SNTG and SNTGO. Liu et al. (2014) predicted 3 ways in which pH affects the adsorption process in pharmaceuticals. Firstly, an increase in pH may cause dissociation of hydrophobic neutral molecules to hydrophilic, negatively charged species, thereby reducing hydrophobic interaction. Secondly, electrostatic repulsion would increase with an increase in solution pH, thereby suppressing electrostatic interaction between the adsorbent and the adsorbate and thirdly, a higher pH could increase π donor ability of the adsorbate, thereby causing π - π interaction. In this study the surface properties of SNTGO and SNTG, such as protonation-deprotonation transition, and surface charge of functional groups were affected by pH as the range varied from 2 - 10. The adsorption of SMZ on SNTGO and SNTG decreased over the pH range by more than 80% which suggested a variety of mechanisms may be responsible for the adsorption. It should be noted that the visibly seen pH effects on adsorption was in agreement with the pH-controlled distribution of the protonated species of SMZ.

The removal of SMZ is highest in an acidic pH (Nam et al., 2015). SMZ at p*K*a $\leq$ 1.7 is cationic, at p*K*a $\leq$ 5.7 it exists as zwitterions (neutral SMZ species) and at p*K*a $\geq$ 5.7, it is anionic. At pH 2, the –COOH functional groups remain protonated, at pH > 5 most of the –COOH groups deprotonate and at pH 9, all the SMZ molecules become deprotonated. Ionizable pharmaceuticals are known to interact with adsorbents through electrostatic attraction or repulsion because of their p*K*a value.

The surface of SNTGO contains a variety of oxygen rich functional groups (C=O, COOH) and SNTG has a carbon rich surface (C=C) and it is these groups which are responsible for adsorption. In solution, SNTGO and SNTG have a negatively charged surface as observed by Li et al., (2013). When the pH is ≤ p*K*a 1.7, SMZ is made acidic, it becomes cationic, thus it binds to the negatively charged surface of the oxygen rich SNTGO and SNTG through electrostatic ion interaction and cation- π bonding. However, at neutral pH, a hydrophobic effect is responsible for the adsorption of SMZ on SNTGO and SNTG. At pH above 7, all SMZ is deprotonated and becomes negatively charged and electric repulsion occurs between anions of SMZ and the negative charge on the GO/G present on SNTGO and SNTG, respectively. Hence, highest adsorption is obtained at acidic pH values which then decrease as the pH becomes more basic.

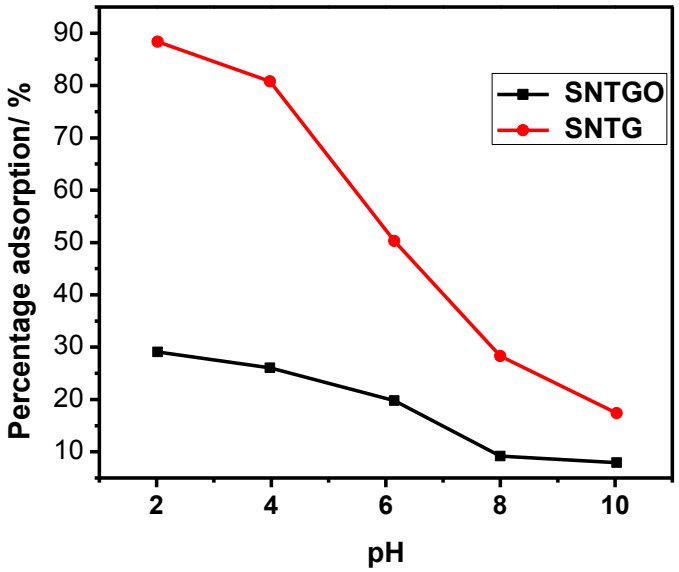

Figure 5.7 Effect of pH on sorption of SMZ onto SNTGO and SNTG (Conditions: 15 mL of 12.5 ppm SMZ, equilibration time 180 mins, adsorbent dose 50 mg, temperature 25 °C).

5.6.2 Effect of ionic strength

Wastewater effluent containing pharmaceutical contaminants often have high conductivity which may affect the behaviour of pharmaceuticals during remediation. This makes it necessary to study the effect of ionic strength on the adsorption behaviour of SMZ on SNTGO and SNTG because an increase in ionic strength may lead to a decrease in adsorption. The ionic strength was studied by adjusting 15 mL of 12.5 ppm SMZ solutions (pH 2) with 10, 20, 40 and 80 mM NaCl

solution, and the result is presented in Figure 5.8. At 20 mM NaCl, there was a slight increase in percentage adsorption of SMZ with SNTG from 86.5% - 89.2% and for SNTGO, from 29% - 30.5%. At pH 2 of this study, SMZ is neutral and the adsorbent has a negative charge. Therefore any adsorption that occurs here is due to hydrophobic interaction via the π-electrons. When NaCl is added in solution, it dissociates into Na^+ and Cl^-. The Na^+ is attracted to the π-electrons of the adsorbent pulling the electrons on one side of the π-bond towards it, leaving a high electron density on the other side. This results in increased π-interaction between the adsorbent and more adsorbate resulting in the increase in adsorption observed. However, when more NaCl is added, Na^+ is attracted to more π-electons and hence the electron density is more evenly distributed resulting in a slight decrease in π-interaction between the adsorbate and adsorbent, leading to the slight decrese in adsorption. Any further increase in NaCl concentration, the Na^+ has no more π-electrons to interact with and thus there is no change in adsorption on π-interactions in the presence of cations (Sarmah and Bhattacharyya, 2016).

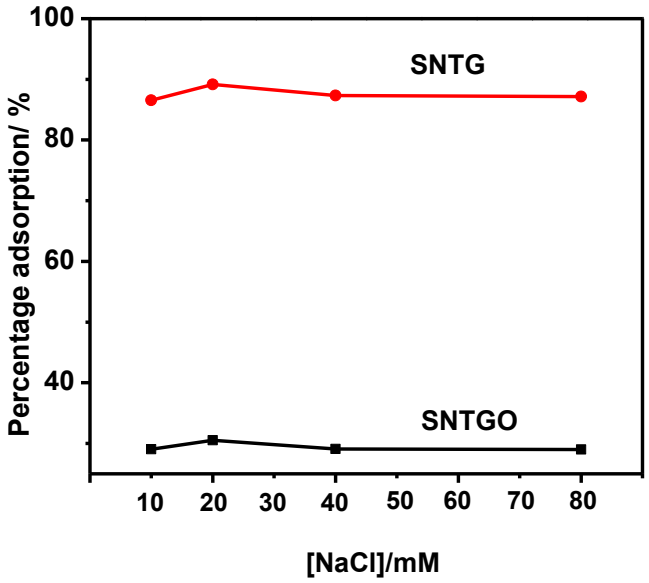

Figure 5.8 Effect of ionic strength on sorption of SMZ onto SNTGO and SNTG (Conditions: 15 mL of 12.5 ppm SMZ, pH 2, equilibration time 180 mins, adsorbent dose 50 mg, temperature 25 °C).

5.6.3 Effect of adsorbent dose

The effect of SNTGO and SNTG dose on the adsorption of SMZ was studied. Adsorbent dose is important because the adsorbent surface provides the active sites for SMZ to adsorb on. An increase in adsorption will therefore result when there are more active sites present. Adsorbent masses of 0.01, 0.02, 0.03, 0.04, 0.05 and 0.06 g of SNTG gave a percentage uptake of 21.0, 35.0, 45.4, 48.3, 59.6 and 60.1%, respectively, while for SNTGO, the percentage uptake was 10.0, 10.1, 13.3, 17.4, 19.8 and 19.9% adsorption, respectively (Figure 5.9) for the same mass of SNTGO. It can be seen that the percentage uptake of SNTGO and SNTG increased linearly up to a mass of 0.05 g of adsorbent. This was due to an increased adsorption surface area because of the increase in adsorbent mass, thereby creating more available interaction sites for the SMZ molecules in solution. Any further increase in adsorbent dose resulted in the percentage adsorption capacity remaining constant for both adsorbents. Adsorption percentage of SMZ molecules was unaffected by an increase in mass of SNTGO and SNTG after 0.05 g (Oyetade et al., 2016). Experiments thereafter, were carried out using a mass of 0.05 g for both adsorbent.

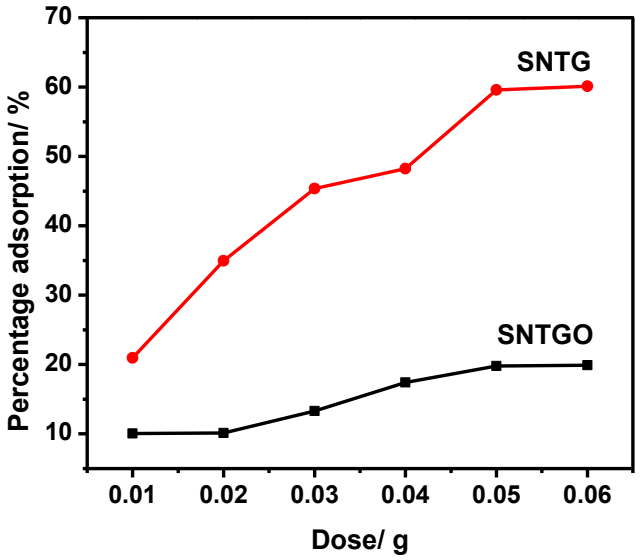

Figure 5.9 Effect of dose on sorption of SMZ onto SNTGO and SNTG (Conditions: 15 mL of 12.5 ppm SMZ, pH 2, equilibration time 180 mins, adsorbent dose 10-60 mg, temperature 25 °C, ionic strength 20 mM NaCl)

5.6.4 Effect of contact time

The effect of contact time on the adsorption of SMZ by SNTGO and SNTG was studied between 2 and 1440 min. The percentage removal of SMZ by SNTGO and SNTG increased with time (Figure 5.10). Equilibrium was obtained within 20 mins for both SNTGO and SNTG, and thereafter the percentage adsorbed remained constant. Adsorption was therefore very fast initially when there were available adsorption sites hence, the rate of removal of the pollutant was rapid and gradually decreased with time until equilibrium was reached. As adsorption sites became occupied, there were fewer sites available, resulting in reduced sorption. This was due to the unavailability of adsorption sites that were available for bonding. Thus with time, the vacant adsorption sites left became difficult to occupy as a result of repulsive forces between solute molecules in the solid and bulk phases (Yu et al., 2015b). Although, the sorption process was fast for both adsorbents, higher removal efficiency was observed for SNTG because of the higher percentage of carbon ensuring its more hydrophobic nature.

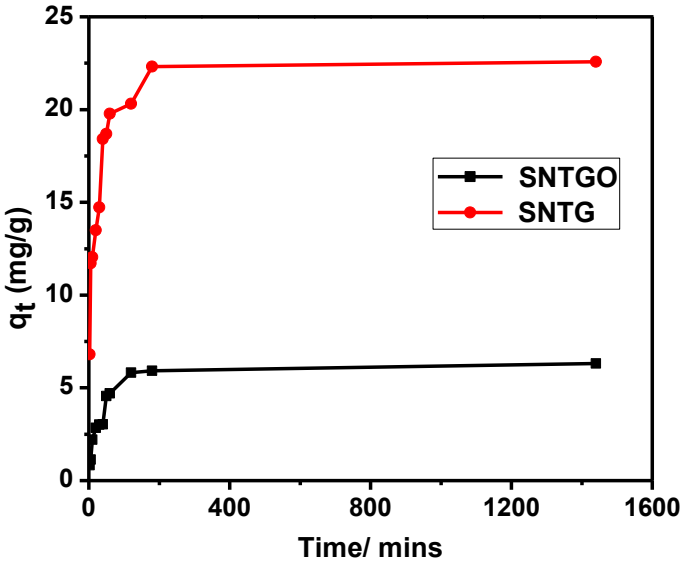

Figure 5.10 Effect of contact time on sorption of SMZ on SNTGO and SNT (Conditions: 15 mL of 12.5 ppm SMZ, pH 2, equilibration time 180 mins, dose 50 mg, temperature 25 °C, ionic strength, 20 mM NaCl)

5.6.5 Effect of temperature

The effect of temperature is shown in Figure 5.11. An increase in adsorbate temperature caused an increase in volume of internal pores of the adsorbents, an increase in rate of diffusion across the internal and external boundary layers and a decrease in the viscosity of the adsorbate solution (Khan et al., 2012). The temperature was studied between 293-313 K. Figure 5.11 shows that the adsorption capacity initially was constant but a further increase in temperature led to a slight decrease in adsorption of SMZ for both adsorbents. At high temperature, the adsorbate molecules become more energetic and move towards the pores of the adsorbent. However when too many adsorbate molecules move towards the pores, the pore of the adsorbent tends to clog up thus reducing the ability of the adsorbent to adsorb the adsorbate. Thus the pore volume decreased and the equilibrium capacity of the adsorbent reduced with an increase in temperature. This effect of temperature on the adsorbents is indicative that firstly, at a point source the adsorbent can be used without significant manipulation in temperature and secondly, the adsorbents function well even at reasonably higher temperatures.

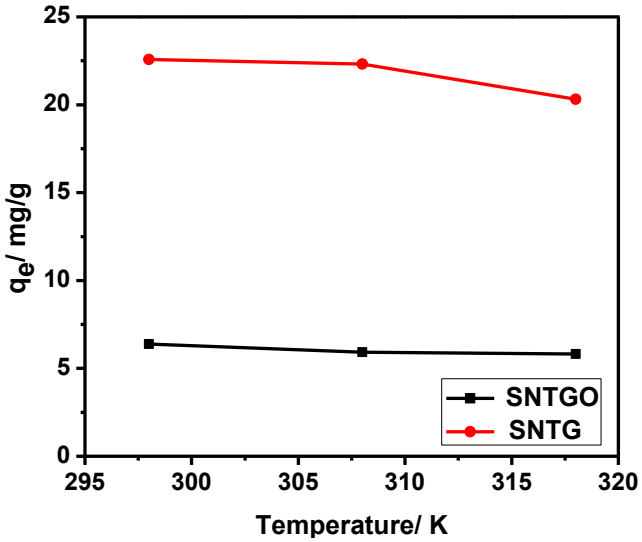

Figure 5.11 Effect of temperature on the adsorption of SMZ by SNTGO and SNTG

5.6.6 Adsorption isotherms

Isotherm models are important in understanding the interaction between adsorbents and the adsorbate. Four isotherm models; Langmuir, Freundlich, Temkin and Dubinin-Radushkevich (D-R)

were applied to the equilibrium data with the equations presented in Table 5.2. The isotherm parameters for both adsorbents are presented in Table 5.5. The best fit model was Freundlich for both adsorbents based on the high value of the correlation coefficients obtained. The Freundlich isotherm model is based on the phenomena of heterogeneous surfaces with several adsorption mechanisms involved, where K_F and N are the Freundlich constants related to the adsorption capacity and adsorption intensity, respectively. SNTGO had a lower K_F value as compared to SNTG; hence, it shows that a lesser amount of SMZ was adsorbed on it. This is consistent with the q_m value from the Langmuir isotherm obtained for SNTGO and SNTG. The Langmuir adsorption capacity q_m for SNTGO and SNTG was 125 and 248 mg/g, respectively.

The favourability for adsorption can be quantified by the separation factor, R_L and is defined as:

$$R_L = \frac{1}{1+K_1 C_0} \tag{5.3}$$

Where K_1 is the equilibrium constants (mg/L) from the Langmuir isotherm expressed in equation 3, and C_0 is the adsorbate concentration (mg/L). The nature of the adsorption process is either unfavourable ($R_L > 1$), linear ($R_L = 1$), favourable ($0 < R_L < 1$) or irreversible ($R_L = 0$). The measured SMZ adsorption at equilibrium yield R_L values of 0.031 for SNTGO and 0.009 for SNTG, which indicates favourable adsorption on both materials. This is consistent with the N value obtained from the Freundlich isotherm, which gives values greater than 1 indicating favourable adsorption. The N values are usually higher for nanocomposites and this is an indication of a strong bond between the adsorbate (SMZ) and the adsorbents. N values less than 10, indicates favourable adsorption. The D-R model was used to describe adsorption on both homogeneous and heterogeneous surfaces (Jovanović et al., 2011). E values obtained from the D-R plots were below 8 kJ/mol, which indicated that the adsorption mechanism was not entirely a chemical process.

Table 5.5 Isotherm parameters for the adsorption of SMZ onto SNTGO and SNTG

Isotherm	Parameter	SNTGO	SNTG
Langmuir	q_m/mg/g	125	248
	b/ L/mg	0.39	3.40
	R^2	0.7356	0.7723
Freundlich	K_F	2.17	5.01
	N	1.13	1.28
	R^2	0.9978	0.9929
Dubunin-Radushkevich	E/ kJ/mol	2.45	5.00
	q_D/mg/g	118	215
	B/ mol/kJ^2	1.0×10^{-10}	2.0×10^{-10}
	R^2	0.9148	0.9959
Temkin	B	21.5	35.3
	b/ J/mol	11.2	70.2
	A/ L/g	27.6	48.6
	R^2	0.946	0.928

Table 5.6 summarises the SMZ adsorption capacities of different carbon based nanocomposites. The SNTGO and SNTG exhibit excellent adsorption capacities for SMZ. The results obtained compared favourably with results from other studies. SNTG had a significant adsorption of SMZ.

Table 5.6 Comparison of q_m values to other studies of SMZ on different adsorbents

Adsorbents	q_m values/ mg/g	References
Mn-Ferrite activated carbon	217	(Wan et al., 2014)
Rice biochar	1.83	(Han et al., 2013)
Activated carbon	185.19	(Çalışkan and Göktürk, 2010)
GO	240	(Chen et al., 2015)
SNTGO	125	This study
SNTG	248	This study

5.6.7 Thermodynamic parameters

The effect of temperature on the adsorption of SMZ was investigated in the range of 293 – 323 K. The results revealed that the adsorption of SMZ decreased with increasing temperature. Thermodynamic parameters such as enthalpy change $\Delta H°$ and entropy change $\Delta S°$ were calculated from the linear plot of ln K_d *vs* 1/T using equation 4 below and Gibbs free energy $\Delta G°$ was calculated from equation 5.5. Thermodynamic properties of SMZ adsorption on SNTGO and SNTG are presented in Table 5.7. The adsorption process can be described as being favourable and spontaneous because negative $\Delta G°$ values were obtained.

Table 5.7 Thermodynamic parameters for the adsorption of SMZ onto SNTGO and SNTG

Adsorbent	Temperature/ K	$\Delta G°$/ kJ/mol	$\Delta H°$/ kJ/mol	$\Delta S°$/ kJ/mol
SNTG	293	-0.258	-0.452	0.868
	303	-0.266		
	313	-0.275		
SNTGO	293	-0.0698	-0.433	0.236
	303	-0.0722		
	313	-0.0764		

The change in Gibbs energy is calculated from the following equation:

$$\Delta G = -RT \ln K \tag{5.4}$$

Where $\Delta G°$ is the standard energy change (J/mol), R is the gas constant (8.314 J/mol/K), T is absolute temperature, and K_d (L/g) is the equilibrium constant.

A plot of ln K *versus* 1/T had a linear profile, and the values of ΔS and ΔH were obtained from the intercept and slope, respectively, using the Van't Hoff equation:

$$\ln K = -\frac{\Delta H}{RT} + \frac{\Delta S}{R} \tag{5.5}$$

The $\Delta G°$ values obtained for both adsorbents were high and negative, which meant that the adsorption process was favourable and spontaneous. A decrease in the negative value of $\Delta G°$ was observed as the temperature of the adsorbents was increased. A negative $\Delta H°$ value was obtained for both adsorbents which indicated an exothermic adsorption process and this explains the decrease in adsorption at higher temperature. This also affirms that the bonding was weak, being more physical than chemical (Al-Khateeb et al., 2014). The positive $\Delta S°$ values obtained indicate increased disorderliness between adsorbent and adsorbate during the adsorption process. The results obtained from the thermodynamics studies indicate that both adsorbents will be useful in the treatment of effluent from pharmaceutical industries.

5.6.8 Adsorption kinetic studies

In a bid to establish the rate determining step of the adsorption process in this study, 4 kinetic models were utilized; namely pseudo-first order (PFO), pseudo-second order (PSO), intraparticle diffusion (IPD) and Elovich models. The equations are presented in (Table 5.3). The kinetic parameter data of all the models and the R^2 coefficient determined by non-linear regression analysis are presented in Table 5.8. Based on the high R^2 values obtained, it was observed that the experimental data of SNTGO and SNTG best fitted the pseudo-second order model. Also, the calculated q_e values (q_e cal) of the PSO model are closer to the experimental values (q_e exp). The PSO model assumes that the rate-limiting step for SMZ adsorption may be due to ion-exchange between the adsorbent and adsorbate as also observed by Shao et al. (2014). The Elovich model is dependent on the principle of chemisorption through bond sharing and interaction. This proves that a part of the adsorption mechanism of SMZ onto SNTGO and SNTG was *via* chemical interaction through the active groups on SMZ and SNTGO and SNTG. The adsorption process on porous solids can be separated into 3 stages: (i) transfer of adsorbate across liquid film to the exterior surface of the adsorbent otherwise referred to as film diffusion, (ii) adsorbate transfer from the surface to the pores of the internal structure of the adsorbent otherwise called intra-particle diffusion, and (iii) adsorbate is adsorbed onto the active sites on the inner and outer surface of the adsorbent (Ma et al., 2012, Yu et al., 2015b). The last step proceeds rapidly and cannot be the rate-determining step. The rate of adsorption is controlled by outer or inner diffusion or both. In a bid to determine the adsorption mechanism, the experimental data obtained was modelled with

the intraparticle diffusion model. A plot of q_t *versus* $t^{0.5}$ showed that an increase in initial concentration of SMZ increased the diffusion rate. The plot obtained from the IPD shows that it did not pass through the origin and was not linear, signifying that adsorption of SMZ was not solely through the intra-particle diffusion *via* the pores of the adsorbents and it is not the only rate-controlling step (Yu et al., 2015b). A larger *C* value means, influence of surface adsorption in the rate limiting step. In the adsorption of SMZ, a mutual adsorption process of both intraparticle diffusion and surface adsorption was observed.

Table 5.8 Kinetic parameters for the adsorption of SMZ from aqueous solution

Model	Parameter	SNTGO	SNTG
Pseudo-first order	k_1 /min^{-1}	0.0160	0.0201
	q_e, eq/ mg/g	1.25	4.98
	R^2	0.9443	0.9218
$q_{e,\,exp}$	mg/g	6.32	22.5
Pseudo-second order	k_2 /g mg/g	3.18	4.94
	q_e /mg/g	6.42	22.7
	R^2	0.9999	0.9999
Intraparticle diffusion	*K*i /mg/g $min^{-0.5}$	0.14	0.33
	C /mg/g	2.43	13.4
	R^2	0.531	0.453
Elovich	A	1.00	2.60
	B	0.02	7.01
	R^2	0.8669	0.8591

5.6.9 Environmental applications

The percentage removal of SMZ from BLG and WWTP by SNTGO was 22.5 and 26.8 %, respectively. However, for SNTG it was 79.3 % and 76.5 % for BLG and WWTP, respectively. The adsorption was particularly good as the pH of both samples were slightly acidic, hence it aided adsorption. This confirms that SNTGO and SNTG can successfully be used to remove SMZ from environmental samples.

5.7 Desorption Studies

Recycling and regeneration of adsorbents is important in the practical application of adsorbents. An ideal adsorbent is one with high adsorption capacity and excellent desorption ability. This would reduce the cost of the adsorbent and also prevent the introduction of secondary pollutants into the environment. Desorption experiments were carried out by washing the adsorbents with acidic ethanol and 0.01 M NaOH. After successive adsorption-desorption cycles, there was a slight decrease in adsorption capacity. Results showed good desorption efficiencies of 70 and 65 % efficiency for SNTGO after 2 cycles and 76 and 72 % for SNTG, after 2 cycles. The FTIR spectra showed no obvious peak changes after 2 cycles of desorption (Figure 5.12) however, surface area and pore volume were reduced when compared to the originally synthesized adsorbents. SNTGO and SNTG had a surface area of 130 m^2/g and 85 m^2/g and pore volumes of 0.43 and 0.45 cm^3/g, respectively. The decrease in surface area and pore volume is because the SMZ molecule filled the pores and adhered to the surface of the adsorbents. The results are indicative that SNTGO and SNTG are reusable and stable.

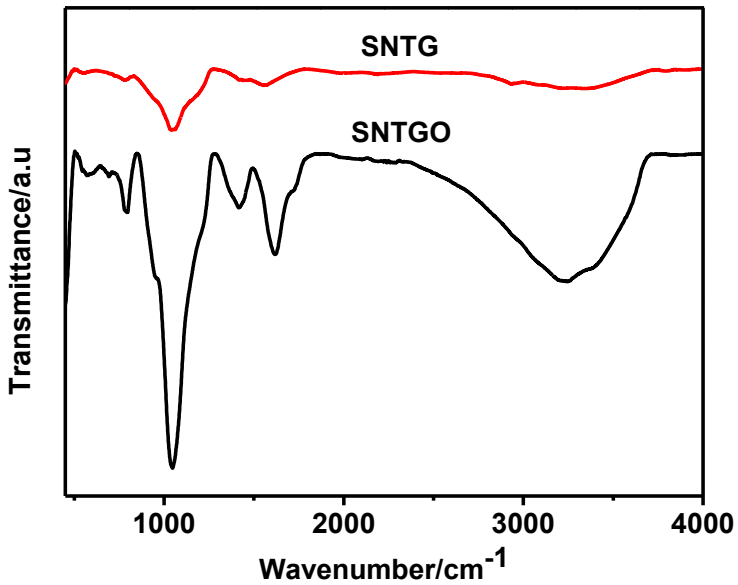

Figure 5.12 FTIR spectra of SNTGO and SNTG after desorption

5.8 Conclusion

In this study, silica nanotubes from elephant grass were synthesized. It was successfully encapsulated with graphene oxide and graphene. Batch adsorption studies were carried out to study the adsorption behaviour of SMZ on SNTGO and SNTG. The adsorbents were effective in the removal of SMZ from aqueous solutions with q_m values of 125 and 248 mg/g obtained for SNTGO and SNTG, respectively. An ionic strength of 20 mM NaCl, temperature of 25 ^{o}C and pH 2 provided the optimum conditions for adsorption. The adsorption kinetics followed the pseudo-second order model and the experimental data best fitted the Freundlich isotherm model. The adsorbents were effective in the treatment of real environmental samples showing that it can be used in the treatment of industrial effluents polluted with SMZ. The adsorbents were still efficient after 2 cycles, thus showing that they can be regenerated.

5.9 Acknowledgments

We gratefully acknowledge the School of Chemistry and Physics, University of KwaZulu-Natal, South Africa, for providing the laboratory facilities and instrumentation used in this research and also to the AAU small grant for financial assistance.

References

Adam, F., Appaturi, J. N., Khanam, Z., Thankappan, R. & Nawi, M. a. M. 2013. Utilization of tin and titanium incorporated rice husk silica nanocomposite as photocatalyst and adsorbent for the removal of methylene blue in aqueous medium. *Applied Surface Science,* 264**,** 718-726.

Al-Khateeb, L. A., Almotiry, S. & Salam, M. A. 2014. Adsorption of pharmaceutical pollutants onto graphene nanoplatelets. *Chemical Engineering Journal,* 248**,** 191-199.

Bouki, C., Venieri, D. & Diamadopoulos, E. 2013. Detection and fate of antibiotic resistant bacteria in wastewater treatment plants: a review. *Ecotoxicology and Environmental Safety,* 91**,** 1-9.

Çalışkan, E. & Göktürk, S. 2010. Adsorption characteristics of sulfamethoxazole and metronidazole on activated carbon. *Separation Science and Technology,* 45**,** 244-255.

Chen, H., Gao, B. & Li, H. 2015. Removal of sulfamethoxazole and ciprofloxacin from aqueous solutions by graphene oxide. *Journal of Hazardous Materials,* 282**,** 201-207.

Dreyer, D. R., Park, S., Bielawski, C. W. & Ruoff, R. S. 2010. The chemistry of graphene oxide. *Chemical Society Reviews,* 39**,** 228-240.

Gibson, L. 2014. Mesosilica materials and organic pollutant adsorption: part B removal from aqueous solution. *Chemical Society Reviews,* 43**,** 5173-5182.

Han, R., Zhang, L., Song, C., Zhang, M., Zhu, H. & Zhang, L. 2010. Characterization of modified wheat straw, kinetic and equilibrium study about copper ion and methylene blue adsorption in batch mode. *Carbohydrate Polymers,* 79**,** 1140-1149.

Han, X., Liang, C.-F., Li, T.-Q., Wang, K., Huang, H.-G. & Yang, X.-E. 2013. Simultaneous removal of cadmium and sulfamethoxazole from aqueous solution by rice straw biochar. *Journal of Zhejiang University Science B,* 14**,** 640-649.

Ho, Y.-S. & Mckay, G. 1998. Sorption of dye from aqueous solution by peat. *Chemical Engineering Journal,* 70**,** 115-124.

Ji, L., Wan, Y., Zheng, S. & Zhu, D. 2011. Adsorption of tetracycline and sulfamethoxazole on crop residue-derived ashes: implication for the relative importance of black carbon to soil sorption. *Environmental Science & Technology,* 45**,** 5580-5586.

Jones, O. A., Lester, J. N. & Voulvoulis, N. 2005. Pharmaceuticals: a threat to drinking water? *TRENDS in Biotechnology,* 23**,** 163-167.

Jovanović, B. M., Vukašinović-Pešić, V. L. & Rajaković, L. V. 2011. Enhanced arsenic sorption by hydrated iron (III) oxide-coated materials—mechanism and performances. *Water Environment Research,* 83**,** 498-506.

Kemper, N. 2008. Veterinary antibiotics in the aquatic and terrestrial environment. *Ecological Indicators,* 8**,** 1-13.

Khan, T. A., Dahiya, S. & Ali, I. 2012. Use of kaolinite as adsorbent: Equilibrium, dynamics and thermodynamic studies on the adsorption of Rhodamine B from aqueous solution. *Applied Clay Science,* 69**,** 58-66.

Kushwaha, A. K., Gupta, N. & Chattopadhyaya, M. 2014. Enhanced adsorption of methylene blue on modified silica gel: equilibrium, kinetic, and thermodynamic studies. *Desalination and Water Treatment,* 52**,** 4527-4537.

Li, M.J., Liu, C.M., Xie, Y.B., Cao, H.B., Zhao, H. and Zhang, Y. 2014. The evolution of surface charge on graphene oxide during the reduction and its application in electroanalysis. *Carbon, 66***,** 302-311.

Li, X., Wang, Z., Li, Q., Ma, J. & Zhu, M. 2015. Preparation, characterization, and application of mesoporous silica-grafted graphene oxide for highly selective lead adsorption. *Chemical Engineering Journal,* 273**,** 630-637.

Lian, F., Sun, B., Song, Z., Zhu, L., Qi, X. & Xing, B. 2014. Physicochemical properties of herb-residue biochar and its sorption to ionizable antibiotic sulfamethoxazole. *Chemical Engineering Journal,* 248**,** 128-134.

Liang, X., Wang, S., Liu, S., Liu, X. & Jiang, S. 2012. A novel octadecylsilane functionalized graphene oxide/silica composite stationary phase for high performance liquid chromatography. *Journal of Separation Science,* 35**,** 2003-2009.

Liu, F.-F., Zhao, J., Wang, S., Du, P. & Xing, B. 2014. Effects of Solution Chemistry on Adsorption of Selected Pharmaceuticals and Personal Care Products (PPCPs) by Graphenes and Carbon Nanotubes. *Environmental Science & Technology,* 48**,** 13197-13206.

Liu, X., Zhang, H., Ma, Y., Wu, X., Meng, L., Guo, Y., Yu, G. & Liu, Y. 2013. Graphene-coated silica as a highly efficient sorbent for residual organophosphorus pesticides in water. *Journal of Materials Chemistry A,* 1**,** 1875-1884.

Loos, R., Locoro, G. & Contini, S. 2010. Occurrence of polar organic contaminants in the dissolved water phase of the Danube River and its major tributaries using SPE-LC-MS 2 analysis. *Water Research,* 44**,** 2325-2335.

Luo, Y.-B., Zhu, G.-T., Li, X.-S., Yuan, B.-F. & Feng, Y.-Q. 2013. Facile fabrication of reduced graphene oxide-encapsulated silica: A sorbent for solid-phase extraction. *Journal of Chromatography A,* 1299**,** 10-17.

Ma, J., Yu, F., Zhou, L., Jin, L., Yang, M., Luan, J., Tang, Y., Fan, H., Yuan, Z. & Chen, J. 2012. Enhanced adsorptive removal of methyl orange and methylene blue from aqueous solution by alkali-activated multiwalled carbon nanotubes. *ACS Applied Materials & Interfaces,* 4**,** 5749-5760.

Marcano, D. C., Kosynkin, D. V., Berlin, J. M., Sinitskii, A., Sun, Z., Slesarev, A., Alemany, L. B., Lu, W. & Tour, J. M. 2010. Improved synthesis of graphene oxide. *ACS Nano,* 4**,** 4806-4814.

Martins, A. F., Mallmann, C. A., Arsand, D. R., Mayer, F. M. & Brenner, C. G. 2011. Occurrence of the antimicrobials sulfamethoxazole and trimethoprim in hospital effluent and study of their degradation products after electrocoagulation. *CLEAN–Soil, Air, Water,* 39**,** 21-27.

Matongo, S., Birungi, G., Moodley, B. and Ndungu, P. 2015. Pharmaceutical residues in water and sediment of Msunduzi River, KwaZulu-Natal, South Africa. *Chemosphere*, *134*,133-140.

Meng, H., Li, Z., Ma, F., Wang, X., Zhou, W. & Zhang, L. 2015. Synthesis and characterization of surface ion-imprinted polymer based on SiO_2-coated graphene oxide for selective adsorption of uranium (vi). *RSC Advances,* 5**,** 67662-67668.

Meynen, V., Cool, P. & Vansant, E.F., 2009. Verified syntheses of mesoporous materials. *Microporous and Mesoporous Materials*, 125(3),170-223.

Nam, S.-W., Jung, C., Li, H., Yu, M., Flora, J. R., Boateng, L. K., Her, N., Zoh, K.-D. & Yoon, Y. 2015. Adsorption characteristics of diclofenac and sulfamethoxazole to graphene oxide in aqueous solution. *Chemosphere,* 136**,** 20-26.

Nielsen, L., Biggs, M. J., Skinner, W. & Bandosz, T. J. 2014. The effects of activated carbon surface features on the reactive adsorption of carbamazepine and sulfamethoxazole. *Carbon,* 80**,** 419-432.

Novoselov, K. S., Geim, A. K., Morozov, S., Jiang, D., Zhang, Y., Dubonos, S. A., Grigorieva, I. & Firsov, A. 2004. Electric field effect in atomically thin carbon films. *Science,* 306**,** 666-669.

Oyetade, O. A., Nyamori, V. O., Martincigh, B. S. & Jonnalagadda, S. B. 2016. Nitrogen-functionalised carbon nanotubes as a novel adsorbent for the removal of Cu (ii) from aqueous solution. *RSC Advances,* 6**,** 2731-2745.

Sarmah, N. and Bhattacharyya, P.K. 2016. Behaviour of cation–pi interaction in presence of external electric field. *RSC Advances, 6,* 100008-100015.

Shao, Y., Wang, X., Kang, Y., Shu, Y., Sun, Q. & Li, L. 2014. Application of Mn/MCM-41 as an adsorbent to remove methyl blue from aqueous solution. *Journal of Colloid and Interface Science,* 429**,** 25-33.

Shi, R., Yan, L., Xu, T., Liu, D., Zhu, Y. & Zhou, J. 2015. Graphene oxide bound silica for solid-phase extraction of 14 polycyclic aromatic hydrocarbons in mainstream cigarette smoke. *Journal of Chromatography A,* 1375**,** 1-7.

Sing, K. S. 1985. Reporting physisorption data for gas/solid systems with special reference to the determination of surface area and porosity (Recommendations 1984). *Pure and Applied Chemistry,* 57**,** 603-619.

Thiele-Bruhn, S. 2003. Pharmaceutical antibiotic compounds in soils–a review. *Journal of Plant Nutrition and Soil Science,* 166**,** 145-167.

Trovó, A. G., Nogueira, R. F., Agüera, A., Fernandez-Alba, A. R., Sirtori, C. & Malato, S. 2009. Degradation of sulfamethoxazole in water by solar photo-Fenton. Chemical and toxicological evaluation. *Water Research,* 43**,** 3922-3931.

Wan, J., Deng, H., Shi, J., Zhou, L. & Su, T. 2014. Synthesized Magnetic Manganese Ferrite Nanoparticles on Activated Carbon for Sulfamethoxazole Removal. *CLEAN–Soil, Air, Water,* 42**,** 1199-1207.

Wang, C., Li, H., Liao, S., Zhang, D., Wu, M., Pan, B. & Xing, B. 2014a. Sorption affinities of sulfamethoxazole and carbamazepine to two sorbents under co-sorption systems. *Environmental Pollution,* 194**,** 203-209.

Wang, J., Chen, Z. & Chen, B. 2014b. Adsorption of polycyclic aromatic hydrocarbons by graphene and graphene oxide nanosheets. *Environmental Science & Technology,* 48**,** 4817-4825.

White, B., 2011. Diagnosis and treatment of urinary tract infections in children. *Am Fam Physician, 83*(4), pp.409-15.

Yang, K., Chen, B. & Zhu, L. 2015. Graphene-coated materials using silica particles as a framework for highly efficient removal of aromatic pollutants in water. *Scientific Reports,* 5, 11641-11653.

Yu, F., Ma, J. & Bi, D. 2015. Enhanced adsorptive removal of selected pharmaceutical antibiotics from aqueous solution by activated graphene. *Environmental Science and Pollution Research,* 22**,** 4715-4724.

Zhang, D., Pan, B., Wu, M., Wang, B., Zhang, H., Peng, H., Wu, D. & Ning, P. 2011. Adsorption of sulfamethoxazole on functionalized carbon nanotubes as affected by cations and anions. *Environmental Pollution,* 159**,** 2616-2621.

Zhang, S., Shao, T., Bekaroglu, S. S. K. & Karanfil, T. 2010a. Adsorption of synthetic organic chemicals by carbon nanotubes: effects of background solution chemistry. *Water Research,* 44**,** 2067-2074.

Zhang, X., Pan, B., Yang, K., Zhang, D. & Hou, J. 2010b. Adsorption of sulfamethoxazole on different types of carbon nanotubes in comparison to other natural adsorbents. *Journal of Environmental Science and Health Part A,* 45**,** 1625-1634.

Zhang, Y., Tian, Z., Xu, J., Zhong, Z., Guo, C., Yu, T. & Chen, Y. 2012. Effects of surfactants on the sorption of sulfamethoxazole by sediment. *Polish Journal of Environmental Studies,* 21, 1505-1511.

Ziylan, A. & Ince, N. H. 2011. The occurrence and fate of anti-inflammatory and analgesic pharmaceuticals in sewage and fresh water: treatability by conventional and non-conventional processes. *Journal of Hazardous Materials,* 187**,** 24-36.

6.0 CHAPTER 6: SYNTHESIS AND CHARACTERISATION OF MCM-41 AND CITRIC GRAFTED MCM-41 FROM MILLET STRAW AND ITS APPLICATION IN ADSORPTION OF METHYLENE BLUE

Samson O. Akpotu and Brenda Moodley*

School of Chemistry and Physics, University of KwaZulu-Natal, Westville Campus, Durban, 4000, South Africa.

*****corresponding author email: moodleyb3@ukzn.ac.za
Telephone: +27 31 2602796
Fax: +27 31 2603091

6.1 Abstract

In this study, millet straw agrowaste was utilized as a precursor in the synthesis of molecular sieve MCM-41. Citric acid-MCM-41 composite was prepared by grafting citric acid (CA) on MCM-41 for improvement of its adsorptive capacity for methylene blue (MB). Characterisation of the adsorbents was carried out using scanning electron microscopy (SEM), high resolution transmission electron microscope (HR-TEM), Brunauer-Emmet-Teller (BET) analysis, thermo-gravimetric analysis (TGA) and fourier transform infrared analysis (FTIR). MB adsorption studies were carried out on the citric acid MCM-41 (SCA-MCM-41) varying parameters such as contact time, pH of solution and the initial MB concentration. It was found that SCA-MCM-41 had a better adsorption capacity than MCM-41. Adsorption capacity was reached within 1 hour. The highest adsorption capacity was highest at pH 8 and decreased thereafter with an increase in pH value of MB. Langmuir, Freundlich and Temkin models were used in analyzing the equilibrium data. Kinetics favoured the pseudo-second order and the best temperature for adsorption was 25 ^{o}C with adsorption being spontaneous and exothermic.

Keywords: *Millet straw, MCM-41, methylene blue, citric acid, adsorption*

6.2 Introduction

Agricultural by-products such as sugar cane bagasse, rice husk ash, and wheat straw are potential raw materials for high value end products which have various applications. This include use as a catalyst, (Sivasubramanian et al., 2013), adsorbent and photo catalysis (Jaroenworaluck et al., 2012) etc. The combustion of these agrowaste materials results in ash which contains various inorganic minerals with a substantial percentage being silica. This extracted silica can be used in the synthesis of MCM-41, which is a siliceous material with unique properties. MCM-41 can be further exploited for adsorption of cationic pollutants by specific surface modification with a tri-carboxylic acid such as citric acid (Kushwaha et al., 2014).

MCM-41 is an amorphous siliceous material that has very distinct properties such as hexagonal *(p6mm)* uniform mesopores, large pore volume and high specific surface area (Qu and Gu, 2014). These properties, especially the surface area can be exploited for selective adsorption. This could be done by the modification of the extensive –OH network on the MCM-41 surface. Citric acid which is a tricarboxylic acid has been employed as a modifier on the surface of adsorbents (Kushwaha et al., 2014, Han et al., 2010, Sajab et al., 2011). This increases its affinity for cationic surfaces such as heavy metals and dyes. At high temperature, a thermochemical reaction occurs between CA and the adsorbents such that the citric acid dehydrates to produce a reactive anhydride which reacts with the hydroxyl group of silica to form an ester linkage. The result is that the free carboxyl groups of citric acid increases the net negative charge on the modified adsorbent surface in solution, making it suitable for cationic adsorption (Kushwaha et al., 2010).

Dyes are the major constituents of textile wastes and the disposal of these wastes are often problematic. Methylene blue (MB) has wide spread usage in the textile industry and has been known to cause a number of illnesses in humans, such as unirary tract problem, central nervous system damage, heart defects (Vutskits et al., 2008). Hence the need for its remediation is very important.

Different approaches have been utilized in the remediation of MB from water such as photodegradation, precipitation, chemical degradation, biodegradation and adsorption (Shao et al., 2014).

Adsorption is the preferred method of choice because of its efficiency, economical advantage and also its ease of use. Citric acid modified adsorbents have been used in the adsorption of MB from aqueous solution with varying degrees of success. MB was adsorbed with CA modified soybeans straw by Han et al. (2010), CA was also used to modify fumed silica and used in the adsorption of MB (Kushwaha et al., 2014). The modified material performed better in both studies above as compared to the unmodified adsorbent.

In this study, MCM-41 a molecular sieve, was synthesized using millet straw, an agrowaste, as a precursor for silica. The synthesised MCM-41 was grafted with citric acid (CA) to form a SCA-MCM-41 composite, which was then applied as an adsorbent. These adsorbents were extensively characterized using thermogravimetric analysis (TGA), elemental analysis (EA), infrared spectroscopy (IR), scanning electron microscopy (SEM), high resolution transmission (HRTEM) and Braunner-Emmet-Teller (BET) surface area analysis. To enhance adsorption, a cationic dye methylene blue was adsorbed with the synthesized adsorbents. The mechanism for MB adsorption and adsorption efficiency as a function of dose, pH, contact time, temperature, adsorption rate and capacity was determined using kinetic and equilibrium isotherm models. To the best of our knowledge, this is the first study to synthesise mesoporous sieve (MCM-41) using agrowaste as a precursor and grafting it with CA. This work also reports on the extensive characterization and its application as an adsorbent for methylene blue from aqueous solution.

6.3 Experimental

6.3.1 Materials

Millet straw was harvested with a sharp stainless steel knife from Kano State, northern Nigeria. Sodium hydroxide (Sigma, 99.99 %), cetyltrimethyl ammonium bromide (Calbiochem, 99.0+%) used as structure directing agent, nitric acid (Sigma, 65 %), butan-1-ol (Merck, 99.0 %), acetone (Sigma, $\geq$99.8 %), and MB (Sigma) were purchased. All chemicals were used without further purification.

6.3.2 Sample pretreatment and silica synthesis

This incorporates both acid and thermal treatments. Millet straw was copiously washed with double distilled water and air dried. About 40 g of clean and ground millet straw was stirred with 1000 mL of 1.0 M HNO_3 at room temperature for 24 hours. Acid treated millet straw was washed with double-distilled water to a neutral pH, dried in an oven at 100 ^oC for 24 hours and calcined in a furnace at 600 ^oC to remove organics (Adam et al., 2013). Nitric acid was used to remove small quantities of soluble minerals (metal oxides) and complete delignification of EG. Millet straw ash was stirred with 1.0 M HNO_3 at 60 ^oC for 24 hrs. This was filtered with Whatman No. 5 filter paper and washed with double-distilled water until a neutral pH was reached and dried at 100 ^oC for 24 hours.

6.3.3 Synthesis of MCM-41 mesoporous silica

MCM-41 was synthesized with a modified procedure of Ghorbani et al. (2013). About 2.5 g of silica from millet straw was dispersed in a solution made by dissolving 1.42 g of NaOH in double-distilled (DD) water in a plastic container. This mixture was refluxed in an oil bath with continuous stirring at 80 ^oC for 24 hrs. Approximately 0.85 g of cetyltrimethylammonium bromide (CTAB) was dissolved in 14.2 mL of DD water. The aqueous solution of CTAB was slowly introduced to the sodium silicate solution while stirring. The pH was adjusted to 11 with 1 M acetic acid, the mixture was stirred at 300 rpm at room temperature for 6 hrs. The gel was transferred to a round bottom flask and heated at 100 ^oC for 72 hrs in a polypropylene bottle. The pH was again adjusted to 11 using acetic acid and aged for 24 hrs. The solid was filtered, washed to a neutral pH and dried at 80 ^oC for 24 hrs. The CTAB template removal was by calcination in air at 550 ^oC for 5 hrs. The obtained MCM-41 was gently broken up with a pestle.

6.3.4 Activation of MCM-41

This was done using a modified procedure of Kushwaha et al. (2014). Approximately 40 mL of 6 M HCl was added to MCM-41 (1 g) and the mixture refluxed at 100 ^oC in a round bottom flask with continuous stirring for 4 hours and then cooled to room temperature. The material was fil-

tered and washed until neutral pH and dried in an oven at 150 ^{o}C for 5 hrs. This was assigned as A-MCM-41.

6.3.5 Synthesis of NH_2-MCM-41

MCM-41 surface was modified in aqueous solution by an easy one-step synthesis. About 1.00 g of MCM-41 was dispersed in ethanol (30 mL) in a 3-necked reflux flask and ultrasonicated for an hr with stirring. Approximately, 500 µL of APTES was added to bind –NH_2. The reaction was stirred with a magnetic stirrer at 50 °C for 8 hrs to obtain a monolayer and positively charged MCM-41. The product was collected by filtration and dried in a vacuum at 60 °C.

6.3.6 Grafting of MCM-41 with citric acid

A 20 mL volume of 0.6 M citric acid was added to 1 g of NH_2-MCM-41. This was sonicated for 45 mins and stirred for 45 mins to make a slurry. It was kept in a vacuum oven at a temperature of 50 ^{o}C for 24 hours which was subsequently increased to 120 ^{o}C for 90 minutes to aid the thermochemical reaction. The material was washed with double-distilled deionized water until a few drops of 0.1 M copper nitrate solution, added to the filtrate, did not turn it cloudy. This signified the complete discharge of excess citric acid. The resultant solid was dried at 70 ^{o}C for 2 hrs and kept in a desiccator until it was characterized. This material was labeled SCA-MCM-41.

6.4 Characterisation of Adsorbents

MCM-41 and CA grafted MCM-41 were characterized using various techniques. The percentage of carbon in the samples was determined using an elemental analyser (Thermo Scientific CHNS/O analyser). N_2 adsorption–desorption isotherms were obtained using a nitrogen adsorption analyzer (Micrometrics Tristar II 3020). MCM-41 was degassed at a temperature of 90 ^{o}C for an hour then ramped up to 200 ^{o}C overnight. CA-grafted samples were degassed (with a Vacprep 061 degasser) at 90 ^{o}C overnight. This temperature was selected to prevent CA decomposition. Surface area and pore size measurement of samples were obtained using the Brunauer–Emmett–Teller (BET) method. The pore volume was calculated from the adsorption branch

based on volume of nitrogen adsorbed at a relative pressure (P/P_o) of approximately 0.99. Low angle (0-5 Θ) and long range (10-90 Θ) x-ray diffraction (XRD) analysis of the samples were carried out on a Bruker D8 XRD with Cu-Kα radiation at 40 mA and 45 kV. Surface morphology was obtained with field-emission scanning-electron microscopy (FESEM), and micrographs were analysed using an operating voltage of 10 kV (Zeiss instrument). Samples were coated with a thin film of gold to minimize surface charging. The ordered nature of samples was determined using high resolution transmission electron microscopy (TEM) (JEOL). Samples were prepared by firstly ultrasonicating in ethanol and placed on copper grids with carbon film. Thermal stability of synthesized materials was determined by heating 5 mg of sample in an aluminium in air at temperature between 25- 900 ^oC at a ramping rate of 5 ^oC/min with SDT Q 600 V 209 Build 20. FTIR (Perkin Elmer Series 100 spectrometer) in the range of 4000 – 400 cm^{-1} was used in the acquisition of data showing the presence of silanol, siloxane and carboxyl functional groups. Quantification of the degree of functionalisation was carried out by elemental analysis and TGA.

6.5 PZC determination

About 0.02 g of sample was dissolved in 0.02 M NaOH in a pH range of 2-10. The pH was adjusted with 0.1 M HCl or 0.1 M NaOH. The PZC value was determined by a plot of final pH *versus* difference in initial and final pH.

6.6. Adsorption Studies

A standard solution of 1000 ppm of MB solution was prepared and diluted to working concentration. The absorbances were read from the UV-3600-Schimadzu UV-VIS-NIR spectrophotometer at a wavelength of 663 nm and a calibration curve. A 20 mL aliquot solution was used in carrying out adsorption experiments. The concentration of the predetermined solution was adjusted using 0.1 M NaOH/HCl, and thereafter a mass of adsorbent was placed in the adsorbate solution and the solution placed on the orbital shaker and equilibrated for 2 hrs. Afterwards, the solution was centrifuged for 3 minutes at 10000 rpm and the supernatant was collected and analysed using a UV-VIS spectrophotometer.

The adsorption capacity of methylene blue at equilibrium time q_e (mg/g) was calculated from the equation:

$$q_e = \frac{(C_o - C_e)V}{W} \quad (6.1)$$

Where C_o and C_e are initial and equilibrium concentrations of MB in mg/L, V is the volume of the solution (L), and *W* is the mass of adsorbent used (g) in the experiment.

The percentage MB removal at equilibrium time was calculated using the equation:

$$\%\ MB\ removal = 100\,\frac{C_o - C_e}{C_o} \quad (6.2)$$

The influence of CA ratio to MCM-41 for the removal of MB was carried out by using 0.03 g of each adsorbent at pH 10 at 25 °C. The effect of pH, adsorbent dose, contact time, initial dye concentration and temperature on adsorption capacity was determined by varying one parameter at a time whilst the others were kept constant.

6.6 Results and Discussion

6.6.1 Characterisation of adsorbent

6.6.1.1 Carbon analysis

The carbon content was determined in the samples. The modified sample SCA-MCM-41 had 4.4% of carbon as compared to none for MCM-41. This was due to the presence of CA grafted on the modified sample.

6.6.1.2 Textural analysis

The N_2 adsorption-desorption isotherm carried out on pristine MCM-41 and SCA-MCM-41 are shown in Figures 6.1 (a) and (b). The pore sizes of the samples were determined using the BJH method and the surface area with a BET method. A type IV isotherm was observed with a low relative pressure of (P/Po = 0.2-0.4) which was due to capillary condensation of nitrogen in the mesopores. CA grafted MCM-41 resulted in the decrease of specific surface area, pore volume and pore diameter (Table 6.1) indicating successful incorporation of CA in MCM-41 as a result of pore blocking and pore filling by citric acid, which was also reported by Wu et al., (2014) and Bhagiyalakshmi et al., (2010).

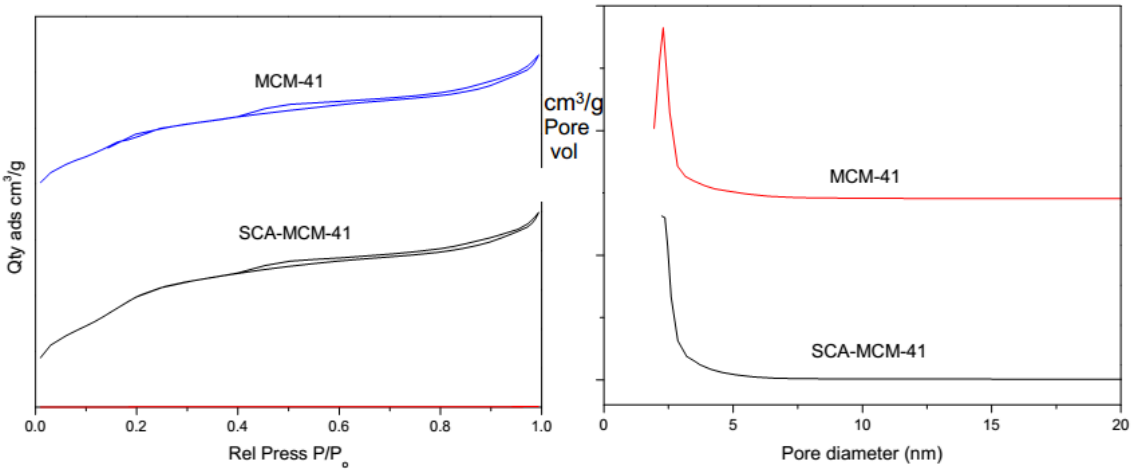

Figure 6.1 (a) N_2-adsorption –desorption isotherm and (b) Pore size distribution of sample

Table 6.1 Textural properties of MCM-41

Sample	SBET (m^2/g)	Pore diameter (nm)	Pore volume (cm^3/g)	References
MCM-41	850.5	3.8	0.87	Present study
SCA-MCM-41	650	2.8	0.65	Present study
MCM-41	1174	4.1	0.98	(Ghorbani et al., 2013)
MCM-41	1101	3.5	0.96	(Bhagiyalakshmi et al., 2010)

6.6.2 X-ray fluorescence analysis

X-ray fluorescence was used in the determination of elemental composition of silica from millet straw. The major composition of the material obtained after calcination was high purity silica (98.2 %). Metal oxide impurities were reduced significantly (< 1.8 %) due to the acid and thermal treatment of the samples. Other metal oxides found were Al (0.518 %), Fe (0.098 %), Ca (0.043 %), K (0.040 %), V (0.045 %) and S (0.053 %), which were negligible impurities and may be from dilution effects of the aqueous solution. Leaching biomass with acid reduces impurities, and synthesis of silica at acidic pH (3) results in a high purity silica (Liou, 2011).

6.6.3 XRD analysis

The profiles of the wide angle XRD and low angle XRD scans obtained at 10-80(Θ) and 1-5(Θ), respectively for MCM-41 and citric acid grafted MCM-41 are shown in Figures 6.2 (a) and (b). MCM-41 and SCA-MCM-41 were characterized by a large amorphous peak between 20-30(Θ) which is present in siliceous materials (Ghorbani et al., 2013). However, in SCA-MCM-41, there were no diffraction peaks corresponding to CA crystals. This was due to the amorphous nature of the material and a well organized silica matrix (Takahashi et al., 2000). The low angle scan obtained at 0-5(Θ) of the MCM-41 outline revealed a well ordered hexagonal mesophase for the unmodified MCM-41, and showed 3 intense peaks at 100, 110, 200 and a fourth not so prominent peak at 210 (Ghorbani et al., 2013, Qu and Gu, 2014). However, SCA-MCM-41 had the same peaks as MCM-41 but was of lesser intensity because of the interaction of CA on silica suppressing the peaks. This may be because of the partial degradation in the ordered mesoporous structure (Liou, 2011) and also due to pore impregnation in the porous channels (Wu et al., 2014), followed by CA-grafting on MCM-41 (Bhagiyalakshmi et al., 2010).

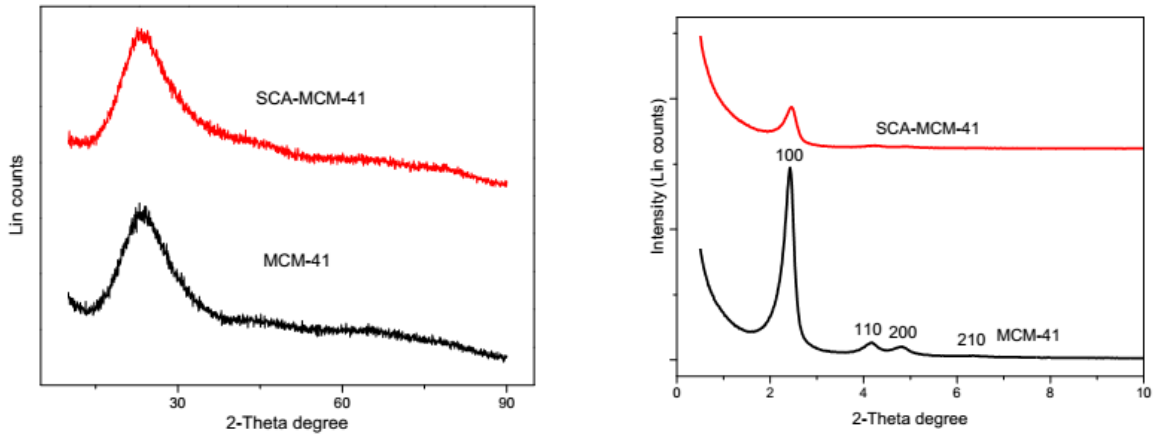

Figure 6.2 (a) Wide angle XRD profiles of MCM-41 and SCA-MCM-41 and (b) Low angle profiles of MCM-41 and SCA-MCM-41

6.6.4 FTIR analysis

The FTIR spectrum of MCM-41 and SCA-MCM-41 are shown in Figure 6.3. The MCM-41 sample had an absorption band around 3400 cm^{-1} which is due to water and –OH stretching groups present. The bands at 960 and 1625 cm^{-1} are due to Si-OH stretching and bending, respectively (Adam et al., 2013). There was a shift in the band at 1625 cm^{-1} in MCM-41 to 1630 cm^{-1} in SCA-MCM-41 which is assigned as the intermolecular hydrogen bond from carboxyl groups which were prominent in SCA-MCM-41 (Takahashi et al., 2000). This shift was due to the presence of the carboxylic acid from the citric acid. Absorption bands at 1050 cm^{-1} and 805 cm^{-1} were due to asymmetric stretching of Si-O-Si and symmetric stretching, respectively (Kushwaha et al., 2014). SCA-MCM-41 had absorption peaks between 1715 cm^{-1} and 1640 cm^{-1} due to carbonyl stretching, either as conjugated or non-conjugated to aromatic rings which was absent in MCM-41. The band at 1430 cm^{-1} is attributed to C-O from the carbonyl group from CA. Vibrations around 1715-1730 cm^{-1} was due to esterification of CA with MCM-41 forming a C=O bond from the COOH group (Kushwaha et al., 2014). Carboxyl groups function as an effective proton donor and aids in deprotonation because it forms coordinated complexes with cationic dyes *via* electrostatic ion interaction. There were peaks due to CTAB as the calcination temperature ensured a complete of the structure directing agent.

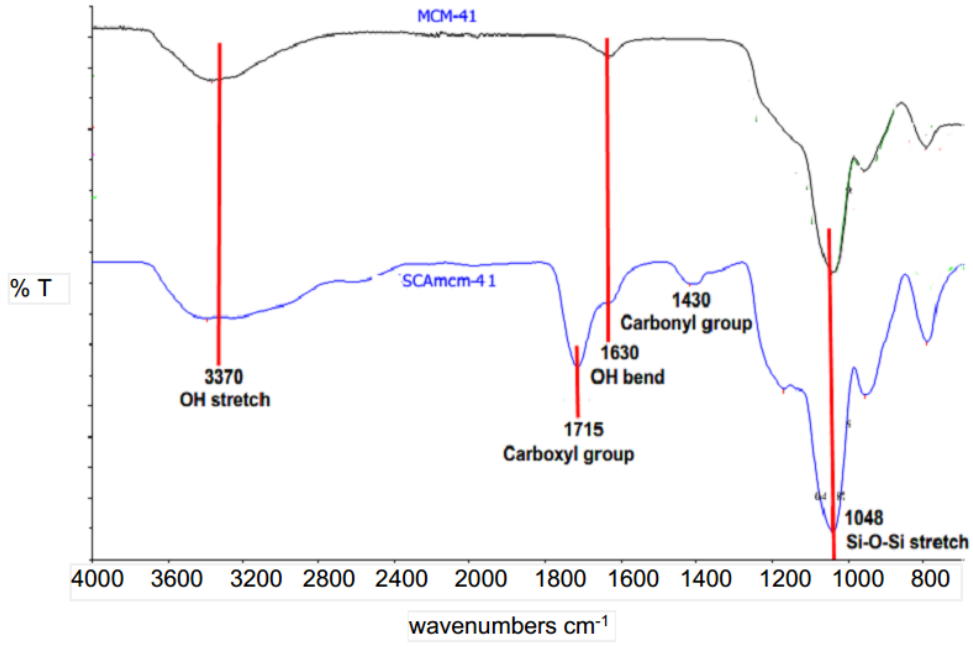

Figure 6.3 FTIR spectra of MCM-41 and SCA-MCM-41

6.6.5 TGA profiles

The TGA and DTA profiles of MCM-41 and SCA-MCM-41 samples are presented in Figure 6.4. MCM-41 showed a 2 step degradation profile. Firstly, there was the removal of physically adsorbed water at 120 °C and resulted in a weight loss of 4.5 %. The subsequent phase had a maximum degradation loss at 350 °C, with a 0.5 % mass loss. The last phase of 350-600 °C resulted in minimal weight loss. At the last phase, loss of water occurred from condensation of the adjacent silanol group, as well as dehydroxylation. Stability of MCM-41 occurred at 600 °C with no further change in mass thereafter. The SCA-MCM-41 sample had a different degradation pattern as MCM-41, but a concurrent loss occurred due to CTAB and CA degradation. At the onset, physisorbed water was removed at 120 °C, and at 120-250 °C there was loss of carbon in CA and CTAB. Lastly, at 350-450 °C there was condensation of the adjacent silanol groups, and the sample became thermally stable.

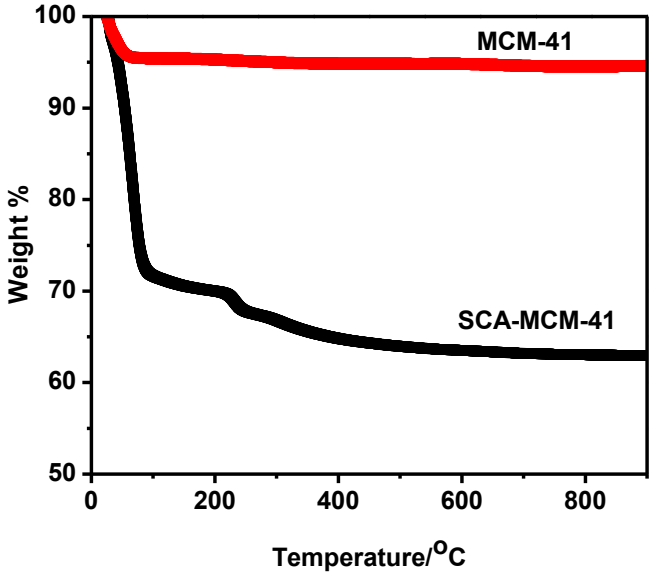

Figure 6.4 TGA profiles of MCM-41 and SCA-MCM-41

6.6.6 Morphological analysis

SEM images of MCM-41 and SCA-MCM-41 samples are presented in Figures 6.5 (a) and (b). MCM-41 appeared as agglomerated spherical particles with pore spaces which may have resulted from the ageing process. The modified sample, SCA-MCM-41, had a type of coverage on the surface of the spherical particles and the pore cavities were now no longer as clearly visible. Therefore, even though there is a covering over the spheres, the spheres are still present indicatiing that the surface properties of SCA-MCM-41 did not significantly change after the citric-acid grafting.

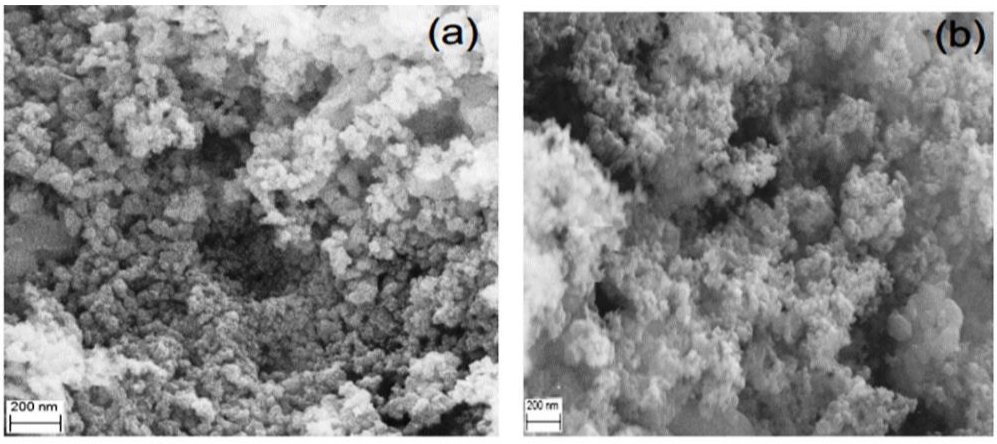

Figure 6.5 (a) FESEM image of MCM-41 and (b) FESEM image of SCA-MCM-41

Images from HRTEM analysis are presented in Figures 6.6 (a) and (b). TEM images revealed a crystallized 3 dimensional structure of MCM-41. It also revealed the hexagonal or honey comb structure which is a unique feature of MCM-41. A cross-sectional measurement of the pore diameter gave a value of 3.55 nm and this is in agreement with BET pore size measurements. MCM-41 can be deemed as mesoporous as it falls under the IUPAC classification of 2-50 nm.

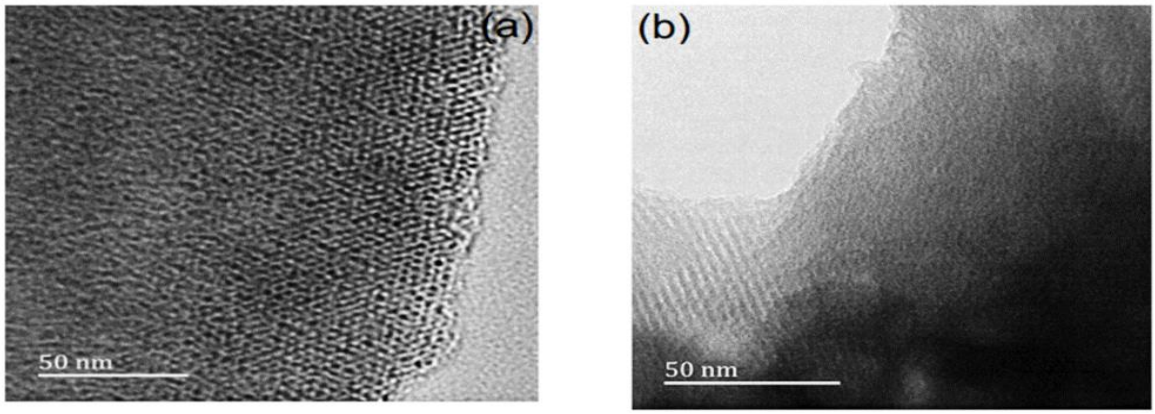

Figure 6.6 (a) HRTEM image of MCM-41 and 6.6 (b) HRTEM image of SCA-MCM-41

6.7 Adsorption Studies

6.7.1 Effect of pH

The effect of pH on the adsorption of MB dye solution was studied over a pH range of 2-10 (Figure 6.7). The adsorption of MB increased from 52 to 89% on MCM-41 and from 68.9 to 96.7% on SCA-MCM-41, as pH increased from 3-7. At low pH (acidic) there is competition between H^+ and MB ions for -OH and –COOH groups on MCM-41 and CA-grafted MCM-41, respectively. This caused a decrease in the amount of MB adsorbed but at higher pH values $–COO^-$ and O^- exist, increasing electrostatic attraction between MB and the adsorbent, resulting in increased MB adsorption, as observed by Kushwaha et al. (2014). This competition causes a decrease in the quantity of MB dye adsorbed. At increased pH, $-O^-$ and $–COO^-$ ion become more prominent and may enhance electrostatic interaction resulting in increasing adsorption capacity for MB. Adsorption capacity of MB after pH 8 was marginal, hence, pH 8 was selected for further studies. The increase in adsorption capacity of SCA-MCM-41 was because of more ($-COO^-$) adsorption sites than in MCM-41 (Sajab et al., 2011). Electrostatic ion attraction is the main

mechanism of adsorption of MB on to SCA-MCM-41, however MB is also possibly adsorbed physically on the pores of the adsorbents This possible physical adsorption was observed at low pH values which showed there was still adsorption occurring which was not due to electrostatic interaction.

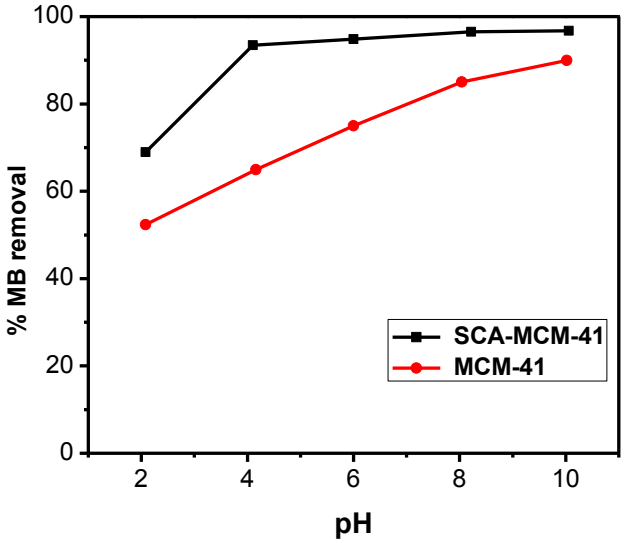

Figure 6.7 Effect of pH on MB removal

6.7.2 Effect of adsorbent dose

Adsorbent dosage is important in measuring the adsorption capacity and removal efficiency, the quantity of adsorbent added to a solution determines the quantity of binding sites available for adsorption. The effect of adsorbent dose (MCM-41 and SCA-MCM-41) on the removal of MB from aqueous solution is shown in Figure 6.8. This figure shows the removal of the MB increases up to a limit 30 mg and it then remains constant. The adsorption of MB on MCM-41 increased from 46.72 to 77.80%, and for SCA-MCM-41 it increased from 50.46 to 95.09% as the adsorbent dose increased. Increased adsorption can be attributed to increased surface area and the availability of more adsorption sites, however the amount adsorbed per unit mass is considerably decreased (Reddy et al., 2012).

The adsorption for both materials increases with an increase in adsorbent dose due to the increase in available sorption sites. However, higher masses of adsorbent lead to aggregation of the adsorbent and reduced surface area resulting in no further adsorption shown by the levelling

of the curve (Figure 6.8). For SCA-MCM-41, aggregation is reached at 30 mg of adsorbent, but at that point almost all the adsorbate has been adsorbed (95.09%). For MCM-41, aggregation is reached at 40 mg of adsorbent dose but due to the fewer number of available sites for adsorption, it only reaches a maximum of 77.80% adsorption shown by the levelling of the curve.

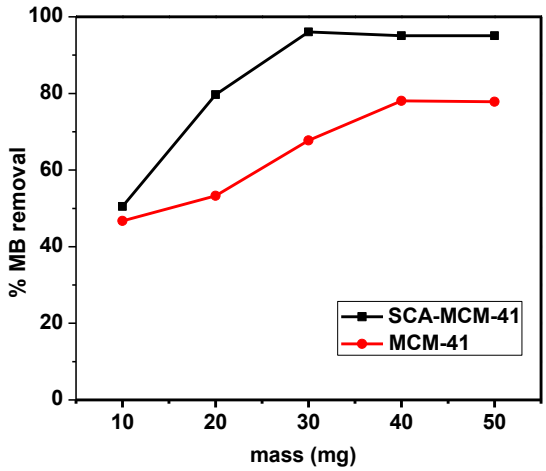

Figure 6.8 Effect of dose on MB removal

6.7.3 Effect of initial concentration

This was carried out at pH 8 and the concentration range was between 30-120 mg/L of MB. The initial low concentration of MB was an important dynamic in overcoming mass transfer resistance of dye molecules between the aqueous solution and adsorbent. As the concentration of MB increased, the gradient concentration became higher which made more dye molecules transfer to SCA-MCM-41, resulting in it having a higher adsorptive capacity and removal efficiency (Van Doorslaer et al., 2015). There was an increase in q_t MB adsorbed from 20.90 to 53.20 mg/g and from 28.28 to 81.34 mg/g for MCM-41 and SCA-MCM-41, respectively, on increasing the initial concentration from 30-120 mg/L (Appendix C 1.1). The decrease in % MB adsorption with an increase in MB concentration is not significant for SCA-MCM-41 which is due to the availability of a large number of available adsorption sites and in the case of MCM-41, the % MB decrease was more due to a lesser amount of adsorption sites. During the initial adsorption process, there was a large amount of adsorbent in the solution with unoccupied sites, therefore the adsorption was rapid. Adsorption rate reduced as time progressed, because the adsorbent sur-

face had become saturated with the dye (sorption sites become occupied by the adsorbate), the diffusion rate of MB into the inner space of SCA-MCM-41 became slower, thereby limiting adsorption (Kushwaha et al., 2014). Agglomeration of MB occurs at high MB concentration which would also slow down the adsorption process (Sajab et al., 2011).

6.7.4 MB adsorption isotherms

The analysis of adsorption equilibria aids in understanding the effect of temperature and adsorbent to adsorbate ratio/interaction on the efficiency of an adsorption process. An increase in temperature causes increased rate of diffusion of the adsorbate molecules across the external boundary layer and in internal pores of the adsorbent particles (Sajab et al., 2011). The equilibrium data analysed in this study are Langmuir, Freundlich, Temkin and Dubinin-Radushkevich isotherm models.

Table 6.2 Adsorption isotherm models

Models	Equation	Reference
Langmuir	$\frac{C_e}{q_e} = \frac{1}{bQ_m} + \frac{C_e}{Q_m}$	Kushwaha et al. (2014)
Freundlich	$ln\, q_e = ln\, K_F + \left(\frac{1}{n}\right) ln\, C_e$	Kushwaha et al. (2014)
Temkin	$ln\, q_e = B\ ln\, A + B\ ln\, C_e$	Kushwaha et al. (2014)
D-R	$ln\, q_e = ln\, qmax - \beta\varepsilon^2$	Shao et al. (2014)

For the Langmuir model, q_e is the adsorption capacity (mg/g) at equilibrium, Q_m is the monolayer adsorption capacity (mg/g), b is the Langmuir constant related to the free energy of adsorption (L/mg) and C_e is the equilibrium concentration (mg/L) of the dye in solution. The values of Q_m and b were calculated from slope ($1/Q_m$) and intercepts ($1/bQ_m$) of the linear plots of C_e/q_e *vs* C_e. For the Freundlich isotherm K_F and N are Freundlich constants related to adsorption capacity (mg/g), 1/n is adsorption intensity of adsorbents. K_F and n were calculated from intercept (ln K_F) and slope (1/n) of the plots of ln q_e *vs* ln C_e. For the Temkin isotherm, B = RT/b, where b is the Temkin constant (J/mol) related to adsorption heat, T = absolute temperature (K), R = gas con-

stant (8.314 J/mol K), and A is the Temkin isotherm constant (L/g). B and A are calculated from slope (B) and intercept (B ln A) of the plot of q_e *vs* ln C_e. The D-R model is applied to make a distinction between chemical and physical adsorption processes with q_e as the adsorption density (mg/g) at equilibrium, q_D = D–R adsorption capacity (mmol/g), b (mol^2/kj^{-2}) = activity coefficient related to the mean adsorption energy and ε = Polanyi potential expressed as equation 3:

$$\varepsilon = RT\ ln(1 + \frac{1}{C_e}) \tag{6.3}$$

where C_e = equilibrium concentration in mol/L and T is the absolute temperature in K. A plot of ln q_e against ε^2 gives a straight line with a slope of β, and intercept of ln q_D gives information about mean free energy E (kj mol/L) of adsorption per molecule of adsorbate and can be calculated using this equation:

$$E = \frac{1}{\sqrt{-2\beta}} \tag{6.4}$$

Correlation coefficient and other parameters calculated from equilibrium data of Langmuir, Freundlich, Temkin and Dubinin-Radushkevich isotherms are shown in Table 6.3. The high R^2 value obtained from both samples fitted into both the Langmuir and Freundlich isotherms and showed both models as being favourable for adsorption. The K_F value obtained indicated a high adsorption capacity with an adsorption intensity value of n>1 showing good adsorption conditions (Kushwaha et al., 2014). Due to adsorbate/adsorbate interaction, Temkin isotherm values indicate heat of adsorption of all molecules in the layer would decrease linearly. Q_m values showed that there was high monolayer adsorption. The mean sorption energy of the D-R model for MCM-41 and SCA-MCM-41 was 3.454 and 5.128 mol^{-1}, respectively. This proves that adsorption was not a chemical process for SCA-MCM-41 and MCM-41 but rather a physical process.

Table 6.3 Isotherm parameters of MB adsorption on MCM-41 and SCA-MCM-41

Isotherm parameters	MCM-41	SCA-MCM-41
Langmuir		
Q_{max} (mg/g)	68.5	88.5
b (L/mg)	0.2926	0.0536
R^2	0.9920	0.9769
Freundlich		
K_F (mg/g(mg/L)$^{-1/n}$)	2.09	3.29
N	8.08	26.7464
R^2	0.970	0.9962
Temkin		
B	159.9	173.8
b (J/mol)	15.5	14.3
A (L/g)	12.4	24.4
R^2	0.999	0.9605
D-R		
q_D (mmol/ g)	0.53	0.79
R^2	0.9524	0.973
E (kJ/mol)	3.454	5.128

6.7.5 Adsorption kinetics

The kinetic studies for adsorption of MB were carried out over a concentration range of 30-120 mg/L for MCM-41 and SCA-MCM-41. The resulting data was fitted into three kinetic models; Lagergren pseudo-first order, pseudo-second order and intraparticle diffusion. Linearised forms of pseudo-first order (equation 6.5), pseudo-second order (equation 6.6) and intraparticle diffusion (equation 6.7) equations are given.

$$ln\ (q_e - q_t) = ln\, q_e\ - ln\, k_{ad} t \tag{6.5}$$

$$\frac{t}{qt} = \frac{1}{K_2\, q_e^2} + \frac{t}{qe} \tag{6.6}$$

$$Q_t\ = K_i t^{0.5} + C \tag{6.7}$$

Where q_e, q_t and k_{ad} (min^{-1}) are amounts of MB adsorbed at equilibrium, at time t (mg/g), and rate constant of adsorption, respectively. The values of the k_{ad} and q_e cal were calculated from the slopes ($-k_{ad}$) and the intercepts ($ln\ q_e$) of the plots of ln ($q_e - q_t$) *vs* t. K_i is the intraparticle rate diffusion constant (mg/g $min^{-1/2}$), *C* is the intercept depicting intra-boundary layer effect, K_2 is the rate constant of adsorption (g/mgmin) and Q_t is the amount of MB adsorbed at time t (mg/g).

The calculated kinetics parameters for adsorption of MB on MCM-41 and SCA-MCM-41 at an initial concentration of 30 mg/L are presented in Table 6.4. From the data obtained, pseudo-second-order appears as the best-fit model with $R^2 > 0.99$ suggesting that the adsorption process is chemical in nature which entails ion exchange between adsorbent and adsorbate (Shao et al., 2014). Intraparticle diffusion showed that an increase in initial concentration of MB increased the diffusion rate of MB. The larger the *C* value, the larger the contribution of surface adsorption in the rate-limiting step (Kushwaha et al., 2014). This signifies a mutual adsorption process of both intraparticle diffusion and surface adsorption.

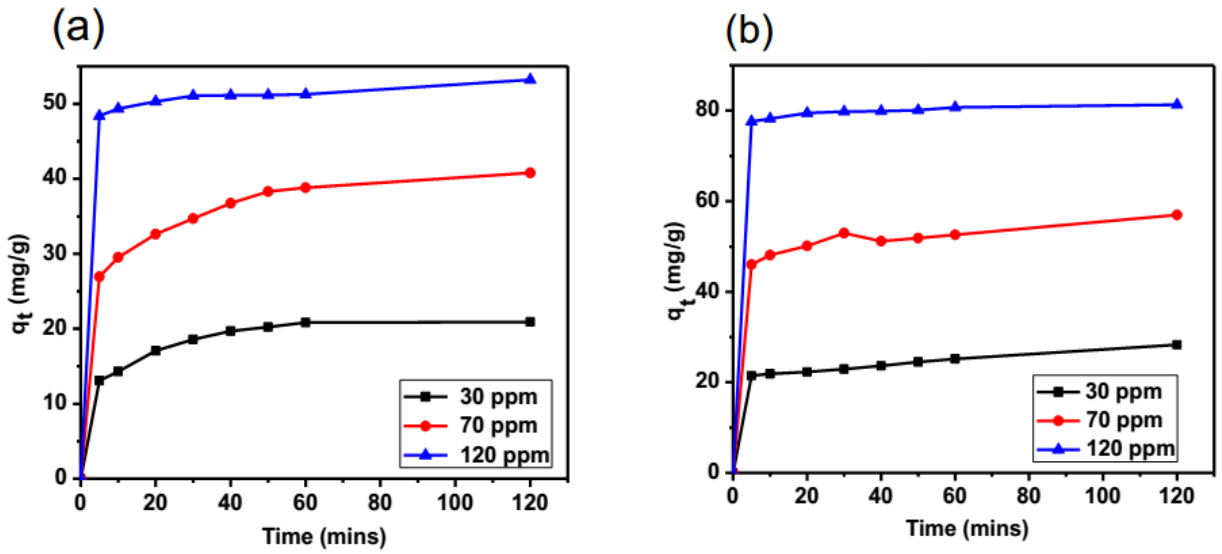

Figure 6.9 (a) Sorption kinetics of MB on MCM-41 and (b) Sorption kinetics of MB on SCA-MCM-41

Table 6.4 Kinetic parameters for adsorption of MB on MCM-41 and SCA-MCM-41

Isotherm parameters	MCM-41	SCA-MCM-41
Pseudo-first order		
k_{ad}	0.0804	0.0169
q_1 (mg/g)	2.88	2.11
R^2	0.8699	0.9834
q_e cal (mg/g)	20.8	28.8
Pseudo-second order		
k_2 (g/mg min)	4.92	4.94
q_e cal (mg/g)	21.83	28.82
R^2	0.9992	0.9993
Intra-particle diffusion		
k_i (mg/g $min^{-1/2}$)	0.8115	0.7894
C	12.3	19.1
R^2	0.9799	0.9624

6.7.6 Effect of temperature

The effect of temperature on adsorption efficiency of SCA-MCM-41 on methylene blue removal is shown in Figure 6.10. A low temperature favours the adsorption process. A temperature increase from 25 ^oC to 65 ^oC caused a reduction in adsorption capacity. The decrease in adsorption capacity is attributed to fast rates of particle vibration, adsorption and desorption between SCA-MCM-41 and MB. An increase in temperature promotes desorption causing a decrease in adsorption capacity (Qu and Gu, 2014). Also, MB molecules are predisposed to leaving the solid phase and moving into the bulk phase due to temperature increase (Kushwaha et al., 2014).

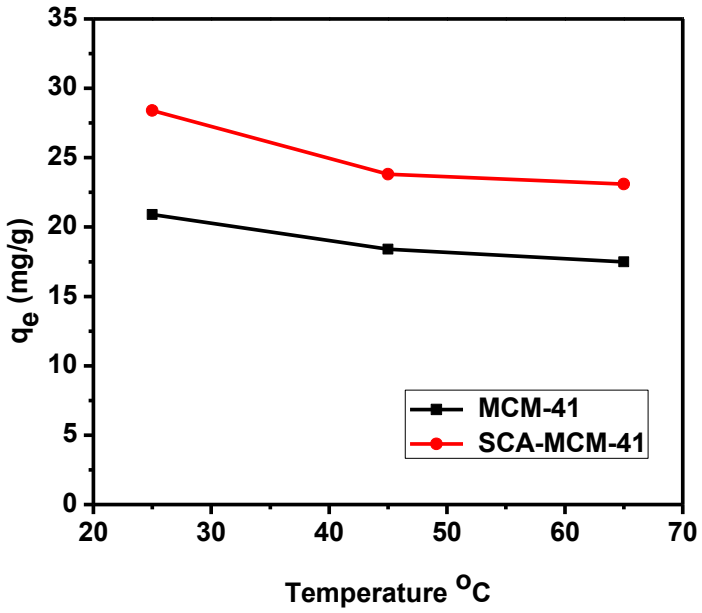

Figure 6.10 Effect of temperature on the removal of MB on MCM-41 and SCA-MCM-41

Three thermodynamic parameters, Gibbs free energy (ΔG^{o}), change in enthalpy (ΔH^{o}) and change in entropy (ΔS^{o}) were calculated using equations 6.8 and 6.9:

$$\ln K_d = \frac{\Delta S^{\circ}}{R} - \frac{\Delta H^{\circ}}{RT} \quad (6.8)$$

$$\Delta G^{0} = -RTlnK_d \quad (6.9)$$

Where T is temperature (K), R is the ideal gas constant and K_d is the distribution coefficient obtained from experimental data using equation 6.5:

$$K_d = \frac{Equilibrium\ concentration\ of\ MB\ adsorbed\ on\ SCAMCM41}{Equilibrium\ concentration\ of\ MB\ in\ solution} = \frac{(Co-Ce)}{Ce} v/m \quad (6.10)$$

ΔH^{o} and ΔS^{o} values were calculated from the slope and intercept of Van't Hoff plots. These values including ΔG^{o} are shown in Table 6.5. A negative $\Delta H°$ value for SCA-MCM-41 suggested that the adsorption process is exothermic. The negative value of $\Delta G°$ shows the reaction as being spontaneous and indicates that the adsorption process is favourable at low temperature (Sajab et al., 2011, Shao et al., 2014, Han et al., 2010). A negative $\Delta S°$ value for SCA-MCM-41 indicates disorderliness at the adsorbent-solution interface (Kushwaha et al., 2014). SCA-MCM-41 has a

more negative Δ*S*° value which suggests a lesser degree of disorderliness compared to MCM-41. As a result, the lesser degree of disorderliness would lead to increased adsorption which confirms the increased adsorption capacity obtained for SCA-MCM-41.

Table 6.5 Thermodynamic parameters for MB adsorption on MCM-41 and SCA-MCM-41

Samples	**T (^{o}C)**	**Δ*G*° (kJ/mol)**	**Δ*H*° (kJ/mol)**	**Δ*S*° (kJ/mol)**
MCM-41	25	-2.2234	-1.6007	-4.4844
	45	-1.3641		
	55	-1.1414		
SCA-MCM-41				
	25	-7.8195	-6.5052	-18.733
	45	-3.8064		
	55	-3.5324		

6.8 Conclusion

CA was successfully grafted onto synthesized MCM-41 from millet straw and characterised. The modified adsorbent (SCA-MCM-41) had an improved adsorptive capacity of MB dye (28.8 mg/g) as compared to unmodified MCM-41 (20.8 mg/g) because of the presence of the carbonyl groups. The equilibrium adsorption data obtained fitted into the Freundlich and Langmuir isotherms. The adsorption process involved intraparticle diffusion and was exothermic and spontaneous. An increase in temperature decreased the adsorption of MB. The optimum pH for adsorption was 8 and optimum temperature was 25 ^{o}C.

6.9 Acknowledgements

We gratefully acknowledge the School of Chemistry and Physics, University of KwaZulu-Natal, South Africa, for providing the laboratory facilities and instrumentation used in this research and also the AAU small grant for financial assistance.

References

Adam, F., Appaturi, J. N., Khanam, Z., Thankappan, R. & Nawi, M. a. M. 2013. Utilization of tin and titanium incorporated rice husk silica nanocomposite as photocatalyst and adsorbent for the removal of methylene blue in aqueous medium. *Applied Surface Science,* 264**,** 718-726.

Bhagiyalakshmi, M., Yun, L. J., Anuradha, R. & Jang, H. T. 2010. Utilization of rice husk ash as silica source for the synthesis of mesoporous silicas and their application to CO_2 adsorption through TREN/TEPA grafting. *Journal of Hazardous Materials,* 175**,** 928-938.

Ghorbani, F., Younesi, H., Mehraban, Z., Çelik, M. S., Ghoreyshi, A. A. & Anbia, M. 2013. Preparation and characterization of highly pure silica from sedge as agricultural waste and its utilization in the synthesis of mesoporous silica MCM-41. *Journal of the Taiwan Institute of Chemical Engineers,* 44**,** 821-828.

Han, R., Zhang, L., Song, C., Zhang, M., Zhu, H. & Zhang, L. 2010. Characterization of modified wheat straw, kinetic and equilibrium study about copper ion and methylene blue adsorption in batch mode. *Carbohydrate Polymers,* 79**,** 1140-1149.

Jaroenworaluck, A., Pijarn, N., Kosachan, N. & Stevens, R. 2012. Nanocomposite TiO_2–SiO_2 gel for UV absorption. *Chemical Engineering Journal,* 181**,** 45-55.

Kushwaha, A. K., Gupta, N. & Chattopadhyaya, M. 2010. Enhanced adsorption of malachite green dye on chemically modified silica gel. *Journal of Chemical and Pharmaceutical Research,* 2**,** 34-45.

Kushwaha, A. K., Gupta, N. & Chattopadhyaya, M. 2014. Enhanced adsorption of methylene blue on modified silica gel: equilibrium, kinetic, and thermodynamic studies. *Desalination and Water Treatment,* 52**,** 4527-4537.

Liou, T.-H. 2011. A green route to preparation of MCM-41 silicas with well-ordered mesostructure controlled in acidic and alkaline environments. *Chemical Engineering Journal,* 171**,** 1458-1468.

Qu, Q. & Gu, Z. 2014. Facile synthesis of hierarchical MCM-41 spheres with an ultrahigh surface area and their application for removal of methylene blue from aqueous solutions. *Analytical Methods,* 6**,** 1397-1403.

Reddy, M. S., Sivaramakrishna, L. & Reddy, A. V. 2012. The use of an agricultural waste material, Jujuba seeds for the removal of anionic dye (Congo red) from aqueous medium. *Journal of Hazardous Materials,* 203**,** 118-127.

Sajab, M. S., Chia, C. H., Zakaria, S., Jani, S. M., Ayob, M. K., Chee, K. L., Khiew, P. S. & Chiu, W. S. 2011. Citric acid modified kenaf core fibres for removal of methylene blue from aqueous solution. *Bioresource Technology,* 102**,** 7237-7243.

Shao, Y., Wang, X., Kang, Y., Shu, Y., Sun, Q. & Li, L. 2014. Application of Mn/MCM-41 as an adsorbent to remove methyl blue from aqueous solution. *Journal of Colloid and Interface Science,* 429**,** 25-33.

Sivasubramanian, G., Shanmugam, C. & Parameswaran, V. 2013. Copper (II) immobilized on silica extracted from foxtail millet husk: a heterogeneous catalyst for the oxidation of tertiary amines under ambient conditions. *Journal of Porous Materials,* 20**,** 417-430.

Takahashi, R., Sato, S., Sodesawa, T., Kawakita, M. & Ogura, K. 2000. High surface-area silica with controlled pore size prepared from nanocomposite of silica and citric acid. *The Journal of Physical Chemistry B,* 104**,** 12184-12191.

Van Doorslaer, X., Haylamicheal, I. D., Dewulf, J., Van Langenhove, H., Janssen, C. R. & Demeestere, K. 2015. Heterogeneous photocatalysis of moxifloxacin in water: Chemical transformation and ecotoxicity. *Chemosphere,* 119**,** S75-S80.

Wu, Y., Zhang, M., Zhao, H., Yang, S. & Arkin, A. 2014. Functionalized mesoporous silica material and anionic dye adsorption: MCM-41 incorporated with amine groups for competitive adsorption of Acid Fuchsine and Acid Orange II. *RSC Advances,* 4**,** 61256-61267.

7.0 CHAPTER 7: SYNTHESIS AND CHARACTERIZATION OF CITRIC ACID GRAFTED MCM-41 AND ITS ADSORPTION OF METHYLENE BLUE

Samson O. Akpotu and Brenda Moodley*

School of Chemistry and Physics, University of KwaZulu-Natal, Westville Campus, Durban, 4000, South Africa.

* corresponding author email: moodleyb3@ukzn.ac.za
Telephone: +27 31 2602796
Fax: +27 31 2603091
First author email: samsonakpotu@yahoo.com

7.1 Abstract

In this study, citric acid (CA) grafted MCM-41 (SCA-MCM-41) was synthesized for improvement of its adsorptive capacity for methylene blue (MB). Characterization of the adsorbent was carried out using scanning electron microscopy (SEM), high resolution transmission electron microscopy (HRTEM), elemental analysis (EA), x-ray diffraction analysis (XRD), textural analysis, thermo-gravimetric analysis (TGA), solid state nuclear magnetic resonance analysis (SSNMR) and fourier transform infrared analysis (FTIR). MB adsorption studies were carried out on citric acid modified MCM-41, varying parameters such as initial dye concentration, pH, adsorbent dose, contact time and temperature. The maximum adsorption capacity of the modified material improved considerably with a q_m of 204.08 mg/g at pH 10 and a temperature of 25 °C. Freundlich and Temkin models were best fitted for the equilibrium data. The adsorption kinetics favoured the pseudo-second-order model. MB adsorption into SCA-MCM-41 was spontaneous and exothermic.

Keywords*: MCM-41, citric acid, methylene blue, adsorption, solgel, grafting*

7.2 Introduction

Industrialisation of the world manufacturing processes however beneficial has brought severe strain on global water resources as effluents are discharged into water bodies. Dyes and pigments when discharged causes harm to aquatic organisms and makes the water unsafe for human consumption, hence, there is an urgent need for remediation. Mobil catalytic material (MCM-41) is a unique class of materials that has excellent properties, such as increased surface area, hexagonal homogenous pores, narrow pore size distribution and thermal stability (Ghorbani et al., 2013). These properties make them suitable as a catalyst support and sorbent for large organic molecules (Janicke et al., 1999, Meléndez-Ortiz et al., 2013). The abundance of extensive -OH groups on the surface of the silica generates sites that can be functionalised for specific adsorption (Kushwaha et al., 2014). Specific adsorption refers to the modification of the surface of MCM-41 with different functional groups tailored towards the adsorption of an adsorbate of choice. Modification of MCM-41 with a tricarboxylic acid can significantly increase its adsorption sites towards cationic surfaces. These cationic surfaces may be heavy metals, dyes or other pollutants. Cationic pollutants such as heavy metals and dyes may present severe environmental problems to man and aquatic life if discharged indiscriminately and therefore its removal from wastewater is important.

Dyes are pigments with widespread industrial use and are often discharged indiscriminately in water systems causing reduction of light penetration in aqueous environs, depleting of oxygen, dispersion of aerosol in the atmosphere and non-degradability (Leme et al., 2015). MB has been used in medicine as an antimalaria agent, in treatment of Alzheimer disease, cardiac surgery and cancer treatment (Ginimuge and Jyothi, 2010). Methylene blue (Figure 7.1) is widely used in textile industry and has been known to cause illnesses in humans such as damage to the nervous system, heart defects and urinary tract infection (Kushwaha et al., 2014).

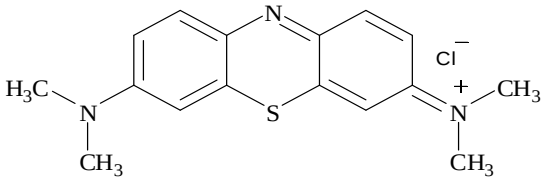

Figure 7.1 **Molecular structure of methylene blue**

Adsorbents such as activated carbon (Song et al., 2012), agrowaste, plant-inorganic composites (Singh et al., 2010), inorganic-organic composites (Adam et al., 2013), nanocomposites and silica (Kushwaha et al., 2014, Qu and Gu, 2014, Wu et al., 2004), have been used for the adsorption of methylene blue dye.

Chemical surface modification of adsorbents is known to increase adsorbent selectivity, capacity and adsorption efficiency (Zhu et al., 2008). Citric acid is a low cost tricarboxylic acid which can be utilized in modification of adsorbents resulting in increased adsorption efficiency. Citric acid derivatised materials have shown tremendous potential in remediating a wide range of pollutants such as heavy metals (Zhu et al., 2008, Marshall et al., 1999, Kandah et al., 2008, Douglas et al., 2006), and organic dyes (Kushwaha et al., 2014, Kushwaha et al., 2010). At elevated temperatures, a thermochemical reaction occurs between citric acid and the adsorbent such that citric acid dehydrates to produce a reactive anhydride which reacts with the hydroxyl groups of silica to form an ester linkage. The resulting effect is that the free carboxyl groups of citric acid increases the net negative charge on the modified adsorbent surface in a solution, making it suitable for cationic adsorption (Zhu et al., 2008).

Marshall et al. (1999) and Douglas et al. (2006) modified soybean hulls with citric acid and used it in the adsorption of Cu^{2+} which showed an increase in adsorption as compared to the unmodified adsorbent. Zhu et al. (2008) showed that modification of soybean straw with citric acid greatly increased the adsorption of Cu^{2+}, Kandah et al. (2008) modified sheep manure with citric acid and showed an increase in its adsorption of Co as compared to the unmodified form. Kushwaha et al. (2010) modified silica gel with oxalic and citric acids, and used it in the adsorption of malachite green. The results obtained showed silica gel modified with citric acid (tricarboxylic acid) had better adsorption capacity than silica gel modified with oxalic acid (dicarboxylic acid). Overall, the modified material showed an improved adsorption as compared to the unmodified silica gel. The modified silica gel with citric acid was used in the adsorption of methylene blue and showed a two-fold increase in its adsorptive capacity.

Thus, the grafting of citric acid on the surface of MCM-41 was expected to produce an adsorbent with unique properties and improved adsorptive abilities for cationic dyes. Ho et al. (2003) pre-

viously synthesised ordered mesoporous silica with carboxylic acid, however, toluene and cyanide was used in the synthesis process. These chemicals are difficult to handle, known to be highly toxic to both humans and the environment, if not properly disposed (Ikeda and Ohtsuji, 1971, Gijzen et al., 2000). The time of synthesis was also very long (over 48 hrs), thus making synthesis labourious and unnecessarily cumbersome. Also, the use of inert gas and high temperatures for extended periods may not be necessary as this contributes to the cost of production of the adsorbent.

In this study we report a time efficient (< 10 hrs), and environmentally friendly method for the synthesis of citric acid grafted MCM-41. The impact of carboxylic groups on mesoporous silica for the removal of a cationic dye was studied. MCM-41 and citric acid grafted MCM-41 were synthesized. The two adsorbents were characterized using thermogravimetric analysis (TGA), elemental analysis (EA), solid state nuclear magnetic resonance (SSNMR), infrared spectroscopy (IR), scanning electron microscopy (SEM), transmission electron microscopy (TEM) and textural analysis. Methylene blue (MB) was utilized in adsorption testing of the synthesized materials. The mechanism for MB adsorption and adsorption efficiency as a function of dose, pH, contact time, temperature, adsorption rate and capacity was determined using kinetic and equilibrium isotherm models.

7.3 Experimental

7.3.1 Chemicals

Tetraethylorthosilicate (TEOS) 98% (Aldrich), cetyltrimethylammonium bromide (CTAB) 99+% (Calbiochem), ammonium hydroxide 25% (BDH chemicals), absolute ethanol (Merck), methylene blue (Sigma Aldrich), 37% HCl, 3-aminopropyltriethoxysilane (APTES) and citric acid (CA) monohydrate obtained from Thomas Baker were used in the experimental.

7.3.2 Synthesis of MCM-41

MCM-41 was synthesized using a modified method from Parida et al. (2012). About 2.4 g of CTAB was dissolved in 120 mL of ultra-pure water at room temperature. A 10.25 mL aliquot of ammonium hydroxide was added to a beaker containing CTAB and water, under stirring with a magnetic stirrer. A 10 mL aliquot of ethanol was added to the mixture. This was allowed to stir for 30 minutes and a further 10 mL of tetraethylorthosilicate (TEOS) was added to the clear solution and stirred vigorously at 300 rpm for an hour. The slurry was vacuum filtered, washed with double-distilled deionised water to a neutral pH, expelling the surfactant and ammonia solution. The resultant powder was dried in an oven (Vindon Solid State) at a temperature of 110 °C for 24 h. The dried powder was broken up gently with a mortar and pestle before calcination in muffle furnace (Kittec Squardro) at 550 °C for 5 h and with a ramp rate of 2 °C/min to remove CTAB.

7.3.3 Activation of MCM-41

Activation of MCM-41 was achieved by modifying the method of Kushwaha et al. (2014). Approximately 40 mL of 6 M HCl was added to MCM-41 (1 g) in a 3 necked flask and the mixture refluxed at 100 °C using a double-walled condenser with continuous stirring for 4 h, and then left to cool to room temperature. The resulting material was vacuum filtered and washed with double distilled water until a neutral pH was reached, and dried in an oven at 150 °C for 5 h. This was assigned as A-MCM-41.

7.3.4 Synthesis of NH_2-MCM-41

MCM-41 surface was modified by in aqueous by an easy one-step synthesis. About 1.00 g of MCM-41 was dispersed in ethanol (30 mL) in a round bottom flask and ultrasonicated for an hr with stirring. Approximately, 500 µL of APTES was added to bind $–NH_2$. The reaction was stirred at 50 °C for 8 h to obtain a monolayer and positively charged MCM-41. The product was collected by filtration and dried under vacuum at 60 °C.

7.3.5 Grafting of A-MCM-41 with citric acid

A 20 mL volume of 0.6 M citric acid, prepared in water, was added to 1 g of NH_2-MCM-41. This was sonicated for 45 mins and stirred for 45 mins to make a slurry. It was kept in a vacuum oven at a temperature of 50 °C for 24 hours which was subsequently increased to 120 °C for 90 minutes to aid the thermochemical reaction. The material was washed with double-distilled de-ionized water until a few drops of 0.1 M copper nitrate solution added to the filtrate did not turn cloudy. This signified the complete discharge of excess citric acid and a neutral pH has been reached. The resultant solid was dried at 70 °C for 2 hrs and kept in a desiccator until it was characterized. This material was labelled 0.6SCAMCM-41. The same process was repeated using 0.8, 1.0, 1.2 and 1.4 M citric acid, and the samples were designated 0.8SCA-MCM-41, 1.0SCA-MCM-41, 1.2SCA-MCM-41, and 1.4SCA-MCM-41, respectively.

7.4 Characterisation of Synthesised Materials

MCM-41 and CA grafted MCM-41 were characterized using various techniques. The percentage of carbon in the samples was determined using an elemental analyser (Thermo Scientific CHNS/O analyser). N_2 adsorption–desorption isotherms were obtained using a nitrogen adsorption analyzer (Micrometrics Tristar II 3020). MCM-41 was degassed at a temperature of 90 °C for an hour and then ramped up to 200 °C overnight. CA-grafted samples were degassed at 90 °C overnight. This temperature was selected to prevent CA decomposition. Surface area and pore size measurement of samples were obtained using the BET method. The pore volume was calculated from the adsorption branch based on volume of nitrogen adsorbed at a relative pressure (P/P_o) of approximately 0.99. Low angle (0-5 Θ) and long range (10-90 Θ) x-ray diffraction (XRD) analysis of samples were carried out on a Bruker D8 XRD with Cu-Kα radiation at 40 mA and 45 kV. Surface morphology was obtained with field-emission scanning-electron microscopy (FESEM), micrographs were analysed using an operating voltage of 10 kV (Zeiss instrument). Samples were coated with a thin film of gold to minimize surface charging. The ordered nature of samples was determined using high resolution transmission electron microscopy (TEM) (JEOL). Samples were prepared by firstly ultrasonicating in ethanol and placed on copper grids with carbon film. Thermal stability of synthesized materials was determined by heating 5

mg of samples in aluminium pans in air at 900 °C at a ramping rate of 5 °C/min with SDT Q 600 V 209 Build 20. FTIR (Perkin Elmer Series 100 spectrometer) in the range of 4000 – 400 cm^{-1} was used in the acquisition of data showing the presence of silanol, siloxane and carboxyl functional groups. ^{29}Si and ^{13}C magic angle spinning (MAS) NMR spectra were measured on a Bruker D8 Advance NMR operating under a static magnetic field.

7.4.1 Point of Zero Charge (PZC) determination

About 0.02 g of sample was suspended in 0.02 M NaOH in a pH range of 2-10. The pH was adjusted with 0.1 M HCl or 0.1 M NaOH and the PZC value was determined by a plot of final pH *versus* difference in initial and final pH (Khan et al., 2013).

7.5 Adsorption Studies

A MB stock solution of 1000 ppm was prepared and diluted to various working solution concentrations and the absorbances read from the UV-3600-Shimadzu UV-VIS-NIR spectrophotometer at a wavelength of 663 nm to produce a calibration curve. Adsorption experiments were carried out using 20 mL aliquot solutions. The MB solution of predetermined concentration (pH adjusted with 0.1 M NaOH or HCl) and a specific mass of adsorbent were placed on the orbital shaker (Scientific Engineering) to equilibrate for 2 hrs. After adsorption, the MB solution was centrifuged at 10000 rpm for 3 minutes and the supernatants were analysed using a UV-spectrophotometer.

The adsorption capacity of methylene blue at equilibrium time q_e (mg/g) was calculated from the equation:

$$q_e = \frac{(C_o - C_e)V}{W} \qquad (7.1)$$

Where C_o and C_e are initial and equilibrium concentrations of MB in mg/L, V is the volume of the solution (L), and *W* is the mass of adsorbent used (g) in the experiment.

The percentage MB removal at equilibrium time was calculated using the equation:

$$\%\, MB\ removal = 100\,\frac{C_o - C_e}{C_o} \qquad (7.2)$$

The influence of CA ratio to MCM-41 for the removal of MB was carried out by using 12.5 mg of each adsorbent at pH 6 at a temperature of 25 °C. The effect of pH (6-11), adsorbent dose (5-40 mg), contact time (5-120 mins), initial dye concentration (30 mg/L) and temperature (293 to 323 K) on adsorption capacity was determined by varying one parameter at a time while the others were kept constant, unless otherwise stated.

7.6 Results and Discussion

7.6.1 Characterisation of adsorbents

7.6.1.1 XRD profiles

Figure 7.2 (a) shows the wide angle scan XRD profile obtained at 10-80(Θ) for unmodified MCM-41 and citric acid grafted MCM-41. In unmodified MCM-41, 0.6SCA-MCM-41, 0.8SCA-MCM-41 and 1.0SCA-MCM-41, there were no diffraction peaks corresponding to CA crystals. Only a large amorphous peak between 20 and 30(Θ) characteristic of siliceous materials was observed, indicating the amorphous nature of the samples (Takahashi et al., 2000, Simonutti et al., 1999), and a well-organized silica matrix. However, a crystalline material was observed at higher citric acid concentrations that produced 1.2SCA-MCM-41 and 1.4SCA-MCM-41. This may be a result of CA crystals being overloaded on the silica support. Figure 7.2 (b) shows low angle scan XRD profiles for all samples obtained between 0-5(Θ). The profile of MCM-41 showed 3 intense peaks, one at 100 (2.5(Θ)) and two higher order reflection peaks at 110 (4.2(Θ)) and 200 (4.8(Θ)). These peaks are indicative of mesophase materials, (Qu and Gu, 2014) and confirms the synthesis of MCM-41 (Monash and Pugazhenthi, 2010). As the CA concentration increased, there was a reduction in the intensity of these peaks. The differences in CA concentration led to variation in XRD peaks suggesting that CA concentration played a vital part in the silica phase. However, for samples with higher CA concentration, the two diffraction peaks (110 and 200 at

4.2 and 4.8(Θ), respectively) disappeared signifying partial reduction in orderliness of mesoporous structure. Mesoporous materials synthesized at basic pH possess a well resolved extremely ordered hexagonal mesostructured (Monash and Pugazhenthi, 2010), which is now lost due to the increase in CA concentration. The decreased peak intensities of the citric acid grafted MCM-41 is due to higher contrast between silica and the carboxyl group, loss of space and correlation of pores.

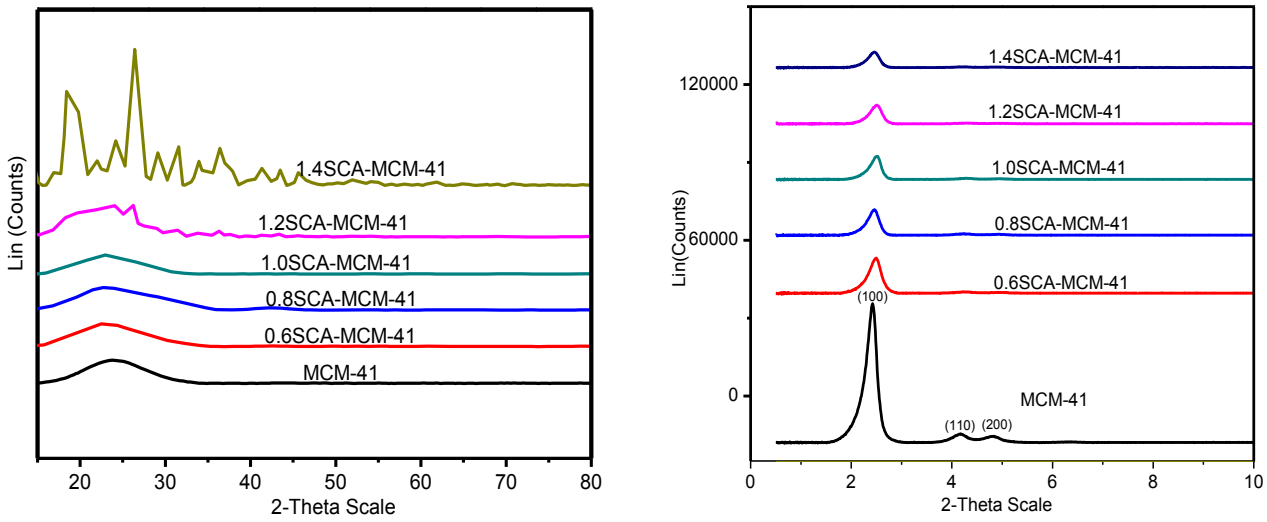

Figure 7.2 (a) Wide angle XRD profiles and (b) Low angle XRD profiles

7.6.1.2 FTIR studies

The FTIR spectra are shown in Figure 7.3. Absorption bands around 3400 cm^{-1} for all samples are indicative of water and –OH stretching groups present. Bands at 960 and 1630 cm^{-1} in MCM-41 are due to the stretching and bending, respectively of the hydroxyl substituent attached to Si. The band around 1630 cm^{-1} in CA grafted MCM-41 is assigned as the intermolecular hydrogen bond from the carboxyl groups. This is further confirmed by the ^{29}Si and ^{13}C NMR studies. The absorption peak found around 1050 cm^{-1} and 805 cm^{-1} are due to asymmetric stretching of Si-O-Si and symmetric stretching, respectively (Kushwaha et al., 2014). All modified samples had absorption bands between 1736 cm^{-1} and 1640 cm^{-1} due to carbonyl stretching (Kushwaha et al., 2014), either as conjugated or non-conjugated to aromatic rings which was not found in the unmodified material. The band in the region of 1425 cm^{-1} can be attributed to C-O from the carboxyl group from CA which was also not present in the unmodified material. CA grafting result-

ed in vibrations around 1715-1730 cm^{-1}, which is due to esterification of CA with MCM-41 forming a C=O bond from the COOH group in CA (Kushwaha et al., 2014). The carboxyl group of the modified material is thought to function as an efficient proton donor and aids in deprotonation as it forms coordinated complexes with cationic dyes (Han et al., 2010) *via* electrostatic ion interaction.

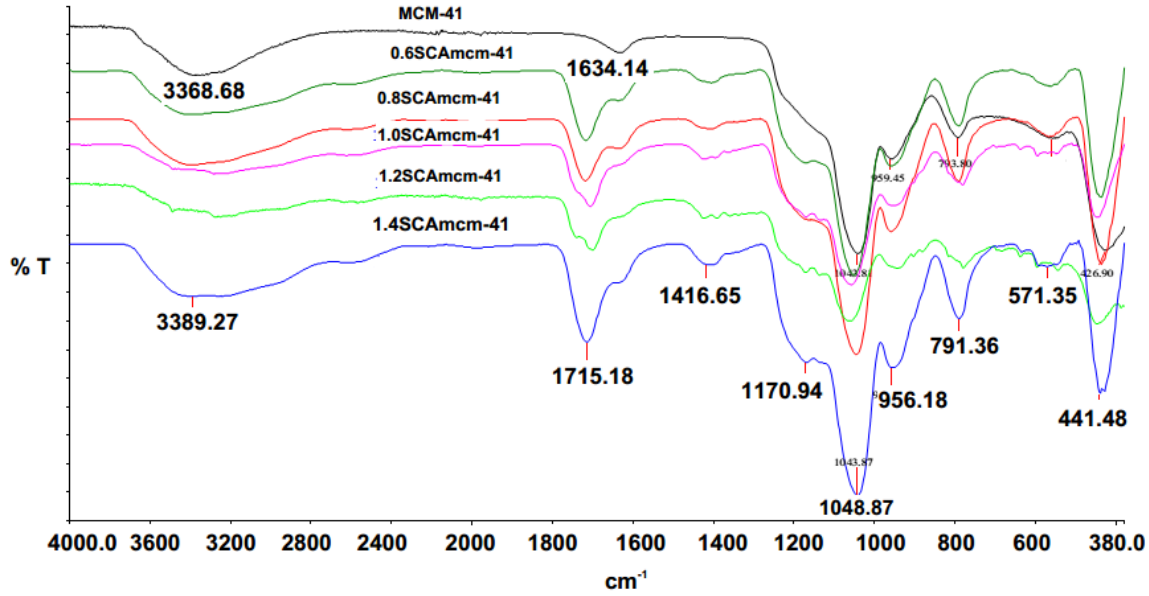

Figure 7.3 FTIR spectra of unmodified and modified MCM-41

7.6.1.3 TGA-DSC profiles

The thermal profile of MCM-41 and CA grafted MCM-41 samples (Appendix B 1.1) showed that 0.6SCA-MCM-41 displayed better stability when compared to the other grafted samples. MCM-41 degradation profile was depicted as a 3 step process. Firstly, there was the removal of physically adsorbed water which occurred as weight loss of 4.5% at about 150 °C. The subsequent phase had a degradation loss in mass of about 0.5% at 350 °C. Within this temperature range, there was a slight but gradual loss in mass, which can be attributed to decomposition of residual carbon, loss of water from the condensation of adjacent silanol groups, dehydroxylation and removal of the CTAB organic template. Beyond 650 °C, the thermal profile showed that MCM-41 is thermally stable, with no noticeable change in mass occurring thereafter.

For CA-grafted silica, mass loss occurred at the same temperature range as it did for MCM-41. However, there was simultaneous mass loss due to CTAB and CA degradation for each sample. Initially, there was removal of physisorbed water in CA and CTAB at 150 °C. At 150-350 °C, there was further mass loss as carbon present in CTAB and CA decomposed. At 350-650 °C, degradation occurred due to loss of water on condensation of adjacent silanol groups and removal of the CTAB template and residual carbon in CA. The total mass loss for all samples increased as CA concentration increased, thereby substantiating the XRD (as the material becomes more crystalline), textural analysis (reduction in surface area and pore volume) and ^{13}C Cross Polarisation Magic Angle Spinning-NMR analysis.

7.6.1.4 NMR studies

Figures 7.4 (a) and 7.4 (b) show ^{29}Si and ^{13}C spectra, respectively. The SiO_4 repetitive unit is denoted as Q^n with formula $Si(OSi)_n(OH)_{4-n}$ (Takahashi et al., 2000). All ^{29}Si samples exhibited 3 peaks at -90, -100 and -110 ppm and were designated as Q^2, Q^3 and Q^4 species, respectively. These are typical of siliceous based materials. The peaks at -90 ppm (Q^2) are due to the silica atom possessing a geminal silanol $(Si\text{-}O)_2Si\text{-}(OH)_2$, -100 ppm ($Q^3$) is due to silicon atoms possessing a lone -OH group $(Si\text{-}O)_3Si\text{-}OH$ and at -110 ppm (Q^4) is as a result of the silica atom without –OH groups, $Si(Si\text{-}O)_4$ (Takahashi et al., 2000). On all samples, the Q^4 species were dominant which was due to condensation of silanol with Q^3 and very little Q^2 present. In MCM-41, these peaks were barely visible, however, as citric acid concentration increased, it was observed there was an increasing shift (ppm) towards Q^3 and Q^2 species which may be due to the presence of substantial amounts of silanol on the surface.

Solid-state single pulse excitation (SPE) MAS ^{13}C NMR spectra of all samples were obtained at room temperature (Figure 7.4 (b)). All CA-grafted MCM-41 showed a resonance peak at 44.2 ppm, which is due to the methyl carbon in the ethoxyl group (CH_3CH_2OSi). In contrast, at higher CA concentration (1.2 and 1.4 M), this peak splits into 2 depicting the structure of the methyl carbon in pure CA. The peak observed at 72.5 ppm is due to the methylene carbon in the ethoxyl group and the peaks between 172-182 ppm are attributed to the carboxyl carbons of the CA (Takahashi et al., 2000). At low CA concentration only the peak at 44.2 ppm was observed due

to the amorphous nature of the samples. The presence of carboxyl peaks in samples 1.0SCA-MCM-41, 1.2SCA-MCM-41 and 1.4SCA-MCM-41 is due to the high concentration of citric acid grafted on them. This is substantiated from FTIR, TGA and XRD analysis results showing more crystalline samples at a higher CA concentration. Further confirmation of increasing crystallinity with increasing CA content is seen as the intensity of all the peaks increased as CA concentration increased in the modified MCM-41 (Takahashi et al., 2000).

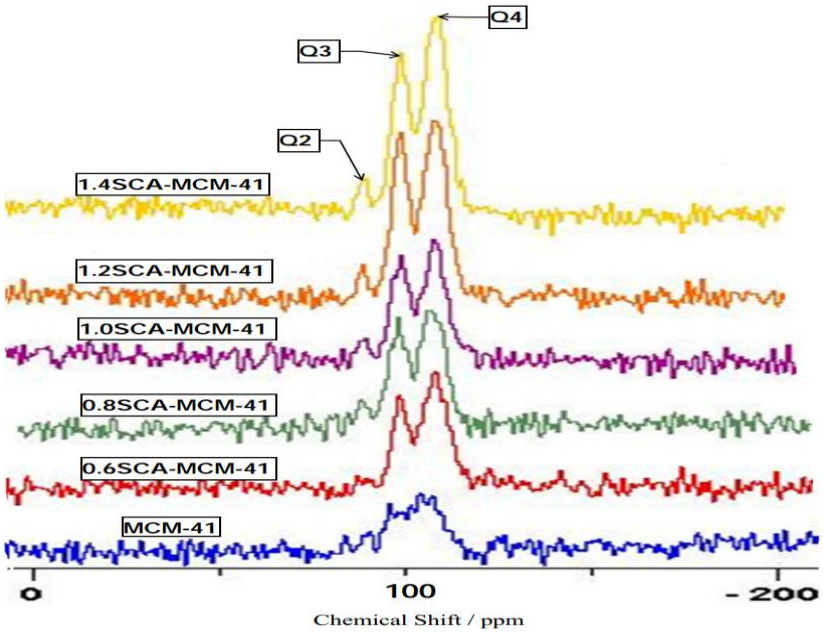

Figure 7.4 (a) Changes in ^{29}Si MAS NMR

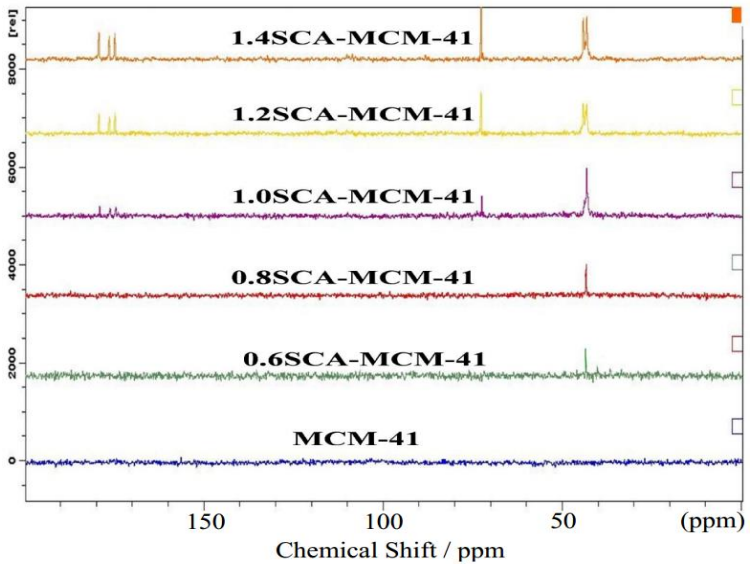

Figure 7.4 (b) ^{13}C MAS NMR spectra

7.6.1.5 Elemental analysis

This was carried out to determine the percentage of carbon in the samples. There was a general increase in carbon content of samples as CA concentration was increased from 0, 4.0, 4.8, 6.2, 8.8 and 14.2% for MCM-41, 0.6SCA-MCM-41, 0.8SCA-MCM-41, 1.0SCA-MCM-41, 1.2SCA-MCM-41 and 1.4SCA-MCM-41, respectively. This is indicative that different percentages of carbon were grafted on MCM-41 and which contributed to the increase in the hydrophobic nature of the adsorbents.

7.6.1.6 Textural analysis

Figures 7.5 (a) and 7.5 (b) showed the N_2 adsorption-desorption isotherms and pore size distribution graphs, respectively, of MCM-41 and CA grafted MCM-41 samples. A distinctive type IV adsorption isotherm for mesoporous solids was observed for both unmodified and modified samples. This indicated that ordered nature of the pores was relatively undisturbed. At low pressure between ($P/P_o \leq 0.2$) N_2 adsorption uptake by MCM-41 showed a linear increase due to monolayer-multi-layer adsorption on the walls of the pores. Between pressures of 0.20 and 0.40, there was a rapid increase in adsorbed volume which may be attributed to capillary condensation of N_2 in the pore channels and a narrow pore size distribution of uniform size (Monash and Pugazhenthi, 2010). At relatively high pressure, between 0.46-0.99, there was minimal linear increment in the multilayer adsorption of N_2. MCM-41 had a H2 hysteresis loop which indicated uniform and regular pores. Larger hysteresis loops were present on all CA grafted samples which was due to the presence of larger mesopores. MCM-41 is often characterized by specifically large surface area, pore sizes, large pore volume and high hexagonal nature. Table 7.1 shows the BET surface area, total pore volume, and average pore size of the samples.

Table 7.1 Surface area, pore diameter and pore volume measurements for MCM-41 and CA-MCM-41 samples

Sample	SBET(m^2/g)	Pore diameter (nm)	Pore volume (cm^3/g)
MCM-41	1261	2.73	0.93
0.6SCA-MCM-41	808	3.01	0.61
0.8SCA-MCM-41	780	2.61	0.51
1.0SCA-MCM-41	768	2.64	0.50
1.2SCA-MCM-41	604	2.84	0.43
1.4SCA-MCM-41	507	2.97	0.37

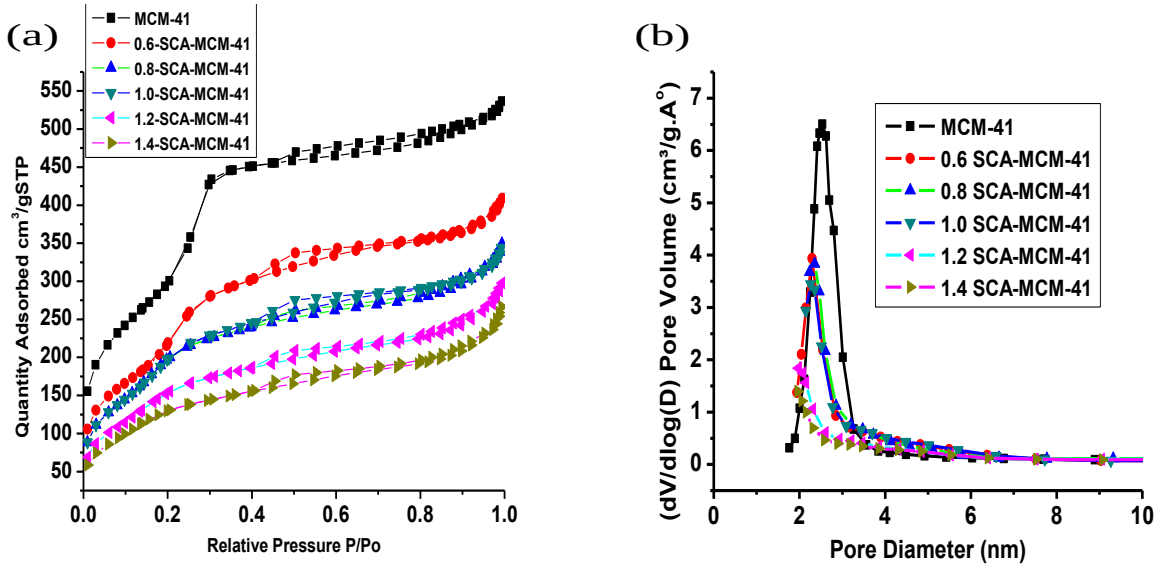

Figure 7.5 (a) N_2 adsorption-desorption isotherms and (b) Pore size distribution of samples

The pore size distribution pattern was between 2-4 nm for all samples which is characteristic of mesoporous materials according to IUPAC (Beck et al., 1992). MCM-41 had a highly mono-modal narrow pore distribution of 2 nm very close to the micropore region. However, there was a small pocket of pores between 6-10 nm for 1.2SCA MCM-41 and 1.4SCA MCM-41. The results indicated that CA grafting on MCM-41 caused a reduction in surface area and pore volume. The reduced surface measurements were more prominent with increased CA concentration. This was as a result of pore filling by citric acid.

7.6.1.7 Analysis of surface morphology

SEM images are shown in Figure 7.6. There are 2 mechanisms for the formation of MCM-41; liquid crystal initiation and silicate anion initiation pathway (Firouzi et al., 1995). The pathway of this study was the former where surfactant micelles were independently organized and preceded by formation of a siliceous framework around aggregates (Qu and Gu, 2014, Firouzi et al., 1995) ensuring the crystalline phase is well formed. The electrostatic templating mechanism in formation of MCM-41 requires a cationic head (CTAB) and a repeating anionic unit (silica) which forms the $S^{+}I^{-}$ template. This affects the rate of deposition and consequently the mesostructure formation. A strong interaction exists when the concentration of surfactant to silica is high, resulting in quick formation of nanospheres, which tends to aggregate to layers of spheres forming rod-like particles. Rod-like particle formation is further enhanced by addition of ethanol as it causes the rate of polymerization to be reduced. The morphological appearance of MCM-41 comprised a mixture of spheres and rods with a mean size of 91 nm and at a close view was made up of small grain particles with an average diameter size of 3 nm, clearly showing uniform aggregation with large cavities and large pore volume (Figures 7.6 (b), 7.6 (c) and 7.6 (d)). An enlarged view of 0.6SCA-MCM-41, 0.8SCA-MCM-41 and 1.0SCA-MCM-41 SEM images revealed coating by citric acid as it is visible on small grain like spheres of MCM-41 (Figure 7.6 (e)). SEM images of 1.2SCA-MCM-41 and 1.4SCA-MCM-41 showed a more homogenous cover of citric acid and reduced cavities and pore volume (Figures 7.6 (e) and 7.6 (f)). This is in agreement with results of BET, XRD and ^{13}CP MAS-NMR analysis.

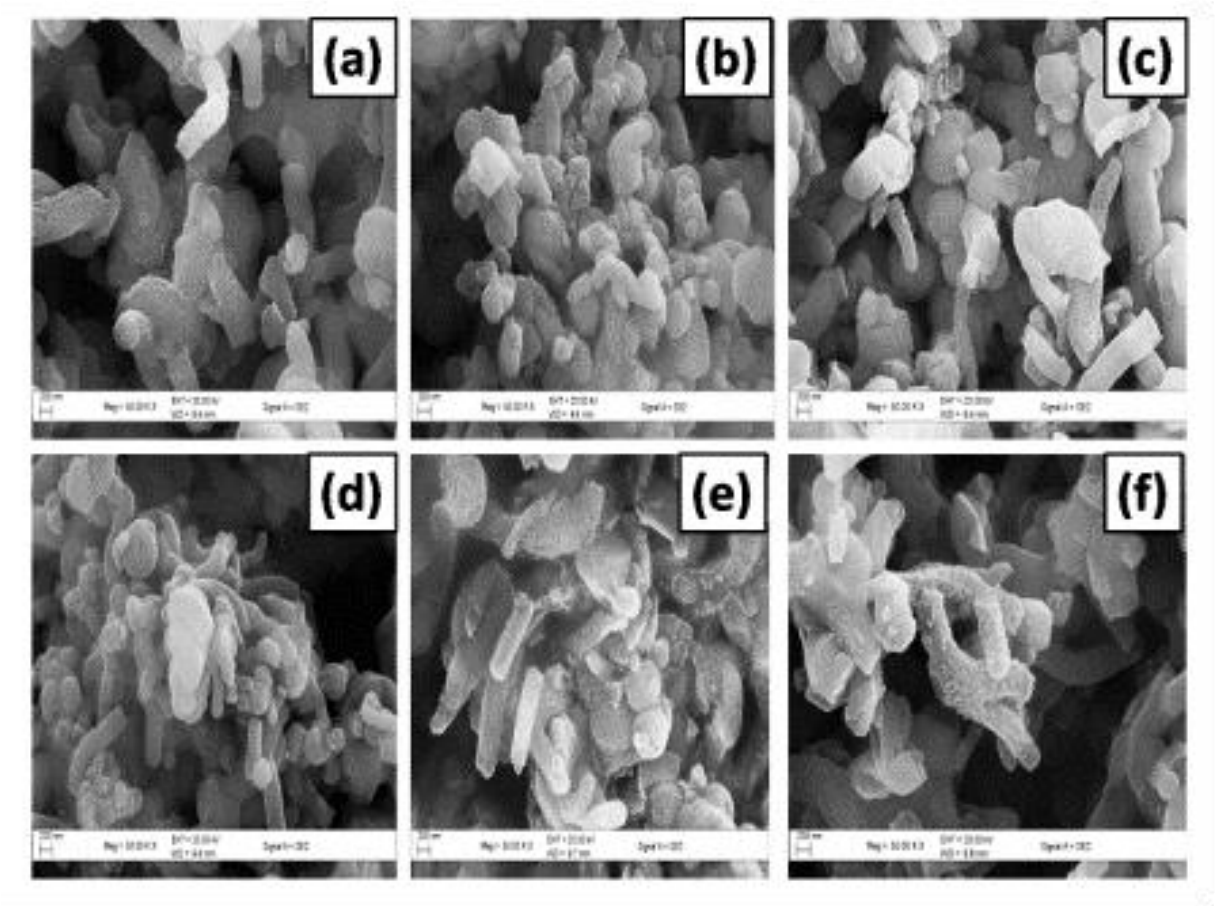

Figure 7.6 Scanning electron micrographs of (a) MCM-41 (b) 0.6SCA-MCM-41 (c) 0.8SCA-MCM-41 (d) 1.0SCA-MCM-41 (e) 1.2SCA-MCM-41 (f) 1.4SCA-MCM-41

High resolution transmission electron microscopy images of all samples are presented in Figures 7.7 (a-g). All samples showed a one dimensional, highly ordered hexagonal honey comb structure of silicate material typical of MCM-41. Data obtained from XRD studies further confirms the hexagonal order of the MCM-41 mesopores. The ordered morphology shows a hexagonal shape with visible monomodal pore sizes of 2.3 nm on the (100) crystal face (Figure 7.7 (a)) and a uniform wall of parallel channels on 110 crystal face. The pore size of 2.3 nm was in agreement with values of 2.0 nm obtained from BET measurements. Samples with high citric acid content 1.2SCA-MCM-41 and 1.4SCA-MCM-41 (Figures 7.7 (f) and 7.7 (g)) showed some of level of reduction of its ordered nature because of degradation which was also confirmed by XRD analysis.

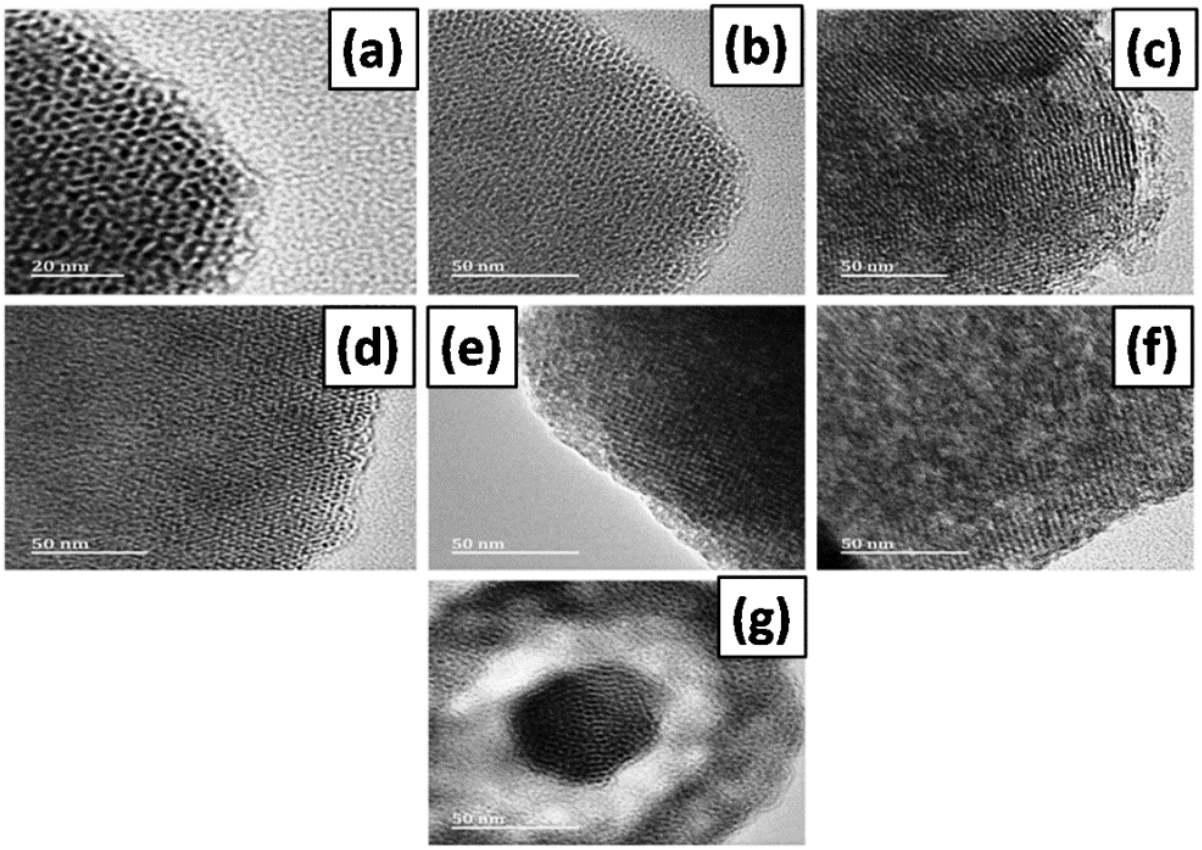

Figure 7.7 Transmission electron micrographs of (a) MCM-41 at 20 nm (b) MCM-41 at 50 nm (c) 0.6SCA-MCM-41 at 50 nm (d) 0.8SCA-MCM-41 at 50 nm (e) 1.0SCA –MCM-41 at 50 nm (f) 1.2SCA-MCM-41 at 50 nm (g) 1.4SCA-MCM-41 at 50 nm

7.7 Adsorption Studies

7.7.1 Effect of citric acid content on MB removal efficiency

This was determined experimentally by comparing the adsorption capacity of MCM-41 to 0.6, 0.8, 1.0, 1.2 and 1.4 M CA grafted MCM-41 in the adsorption of MB and showed that CA enhanced MB removal efficiency compared to unmodified MCM-41. At pH 6, unmodified MCM-41 produced an adsorption efficiency of 27.8% which was appreciably increased to 50.9% when 0.6 MCA was used. However, a further increase in CA concentration was detrimental to the removal of MB as seen in Figure 7.8. This is further confirmed by the BET results which showed

that 0.6 M CA had the highest surface area of all the modified adsorbents. Hence, 0.6 M was adopted as the optimum concentration of CA needed for modification.

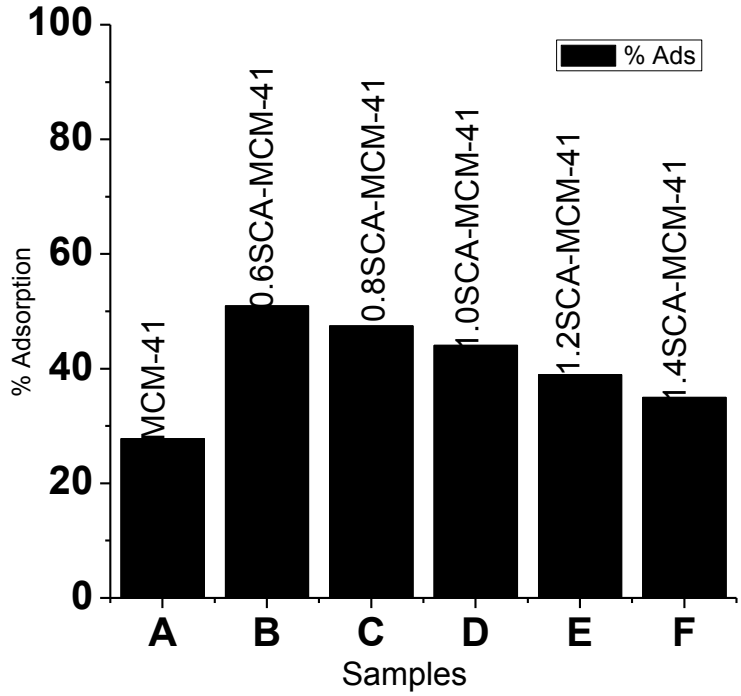

Figure 7.8 Effect of citric acid concentration on removal of MB (C_o, 30 ppm, adsorbent dose 0.15 mg, temperature 25 °C, contact time 60 mins)

7.7.2 Effect of pH on MB adsorption

The effect of pH on MB adsorption capacity of MCM-41 and citric acid grafted MCM-41 was investigated as this plays an important role in the adsorption process. The solution pH influences the degree of ionization of adsorbent and adsorbate, thereby modifying equilibrium and reaction kinetics of the adsorption process (Qu and Gu, 2014). The pH PZC of MCM-41 was observed at pH 5.3, which was higher than that of 0.6-MCM-41 (4.2), 0.8-SCA-MCM-41 (3.9), 1.0-SCA-MCM-41 (3.8), 1.2-SCA-MCM-41 (3.7) and 1.4-SCA-MCM-41 (3.6). When pH is less than PZC, the acidic solution becomes more protonated and the adsorbent surface is positively charged (Reddy et al., 2013). On the other hand, when pH is above PZC, the surface is negatively charged. The adsorption capacity of citric acid grafted MCM-41 was higher than MCM-41 between pH 6-10 before a slight decrease was observed (Figure 7.9). The optimum pH of adsorption for CA-grafted material was 10 for both adsorbents. At low pH (acidic) there is competition

between H^+ and MB ions for -OH and –COOH groups on MCM-41 and CA-grafted MCM-41, respectively. This caused a decrease in the amount of MB adsorbed but at higher pH values – COO^- and O^- exist, increasing electrostatic attraction between MB and the adsorbent, resulting in increased MB adsorption capacity (Kushwaha et al., 2014). This indicated that an exchange of ions may be a major mechanism in MB adsorption (Sajab et al., 2011). A pH value of 10 was selected for CA grafted MCM-41 and MCM-41, respectively. At basic pH greater than 10, decreased MB adsorption may be attributed to the excess OH^- ions competing with the adsorption sites on CA-grafted MCM-41 for MB ions. As a result of the increase in –OH ions there is a reduction in the amount of MB that is adsorbed by the adsorbent as some MB are attracted to the excess OH^- in solution. In aqueous solution, silica becomes rapidly soluble at a pH > 10, this may cause a dissociation of silica particles and hence a decrease in BET surface area (Wu et al., 2004), and may cause a reduction in adsorption capacity. Thus after centrifuging a significant amount of MB still remains in solution and a reduced adsorption is observed. This provides evidence that electrostatic ion exchange reaction may be one of the modes of adsorption between the adsorbent and MB as was also observed by Shao et al. (2014).

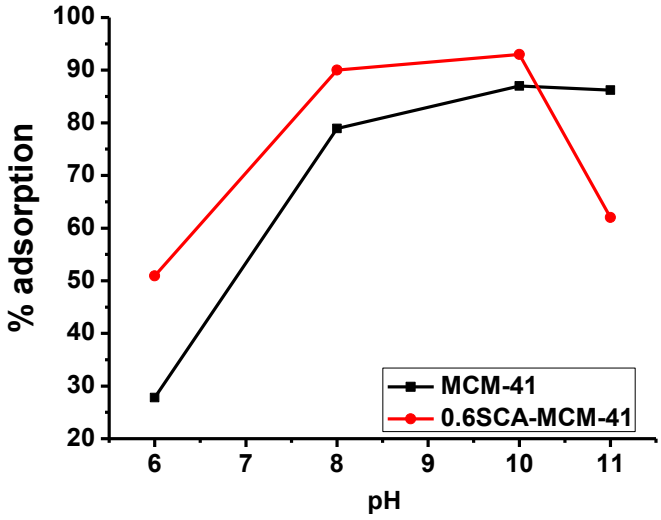

Figure 7.9 Effect of pH on adsorption of MB (C_o, 30 ppm, adsorbent dose 0.15 mg, temperature 25 °C, contact time 60 mins)

7.7.3 Effect of adsorbent dosage

Adsorbent dose is vital in the determination of sorption capacity. The effect of adsorbent dose on adsorption capacity was studied by varying the amount of MCM-41 between 5-40 mg which increased MB adsorption from 37.1 to 91.2% where optimum adsorption occurred at 20 mg. There was minimal increase in adsorption beyond that mass (89.2-91.2%). On the other hand, 0.6SCA-MCM-41 MB adsorption increased from 49.2 to 93.5%, when the dose was increased from 5 to 20 mg with an optimum dose identified as 12.5 mg. Thereafter, only a small increase (93.4–93.5%) was observed when the adsorbent mass was increased from 12.5 to 20 mg (Figure 7.10). The initial increase in percent adsorption with an increase of adsorbent dose was due to the greater availability of the adsorption binding sites until equilibrium was attained. Thereafter there was no significant increase in adsorption. This was because of the likelihood of collisions between solid particles of the adsorbent which resulted in the formation of solid aggregates and consequently decreased surface area and increased diffusion path length which was responsible for the stability in adsorption capacity (Shao et al., 2014).

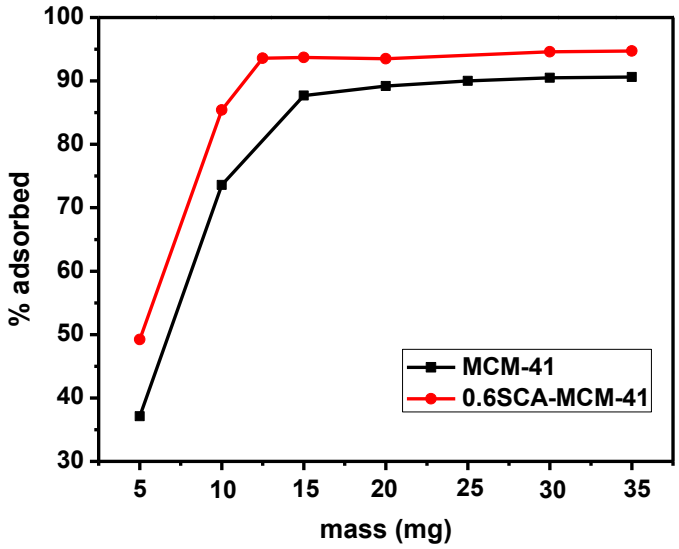

Figure 7.10 Effect of dose on adsorption of MB (C_o, 30 ppm, temperature 25 °C, contact time 60 mins, pH 10)

7.7.4 Effect of temperature

The effect of temperature on adsorption capacity of 0.6SCA-MCM-41 on methylene blue removal is shown in Figure 7.11 (a). A low temperature favours the adsorption process. An increase in temperature from 298 to 328 K caused a decrease in adsorption capacity. The decrease in adsorption capacity is attributed to fast rates of particle vibration, adsorption and desorption between 0.6SCA-MCM-41 and MB. An increase in temperature promotes desorption causing a decrease in adsorption capacity (Qu and Gu, 2014). Also, MB molecules are predisposed to leaving the solid phase and moving into the bulk phase due to temperature increase (Kushwaha et al., 2014).

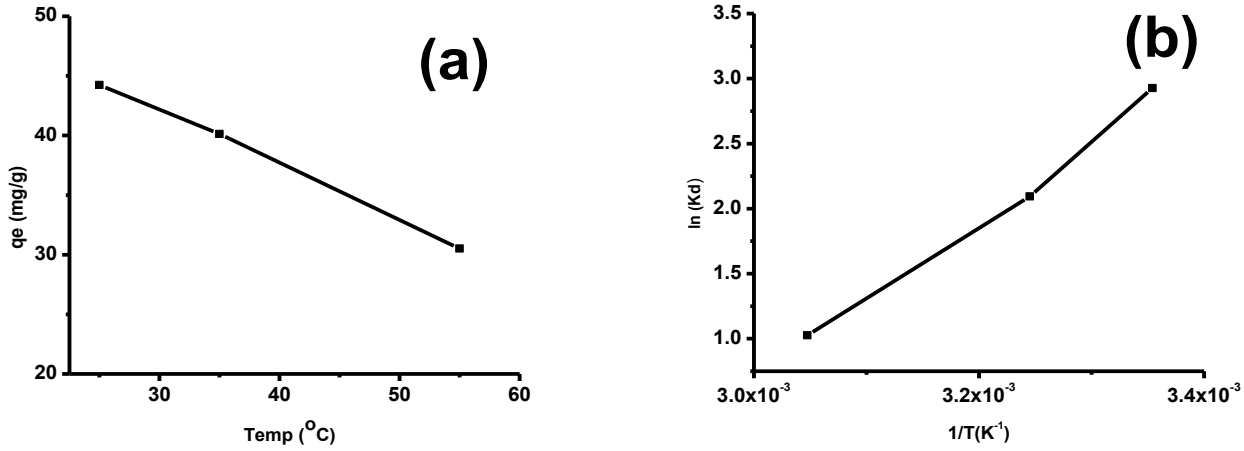

Figure 7.11 (a) Effect of temperature on removal of MB and (b) Plot of ln K_d *versus* 1/T for MB adsorption on 0.6SCA-MCM-41 (C_o, 30 ppm, temperature 25 °C, contact time 60 mins, pH 10, adsorbent dose 0.125 g)

Three thermodynamic parameters, Gibbs free energy ($\Delta G°$), change in enthalpy ($\Delta H°$) and change in entropy ($\Delta S°$) were calculated using equations 7.3 and 7.4:

$$\ln K_d = \frac{\Delta S°}{R} - \frac{\Delta H°}{RT} \quad (7.3)$$

$$\Delta G^0 = -RTlnK_d \quad (7.4)$$

Where T is temperature (K), R is ideal gas constant and K_d is the distribution coefficient obtained from experimental data using equation 7.5:

$$K_d = \frac{Equilibrium\ concentration\ of\ MB\ adsorbed\ on\ 0.6\ SCA\ MCM41}{Equilibrium\ concentration\ of\ MB\ in\ solution} = \frac{(C_o - C_e)}{C_o}\ x\ \frac{v}{m} \qquad (7.5)$$

Where v is the volume (mL) of solution and m (g) is mass of sorbent

$\Delta H°$ and $\Delta S°$ values were calculated from the slope and intercept of Van't Hoff plot (Figure 7.11 (b)). These values including $\Delta G°$ are shown in Table 7.2. The negative $\Delta H°$ values for 0.6SCA-MCM-41 and MCM-41 suggested that the adsorption process is exothermic. The negative values of $\Delta G°$ shows the reaction as being spontaneous and indicates that the adsorption process is favourable at low temperature. A negative $\Delta S°$ value for 0.6SCA-MCM-41 which is the change in entropy value was indicative of less disorderliness at the adsorbent-solution interface during the adsorption (Kushwaha et al., 2014).

Table 7.2 Thermodynamic parameters for MB adsorption on MCM-41 and 0.6SCA-MCM-41

Samples	T (^oC)	$\Delta G°$ (kJ/mol)	$\Delta H°$ (kJ/mol)	$\Delta S°$ (kJ/mol/K)
MCM-41	25	-0.7632	-0.86862	-3.6362
	35	-0.5765		
	55	-0.0113		
0.6SCA-MCM-41				
	25	-2.483	-6.103	-17.61
	35	-1.893		
	55	-0.0687		

7.7.5 Study of adsorption rate and kinetic mechanism

Rate studies were carried out over various contact times at different concentrations of MB to demonstrate the mechanism of adsorption of MB on 0.6SCA-MCM-41. It was observed that equilibrium was reached within 5 minutes for all MB concentrations and no significant change

occurred from 5 to 120 min (Figure 7.12). This implied the rate of MB adsorption was fast even at different concentrations of MB. The resulting data was fitted into three kinetic models; Lagergren pseudo-first order, pseudo-second order and intraparticle diffusion. Linearised forms of pseudo-first order (equation 7.6), pseudo-second order (equation 7.7) and intraparticle diffusion (equation 7.8) equations are given (Kushwaha et al., 2014):

$$\ln(q_e - q_t) = \ln q_e - k_1 t \tag{7.6}$$

$$\frac{t}{qt} = \frac{1}{K_2\, q_e^2} + \frac{t}{qe} \tag{7.7}$$

$$q_t = K_i t^{0.5} + C \tag{7.8}$$

Where q_e, q_t and k_1 (min^{-1}) are amounts of MB adsorbed at equilibrium, at time t (mg/g), and rate constant of adsorption, respectively. The values of the k_1 and q_e cal were calculated from the slopes ($–k_1$) and the intercepts (ln q_e) of the plots of ln (q_e–q_t) *vs* t. K_i is the intraparticle rate diffusion constant (mg/g $min^{-1/2}$), *C* is the intercept depicting intra-boundary layer effect, K_2 is the rate constant of adsorption (g/mg min) and q_t is the amount of MB adsorbed at time t (mg/g). The calculated kinetic parameters for adsorption of MB on MCM-41 and 0.6SCA-MCM-41 at an initial concentration of 30 mg/L are presented in Table 7.3. From the data obtained, pseudo-second-order appears as the best-fit model with $R^2 > 0.9997$ suggesting that the adsorption process is chemical in nature which entails ion exchange between adsorbent and adsorbate (Shao et al., 2014). Intraparticle diffusion showed that an increase in initial concentration of MB increased the diffusion rate of MB. The larger the *C* value, the larger the contribution of surface adsorption in the rate-limiting step (Kushwaha et al., 2014, Lawal and Moodley, 2016). This signifies a mutual adsorption process of both intraparticle diffusion and surface adsorption.

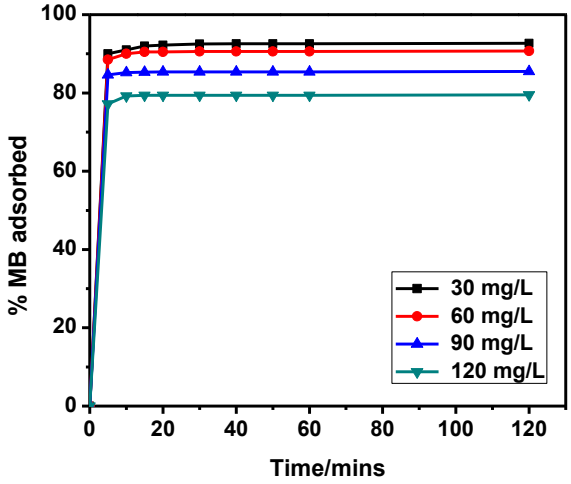

Figure 7.12 Sorption kinetics of MB at different concentrations

Table 7.3 Kinetic parameters for adsorption of MB on MCM-41 and 0.6SCA-MCM-41

Isotherm parameters	MCM-41	0.6SCA-MCM-41
Pseudo-first order		
K_1 (min^{-1})	0.0755	0.0115
q_e^{cal} (mg/g)	1.0591	28.2
R^2	0.8241	0.9514
q_e exp (mg/g)	15.6	44.24
SE %	7.05	8.02
Pseudo-second order		
k_2 (g/mg min)	7.83 x 10^2	1.25 x 10^3
q_e^{cal} (mg/g)	15.92	43.86
R^2	0.9999	0.9997
SE %	0.16	0.19
Intra-particle diffusion		
k_i (mg/g min$^{-1/2}$)	0.5215	0.132
C	12.07	43.13
R^2	0.7336	0.9450
SE %	1.77	0.56

$$SE\bar{x} = \frac{S}{\sqrt{n}}$$

S$E\bar{x}$ = Standard error of the mean, s = Standard deviation of the mean, n = Number of observations of the sample

7.7.6 Adsorption isotherms

Table 7.4 shows the Langmuir, Freundlich, Temkin and Dubinin-Radushkevich models with their equations which describe the sorption of MB on the adsorbent.

Table 7.4 Adsorption isotherm models

Model	Equation	Reference
Langmuir	$\frac{Ce}{qe} = \frac{1}{bQm} + \frac{Ce}{Qm}$	Kushwaha et al. (2014)
Freundlich	$\ln qe = ln\, K_f + \left(\frac{1}{n}\right) ln\, C_e$	Kushwaha et al. (2014)
Temkin	$Qe = B\ \ln A + B \ln C_e$	Kushwaha et al. 2014
D-R	$ln\, qe = ln\, qD - \beta\varepsilon^2$	Shao et al. (2014)

For the Langmuir model, q_e is the adsorption capacity (mg/g) at equilibrium, Q_m is the monolayer adsorption capacity (mg/g), b is the Langmuir constant related to the free energy of adsorption (L/mg) and C_e is the equilibrium concentration (mg/L) of the dye in solution. The values of Q_m and b were calculated from slope ($1/Q_m$) and intercepts ($1/bQ_m$) of the linear plots of C_e/q_e *vs* C_e. For the Freundlich isotherm K_F and n are Freundlich constants related to adsorption capacity (mg/g), 1/n is adsorption intensity of adsorbents. K_F and n were calculated from intercept (ln K_F) and slope (1/n) of the plots of ln q_e *vs* ln C_e. For the Temkin isotherm, B = RT/b, where b is the Temkin constant (J/mol) related to adsorption heat, T = absolute temperature (K), R = gas constant (8.314 J/mol K), and A is the Temkin isotherm constant (L/g). B and A are calculated from slope (B) and intercept (B ln A) of the plot of q_e *vs* ln C_e. The D-R model is applied to make a distinction between chemical and physical adsorption processes with q_e as the adsorption density (mg/g) at equilibrium, q_D = D–R adsorption capacity (mmol/g), β (mol^2/kj^{-2}) = activity coefficient related to the mean adsorption energy and ε = Polanyi potential expressed as equation 7.9:

$$\varepsilon = RT\ l(1 + \frac{1}{C_e}) \qquad (7.9)$$

where C_e = equilibrium concentration in mol/L and T is the absolute temperature in K. A plot of ln q_e against ε^2 gives a straight line with a slope of β, and slope gives information about mean free energy E (kJ/mol) of adsorption per molecule of adsorbate and can be calculated using this equation:

$$E = \frac{1}{\sqrt{2\beta}} \tag{7.10}$$

Table 7.5 shows the correlation coefficient and other parameters calculated from equilibrium data of Langmuir, Freundlich, Temkin and Dubinin-Radushkevich isotherms. Q_m values showed that there was high monolayer adsorption. The K_F value indicates a high adsorption capacity where an adsorption intensity value of n > 1 indicates good adsorption conditions (Kushwaha et al., 2014). Due to adsorbate/adsorbate interaction, Temkin isotherm values indicated that heat of adsorption of all molecules in the layer would decrease linearly and it was the best fit it had a high R^2 value (Kushwaha et al., 2014). The mean sorption energy of the D-R model for MCM-41 and 0.6SCA-MCM-41 was 3.56 and 7.56 kJ/mol, respectively. This indicated that the adsorption process was simultaneously between electrostatic ion interaction and intraparticle diffusion.

Table 7.5 Isotherm parameters of MB adsorption on MCM-41 and 0.6SCA-MCM-41

Isotherm parameters	MCM-41	0.6SCA-MCM-41
Langmuir		
Q_{max} (mg/g)	89.3	204.08
b (L/mg)	0.87	0.039
R^2	0.93	0.976
Freundlich		
K_F (mg/g(mg/L)$^{-1/n}$)	2.23	31.906
N	1.4	1.94
R^2	0.9543	0.9423
Temkin		
B	19.4	45.75
b (J/mol)	127.8	54.18
A (L/g)	40	7.647
R^2	0.993	0.9785
D-R		
q_D (mmol/g)	1.5759	4.79
β (mol^{2}kJ)	0.0394	0.2084
R^2	0.9712	0.965
E (kJ/mol)	3.56	7.56

7.8 Conclusion

CA was successfully grafted onto synthesized MCM-41 and both were characterised. The modified adsorbent (0.6SCA-MCM-41) had an improved maximum adsorption capacity of MB dye (204.08 mg/g) as compared to unmodified MCM-41 (89.3 mg/g) because of the presence of the carboxyl groups. The equilibrium adsorption data obtained fitted into the Temkin, Freundlich and Langmuir isotherms suggesting the material is a favourable adsorbent. The adsorption process involved intraparticle diffusions and was exothermic and spontaneous. An increase in temperature decreased the adsorption of MB. The optimum pH for adsorption was 10 and lower temperatures resulted in higher adsorption capacities.

7.9 Acknowledgements

We gratefully acknowledge the School of Chemistry and Physics, University of KwaZulu-Natal, South Africa, for providing the laboratory facilities and instrumentation used in this research and also to the AAU small grant for financial assistance.

References

Adam, F., Appaturi, J. N., Khanam, Z., Thankappan, R. & Nawi, M. a. M. 2013. Utilization of tin and titanium incorporated rice husk silica nanocomposite as photocatalyst and adsorbent for the removal of methylene blue in aqueous medium. *Applied Surface Science,* 264**,** 718-726.

Beck, J., Vartuli, J., Roth, W., Leonowicz, M., Kresge, C., Schmitt, K., Chu, C., Olson, D. H. & Sheppard, E. 1992. A new family of mesoporous molecular sieves prepared with liquid crystal templates. *Journal of the American Chemical Society,* 114**,** 10834-10843.

Douglas, S., Pongamphai, S., Lerdtrailuck, S., Ponin, S., Polchai, S., Kaewchana, A. & Osataworanun, B. Adsorption of Copper (II) Ion from Aqueous Solution Using Soybean Hulls. The 2nd Joint International Conference on "Sustainable Energy and Environment (SEE 2006), 2006.

Firouzi, A., Kumar, D., Bull, L., Besier, T., Sieger, P., Huo, Q., Walker, S., Zasadzinski, J., Glinka, C. & Nicol, J. 1995. Cooperative organization of inorganic-surfactant and biomimetic assemblies. *Science,* 267**,** 1138-1143.

Ghorbani, F., Younesi, H., Mehraban, Z., Çelik, M. S., Ghoreyshi, A. A. & Anbia, M. 2013. Preparation and characterization of highly pure silica from sedge as agricultural waste and its utilization in the synthesis of mesoporous silica MCM-41. *Journal of the Taiwan Institute of Chemical Engineers,* 44**,** 821-828.

Gijzen, H. J., Bernal, E. & Ferrer, H. 2000. Cyanide toxicity and cyanide degradation in anaerobic wastewater treatment. *Water Research,* 34**,** 2447-2454.

Ginimuge, P.R. & Jyothi, S.D., 2010. Methylene blue: revisited. *Journal of Anaesthesiology, Clinical Pharmacology,* 26(4), 517-520.

Han, R., Zhang, L., Song, C., Zhang, M., Zhu, H. & Zhang, L. 2010. Characterization of modified wheat straw, kinetic and equilibrium study about copper ion and methylene blue adsorption in batch mode. *Carbohydrate Polymers,* 79**,** 1140-1149.

Ho, K. Y., Mckay, G. & Yeung, K. L. 2003. Selective adsorbents from ordered mesoporous silica. *Langmuir,* 19**,** 3019-3024.

Ikeda, M. & Ohtsuji, H. 1971. Phenobarbital-induced protection against toxicity of toluene and benzene in the rat. *Toxicology and Applied Pharmacology,* 20**,** 30-43.

Janicke, M., Landry, C., Christiansen, S., Birtalan, S., Stucky, G. & Chmelka, B. 1999. Low silica MCM-41 composites and mesoporous solids. *Chemistry of Materials,* 11**,** 1342-1351.

Kandah, M. I., Allawzi, M. A. & Allaboun, H. 2008. Improvement of Manure Adsorption Capacity for Cobalt Removal by Chemical Treatment with Citric Acid. *Jordan Journal of Civil Engineering,* 2, 344-354.

Khan, T. A., Nazir, M. & Khan, E. A. 2013. Adsorptive removal of rhodamine B from textile wastewater using water chestnut (Trapa natans L.) peel: adsorption dynamics and kinetic studies. *Toxicological & Environmental Chemistry,* 95**,** 919-931.

Kushwaha, A. K., Gupta, N. & Chattopadhyaya, M. 2010. Enhanced adsorption of malachite green dye on chemically modified silica gel. *Journal of Chemical and Pharmaceutical Research,* 2**,** 34-45.

Kushwaha, A. K., Gupta, N. & Chattopadhyaya, M. 2014. Enhanced adsorption of methylene blue on modified silica gel: equilibrium, kinetic, and thermodynamic studies. *Desalination and Water Treatment,* 52**,** 4527-4537.

Lawal, I. A. & Moodley, B. 2016. Column, kinetic and isotherm studies of PAH (phenanthrene) and dye (acid red) on kaolin modified with 1-hexyl, 3-decahexyl imidazolium ionic liquid. *Journal of Environmental Chemical Engineering,* 4**,** 2774-2784.

Marshall, W., Wartelle, L., Boler, D., Johns, M. & Toles, C. 1999. Enhanced metal adsorption by soybean hulls modified with citric acid. *Bioresource Technology,* 69**,** 263-268.

Meléndez-Ortiz, H. I., Mercado-Silva, A., García-Cerda, L. A., Castruita, G. & Perera-Mercado, Y. A. 2013. Hydrothermal synthesis of mesoporous silica mcm-41 using commercial sodium silicate. *Journal of the Mexican Chemical Society,* 57**,** 73-79.

Monash, P. & Pugazhenthi, G. 2010. Investigation of equilibrium and kinetic parameters of methylene blue adsorption onto MCM-41. *Korean Journal of Chemical Engineering,* 27**,** 1184-1191.

Parida, K., Mishra, K. G. & Dash, S. K. 2012. Adsorption of copper (II) on NH_2-MCM-41 and its application for epoxidation of styrene. *Industrial & Engineering Chemistry Research,* 51**,** 2235-2246.

Qu, Q. & Gu, Z. 2014. Facile synthesis of hierarchical MCM-41 spheres with an ultrahigh surface area and their application for removal of methylene blue from aqueous solutions. *Analytical Methods,* 6**,** 1397-1403.

Reddy, P. M. K., Mahammadunnisa, S., Ramaraju, B., Sreedhar, B. & Subrahmanyam, C. 2013. Low-cost adsorbents from bio-waste for the removal of dyes from aqueous solution. *Environmental Science and Pollution Research,* 20**,** 4111-4124.

Sajab, M. S., Chia, C. H., Zakaria, S., Jani, S. M., Ayob, M. K., Chee, K. L., Khiew, P. S. & Chiu, W. S. 2011. Citric acid modified kenaf core fibres for removal of methylene blue from aqueous solution. *Bioresource Technology,* 102**,** 7237-7243.

Shao, Y., Wang, X., Kang, Y., Shu, Y., Sun, Q. & Li, L. 2014. Application of Mn/MCM-41 as an adsorbent to remove methyl blue from aqueous solution. *Journal of Colloid and Interface Science,* 429**,** 25-33.

Simonutti, R., Comotti, A., Negroni, F. & Sozzani, P. 1999. 13C and 29Si Solid-State NMR of rubber-silica composite materials. *Chemistry of Materials,* 11**,** 822-828.

Singh, V., Singh, S., Pandey, S. & Sanghi, R. 2010. Adsorption behavior of potato starch-silica nanobiocomposite. *Advanced Material Letter,* 1**,** 40-47.

Song, X., Zhang, Y. & Chang, C. 2012. Novel method for preparing activated carbons with high specific surface area from rice husk. *Industrial & Engineering Chemistry Research,* 51**,** 15075-15081.

Takahashi, R., Sato, S., Sodesawa, T., Kawakita, M. & Ogura, K. 2000. High surface-area silica with controlled pore size prepared from nanocomposite of silica and citric acid. *The Journal of Physical Chemistry B,* 104**,** 12184-12191.

Wu, Z., Ahn, I.-S., Lee, C.-H., Kim, J.-H., Shul, Y. G. & Lee, K. 2004. Enhancing the organic dye adsorption on porous xerogels. *Colloids and Surfaces A: Physicochemical and Engineering Aspects,* 240**,** 157-164.

Zhu, B., Fan, T. & Zhang, D. 2008. Adsorption of copper ions from aqueous solution by citric acid modified soybean straw. *Journal of Hazardous Materials,* 153**,** 300-308.

8.0 CHAPTER 8: AS-SYNTHESISED MCM-41 AND ENCAPSULATION OF MCM-41 WITH GRAPHENE/GRAPHENE OXIDE AND THEIR APPLICATION IN THE REMEDIATION OF PHARMACEUTICALS FROM AQUEOUS SOLUTION

Samson O. Akpotu and Brenda Moodley*

School of Chemistry and Physics, University of KwaZulu-Natal, Westville Campus, Durban, 4000, South Africa.

***** corresponding author email: moodleyb3@ukzn.ac.za
Telephone: +27 31 2602796
Fax: +27 31 2603091

8.1 Abstract

In this study, as-synthesised MCM-41 (ASM41) was synthesized and the effect of surfactant template on adsorption was investigated. Previously synthesized MCM-41 was also encapsulated with graphene oxide and graphene, to obtain MCM-41-GO and MCM-41-G, respectively. This was done to maximally exploit the potential of graphene oxide and graphene as adsorbents. These adsorbents were characterised and applied in the remediation of acetaminophen (Acet) and aspirin (Asp) from aqueous media. Elemental analysis revealed that MCM-41-G had the highest % C, followed by MCM-41-GO and ASM41. Adsorption studies showed that ASM41, MCM-41-GO and MCM-41-G were all better adsorbents of the pharmaceuticals in aqueous solution in this study when compared to MCM-41. The improved performance of the modified adsorbents was as a result of their increased hydrophobicity. The pseudo-second order model was the best fit for the adsorption kinetics and the Freundlich isotherm best described the equilibrium. The thermodynamic studies showed that the adsorption process was spontaneous and exothermic. The desorption studies carried out revealed that the adsorbents could be regenerated and reused in the adsorption of Acet and Asp.

Keywords: *ASM41, MCM-41-GO, MCM-41-G, graphene oxide, graphene, aspirin, acetaminophen, adsorption*

8.2 Introduction

Pharmaceuticals comprise of a large group of chemical compounds which are used in the treatment of man and animals. Amongst these drugs, acetaminophen and aspirin (Figure 8.1) are easily available over-the-counter (OTC) drugs and are administered by individuals. Acetaminophen and aspirin are soluble in water and are not completely broken down by human metabolism. These pharmaceuticals are in turn excreted into sewage systems and eventually find their way into water bodies (Khetan and Collins, 2007). Pharmaceuticals are not easily removed from water bodies by conventional water treatment methods and are regarded as "pseudo-persistent" (Carballa et al., 2004, Tambosi et al., 2010). Pharmaceuticals have been implicated in genotoxicity, aquatic toxicity, creation of resistance in pathogenic microbes and are endocrine disruptors (Khetan and Collins, 2007). Due to their persistence and adverse effects, there is an urgent need for remediation of these substances with an efficient sorbent. Adsorption, over the years has been proven to be a reliable technique in the removal of pollutants from wastewater, because of the efficiency of the process and ease of use. Other added advantages include no toxic by-products and the adsorbents can be recycled (Al-Khateeb et al., 2014).

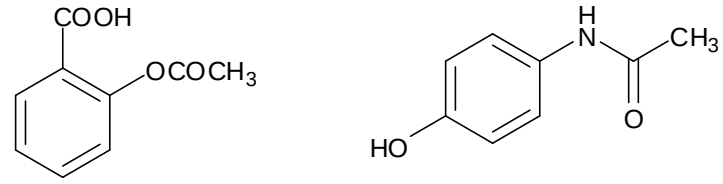

Figure 8.1 Structure of aspirin and acetaminophen

Graphene oxide (GO) and graphene (G) are carbonaceous materials that have found various applications in different fields with huge potential in adsorption. Graphene oxide is made from the oxidation of graphite using strong oxidising agents which create a large array of functional groups such as hydroxyls, ketones, epoxides and carboxyl groups which make it easy to be immobilised on a substrate or as an excellent binder for organic groups (Li et al., 2015, Liu et al.,

2013). Graphene was rediscovered, synthesised and characterised in 2004 by Novoselov et al. (2004). It has a thickness of one carbon atom, arranged in a honey comb lattice structure. It has a theoretical surface area of approximately 2630 m^2/g with a rich π-system, and excellent electrical, thermal and mechanical properties (Yang et al., 2015a, Liu et al., 2013). It has excellent hydrophobic properties which enable it to easily bind to organic pollutants, but the full potential of graphene is often not exploited because it forms aggregates of nanosheets in aqueous solution which reduces the surface area and in turn reduces its adsorption capabilities. In a bid to enable G/GO to reach its maximum adsorption potential, the materials must be immobilised on a substrate. To overcome these challenges, a new class of material termed periodic mesoporous silica-graphene oxide/graphene composites have been developed.

Mobil Catalytic material (MCM-41) is a unique class of materials that has excellent properties, such as increased surface area, homogenous pores, narrow pore size distribution and thermal stability (Ghorbani et al., 2013). However, despite the advantageous properties of MCM-41, the adsorption of organic molecules still remains a challenge. This is because in aqueous solution it is strongly hydrophilic and adsorbs water molecules (Gibson, 2014b). To improve the hydrophobicity of MCM-41, it has been used in the form of as-synthesised for the removal of organic pollutants (Gibson, 2014b). In this form the template of the synthesised MCM-41 is not removed by calcination at high temperature or by refluxing with strong acids. Mangrulkur and co-workers, successfully adsorbed phenol and chloro-phenol with ASM41 with high adsorption capacity when compared to MCM-41. The higher sorption capacity of the ASM41 was attributed to the presence of the surfactant template which improved its hydrophobic properties.

In a bid to develop a material with even greater hydrophobicity and improved sorption capability, a hybrid sorbent with a hydrophobic surface and a large surface area is required. Wang et al. (2010) developed graphene oxide periodic mesoporous silica (GO-PMS) composite with improved thermal, mechanical and electrical properties. GO-PMS developed in another study was applied in the selective adsorption of Pb(II) in aqueous solution with improved efficiency in comparison with the unmodified material (Li et al., 2015). Hence, the encapsulation of PMS with GO is very important for improved adsorptive ability. The coating of PMS serves 3 main purposes: firstly, it helps with an improved dispersion of graphene/graphene oxide because of their hy-

drophobic nature; secondly, it creates a better separation of the adsorbent and adsorbate in water and thirdly, the immobilisation on PMS helps provide a hybrid adsorbent with improved surface area and strongly hydrophobic properties. In a bid to surmount these challenges MCM-41 was synthesized and coated with graphene oxide and graphene.

In this study, we report the encapsulation of MCM-41 with graphene oxide and graphene for the first time and its application as highly efficient adsorbents for the remediation of pharmaceuticals (acetaminophen and aspirin) from wastewater. Also, as-synthesised MCM-41 (ASM41) was applied in the remediation of pharmaceuticals from wastewater. This was done to investigate the hydrophobic effects of the synthesised template in the adsorption of Acet and Asp from aqueous solution. All the adsorbents were characterised using elemental analysis (EA), fourier transform infrared (FTIR) spectroscopy, thermogravimetric analysis (TGA), x-ray diffraction (XRD) studies, textural analysis, scanning electron microscopy (SEM) and transmission electron microscopy (TEM). Acetaminophen and aspirin were selected as model pharmaceutical pollutants to determine the efficiency of the adsorbents as probe molecules and in understanding the adsorption mechanism. The relative low cost of synthesis of ASM41 and MCM-41, coupled with the simple procedure of encapsulation with GO/G and their high efficiency in adsorption makes these materials excellent for the removal of pharmaceutical pollutants from wastewater.

8.3 Experimental

8.3.1 Materials and chemicals

Natural graphite powder, methanol (HPLC grade), hydrazine monohydrate (80%), 3-aminopropyl triethoxysilane (APTES, 99%), HCl (37%), $KMnO_4$, tetraethylorthosilicate (TEOS, 98%) and the pharmaceuticals acetaminophen (Acet) and aspirin (Asp) were obtained from Sigma-Aldrich. Absolute ethanol (Merck), cetyltrimethyl ammoniumbromide (CTAB 99%+) (Calbiochem), H_2SO_4 (98%), H_2O_2 (35%) and H_3PO_4 (80%) were obtained from Promark. All the reagents were analytically pure and were used without further purification. MilliQ water was used in the preparation of the standard solutions and the mobile phase used in chromatography analysis.

8.3.2 Synthesis of MCM-41 and as-synthesised MCM-41

MCM-41 was synthesized using a modified method from Parida et al. (2012). A detailed procedure is found in chapter 7. The uncalcined form of MCM-41 is referred to as as-synthesised MCM-41 (ASM41), where the surfactant was not calcined and retained in the MCM-41 template.

8.3.3 Activation of MCM-41

Activation of MCM-41 was achieved by modifying the method of Kushwaha et al. (2014). A detailed procedure is provided in chapter 7.

8.3.4 Synthesis of NH_2-MCM-41

MCM-41 surface was modified in an aqueous medium by an easy one-step synthesis. A detailed procedure is provided in chapter 7.

8.3.5 Synthesis of GO

GO was synthesized using a modified Tour method (Marcano et al., 2010). A detailed procedure is provided in chapter 5.

8.3.6 Synthesis of MCM-41-GO and MCM-41-G

In this encapsulation procedure, NH_2-MCM-41 was dispersed and sonicated in water. GO (10 mg/L) previously sonicated for 2 hrs was added to the suspension and the pH was adjusted to 7 by adding NH_4OH whilst stirring. It was stirred continuously for 8 hrs and left to settle for an hour. The product was filtered, washed with water and dried in a vacuum oven for 6 hrs at 50 °C. This was labelled as MCM-41-GO. In the synthesis of MCM-41-G, a similar procedure was adopted but the temperature of synthesis was 80 °C and hydrazine monohydrate was added to the mixture to reduce GO to G. The mixture was stirred for 8 hrs, left to settle for an hour, filtered,

washed with water and dried under vacuum. The solid black product was oven dried in a vacuum at 80 °C for 6 hrs. This was labelled MCM-41-G.

8.4 Characterisation of Synthesized Adsorbents

The morphology and microstructure of the adsorbents were analysed by field emission scanning electron microscopy (FESEM, Zeiss instrument, 10 kV operating voltage), and high-resolution transmission electron microscopy (HRTEM, JEOL). X-ray diffraction (XRD) experiments were carried out on an x-ray diffractometer (Bruker D8 Advance, Bruker, AXS, Germany) operating at 45 kV and 40 mA with Cu. The percentage of carbon in the samples was determined using an elemental analyser (Thermo Scientific CHNS/O analyser). N_2 adsorption–desorption isotherms were obtained using a nitrogen adsorption analyzer (Micrometrics Tristar II 3020). MCM-41 was degassed (with Micromeritics VacPrep 061) at a temperature of 90 °C for an hour and then ramped up to 200 °C overnight. CA-grafted samples were degassed at 90 °C overnight. This temperature was selected to prevent CA decomposition. Surface area and pore size measurements of samples were obtained using the BET method. The pore volume was calculated from the adsorption branch based on volume of nitrogen adsorbed at a relative pressure (P/P_o) of approximately 0.99. Fourier transform infrared (FTIR) spectra of the samples were recorded on a Perkin Elmer series 100 spectrometer. Thermogravimetric (TGA) profiles were obtained by weighing 5 mg of sample in an aluminium pan using an SDT Q 600 V 209 Build 20 instrument with a temperature range of 25-900 °C at 10 °C/min in a N_2 environment.

8.4.1 Analytical method

Acetaminophen and aspirin concentrations were quantified using a HPLC system consisting of an Agilent 1200 SL (Agilent Technology, USA) with a pressure grade pump and a UV-Vis detector. Separation was carried out at room temperature with an Agilent Eclispe XDB- C-18 (4.6 x 150 mm, 5 µm particle size) column at a mobile phase flow rate of 0.6 mL/min under isocratic conditions with a mixture of methanol/water (60:40; v/v). The pH of the water was adjusted to 2.3 with H_3PO_4. The sample volume injected was 5 µL.

8.4.2 Adsorption experiments

The pharmaceutical concentrations were determined by HPLC analysis at a wavelength of 254 nm and 210 nm, respectively for acetaminophen and aspirin. Batch adsorption experiments were carried out in PTFE screw cap vials covered with aluminium foil at room temperature to determine the effect of adsorption parameters such as effect of adsorbent dose, adsorption time, effect of ionic strength and pH, and temperature. A 1000 ppm stock solution was prepared, from which several 15.0 mL working solutions of 12.5 mg/L (Acet and Asp) were prepared. The pH of the solution was adjusted using 0.1 M NaOH or 0.1 M HCl to the desired pH. An amount (0.04 g) of the adsorbent was added to the solution and it was shaken with an orbital shaker (Scientific Engineering) for a period of time. Thereafter, the solution was centrifuged at 5000 rpm for a minute to collect the supernatant. The supernatant was filtered through a 0.45 µm cellulose acetate filter and the filtrate injected into the HPLC to determine its concentration. The percentage adsorption was calculated using equation 8.1

$$\%\, adsorption = \frac{(C_o - C_e)}{C_o}\, x\, 100 \qquad (8.1)$$

Where C_0 is the initial concentration (mg/L) and C_e is the equilibrium concentration after a set time in mg/L.

Kinetic studies were carried out using 150 mg of adsorbent with 200 mL of 25, 50, 100 and 200 mg/L of Acet and Asp solution and the pH was adjusted to 2, using 0.1 M NaOH/0.1 M HCl solutions. Aliquots of the solution were withdrawn periodically (2 – 1440 mins), filtered off and the concentration of Acet and Asp adsorbed was determined. The experimental data obtained were applied to the pseudo-first order, pseudo-second order, intraparticle diffusion and Elovich kinetic models. The equations for these models are shown in Table 8.1. The adsorption capacity was calculated using equation 2:

$$q = \frac{(C_o - C_e)V}{m} \qquad (8.2)$$

Where q is the amount of Acet and Asp adsorbed by the adsorbents in mg/g, *V* is the initial volume of solution in L and m is the adsorbent mass in g.

Table 8.1 Kinetic models

Models	Equation	Reference
Pseudo first-order	$ln\left(q_e - q_t\right) = \ln q_e - ln\ k_i t$	(Ho and McKay, 1998)
Pseudo second-order	$\frac{t}{q_t} = \frac{1}{K_2\, q_e^2} + \frac{t}{q_e}$	(Ho and McKay, 1998)
Intraparticle diffusion	$q_t = K_i t^{0.5} + C$	(Kushwaha et al., 2014)
Elovich	$q_t = a\ ln\ t + b$	(Han et al., 2010)

Where q_e and q_t are the amount of Acet and Asp adsorbed (mg/g) at equilibrium and time t (mins), respectively; k_i is the rate constant of the pseudo first-order kinetic model (min^{-1}). K_2 is the rate constant (g/mg/min) of pseudo second-order kinetic model for adsorption. For the intraparticle diffusion model, *C* (mg/g) is the intercept and K_i is the intraparticle diffusion rate constant (g/mg/ $min^{0.5}$) for adsorption. The Elovich coefficient is obtained from the plot of q_t *versus* ln t. The initial adsorption rate, a, and the desorption constant, b, were calculated from the intercept and slope, *x* is the ratio of a:b and is the initial adsorption rate (mg/g min).

For thermodynamic studies, 0.04 g of the adsorbent was placed in the Acet and Asp solution and adjusted to pH 4. The mixture was agitated in a thermostatic shaker bath at varying temperatures of 293, 303 and 313 K for 24 hrs. The solutions were centrifuged at 4000 rpm for 1 min and filtered with a 0.45 µm filter before the concentration of the filtrate was determined using HPLC. The equilibrium data obtained were analysed with the following isotherm models; Langmuir, Freundlich, Temkin and Dubinin-Radushkevich models. The equations for these models are presented in Table 8.2. Thermodynamic parameters such as change in enthalpy (ΔH°), change in Gibbs energy (ΔG°), and change in entropy (ΔS°), were also calculated. Experiments were carried out in duplicate and blanks were also carried out to ensure the integrity of the analytical procedure.

Table 8.2 Adsorption isotherm models

Models	Equation	Reference
Langmuir	$\frac{C_e}{q_e} = \frac{1}{bq_m} + \frac{C_e}{q_m}$	(Kushwaha et al., 2014)
Freundlich	$\ln q_e = ln\, K_F + \left(\frac{1}{n}\right) \ln C_e$	(Kushwaha et al., 2014)
Temkin	$ln\, q_e = B \ln A + B\ lnC_e$	(Kushwaha et al., 2014)
D-R	$\ln q_e = lnq_m - \beta\varepsilon^2$	(Shao et al., 2014)

Where C_e is the equilibrium concentration of pharmaceuticals in solution (mg/L), q_e is the amount of pharmaceuticals adsorbed per unit of the adsorbent at equilibrium time (mg/g), b is the Langmuir constant related to the free energy of adsorption (L/mg), q_m is the theoretical limit of adsorption capacity when the monolayer surface is fully covered with molecules (mg/g), K_F and n are Freundlich constants. In the Temkin isotherm, B = RT/b where b is Temkin constant in J/mol and A is the Temkin isotherm constant (L/g). R is the gas constant in J/mol/K) and T is temperature K.

In the D-R model, β is a constant related to the mean free energy (mol^2/kJ^2) and ε is the Polanyi potential defined as:

$$\varepsilon = RTln\ (1 + \frac{1}{Ce}) \tag{8.3}$$

E is the mean free energy in kJ/mol/L of the adsorption per molecule of the adsorbate and is calculated using the equation:

$$E = \frac{1}{\sqrt{-2B}} \tag{8.4}$$

8.4.3 Real water samples

The details of the real water samples are provided in chapter 5.

8.4.4 Adsorbent regeneration

In order to regenerate the adsorbents used, it was washed with acidic ethanol at a pH of 2. It was then dried in a vacuum oven at a temperature of 60 °C and the adsorption capacity was calculated. The washing and recycling was carried out 2 times.

8.5 Results and Discussion

The materials synthesized were characterized with various techniques to determine the suitability of its properties in the removal of Acet and Asp from solution. The results for the adsorption of Acet and Asp with MCM-41, ASM41, MCM-41-GO and MCM-41-G were determined with a batch adsorption process.

8.5.1 Synthesis of MCM-41 and ASM41

MCM-41 and ASM41 were synthesized using TEOS as a precursor. The FTIR spectrum (Figure 8.4) showed the appearance of sharp peaks at 3340 cm^{-1} (-OH stretching), 1630 cm^{-1} (-OH bending), 1047 cm^{-1} (Si-O-Si asymmetric stretching) and 780 cm^{-1} (Si-O-Si symmetric bending) respectively. In ASM41, the absorption bands observed around 2922 and 2852 cm^{-1} are due to the bending of $–CH_2$ and $–CH_3$ of the CTAB surfactant.

8.5.2 Characterisation of adsorbents

The synthesized adsorbents were characterized with a number of techniques as discussed below.

8.5.2.1 Thermogravimetric analysis

TGA was carried out to determine the thermal stability, purity and volatile portion of ASM41, MCM-41, GO, MCM-41-GO and MCM-41-G with a temperature range from 25 °C to 900 °C (Figure 8.2). The weight loss below 100 °C for all the samples was attributed to the removal of physisorbed water. In MCM-41 and ASM41, there were further weight losses of 1% and 10% between 350 – 450 °C, respectively. This loss in weight was due to the decomposition of the residual carbon and condensation of the adjacent silanol as was also observed by Liou (2011). Thereafter, no mass loss was observed. In GO, there was a remarkable weight loss between 200 °C to 250 °C and this was characterized by the removal of the oxygen containing functional group which was also observed by Liu et al. (2013). In MCM-41-GO and MCM-41-G, there was a lower % weight loss when compared to GO alone which can be attributed to the successful coating of graphene oxide and graphene on MCM-41, respectively. MCM-41 has a higher thermal stability than GO and G, therefore, the coating on MCM-41 helped increase their thermal stabilities. The weight loss before 250 °C was insignificant and this is indicative of the stability of both materials. However, at 250 °C to 550 °C, MCM-41-GO and MCM-41-G lost 13.5% and 16% amount of its weight, respectively. This loss in weight is due to the thermal decomposition of (carbon) graphene oxide and graphene on MCM-41-GO and MCM-41-G, respectively. This is an indication of the successful synthesis of MCM-41-GO and MCM-41-G.

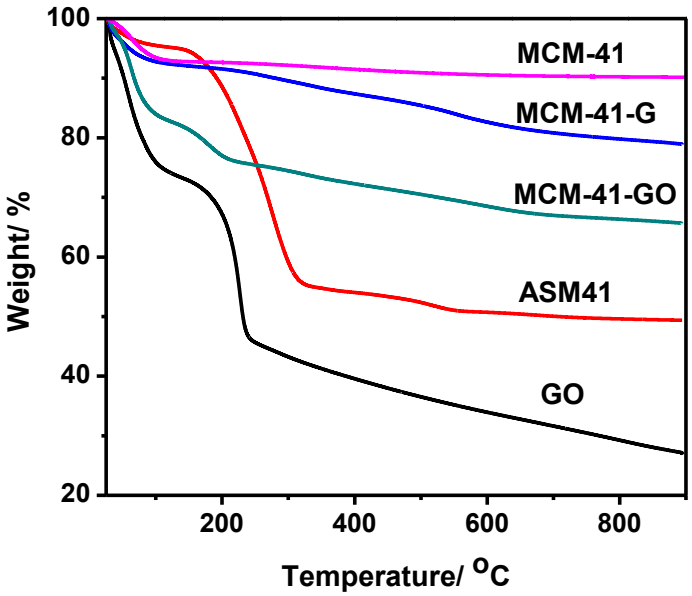

Figure 8.2 TGA profiles of GO, ASM41, MCM-41-GO, MCM-41-G, MCM-41

8.5.2.2 Elemental analysis (EA)

The elemental compositions of the samples are presented in Table 8.3. GO, ASM41, MCM-41, MCM-41-GO and MCM-41-G, had carbon contents of 37.6%, 32.5%, 0.5%, 14.5% and 18.4%, respectively. MCM-41-G had a lower H/C ratio than MCM-41-GO which implied it is more aromatic than MCM-41-GO and also, the lower O/C ratio observed indicated that MCM-41-G was less hydrophilic than MCM-41-GO, as was also observed by Wang et al. (2014b). However, interestingly, based on the H/C and O/C ratios, ASM41 appeared to be hydrophobic and it is also the least hydrophilic material and this can be attributed to the presence of CTAB in the microstructure. The presence of carbon in MCM-41-GO and MCM-41-G proves that G and GO had been successfully coated on MCM-41-G and MCM-41-GO, respectively.

Table 8.3 Elemental composition and atomic ratios, and surface areas (SA) of MCM-41, GO, ASM41, MCM-41-GO and MCM-41-G

Sample	MCM-41	ASM41	GO	MCM-41-GO	MCM-41-G
C/%	0.95	32.5	37.6	14.9	18.4
H/%	1.77	6.42	2.23	2.52	1.70
O/%	97.1	59.0	59.5	80.6	76.8
N/%	0.152	2.07	0.58	1.95	3.09
H/C	22.4	2.37	0.71	2.02	1.13
O/C	76.5	1.36	1.75	4.07	3.14
SA/m^2/g	1261	14	38	327	50.9
Pore volume/cm^3/g	0.93	0.022	0.017	0.34	0.17
Average pore size/nm	2.73	39	38.2	37.6	36.5

8.5.2.3 Textural analysis

The N_2 adsorption/desorption isotherms of the adsorbents are presented in Figure 8.3. A comparison of the amount of N_2 adsorbed/desorbed, revealed that at low or high pressure, previously synthesized MCM-41 was the material with the highest surface area. The detailed analyses of textural properties of the adsorbents are shown in Table 8.3. It was observed that, there was a tremendous decrease in surface area and pore volume of ASM41 when compared to MCM-41.

This can be attributed to the retained template (CTAB) and blocked pore channels in ASM41, as compared to the hollow cavity of MCM-41 which was calcined. This was also observed by Mangrulkar and co-workers (Mangrulkar et al., 2008). GO had a surface area and pore volume of 38 m^2/g and 0.017 cm^3/g, respectively but there was a significant reduction in the surface area and pore volume of MCM-41-GO compared to MCM-41 and this became more prominent in MCM-41-G. This reduction can be attributed to the (carbon) coating of GO and G on MCM-41-GO and MCM-41-G, respectively. All the adsorbents were of mesoporous nature because the pore diameters were less than 50 nm. Despite their relatively moderate surface areas, MCM-41-GO and MCM-41-G are expected to have improved sorption capacities for the removal of pharmaceuticals from aqueous solution as a result of their increased hydrophobicity. The reduced surface area is an indication that GO and G was successfully coated on MCM-41.

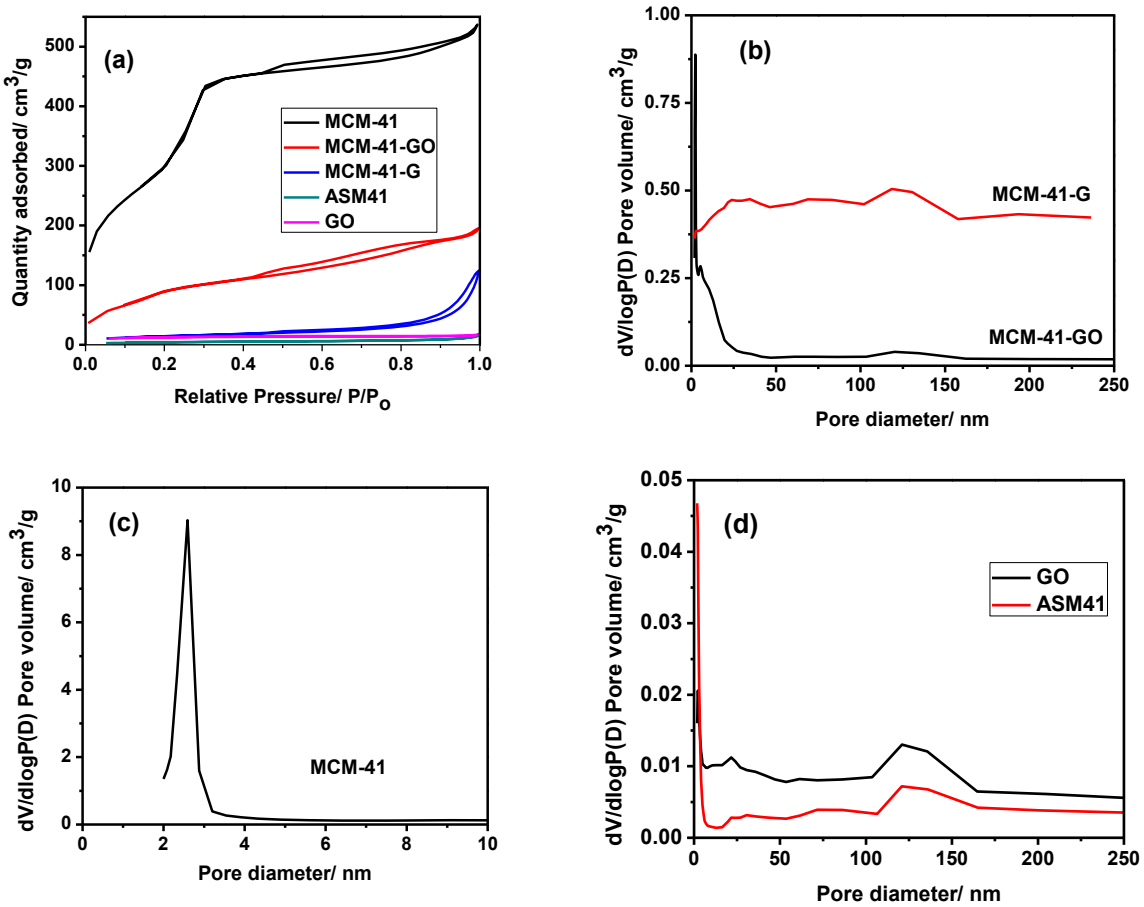

Figure 8.3 (a) N_2 adsorption-desorption of samples and pore size distribution of (b) MCM-41-GO and MCM-41-G (c) MCM-41 and (d) GO and ASM41

8.5.2.4 FTIR spectral analysis

The FTIR spectra of MCM-41, ASM41, GO, MCM-41-G and MCM-41-GO are shown in Figure 8.4. The broad peak at approximately 3240 cm^{-1} in all samples is due to the -OH stretching vibration. In GO, the peak at 1364 cm^{-1} is due to a carbonyl group and the peaks present at 1727 cm^{-1} an 1632 cm^{-1} are due to C=O stretching. The peaks in the GO FTIR spectrum at 1226 cm^{-1} and at 1065 cm^{-1} are due to C-O (epoxy) and C-O alkoxyl vibrations, respectively. A similar result was reported by Liu et al. (2013) and Marcano et al. (2010). ASM41, MCM-41, MCM-41-GO and MCM-41-G had peaks which are typically found on siliceous material. This indicated that the synthesized MCM-41 was successfully coated with GO and G. In MCM-41-GO, the peaks at 1620 cm^{-1} and 1413 cm^{-1} are due to -C=O stretching vibration. MCM-41-GO had a profile similar to GO and this shows that the coating of GO on MCM-41 was successful. MCM-41-G had no carbonyl, C-O-C and epoxy group peaks. The band around 1038 cm^{-1} in the MCM-41-G spectrum was due to the Si-O-Si/Si-O-C asymmetric vibration and Si-O-C was linked by covalent bonds. A similar result was also observed by Liu et al. (2013). This proves that the -COOH group on MCM-41-GO was converted to a Si-O-C bond to give MCM-41-G as also observed by Meng et al. (2015). The peaks around 780 and 430 cm^{-1} were assigned as Si-O-Si symmetric and bending vibrations, respectively. The peak around 1556 cm^{-1} seen in MCM-41-G is due to -C=C- which was assigned as an amide group stretching vibration which means the vinyl group was successfully introduced into MCM-41-G (Meng et al., 2015). The MCM-41-G spectrum revealed that MCM-41 was coated successfully with graphene. In ASM41, there were peaks present which were typical of ammonia at 1210 - 1530 cm^{-1} as observed by Mangrulkar et al. (2008). The peaks at 2922 and 2852 cm^{-1} were due to the bending of $–CH_2$ and $–CH_3$ of the CTAB, respectively and contributed to the hydrophobicity of ASM41. Similar peaks were observed by Mangrulkar et al. (2008) and Thuc and Thuc (2013).

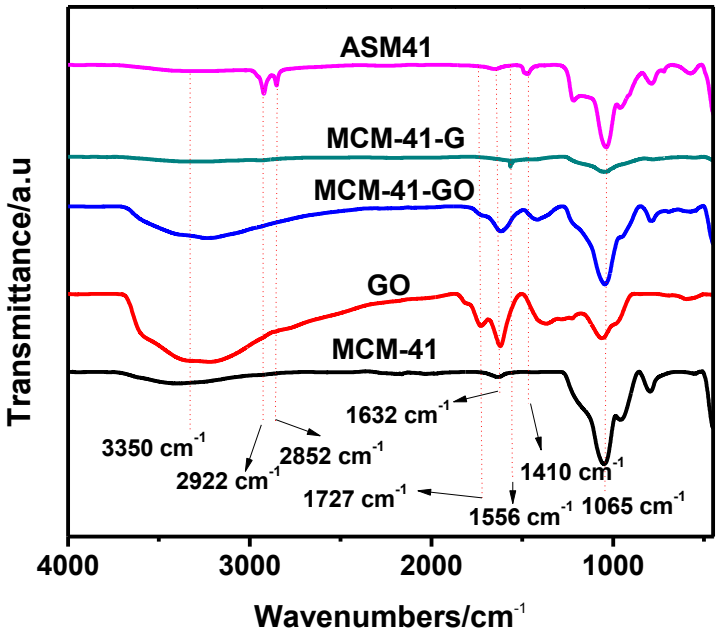

Figure 8.4 FTIR spectra of adsorbents

8.5.2.5 XRD analysis

The XRD profiles for MCM-41, ASM41, GO, MCM-41-GO and MCM-41-G are shown in Figure 8.5. Low angle XRD scans of siliceous samples were obtained between 0-5(Θ). The profile of ASM41 and MCM-41 showed 3 intense peaks, one at 100 and two higher order reflection peaks at 110 and 200. These peaks are the distinguishing features for hexagonal symmetry of MCM-41 and is typical for mesophase materials (Qu and Gu, 2014, Liou, 2011). The higher order reflection peaks at 110 and 200 are suppressed in MCM-41-GO and MCM-41-G. The degree of suppression of the higher order reflection peaks was more prominent in MCM-41-G when compared to MCM-41-GO. This can be attributed to coating of MCM-41-G with a higher percentage of (carbon) graphene. The XRD scan for GO revealed a very intense peak (001) at 2(Θ) = 9.74 which fits the inter-planar spacing of 0.87 nm, which was also observed by Marcano et al. (2010). The XRD profiles of MCM-41, ASM41, MCM-41-GO and MCM-41-G had the amorphous nature of silica with a broad peak centred at 2(Θ) = 23. The MCM-41-GO peak present at 2(Θ) = 26.19 is typical of graphite (002) and resulted from the GO containing oxygen functional groups on the surface of MCM-41-GO being partially transformed. The reaction was promoted

by the chemical interaction between the GO and the MCM-41. A similar observation was recorded by Li et al. (2015). In MCM-41-G, the peak present at 2(Θ) =25.5 is characteristic of graphene and was also observed by Luo et al. (2013). The peaks of GO and G on MCM-41-GO and MCM-41-G, showed that the encapsulation with GO/G was successful.

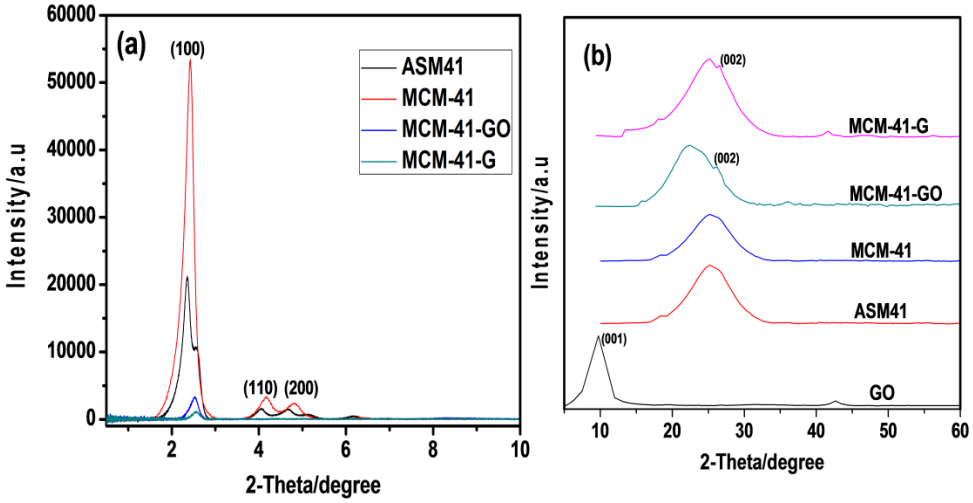

Figure 8.5 (a) Low angle scans of adsorbents and (b) Wide angle scans of adsorbents

8.5.2.6 FESEM and HRTEM image analysis

Figures 8.6 and 8.7 display the FESEM and HRTEM images of ASM41, MCM-41, GO, MCM-41-GO and MCM-41-G, respectively. The HRTEM images of ASM41 and MCM-41 had an ordered morphology of 3 dimensional hexagonal shape/honey comb structure. A uniform wall of parallel channels was also a distinguishable feature present on MCM-41 and ASM41. This is usually a distinguishing feature for MCM-41 (Liou, 2011, Ghorbani et al., 2013). For MCM-41, a pore size of 2.3 nm was obtained and this was in accordance with the value obtained from the BET measurements. The TEM morphology of the GO sheets revealed it to have a smooth transparent surface with large visible pores (Figure 8.7 (a)). The SEM morphology of MCM-41-GO (Figure 8.7 (d)) and MCM-41-G (Figure 8.7 (e)) appeared modified from the coating of graphene oxide and graphene. MCM-41-GO had a thin film of transparent graphene oxide on its surface and in contrast, there was a thick stack of graphene sheets on the surface of MCM-41-G and the transparency of the graphene film on the surface became lost. This is due to the reduction of graphene oxide to graphene *via* a chemical method with hydrazine hydrate. The SEM images for

ASM41 and MCM-41, appeared as small agglomerated spheres with an average diameter size of 3 nm. Also clearly visible on MCM-41 was the large cavities and large pore volume. GO, appeared as a thin transparent film with large pores and with some aggregation. MCM-41-GO had less coating on its surface as compared to MCM-41-G and this is due to more coating of carbon on MCM-41-G. The image analysis shows that the encapsulation with graphene oxide and graphene was successful.

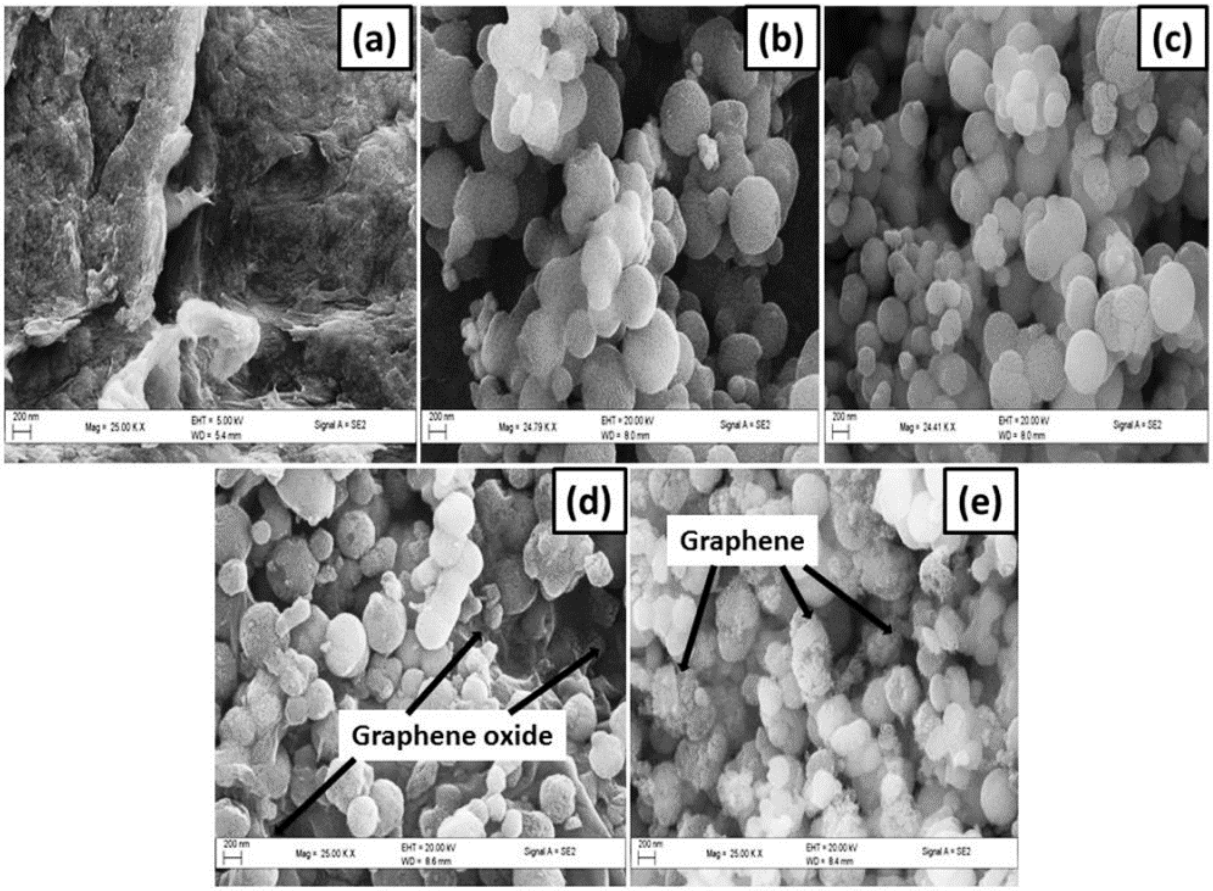

Figure 8.6 FESEM images of (a) GO (b) ASM41 (c) MCM-41 (d) MCM-41-GO (e) MCM-41-G

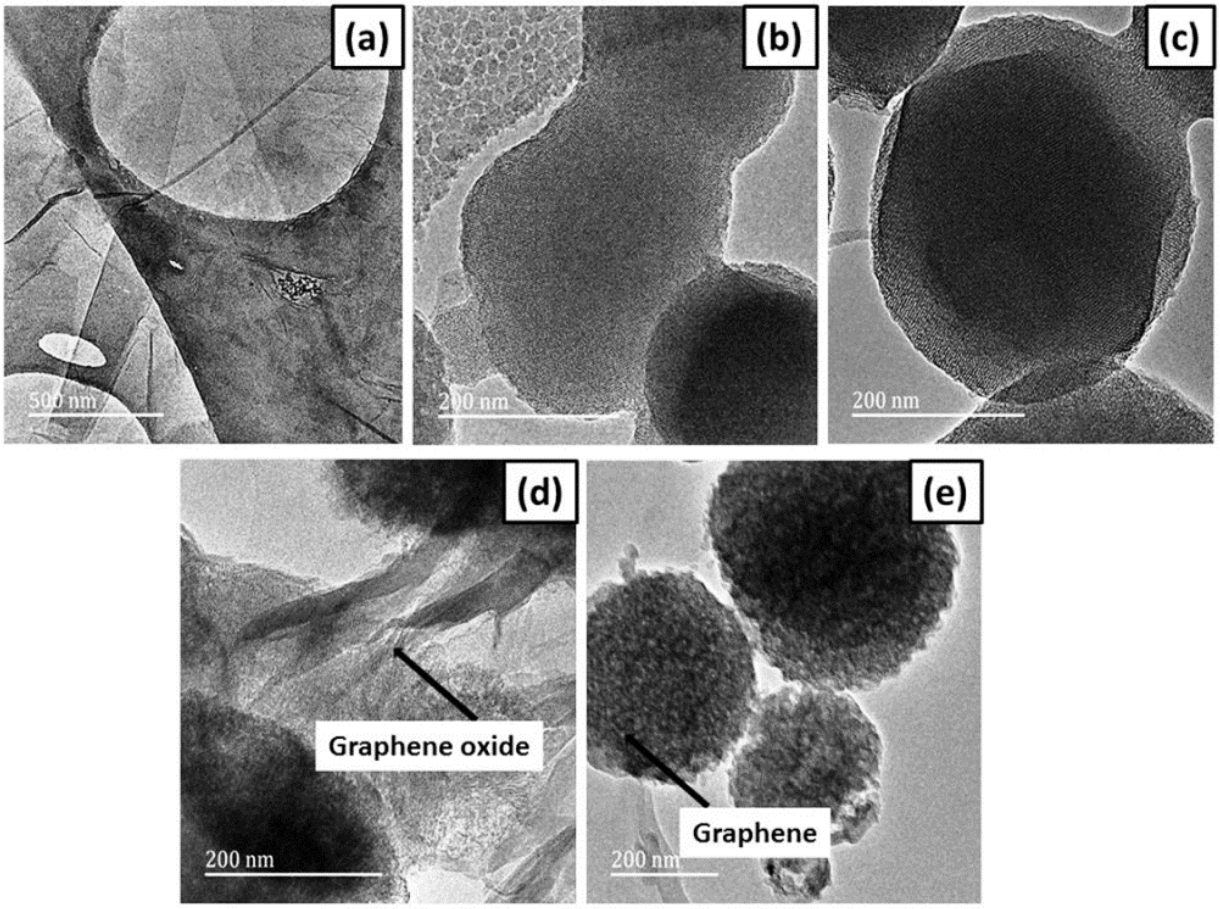

Figure 8.7 HRTEM images of (a) GO (b) ASM41 (c) MCM-41 (d) MCM-41-GO (e) MCM-41-G

8.6 Batch Adsorption Studies

Batch adsorption experiments were carried to determine the efficiency of ASM41, MCM-41, MCM-41-GO and MCM-41-G on the remediation of Acet and Asp from a simulated wastewater solution. The role of pH, ionic strength, adsorbent dose, contact time and temperature were investigated to determine the most suitable conditions for the remediation of Acet and Asp. Thermodynamics, kinetics and isotherm studies were also carried out.

8.6.1 Influence of the surfactant template on the adsorption of Acet and Asp by MCM-41 and ASM41

The surfactant CTAB was used as the structure directing agent (SDA) in the synthesis of MCM-41. The uniform mesopore channels are created by calcining the as-synthesised MCM-41. However, in ASM41, the cationic surfactant CTAB was intentionally left in the structure to increase its hydrophobicity. This SDA consequently affects the porosity, surface area and surface chemistry and the adsorbent behaviour of the as-synthesised adsorbent (Mangrulkar et al., 2008). The adsorption pattern of Acet and Asp on MCM-41 and ASM41 was studied to determine the effect of the SDA. From Figure 8.10, it can be seen that the adsorption of Acet and Asp on ASM41 was significantly higher than on MCM-41. This could be attributed to different functional groups present on the surface of both adsorbents. MCM-41 has silanol and siloxane on its surface, and in aqueous solution becomes very hydrophilic. In contrast, ASM41 has quaternary alkyl ammonium groups on its surface from the SDA, thereby changing its surface chemistry making it form a hydrophobic pocket for trapping pharmaceutical molecules. Therefore, ASM41 has a better adsorptive ability for organic pollutants; hence, its adsorption of Acet and Asp was higher. Mangrulkar et al. (2008), observed a similar effect when as-sythensised MCM-41 and MCM-41 were applied in the adsorption of phenolic compounds.

8.6.2 Effect of pH

Figure 8.8 shows the effect of pH on the adsorption of Acet and Asp on MCM-41, ASM41, MCM-41-GO and MCM-41-G. The adsorption of pharmaceuticals is strongly pH dependent. The pH of a solution can affect the degree of ionization, dissociation of functional groups, and structure of the adsorbates and also the functionality of the adsorbent surface. Adsorption could be based on electrostatic and non-electrostatic ion interaction. The removal of these pharmaceuticals was greatly affected under acidic conditions (pH < p*K*a) than at basic conditions (pH > p*K*a) (Bui et al., 2013, Nam et al., 2015) Acet (p*K*a 1 = 3.5 and p*K*a 2 = 9.8) and Asp (p*K*a, 3.5) exists as unionised neutral molecules at acidic pH and as the pH becomes more basic the molecules are ionised. Any attraction in acid pH was due to interactions with the adsorbent surface through non-electrostatic attraction and hydrophobic effects. When the pH was above 5, acidic

pharmaceuticals become negatively charged and this together with the negatively charged adsorbent surface, causes electrostatic repulsion. The results show the removal of Asp was less sensitive to the pH variation of the pharmaceutical solution and remains almost constant over the pH range of 2-10, except for MCM-41-G. For MCM-41-G, the highest adsorption for Asp was recorded at pH 2. However, as the solution was made more basic, there was electrostatic repulsion between the negatively charged adsorbent and the Asp which led to a decrease in adsorption.

The adsorption process of charged pollutants on ionic surfactants differs significantly from the conventional adsorption process. Usually, the surfactant molecule forms a mono or bilayer on the charged pollutant surface which is dependent on the surfactant concentration (Sen et al., 2012, Gibson, 2014b). In the adsorption of Asp by ASM41, as a result of small changes over the pH range studied from 2-10, electrostatic interaction is not the primary adsorption mechanism, and other mechanisms such as π - π and hydrophobic effects between the cationic CTAB surface and the Asp organic molecules are likely to be responsible for adsorption. The adsorption of Asp on to MCM-41-GO and MCM-41-G was also *via* hydrophobic and $\pi - \pi$ interactions because of the negligible change in adsorption capacity over the pH range of 2-10.

A pH value of 4 was subsequently selected for the rest of the studies as there was no significant difference between the percentage adsorbed at pH 2 and 4. Also, pH 4 better simulates real environmental conditions as opposed to pH 2.

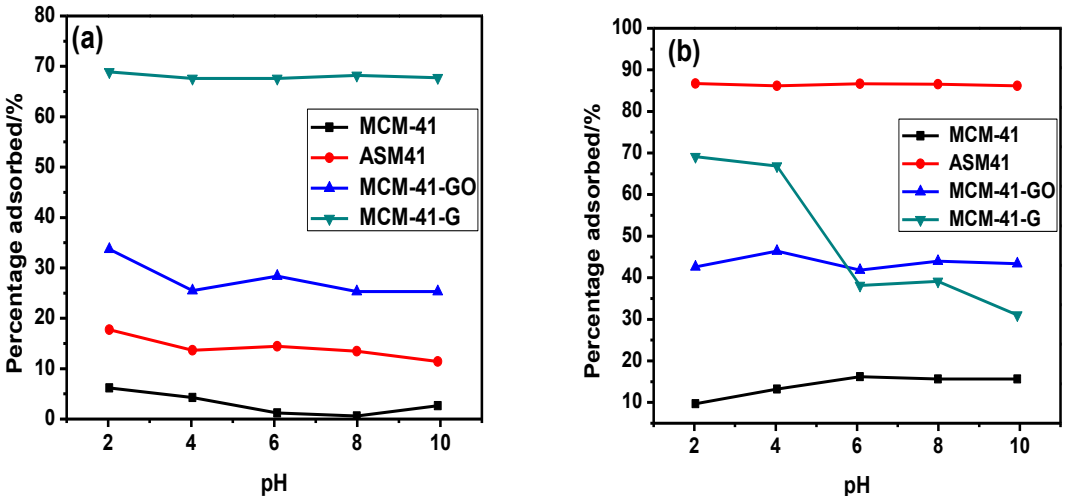

Figure 8.8 (a) Effect of pH on sorption of Acet and (b) Effect of pH on the sorption of Asp on the adsorbents (Conditions: 15 mL of 12.5 ppm Acet and Asp, equilibration time 180 mins, adsorbent dose 40 mg, temperature 25 °C.

8.6.3 Effect of ionic strength

The effect of ionic strength on the adsorption behaviour of Acet and Asp on ASM41, MCM-41, MCM-41-GO and MCM-41-G was studied. The ionic strength was studied by adjusting 15 mL of 12.5 ppm pharmaceutical solutions with 10, 20, 40 and 80 mM NaCl solution. The results are shown in Figure 8.9. The activity coefficients of H_3O^+, OH^- and the adsorbate are affected by the ionic strength as observed by Ma et al. (2012). At 20 mM NaCl, there was a slight increase in percentage adsorption for both Acet and Asp, with all adsorbents. However, subsequent increases in ionic strength after 20 mM did not result in a significant change in adsorption. The slight decrease may be due to the hindering effect caused by the availability of positively charged sodium ions in solution and the competition between pharmaceuticals present in solution for adsorption onto the available adsorption sites. A similar observation was made by Al-Khateeb et al. (2014). This indicated that the overall adsorption mechanism process for all the adsorbents were not due to primarily a single mechanism. A combination of processes such as electrostatic attraction, hydrophobic and $\pi - \pi$ effects was responsible for the adsorption.

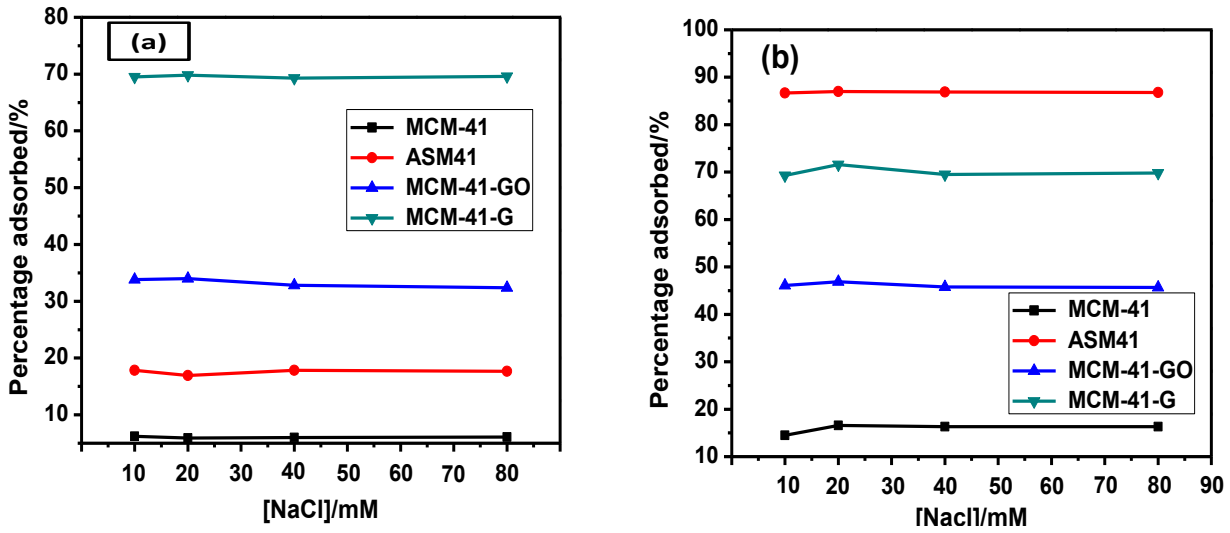

Figure 8.9 (a) Effect of ionic strength on sorption of Acet and (b) Effect of ionic strength on the sorption of Asp on the adsorbents (Conditions: 15 mL of 12.5 ppm Acet and Asp, equilibration time 180 mins, adsorbent dose 40 mg, temperature 25 °C, pH 4).

8.6.4 Effect of adsorbent dose

The effect of adsorbent dose of MCM-41, ASM41, MCM-41-GO and MCM-41-G on the adsorption of Acet and Asp was studied. The results are presented in Figure 8.10. The masses of adsorbent used were 0.01, 0.02, 0.03, 0.04, 0.05 and 0.06 g. For Acet, the percentage adsorption was 0.74 - 11, 4.90 – 23.0, 18.3 – 30.1 and 20.3 – 77.8%, for MCM-41, ASM41, MCM-41-GO and MCM-41-G, respectively. The optimum adsorbent dose was 0.04 g for all the adsorbents with optimum percentage adsorption of 8.68, 19.3, 27.8 and 77.8% for MCM-41, ASM41, MCM-41-GO and MCM-41-G, respectively. It can be seen that the percentage adsorption increases up to 0.04 g and subsequently forms a plateau. However, in contrast, Asp was adsorbed on to the adsorbents optimally at very low dosage, with 0.02 g being the optimum dose in MCM-41. All other adsorbents had 0.01 g as the optimum dose. Interestingly, as can be seen, the effect of dose on Asp was not significant. At low or high doses, the overall percentage adsorption did not change by more than 10%. The maximum percentage removal recorded for MCM-41, ASM41, MCM-41-GO and MCM-41-G were 9.3, 94.6, 25.5 and 38.0%, respectively. The higher percentage removal of Asp at lower doses, could be due to the exposure of all active sites for adsorption causing higher adsorption percentage removal. Higher adsorbent doses, may be detrimental to the

adsorption process as it may enhance the probability of collision causing adsorbent particles to aggregate, thus reducing surface area causing a decrease in the percentage removal (Sajab et al., 2011, Shao et al., 2014). However, for this study 0.04 g was chosen as the optimum dose because it was the optimal dose for Acet and a change in mass did not significantly affect Asp adsorption for all the adsorbents.

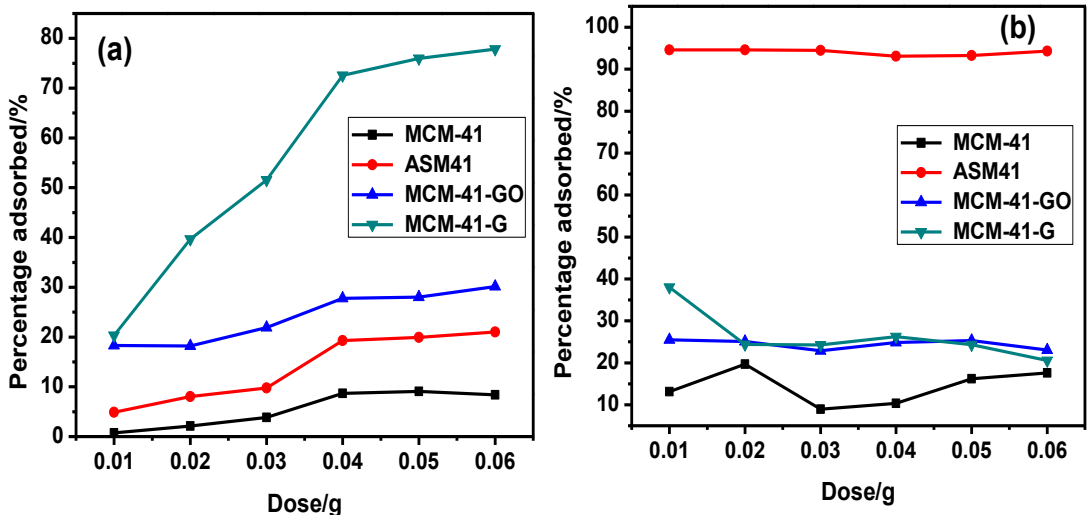

Figure 8.10 (a)Effect of dose on sorption of Acet and 8.10 (b) Effect of dose on the sorption of Asp on the adsorbents (Conditions: 15 mL of 12.5 ppm Acet and Asp, equilibration time 180 mins, temperature 25 °C, pH 4).

8.6.5 Effect of contact time

The effect of contact time for the adsorption of Acet and Asp on MCM-41, ASM41, MCM-41-GO and MCM-41-G was studied between 2 -1440 mins (Figure 8.11). Most of the Acet and Asp (70%) were removed before 30 mins. The initial rapid rate of removal is because of the number of available active sites on the surface of the adsorbent materials which resulted in increased rapid adsorption. After 30 mins, the adsorption rate became slower due to the agglomeration of the Acet and Asp on the active sites of the adsorbents.

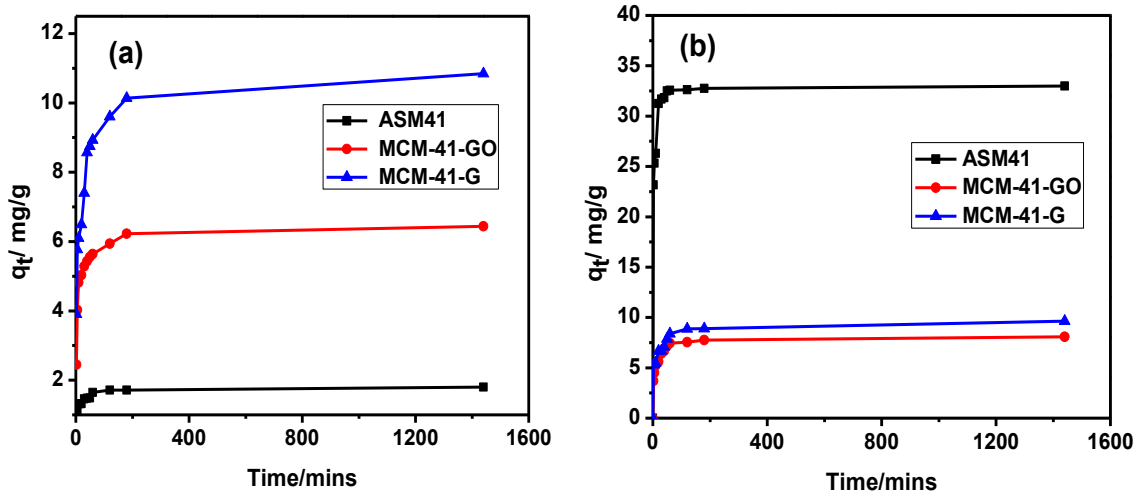

Figure 8.11 (a) Effect of contact time on sorption of Acet and (b) Effect of contact time on the sorption of Asp on the adsorbents (Conditions: 15 mL of 12.5 ppm Acet and Asp, equilibration time 1440 mins, adsorbent dose 40 mg, temperature 25 °C, pH 4).

8.6.6 Effect of temperature

The effect of temperature on the adsorption efficiency of all the adsorbents is shown in Figure 8.12. The range of temperatures studied was from 293-313 K. Figure 8.12 shows a slight decrease in adsorption capacity as the temperature increased with lower temperatures affording a better removal of Acet and Asp. This may be attributed to the pollutant molecules gaining kinetic energy when there was an increase in temperature, thus resulting in the molecules moving away from the solid phase into the bulk phase. A similar observation was made by Kushwaha et al. (2014). This slight variation in adsorption capacity of the adsorbent is indicative that the adsorbents could be used over a range of temperatures, however a lower temperature of 298 K is optimal. This effect of temperature on the adsorbents is indicative that firstly, the adsorbents can be used at point source without a manipulation in temperature and secondly, the adsorbents are useful across a wide range of temperatures.

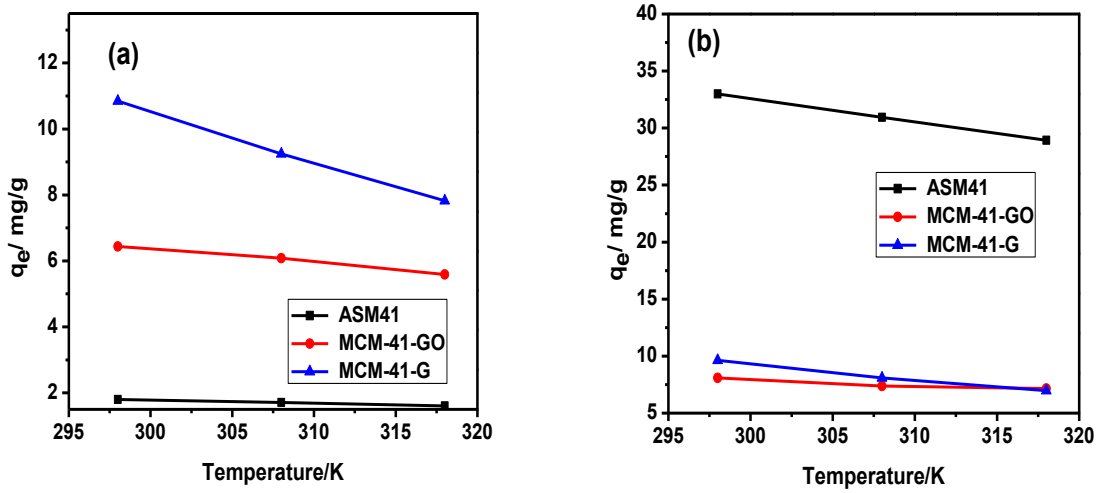

Figure 8.12 (a) Effect of temperature on the adsorption of Acet and (b) Effect of temperature on the adsorption of Asp (Conditions: 15 mL of 12.5 ppm Acet and Asp, equilibration time 180 mins, pH 4).

8.6.7 Adsorption isotherms

The isotherm models were computed based on the experimental data obtained from the non-linear regression analysis of Freundlich (Kushwaha et al., 2014), Langmuir (Ma et al., 2012), Dubinin-Radushkevich (D-R) (Shao et al., 2014) and Temkin (Kushwaha et al., 2014) models, with equations presented in Table 8.2. The isotherm parameters for the adsorbents are presented in Table 8.4. Based on the determination coefficient, the Freundlich isotherm was the best fit for the adsorption data when compared to the other isotherms for both Acet and Asp. The suitability of the Freundlich model suggests that the adsorption process is heterogeneous with several adsorption mechanisms involved in the adsorption process. Freundlich constants K_F and n are the adsorption capacity and adsorption intensity respectively. In the adsorption of Acet, MCM-41-G had a higher K_F value than the other 2 adsorbents, which indicated that it had adsorbed a greater amount of Acet. In the adsorption of Asp, ASM41 had a higher K_F value than MCM-41-GO and MCM-41-G which meant it was a better adsorbent and correlates with the value obtained from the Langmuir isotherm. N values > 1, indicated that the adsorption of both Acet and Asp was favourable with all adsorbents.

The q_m values obtained from the Langmuir isotherm are consistent with the K_F value from the Freundlich isotherm. In the adsorption of Acet, the q_m value for MCM-41-G was 556 mg/g

which was almost double and triple that of the q_m values of MCM-41-GO and ASM41, respectively. In Asp adsorption, the q_m value was largest for ASM41 and smallest for MCM-41-GO. This could be attributed to the amount of carbon present in the different adsorbents and the structure of the adsorbate. ASM41 had the highest percentage of carbon suggesting that the adsorption was primarily by $\pi - \pi$ interactions thus leading to the highest percentage adsorption. The result suggests that the modification of MCM-41 with carbon functionality affects the hydrophobicity of the adsorbents. Thus, this modification enables the adsorbents to have higher sorption capacities for these hydrophobic adsorbates.

The D-R model was chosen to understand the adsorption mechanism between homogeneous and heterogeneous surfaces (Shao et al., 2014). The D-R model distinguishes primarily between physical and chemical adsorption of the pharmaceuticals on ASM41, MCM-41-GO and MCM-41-G. The isotherm constant, E (kJ/mol) and R^2 values are shown in Table 8.4. An E value of between 1 - 8 kJ/mol represents physical adsorption and between 8 – 16 kJ/mol is indicative of a chemical adsorption process. All the values for E, the mean sorption energy obtained, were less than 8 kJ/mol. These values indicated that physical adsorption was the dominating adsorption process for Acet and Asp adsorption on all adsorbents.

Table 8.4 (a) Isotherm parameters for the adsorption of Acet onto different adsorbents

Isotherm	Parameters	ASM41	MCM-41-GO	MCM-41-G
		Acetaminophen		
Langmuir	q_m/ mg/g	121.9	322.6	555.6
	b/ L/mg	12.7	3.03	1.51
	R^2	0.9078	0.8624	0.7888
Freundlich	K_F	3.68	28.1	38.6
	N	1.05	1.07	1.08
	R^2	0.9998	0.9999	0.9993
Dubunin-Radushkevich	E/ kJ/mol	2.5	3.0	3.9
	q_D/ mg/g	76	120	345
	B/ mol/kJ^2	1.0×10^{-10}	2.0×10^{-10}	2.4×10^{-10}
	R^2	0.943	0.987	0.956
Temkin	B	468.1	135.3	80.2
	b/ J/mol	5.30	18.3	30.9
	A/ L/g	15.8	51.6	81.7
	R^2	0.9296	0.9240	0.9130

Table 8.4 (b) Isotherm parameters for the adsorption of Asp onto different adsorbents

Isotherm	Parameters	ASM41	MCM-41-GO	MCM-41-G
		Aspirin		
Langmuir	q_m/ mg/g	909.1	714.3	769.2
	b/ L/mg	0.091	2.64	2.03
	R^2	0.8869	0.9921	0.9928
Freundlich	K_F	116	82.4	96.7
	N	1.03	1.08	1.04
	R^2	0.9994	0.9999	0.9991
Dubunin-Radushkevich	E/ kJ/mol	7.2	4.3	5.2
	q_D/ mg/g	824	539	612
	B/ mol/kJ^2	4.0×10^{-10}	1.0×10^{-10}	1.5×10^{-10}
	R^2	0.9880	0.9125	0.945
Temkin	B	27.2	100	84.5
	b/ J/mol	91.1	24.8	29.3
	A/ L/g	86.9	74.1	84.8
	R^2	0.9183	0.9279	0.9293

Table 8.5 summarises the Acet and Asp adsorption capacities of different adsorbents. ASM41, MCM-41-GO and MCM-41-G exhibited excellent adsorption capacities for Acet and Asp. The results obtained compared favourably with results from other studies in literature. MCM-41-G gave a significant adsorption of Acet, and ASM41 had a high uptake of Asp.

Table 8.5 Comparison of q_m values to other studies of Acet and Asp on different adsorbents

Adsorbents	q_m values/mg/g	References
	Aspirin	
N-CNT/β-CD	71.9	(Mphahlele et al., 2015)
Fe/N-CNT/ β-CD	105	(Mphahlele et al., 2015)
Graphene	18.07	(Al-Khateeb et al., 2014)
MCM-41-GO	714	This study
MCM-41-G	769	This study
ASM41	909	This study
	Acetaminophen	
Graphene	12.98	(Al-Khateeb et al., 2014)
Activated Carbon (AC)	498-722	(Hoegberg et al., 2002)
Sediment colloid	436	(Zhao et al., 2015)
Solid particle	44.4	(Zhao et al., 2015)
Tea waste AC	99.42	(Dutta et al., 2015)
MCM-41-GO	322.6	This study
MCM-41-G	555.6	This study
ASM41	121.9	This study

8.6.7.1 Thermodynamic parameters

The effect of temperature on the adsorption of Acet and Asp was investigated in the range of 293 – 323 K (Table 8.6). The mean free energy of adsorption ($\Delta G°$) was calculated with the equation:

$$\Delta G = -RTln\ K_0 \quad (8.5)$$

A plot of ln K *versus* 1/T had a linear profile, and the values of $\Delta S°$ and $\Delta H°$ were obtained from the intercept and slope, respectively, using the Van't Hoff equation:

$$\ln K_0 = -\frac{\Delta H}{RT} + \frac{\Delta S}{R} \quad (8.6)$$

The negative $\Delta G°$ values obtained for all the adsorbents, meant that the adsorption of Acet and Asp was thermodynamically favourable and spontaneous. The negative $\Delta H°$ values obtained for

the adsorbents indicated an exothermic adsorption process which further explains the decrease in adsorption at higher temperature. This also correlated with the $\Delta G°$ results, which showed the dominant mode of adsorption was physisorption. A similar result was recorded by Ma et al. (2012). The $\Delta S°$ values obtained indicated decreased randomness/disorderliness between the adsorbent and adsorbate during the adsorption process.

Table 8.6 Thermodynamic parameters for the adsorption of Acet and Asp onto adsorbents

Adsorbent	Temperature/ K	Δ*G*°/kJ/mol	Δ*H*°/kJ/mol	Δ*S*°/kJ/mol
		Acetaminophen		
ASM41	293	-2.076	-0.5745	-5.039
	303	-2.125		
	313	-2.176		
MCM-41-GO	293	-2.148	-0.8261	-4.439
	303	-2.193		
	313	-2.237		
MCM-41-G	293	-4.800	-2.174	-8.259
	303	-4.717		
	313	-4.635		
		Aspirin		
ASM41	293	-7.240	-3.921	-11.14
	303	-7.352		
	313	-7.463		
MCM-41-GO	293	-1.931	-0.7342	-4.024
	303	-1.971		
	313	-2.011		
MCM-41-G				
	293	-4.351	-1.977	-7.967
	303	-4.430		
	313	-4.510		

8.6.8 Adsorption kinetics

Four kinetic models were utilized to determine the rate determining step namely: pseudo-first order (PFO), pseudo-second order (PSO) and intraparticle diffusion (IPD) and Elovich models. The equations for the models are presented in Table 8.1. In a bid to understand the adsorption process, the PFO, PSO, IPD and Elovich models were fitted to the experimental data obtained from the batch adsorption experiments. The R^2 values determined by non-linear regression analysis are presented in Table 8.7. The R^2 value of the PSO kinetic model is much higher than the other models. The experimental q_e values from the PSO model are much closer to the calculated q_e values, when compared to the others. Therefore, the PSO model best describes the adsorption behaviour of Acet and Asp on ASM41, MCM-41-GO and MCM-41-G. The Elovich model is dependent on the principle of chemisorption through bond sharing and interaction. This proves that a part of the adsorption mechanism of Acet and Asp onto ASM41, MCM-41-GO and MCM-41-G was *via* chemical interaction through the active groups on Acet and Asp on the adsorbents surfaces. In a bid to determine the rate controlling step involved in the adsorption of Acet and Asp, the IPD model was used. A plot of q_t *vs* $t^{0.5}$ did not pass through the origin which indicated that IPD was not the sole rate controlling step (Al-Degs et al., 2006, Ma et al., 2012) due to the large *C* values of the linear portion of the plots (Doğan et al., 2009).

Table 8.7 (a) Kinetic parameters for the adsorption of Acet from aqueous solution

Model	Parameter	ASM41	MCM-41-GO	MCM-41-G
		Acetaminophen		
Pseudo-first order	k_1/min^{-1}	0.65	0.75	1.62
	q_e, eq/mg/g	0.81	7.46	8.47
	R^2	0.8667	0.881	0.9081
$q_{e,\,exp}$	mg/g	1.80	6.43	10.8
Pseudo-second order	k_2/min^{-1}	3.41	0.9835	1.008
	q_e /mg/g	1.81	6.46	10.9
	R^2	0.9999	0.9999	0.9999
Intraparticle diffusion	*K*i/mg/g min$^{-0.5}$	0.0155	0.0165	0.1506
	C/mg/g	1.35	4.54	6.49
	R^2	0.5484	0.3877	0.5288
Elovich	A	0.1126	0.581	1.33
	B	1.08	3.10	3.77
	R^2	0.8937	0.8247	0.9168

Table 8.7 (b) Kinetic parameters for the adsorption of Asp from aqueous solution

Model	Parameter	ASM41	MCM-41-GO	MCM-41-G
		Aspirin		
Pseudo-first order	k_1/min^{-1}	1.34	1.05	1.33
	q_e, eq/mg/g	5.00	0.70	0.90
	R^2	0.6801	0.8362	0.8644
$q_{e,\,exp}$	mg/g	33.0	8.07	9.63
Pseudo-second order	k_2/min^{-1}	0.0407	0.820	1.00
	q_e /mg/g	33.0	8.11	9.68
	R^2	0.9999	0.9999	0.9999
Intraparticle diffusion	*K*i/mg/g min$^{-0.5}$	0.1766	0.0933	0.1146
	C/mg/g	28.7	5.52	6.24
	R^2	0.2596	0.4383	0.574
Elovich	A	1.66	0.7486	0.8124
	B	24.20	3.66	4.34
	R^2	0.7078	0.8730	0.8913

8.7 Regeneration Studies

Recycling and regeneration of adsorbents is important in the practical application of adsorbents. An ideal adsorbent is one with high adsorption capacity and excellent desorption ability. This would reduce the cost of always preparing new adsorbents and also reduce the introduction of secondary pollutants into the environment. Desorption experiments were carried out by washing the adsorbents with acidic ethanol and 0.01 M NaOH. After successive adsorption-desorption cycles, there was a slight decrease in adsorption capacity. Results showed good desorption efficiencies of 85 and 76% for MCM-41-GO, 85 and 82% for MCM-41-G, and 83 and 79% for ASM41 for Acet and Asp, respectively after 2 desorption cycles. The FTIR spectra showed no obvious peak changes after 2 cycles of desorption. However, there was a slight change in the surface area of all the adsorbents after 2 desorption cycles. The results are indicative that ASM41, MCM-41-GO and MCM-41-G are reusable and stable.

8.8 Conclusion

In this study, ASM41 was synthesised. Previously synthesized MCM-41 was successfully coated with graphene oxide and graphene. Batch adsorption studies were carried out to study the adsorption behaviour of Acet and Asp on MCM-41, ASM41, MCM-41-GO and MCM-41-G. The carbon present in the adsorbents confers a degree of hydrophobicity to the adsorbent. The least adsorption for Acet and Asp was recorded with MCM-41 because of its highly hydrophilic nature. All the adsorbents were effective in the removal of Acet and Asp from aqueous solution but ASM41 was the best adsorbent for Asp at a pH of 2, adsorbent dose of 40 mg and a temperature of 25 °C. MCM-41-G was the best adsorbent for Acet at pH 2, adsorbent dose of 40 mg and a temperature of 25 °C. The adsorption kinetics fitted the pseudo-second order model and the best fit isotherm was the Freundlich model. The adsorbents were also effective in the treatment of real environmental samples. The adsorbents showed they were still efficient after 2 cycles of regeneration.

8.9 Acknowledgments

We gratefully acknowledge the School of Chemistry and Physics, University of KwaZulu-Natal, South Africa, for providing the laboratory facilities and instrumentation used in this research and also to the AAU small ggrant for provision of financial support.

References

Al-Degs, Y. S., El-Barghouthi, M. I., Issa, A. A., Khraisheh, M. A. & Walker, G. M. 2006. Sorption of Zn (II), Pb (II), and Co (II) using natural sorbents: equilibrium and kinetic studies. *Water Research,* 40**,** 2645-2658.

Al-Khateeb, L. A., Almotiry, S. & Salam, M. A. 2014. Adsorption of pharmaceutical pollutants onto graphene nanoplatelets. *Chemical Engineering Journal,* 248**,** 191-199.

Carballa, M., Omil, F., Lema, J. M., Llompart, M. A., García-Jares, C., RodríGuez, I., Gomez, M. & Ternes, T. 2004. Behavior of pharmaceuticals, cosmetics and hormones in a sewage treatment plant. *Water Research,* 38**,** 2918-2926.

Doğan, M., Abak, H. & Alkan, M. 2009. Adsorption of methylene blue onto hazelnut shell: kinetics, mechanism and activation parameters. *Journal of Hazardous Materials,* 164**,** 172-181.

Dutta, M., Das, U., Mondal, S., Bhattachriya, S., Khatun, R. & Bagal, R. 2015. Adsorption of acetaminophen by using tea waste derived activated carbon. *International Journal of Environmental Sciences,* 6**,** 270-281.

Ghorbani, F., Younesi, H., Mehraban, Z., Çelik, M. S., Ghoreyshi, A. A. & Anbia, M. 2013. Preparation and characterization of highly pure silica from sedge as agricultural waste and its utilization in the synthesis of mesoporous silica MCM-41. *Journal of the Taiwan Institute of Chemical Engineers,* 44**,** 821-828.

Gibson, L. 2014. Mesosilica materials and organic pollutant adsorption: part B removal from aqueous solution. *Chemical Society Reviews,* 43**,** 5173-5182.

Han, R., Zhang, L., Song, C., Zhang, M., Zhu, H. & Zhang, L. 2010. Characterization of modified wheat straw, kinetic and equilibrium study about copper ion and methylene blue adsorption in batch mode. *Carbohydrate Polymers,* 79**,** 1140-1149.

Ho, Y.-S. & Mckay, G. 1998. Sorption of dye from aqueous solution by peat. *Chemical Engineering Journal,* 70**,** 115-124.

Hoegberg, L. C. G., Angelo, H. R., Christophersen, A. B. & Christensen, H. R. 2002. Effect of ethanol and pH on the adsorption of acetaminophen (paracetamol) to high surface activated charcoal, in vitro studies. *Journal of Toxicology: Clinical Toxicology,* 40**,** 59-67.

Khetan, S. K. & Collins, T. J. 2007. Human pharmaceuticals in the aquatic environment: a challenge to green chemistry. *Chemical Reviews,* 107**,** 2319-2364.

Kushwaha, A. K., Gupta, N. & Chattopadhyaya, M. 2014. Enhanced adsorption of methylene blue on modified silica gel: equilibrium, kinetic, and thermodynamic studies. *Desalination and Water Treatment,* 52**,** 4527-4537.

Li, X., Wang, Z., Li, Q., Ma, J. & Zhu, M. 2015. Preparation, characterization, and application of mesoporous silica-grafted graphene oxide for highly selective lead adsorption. *Chemical Engineering Journal,* 273**,** 630-637.

Liou, T.-H. 2011. A green route to preparation of MCM-41 silicas with well-ordered mesostructure controlled in acidic and alkaline environments. *Chemical Engineering Journal,* 171**,** 1458-1468.

Liu, X., Zhang, H., Ma, Y., Wu, X., Meng, L., Guo, Y., Yu, G. & Liu, Y. 2013. Graphene-coated silica as a highly efficient sorbent for residual organophosphorus pesticides in water. *Journal of Materials Chemistry A,* 1**,** 1875-1884.

Luo, Y.-B., Zhu, G.-T., Li, X.-S., Yuan, B.-F. & Feng, Y.-Q. 2013. Facile fabrication of reduced graphene oxide-encapsulated silica: A sorbent for solid-phase extraction. *Journal of Chromatography A,* 1299**,** 10-17.

Ma, J., Yu, F., Zhou, L., Jin, L., Yang, M., Luan, J., Tang, Y., Fan, H., Yuan, Z. & Chen, J. 2012. Enhanced adsorptive removal of methyl orange and methylene blue from aqueous solution by alkali-activated multiwalled carbon nanotubes. *ACS Applied Materials & Interfaces,* 4**,** 5749-5760.

Mangrulkar, P. A., Kamble, S. P., Meshram, J. & Rayalu, S. S. 2008. Adsorption of phenol and o-chlorophenol by mesoporous MCM-41. *Journal of Hazardous Materials,* 160**,** 414-421.

Marcano, D. C., Kosynkin, D. V., Berlin, J. M., Sinitskii, A., Sun, Z., Slesarev, A., Alemany, L. B., Lu, W. & Tour, J. M. 2010. Improved synthesis of graphene oxide. *ACS Nano,* 4**,** 4806-4814.

Meng, H., Li, Z., Ma, F., Wang, X., Zhou, W. & Zhang, L. 2015. Synthesis and characterization of surface ion-imprinted polymer based on SiO_2-coated graphene oxide for selective adsorption of uranium (vi). *RSC Advances,* 5**,** 67662-67668.

Mphahlele, K., Onyango, M. S. & Mhlanga, S. D. 2015. Adsorption of aspirin and paracetamol from aqueous solution using Fe/N-CNT/β-cyclodextrin nanocomopsites synthesized via a benign microwave assisted method. *Journal of Environmental Chemical Engineering,* 3**,** 2619-2630.

Novoselov, K. S., Geim, A. K., Morozov, S., Jiang, D., Zhang, Y., Dubonos, S. A., Grigorieva, I. & Firsov, A. 2004. Electric field effect in atomically thin carbon films. *Science,* 306**,** 666-669.

Parida, K., Mishra, K. G. & Dash, S. K. 2012. Adsorption of copper (II) on NH_2-MCM-41 and its application for epoxidation of styrene. *Industrial & Engineering Chemistry Research,* 51**,** 2235-2246.

Qu, Q. & Gu, Z. 2014. Facile synthesis of hierarchical MCM-41 spheres with an ultrahigh surface area and their application for removal of methylene blue from aqueous solutions. *Analytical Methods,* 6**,** 1397-1403.

Sajab, M. S., Chia, C. H., Zakaria, S., Jani, S. M., Ayob, M. K., Chee, K. L., Khiew, P. S. & Chiu, W. S. 2011. Citric acid modified kenaf core fibres for removal of methylene blue from aqueous solution. *Bioresource Technology,* 102**,** 7237-7243.

Sen, T. K., Thi, M. T., Afroze, S., Phan, C. & Ang, M. 2012. Removal of anionic surfactant sodium dodecyl sulphate from aqueous solution by adsorption onto pine cone biomass of Pinus Radiate: equilibrium, thermodynamic, kinetics, mechanism and process design. *Desalination and Water Treatment,* 45**,** 263-275.

Shao, Y., Wang, X., Kang, Y., Shu, Y., Sun, Q. & Li, L. 2014. Application of Mn/MCM-41 as an adsorbent to remove methyl blue from aqueous solution. *Journal of Colloid and Interface Science,* 429**,** 25-33.

Tambosi, J. L., Yamanaka, L. Y., José, H. J., Moreira, R. D. F. P. M. & Schröder, H. F. 2010. Recent research data on the removal of pharmaceuticals from sewage treatment plants (STP). *Química Nova,* 33**,** 411-420.

Thuc, C. N. H. & Thuc, H. H. 2013. Synthesis of silica nanoparticles from Vietnamese rice husk by sol–gel method. *Nanoscale Research Letters,* 8**,** 1-10.

Wang, J., Chen, Z. & Chen, B. 2014. Adsorption of polycyclic aromatic hydrocarbons by graphene and graphene oxide nanosheets. *Environmental Science & Technology,* 48**,** 4817-4825.

Wang, Z.-M., Wang, W., Coombs, N., Soheilnia, N. & Ozin, G. A. 2010. Graphene Oxide− Periodic Mesoporous Silica Sandwich Nanocomposites with Vertically Oriented Channels. *ACS Nano,* 4**,** 7437-7450.

Yang, K., Chen, B. & Zhu, L. 2015. Graphene-coated materials using silica particles as a framework for highly efficient removal of aromatic pollutants in water. *Scientific Reports,* 5**,** 11641-11653.

Zhao, Y., Yang, S., Wang, G. & Han, M. 2015. Adsorption behaviors of acetaminophen onto the colloid in sediment. *Polish Journal of Environmental Studies,* 24, 853-861.

9.0 CHAPTER 9: SYNTHESIS OF MCM-48, ENCAPSULATION WITH GRAPHENE OXIDE/GRAPHENE AND ITS APPLICATION IN REMEDIATION OF PHARMACEUTICALS FROM AQUEOUS SOLUTION

Samson O. Akpotu and Brenda Moodley*

School of Chemistry and Physics, University of KwaZulu-Natal, Westville Campus, Durban, 4000, South Africa.

***** corresponding author email: moodleyb3@ukzn.ac.za
Telephone: +27 31 2602796
Fax: +27 31 2603091

9.1 Abstract

This study was carried out to determine the efficiency of as-synthesised MCM-48 (ASM48), graphene oxide encapsulated MCM-48 (M48GO) and graphene encapsulated MCM-48 (M48G) in the remediation of pharmaceuticals (caffeine (CAF) and phenacetin (PHE)) from aqueous solution. ASM48 had improved hydrophobic properties for adsorption compared to MCM-48 and was therefore performed better in remediation applications. The adsorbents were characterised with a host of different techniques. The optimisation experiments showed that the adsorption capacity of the adsorbents for the pharmaceuticals increased with increasing adsorbate concentration and contact time but decreased with an increase in adsorbent mass and temperature. The optimum pH for adsorption of the selected pharmaceuticals was 2. Hydrophobic interaction was the dominant mechanism of adsorption which was controlled by the pH-p*K*a interaction between the adsorbents and adsorbates. The sorption kinetics showed that the data fitted the pseudo second order and intraparticle diffusion model. The equilibrium data obtained showed that it fitted the Freundlich adsorption isotherm. M48G was the best adsorbent and had a maximum adsorption capacity of 153.8 and 212.7 mg/g for CAF and PHE, respectively. Thermodynamic studies showed the adsorption process as spontaneous and exothermic. The desorption studies carried

out revealed that the adsorbents could be regenerated and reused in the adsorption of CAF and PHE.

Keywords: *MCM-48, as-synthesised, graphene oxide, graphene, caffeine, phenacetin, adsorption*

9.2 Introduction

Over the last decade pharmaceuticals have gained much attention as emerging contaminants (Khetan and Collins, 2007, Jones et al., 2005). These pharmaceuticals are found in trace concentrations in all environmental media (Bui et al., 2013). They have been detected in aqueous systems and in soil at concentration levels from a few µg/L to about a 100 µg/L particularly in effluents from the pharmaceutical industry (Larsson et al., 2007). Pharmaceuticals are suspected of causing unknown chronic toxic effects in the environment and may cause resistance of microorganisms against antibiotic drug usage (Martínez, 2008). Hence, there is an urgent need to remove these emerging contaminants from environmental media. However, conventional water treatment systems are not designed to effectively remove pharmaceuticals from water systems (Castiglioni et al., 2006, Bui et al., 2013). It has therefore become imperative to develop water treatment systems that are efficient in the removal of pharmaceuticals from water systems.

Amongst the technologies available, adsorption is the most preferred method for the removal of pharmaceuticals from water systems. This is due to its inherent advantages such as ease of use, uncomplicated technology, and no by-products. Many materials have been applied in the adsorption of pharmaceuticals with varying degrees of success. These materials include activated carbon (Snyder et al., 2007), zeolites (Martucci et al., 2012), graphene oxide (Nam et al., 2015), graphene (Al-Khateeb et al., 2014) and ordered mesoporous silica (OMS) (Bui and Choi, 2009). OMS was first synthesised in 1992 (Beck et al., 1992) with enormous potential in remediating pharmaceuticals from wastewater. MCM-48 is a class of OMS that has excellent properties such as large surface area (> 1000 m^2/g), homogenous pores, narrow pore size distribution, cubic *Ia3d* symettry and thermal stability (Gibson, 2014b). However, due to its strong hydrophilic properties, it has a very low adsorptive capacity for pharmaceuticals. Hence, in a bid to exploit its true

adsorptive capabilities, MCM-48 was made more hydrophobic by coating with a more hydrophobic material such as graphene oxide/graphene or converted into as-synthesised (ASM48).

As-synthesised MCM-48 is made by retaining the surfactant template in the MCM-48. The surfactant is often times a long chain carbon and confers hydrophobicity on an otherwise strongly hydrophilic material. This has been applied by Mangrulkar and co-workers with increased adsorptive ability for phenols in aqueous systems (Mangrulkar et al., 2008). Graphene and graphene oxide are strongly hydrophobic materials and are good adsorbents for organic pharmaceutical molecules but are not able to achieve their true potential for adsorption. This is because graphene is unable to form aggregated nanosheets (Yang et al., 2015a) and graphene oxide is extremely difficult to separate from the adsorbate (Liu et al., 2013). To overcome these challenges in both materials, the graphene/graphene oxide is anchored on an OMS to produce a hybrid material. This hybrid material combines the uniqueness of the individual materials such as large surface area of the OMS and high hydrophobicity of the graphene oxide/graphene. Siliceous materials coated with graphene/graphene oxide have shown improved adsorption for organic pollutants (Liu et al., 2013, Yang et al., 2015a). Modified OMS has also shown improved adsorption for pharmaceuticals (Bui et al., 2013, Bui et al., 2011).

Caffeine is a basic pharmaceutical with a p*K*a value > 14. It is a central nervous system stimulant and is present in many analgesic drugs and beverages. Phenacetin is a neutral pharmaceutical with a p*K*a value > 14. It is a metabolite of paracetamol and is also an analgesic. Its usage has been banned in the USA and India because of long term kidney and liver damage associated with ingestion. Hence, the need to remediate these pharmaceuticals from wastewater (Dubach et al., 1991). Their structures are shown in Figure 9.1.

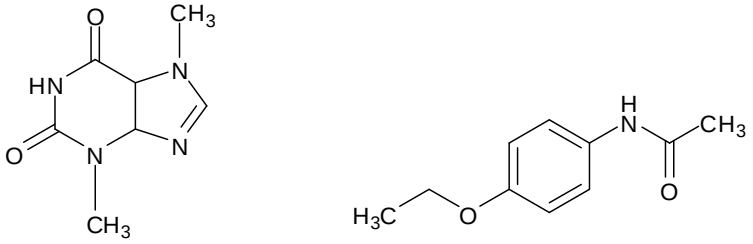

Caffeine Phenacetin

Figure 9.1 Structure of caffeine and phenacetin

In this study, we report the encapsulation of MCM-48 with graphene oxide and graphene for the first time and its application as highly efficient adsorbents for the remediation of pharmaceuticals (CAF and PHE) from wastewater. Also, as-synthesised MCM-48 (ASM48) was synthesised and applied in the remediation of pharmaceuticals from aqueous solution. This was done to investigate the hydrophobic effects of the synthesised template in the adsorption of CAF and PHE from aqueous solution. All adsorbents were characterised using elemental analysis (EA), fourier transform infrared (FTIR) spectroscopy, thermogravimetric analysis (TGA), x-ray diffraction (XRD) studies, textural analysis, scanning electron microscopy (SEM) and transmission electron microscopy (TEM). Caffeine and phenacetin were selected as model pharmaceutical pollutants to determine the efficiency of the adsorbents as well as to understand the adsorption mechanism. The relative low cost of synthesis of ASM48, the simple encapsulation procedure of MCM-48 with GO and G, and their high efficiency makes these materials excellent adsorbents for the removal of pharmaceutical pollutants in wastewater.

9.3 Experimental

9.3.1 Materials and chemicals

Natural graphite powder, methanol (HPLC grade), hydrazine monohydrate (80 %), 3-aminopropyl triethoxysilane (APTES, 99 %), HCl (37 %), $KMnO_4$, tetraethylorthosilicate (TEOS, 98 %) and the pharmaceuticals, caffeine (CAF) and phenacetin (PHE) were obtained from Sigma-Aldrich. Absolute ethanol (Merck), cetyltrimethyl ammoniumbromide (CTAB 99 %+) (Calbiochem), H_2SO_4 (98 %), H_2O_2 (35 %) and H_3PO_4 (80 %) were obtained from Promark. All the reagents were analytically pure and were used without further purification. MilliQ water was used in the preparation of the standard solutions and the mobile phase used in chromatography analysis.

9.3.2 Synthesis of MCM-48 and as-synthesised MCM-48

MCM-48 was synthesized using a modified method from Peng et al. (2011). About 2.4 g of CTAB was dissolved in 100 mL of ultra-pure water at room temperature. A 75 mL aliquot of

ethanol was added to the mixture. An 18 mL aliquot of ammonium hydroxide was added to a beaker containing CTAB, ethanol and water under stirring. This was allowed to stir for 30 minutes and 3.6 mL of tetraethylorthosilicate (TEOS) was added to the clear solution and stirred vigorously at 300 rpm for 4 hrs. The slurry was filtered and washed with double-distilled deionised water to a neutral pH, expelling the surfactant and ammonia solution. The resultant powder was dried in an oven at a temperature of 110 °C for 24 hrs. This was labelled as as-synthesised MCM-48 (ASM48). The dried powder was broken up gently with a pestle properly before calcination at 550 °C for 5 hrs and with a ramp rate of 2 °C/min for CTAB removal in order to obtain MCM-48.

9.3.3 Activation of MCM-48

Activation of MCM-48 was achieved by modifying the method used by Kushwaha et al. (2014). A similar procedure was used in the activation of MCM-41 described in chapter 4. A detailed procedure is provided in chapter 5.

9.3.4 Synthesis of NH_2-MCM-48

MCM-48 surface was modified by an aqueous, easy one-step synthesis. A similar procedure was used in the synthesis of NH_2-MCM-41 and a detailed procedure is provided in chapter 5.

9.3.5 Synthesis of GO

GO was synthesized using a modified Tour method (Marcano et al., 2010). A detailed procedure is provided in chapter 5.

9.3.6 Synthesis of M48GO and M48G

In this encapsulation process, NH_2-MCM-48 was dispersed and sonicated in water. GO (10 mg/L), previously sonicated for 2 hrs was added to the suspension and the pH was adjusted to 7 by adding NH_4OH whilst stirring. It was stirred continuously for 8 hrs and left to settle for an

hour. The product was filtered, washed with water and dried in a vacuum oven for 6 hrs at 50 °C. This was labelled as M48GO. In the synthesis of M48G, a similar procedure was adopted to M48GO but the temperature of synthesis was 80 °C and hydrazine monohydrate was added to the mixture to reduce GO to G. The mixture was stirred for 8 hrs, left to settle for an hour, filtered, washed with water and dried under vacuum. The solid black product was oven dried in a vacuum at 80 °C for 6 hrs. This was labelled M48G.

9.4 Characterisation of Samples

The FTIR spectra of the adsorbent samples were recorded on a Perkin Elmer series 100 spectrometer. Thermogravimetric (TGA) profiles were obtained using 5 mg of sample in an aluminium pan on an SDT Q 600 V 209 Build 20 between 25-900 °C at 10 °C/min in a N_2 environment. The information on surface morphology and microstructure of the adsorbents were obtained by analysis on a field emission scanning electron microscope (FESEM, Zeiss instrument, 10 kV operating voltage), and high-resolution transmission electron microscope (HRTEM, JEOL). X-ray diffraction (XRD) experiments were carried out on an x-ray diffractometer (Bruker D8 Advance, Bruker, AXS, Germany) operating at 45 kV and 40 mA with Cu. The carbon content of the samples was determined using an elemental analyser (Thermo Scientific CHNS/O analyser). N_2 adsorption–desorption isotherms were obtained using a nitrogen adsorption analyzer (Micrometrics Tristar II 3020). The samples were degassed at a temperature of 90 °C with a Micromeritics VacPrep 061 for an hour and then ramped up to 200 °C overnight. Surface area and pore size measurements of samples were obtained using the BET method. The pore volume was calculated from the adsorption branch based on volume of nitrogen adsorbed at a relative pressure (P/P_o) of approximately 0.99.

9.5 Adsorption Experiments

The pharmaceutical concentrations were determined by HPLC measurements at a wavelength of 210 nm and 254 nm, respectively for caffeine and phenacetin. Batch adsorption experiments were carried out using PTFE screw cap vials covered with aluminium foil at room temperature to determine the effect of adsorption parameters such as adsorbent dose, adsorption time, pH and

temperature. A 1000 mg/L stock solution was prepared, from which several 15.0 mL working solutions of 12.5 mg/L (CAF and PHE) were prepared.

9.5.1 Analytical method

Caffeine and phenacetin concentrations were quantified using a HPLC system consisting of an Agilent 1200 SL (Agilent Technology, USA) with a pressure grade pump and a UV-Vis detector at a wavelength of 210 nm for CAF and 254 nm for PHE. Separation was carried out at room temperature with an Agilent Eclispe XDB- C-18 (4.6 x 150 mm, 5 µm particle size) column at a mobile phase flow rate of 0.6 mL/min under isocratic conditions with a mixture of methanol/water (60:40; v/v). The pH of the water was adjusted with H_3PO_4 to 2.3. The sample volume injected was 5 µL.

9.6 Adsorption Kinetics

Batch adsorption experiments were determined by adding about 40 mg of the adsorbent to 15 mL of 12.5 mg/L pharmaceutical aqueous solution (CAF and PHE solution) in a series of beakers covered with aluminium foil. The mixture was agitated on a shaker at 25 °C for 180 mins. At set times, the solutions were centrifuged and filtered through a 0.45 µm filter and the residual concentration of the filtrate was determined by analysis using the HPLC-UV instrument. The concentration of CAF and PHE in the supernatant solution was calculated from their calibration curves. Batch adsorption studies were carried out by varying the pH of the solution (2 -10) using 0.1 M NaOH/HCl, dose, contact time, initial adsorbate concentration and temperature. Thermodynamic and adsorption isotherm studies were also carried out. The amount of adsorbate adsorbed on to the adsorbents at time *t*, and q_t (mg/g) were calculated using equation 9.1:

$$q_t = \frac{(C_o - C_e)V}{m} \tag{9.1}$$

The removal efficiency of the pharmaceuticals in solution, and the percentage adsorption were calculated as:

$$\% \, adsorption = \frac{(C_o - C_e)}{C_o} \, x \, 100 \quad (9.2)$$

Where C_0 and C_e are the initial and equilibrium concentrations of the pharmaceutical solutions, respectively, *V* is the solution volume (L) and m is the mass of the adsorbent (g).

Kinetic studies were carried out using 150 mg of adsorbent with 200 mL of 25, 50, 75 and 100 mg/L of CAF and PHE solution with the pH adjusted to 2. Aliquots of the solution were withdrawn periodically (2 – 1440 mins), filtered off, and the concentration of (CAF and PHE) adsorbed was determined.

9.6.1 Adsorption isotherms

Three models were selected to explain the isothermal relationship between the adsorbents and adsorbate. These were the Langmuir (Langmuir, 1918), Freundlich (Freundlich, 1906) and Temkin (Kushwaha et al., 2014) models. The linear form of the Langmuir equation is presented in equation 3:

$$\frac{C_e}{q_e} = \frac{1}{bq_m} + \frac{C_e}{q_m} \quad (9.3)$$

Where b is the Langmuir constant related to the energy of adsorption (L/mg), q_m is the maximum adsorption capacity (mg/g) and is obtained by plotting C_e/q_e *vs* C_e. q_e is the amount of pharmaceuticals adsorbed per unit of the adsorbent at equilibrium time (mg/g)

The Freundlich adsorption isotherm equation is given in equation 9.4:

$$\ln q_e = ln \, K_f + \left(\frac{1}{n}\right) \ln C_e \quad (9.4)$$

Where C_e is the equilibrium concentration of the pharmaceuticals in solution (mg/L). K_f is the Freundlich constant for adsorption capacity and *n* gives information about the adsorption intensity.

The Temkin adsorption isotherm equation is given in equation 9.5:

$$ln\, q_e = B \ln A + B\ lnC_e \quad (9.5)$$

Where B = RT/b, and b is the Temkin constant in J/mol, T is the absolute temperature (K), R is the gas constant (8.314 J/mol/K), A is the Temkin isotherm constant (L/g).

9.6.2 Adsorption kinetics

Adsorption kinetics were carried out to determine the rate determining step and adsorption mechanism. The data obtained from the adsorption studies was fitted and analysed with the pseudo-first order (PFO) (Ho and McKay, 1998), pseudo-second order (PSO) (Ho et al., 2003) and the intraparticle diffusion (IPD) (Weber and Morris, 1963) models.

The PFO equation is given in equation 9.6:

$$ln\ (q_e - \ q_t) = \ln q_e - \ ln\ k_i t \quad (9.6)$$

Where q_t and q_e are the quantity of pharmaceuticals adsorbed (mg/g), at time t and equilibrium time, respectively. k_i (min^{-1}) is the adsorbate rate constant obtained from plotting $ln(q_e - q_t)$ *vs t*.

The PSO equation is given in equation 9.7:

$$\frac{t}{q_t} = \frac{1}{K_2\, q_e^2} + \frac{t}{q_e} \quad (9.7)$$

Where K_2 is the PSO rate constant (g/mg/min) and constants K_2 and q_e (mg/g) are obtained by plotting t/q_t *vs t.*

The IPD equation is given in equation 9.8:

$$q_t = K_i t^{0.5} + C \quad (9.8)$$

Where q_t is the amount adsorbed at time *t*, K_i is the rate constant of IPD [(mg/g) $min^{0.5}$], $t^{0.5}$ is the square root of time and *C* is the intercept depicting intra-boundary layer effect.

9.6.3 Thermodynamic studies

This provides detailed information about changes in energy as regards adsorption. The effect of temperature on the adsorption of CAF and PHE was investigated in the range of 293 – 323 K. The mean free energy of adsorption ($\Delta G°$) was calculated with the equation:

$$\Delta G = -RT ln\, K_0 \quad (9.9)$$

A plot of ln K *versus* 1/T had a linear profile, and the values of (ΔS) and (ΔH) were obtained from the intercept and slope, respectively, using the Van't Hoff equation:

$$\ln K_0 = -\frac{\Delta H}{RT} + \frac{\Delta S}{R} \quad (9.10)$$

9.6.4 Adsorbent regeneration

In order to regenerate the adsorbents used, it was washed with acidic ethanol at a pH of 2. It was then dried in a vacuum oven at a temperature of 60 °C and the adsorption capacity was calculated. The washing and recycling was carried out 2 times.

9.7 Results and Discussion

9.7.1 Characterisation of adsorbents

FTIR spectroscopy was used to determine the functional groups present on the surface of the adsorbents (Figure 9.2). On all adsorbents, a broad peak around 3230 cm^{-1} was prominent and was due to –OH vibrations. In GO, the peaks observed at 1729 cm^{-1} and 1634 cm^{-1} were due to C=O

stretching and the peak at 1364 cm^{-1} was due to the carbonyl group, respectively. A similar observation was recorded in studies by Marcano et al. (2010). ASM48, MCM-48, M48GO and M48G had peaks that typically define siliceous material. This implied that the synthesized MCM-48 was successfully encapsulated with GO and G. In M48GO, the peaks at 1622 cm^{-1} and 1415 cm^{-1} are due to -C=O stretching vibration. M48GO had a profile similar to GO and this shows that the encapsulation of GO on MCM-48 was successful. M48G had no carbonyl, C-O-C and epoxy group peaks. The band around 1048 cm^{-1} for M48G was due to the Si-O-Si/Si-O-C asymmetric vibration and Si-O-C was linked by covalent bonds. A similar observation was also recorded by Liu et al. (2013). This implied that the -COOH group in the GO was converted to a Si-O-C bond as was also observed by Meng et al. (2015). The peaks around 780 and 430 cm^{-1} in the M48G spectrum were assigned as Si-O-Si symmetric and bending vibrations, respectively. The peak around 1555 cm^{-1} seen in M48G is a -C=C- which is assigned to the amide group stretching vibration which means the vinyl group was successfully introduced into M48G (Meng et al., 2015). The M48G spectrum revealed that MCM-48 was successfully encapsulated with graphene. In ASM48, there were peaks present which were typical of ammonia at 1415 - 1533 cm^{-1} also observed by Mangrulkar et al. (2008). The peaks at 2925 and 2850 cm^{-1} were due to the bending of $–CH_2$ and $–CH_3$ of the CTAB, respectively which impacted the hydrophobicity of ASM48. Similar vibrations were observed by Mangrulkar et al. (2008) for the synthesis of as-synthesised MCM-41.

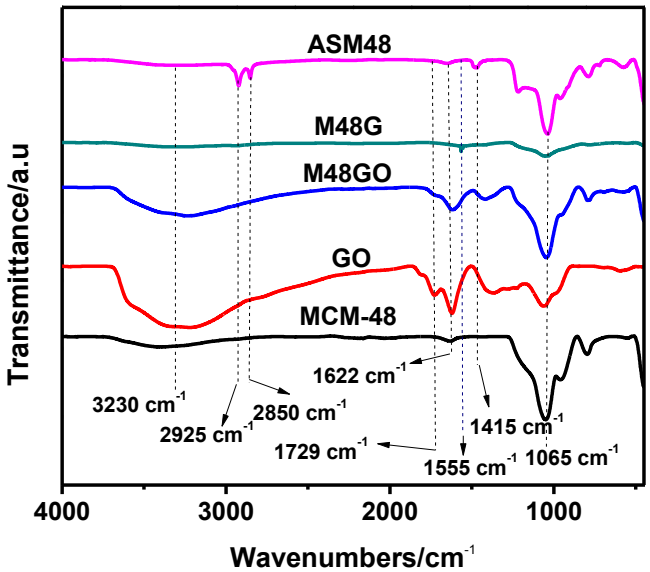

Figure 9.2 FTIR spectra of adsorbents

Thermogravimetric analysis was carried out on all the adsorbents in the temperature range between 25 °C to 900 °C (Figure 9.3). All the adsorbents exhibited weight loss below 120 °C and this was due to the expulsion of physisorbed water. MCM-48 and ASM48 had 3 stages of weight loss. At stage one below 120 °C, approximately 10% weight loss occurred. Stage had weight losses of 41.5% and 2% between 150 – 350 °C for ASM48 and MCM-48, respectively. This degradation is attributed to the decomposition of residual carbon as was also observed by Thuc and Thuc (2013). This explains the drastic weight loss in ASM48, as the long chain carbon template of the ionic surfactant CTAB remained as part of the structure. In the third stage between 350 – 650 °C, there was minimal weight loss before both adsorbents became thermally stable. The loss at this stage was attributed to condensation of adjacent silanol groups. GO is usually characterized by a sharp decline in weight between 150 °C – 250 °C. This decline is attributed to the removal of oxygen containing functional groups. A similar observation was made by Marcano et al. (2010). From the thermal profiles of M48GO and M48G, it was observed that the materials had more stability when compared to GO. This is indicative that the encapsulation of MCM-48 with GO and G was successful. The weight loss for M48GO and M48G occurred in 3 phases with the first phase occurring before 150 °C. The second phase occurred between 150 °C and 250 °C and the weight loss recorded was 6.5 and 14.5% for M48GO and M48G, respectively. This is due to decomposition of carbon. The final stage had a weight loss of 1 and 14% for M48G and M48GO, respectively, at a temperature above 250 °C. This loss can be attributed to the removal of oxygen functionality present on the surface of the adsorbents with M48GO having a higher oxygen content.

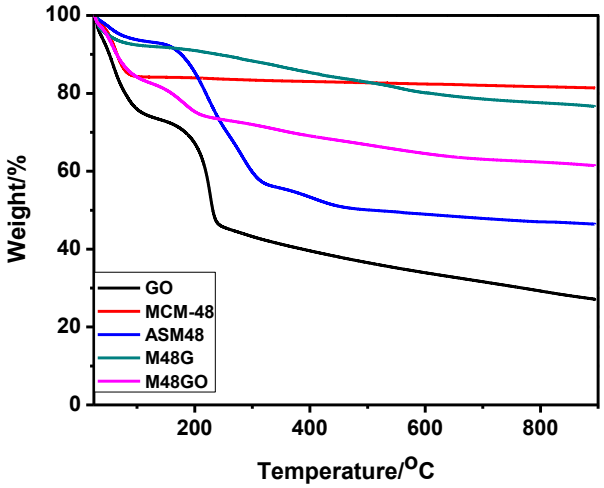

Figure 9.3 TGA profiles of adsorbents

The elemental compositions of the adsorbents are presented in Table 9.1. GO, ASM48, MCM-48, M48GO and M48G, had carbon contents of 37.6%, 35.1%, 0.9%, 16.2% and 22.4%, respectively. The high carbon composition and the highly hydrophobic nature of ASM48 is attributed to the CTAB present in the template of ASM48. The lower H/C ratio of M48G when compared to M48GO implies that it is more aromatic and also, the lower O/C ratio of M48G implies that it is less hydrophilic than M48GO as also observed by Wang et al. (2014b). The presence of carbon shown from the EA results proved that the encapsulation process was successful. ASM48 appeared to be very hydrophobic based on the H/C and O/C indices. This hydrophobicity stems from the presence of the long carbon chain from the highly hydrophobic surfactant CTAB in the microstructure.

Table 9.1 Elemental composition and atomic ratios, and surface areas (SA) of MCM-48, GO, ASM48, M48GO and M48G

Sample	MCM-48	ASM48	GO	M48GO	M48G
C/%	0.90	35.1	37.6	16.2	22.4
H/%	2.31	7.07	2.23	2.51	1.84
O/%	96.7	55.7	59.5	79.3	72.2
N/%	0.13	2.16	0.58	2.04	3.55
H/C	31.0	2.43	0.71	1.87	0.99
O/C	80.9	1.19	0.48	3.69	2.43
SA/m^2/g	1028	16	39	119	65.3
Pore volume/cm^3/g	0.67	0.05	0.017	0.20	0.17
Average pore size/nm	2.54	12	38.2	6.9	11.8

N_2 adsorption-desorption isotherms of the adsorbents are presented in Figure 9.4 which showed that MCM-48 had the highest amount of N_2 adsorbed at low or high pressure. The detailed textural properties are presented in Table 9.1. ASM48 had a very low surface area and pore volume when compared to MCM-48. This is because of the presence of the CTAB surfactant in the template of the ASM48 which caused pore channels/cavities to be blocked, hence, the low surface area. Synthesised GO had a surface area and pore volume of 39 m^2/g and 0.017 cm^3/g, respectively. The surface area and pore volume of M48GO and M48G were significantly reduced compared to MCM-48, and more so in M48G. This can be explained as a result of the coating of hy-

drophobic carbonaceous material on MCM-48. M48G had more carbon coating than M48GO, which accounted for its reduced surface area and pore volume. This confirms the successful encapsulation and correlates with the results obtained from the EA. All the adsorbents were of mesoporous nature because the pore diameter was less than 50 nm.

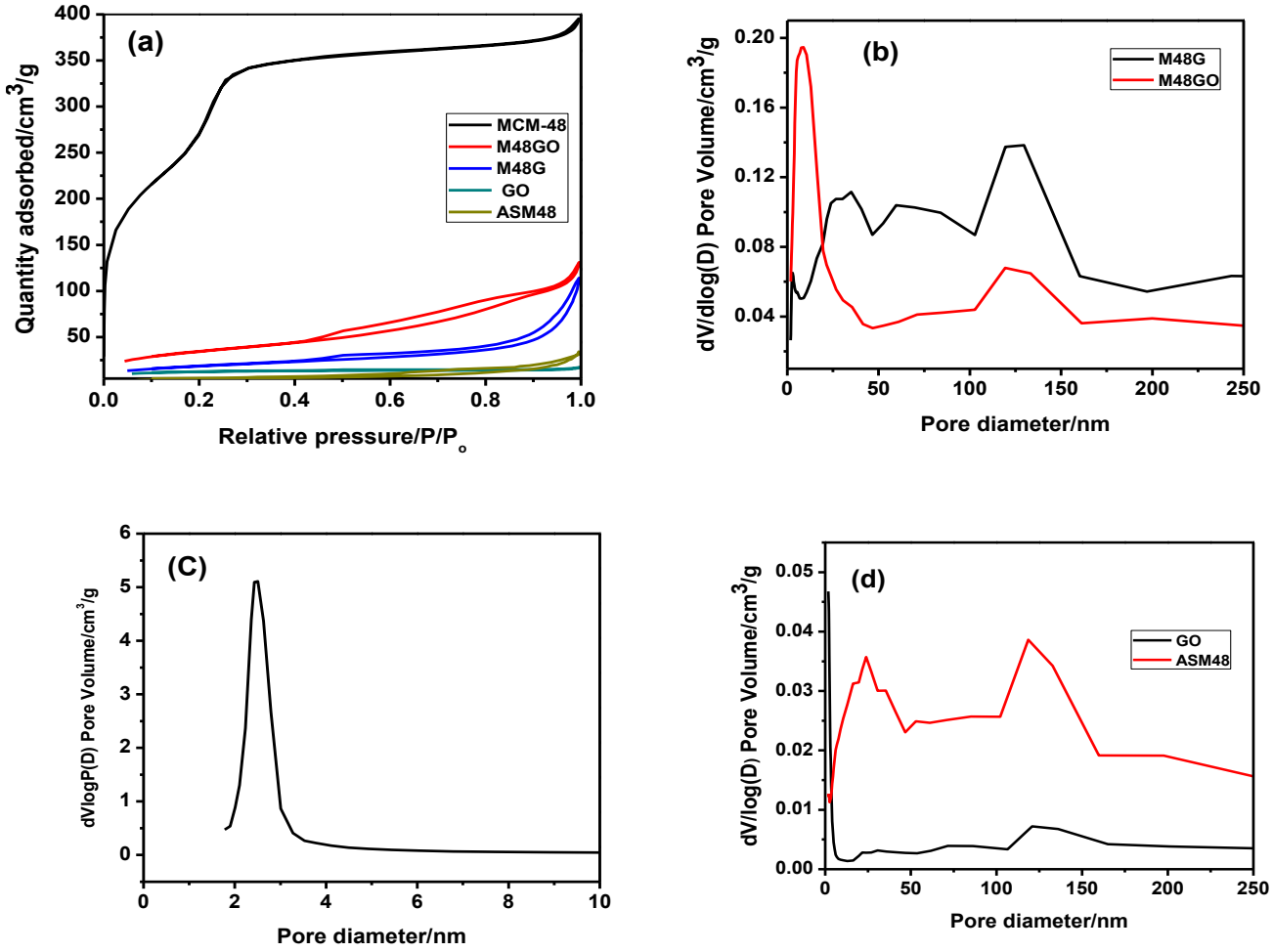

Figure 9.4 (a) N_2 adsorption-desorption of samples and pore size distribution of (b) M48GO and M48G (c) MCM-48 and (d) GO and ASM48

The XRD profiles of all the adsorbents are presented in Figure 9.5. The low angle XRD patterns of ASM48, MCM-48, M48GO and M48G are shown in Figure 9.5 (a). Clearly, it can be seen that the Braggs reflection which is characteristic of mesoporous MCM-48 material with unique cubic Ia3d symmetry is prominent in all the adsorbents. MCM-48 clearly exhibited 5 peaks in the 2 θ range from 2-6 with these reflections present at 211, 220, 321, 400 and 420 with 211 being

the principal peak. These reflections were also observed in similar studies by Peng et al. (2011) and Chen et al. (2013). It was observed that reaction conditions played an important role in the structure of MCM-48. The peaks became suppressed when GO was encapsulated and even more so with G. In Figure 9.5 (b) for the wide angle XRD scan, GO had a sharp peak at 2(θ) = 9.74. In contrast, MCM-48, ASM48, M48GO and M48G all had a broad peak at 2(θ) = 24 which is typical of siliceous materials. However, M48GO and M48G had marked inflections at 2(θ) = 26.21 and 25.4, respectively. These peaks are typical of oxygen containing functional groups by GO and chemical interaction by the reduced GO (graphene) on M48GO and M48G as also observed by Li et al. (2015) and Luo et al. (2013). The presence of this signifies a successful encapsulation process.

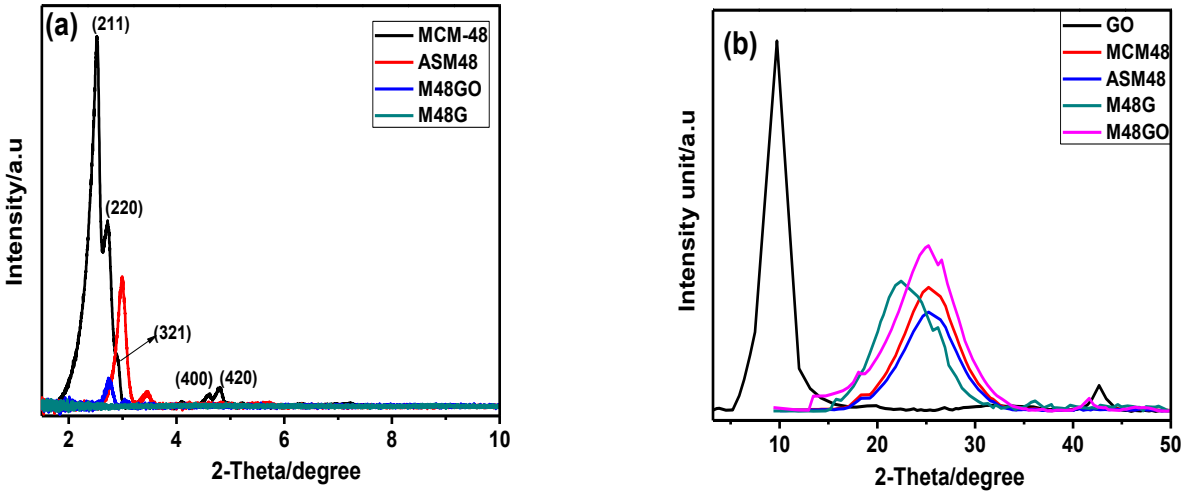

Figure 9.5 (a) Low angle scans of adsorbents and (b) Wide angle scans of adsorbents

To further confirm the Ia3d cubic mesostructure of MCM-48, HRTEM images were obtained which were in agreement with XRD analysis. Each nanosphere in the FESEM images appear as a single crystal like structure with ordered mesoporous channels extending through the material. The mesoporous nanospheres show discernible cavities associated with crystalline MCM-48. GO sheets appeared as large particleswith a transparent outlook. M48GO appeared to be coated with a transparent film of GO on its surface. M48G appeared as stacks of graphene sheets on MCM-48, thereby losing its transparency due to stacking by graphene sheets as a result of the in-situ reduction of graphene oxide to graphene. FESEM image analysis of MCM-48 and ASM48, revealed that it was comprised of uniform nano spherical particles with an average diameter of 200 nm with no agglomeration. Interparticle voids were also observed between these spheres.

M48GO had a thin layer of graphene oxide on its surface and also graphene oxide sheets filling the interparticle voids. In contrast, M48G, had stacks of graphene sheets layered over the surface of MCM-48, thereby losing its transparency and forming aggregates.

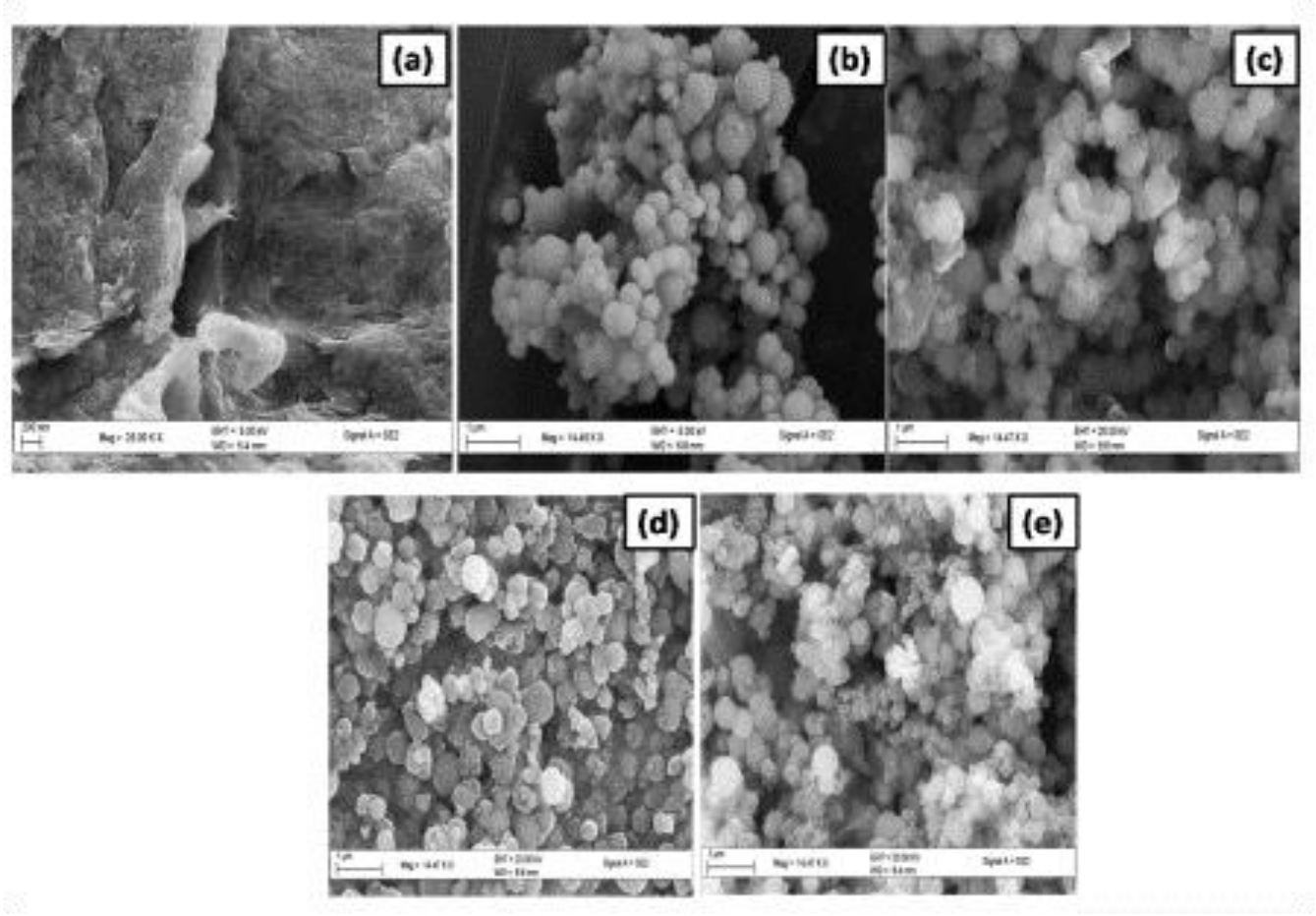

Figure 9.6 FESEM images (magnification = 25000) of (a) GO (b) ASM48 (c) MCM-48 (d) M48GO (e) M48G

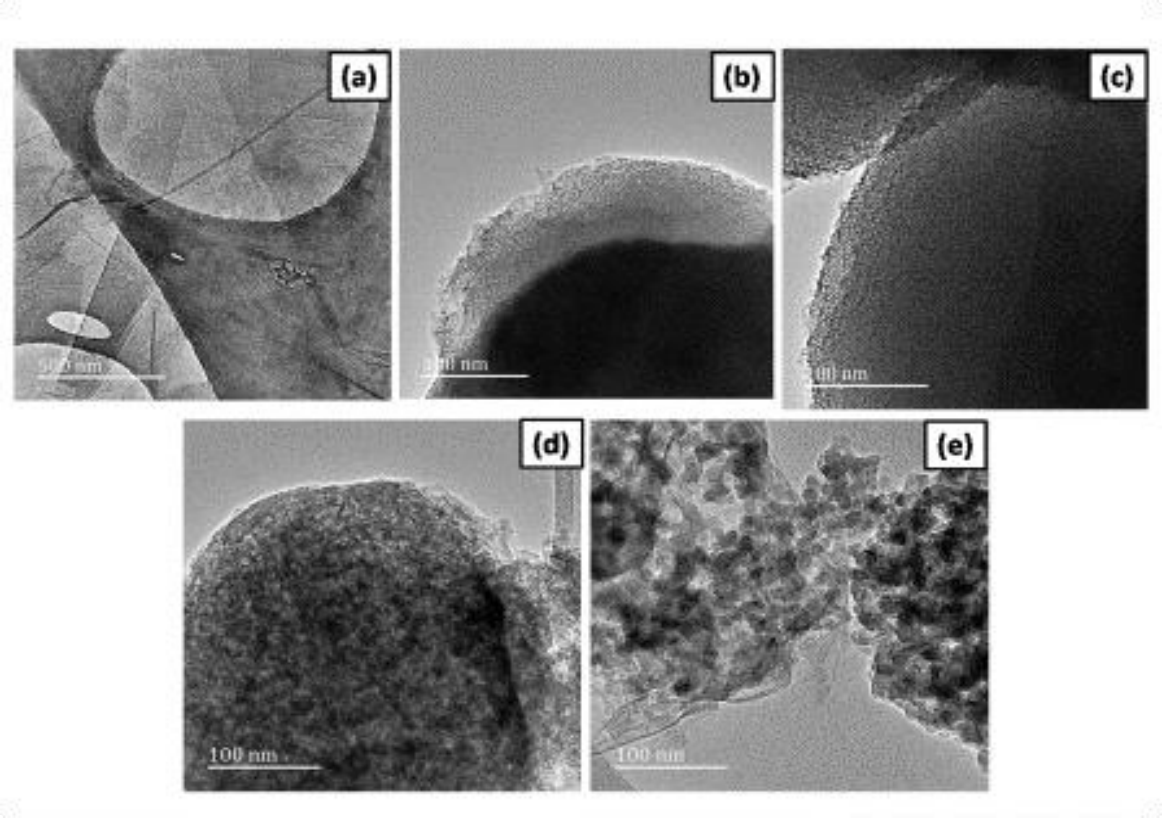

Figure 9.7 HRTEM images of (a) GO (b) ASM48 (c) MCM-48 (d) M48GO (e) M48G

9.8 Batch Adsorption Studies

Batch adsorption experiments were carried out to determine the efficiency of ASM48, M48GO and M48G on the removal of CAF and PHE from a simulated wastewater solution. The role of pH, ionic strength, adsorbent dose, contact time and temperature were investigated to determine the most suitable conditions for the remediation of CAF and PHE. Thermodynamics, kinetics and isotherm studies were also carried out.

9.8.1 Effect of pH

Ionisable pharmaceutical pollutants interact with adsorbent surfaces through electrostatic attraction or repulsion and this depends on their p*K*a values (Nam et al., 2015). Figure 9.8 shows the effect of pH on the adsorption of CAF and PHE on ASM48, M48GO and M48G. The pH of a solution is an important parameter that affects the adsorption process. The effect of pH was stud-

ied in the range of 2-10. A low pH of 2 (pH < p*K*a) (acidic condition), favoured the adsorption of caffeine and phenacetin on all the adsorbents as compared to basic conditions (pH > p*K*a). However, the effect of pH on adsorption was negligible because the pH range studied was below the pharmaceuticals' p*K*a values. Caffeine is a basic pharmaceutical with a p*K*a > 14 and phenacetin is a neutral pharmaceutical with a p*K*a > 14. At acidic pH, pH < p*K*a, CAF and PHE exist in solution as neutral molecules interacting with the adsorbent surface primarily through hydrophobic interactions which is a non-electrostatic interaction. As the pH of the solution is increased gradually with the addition of further amounts of NaOH, the adsorption percentage of PHE and CAF are seen to decrease. This is due to the solution becoming more basic, resulting in PHE and CAF becoming ionised (deprotonated) thus leading to an electric repulsion between the negative adsorbent surface and the adsorbate molecules. At a pH of 7 and above, the surface of both adsorbents and the pharmaceutical is negative, therefore very little interaction occurs. During the changes in pH, there is very little adsorption due to electrostatic interactions and hence, the main mechanism for adsorption is the hydrophobic effect.

In the adsorption of PHE on to the different adsorbents, it was observed that there was a higher sorption capacity with ASM48 than with M48GO. This could be attributed to the longer chain length of PHE and the conjugated double bonds present in PHE which preferred interactions with the hydrophobic ASM48. Therefore, the dominant mechanism of interaction between ASM48 and PHE molecules in solution may be attributed to the lateral hydrophobic chain and head group interaction as was also observed by Sen et al. (2012). Also, the longer carbon chain length of PHE encourages adsorption laterally along the surfactant molecules, and the conjugated structure causes a π-π interaction between the surfactant and PHE molecules in solution as was also observed by Zhao et al. (2005). In ASM48, the improved adsorption observed for both pharmaceuticals compared to MCM-48 was as a result of its increased hydrophobicity by retaining the long chain cationic SDA and reducing silanol density. This reduced silanol density has probably led to increased adsorption of anionic and hydrophobic pollutants (Bui et al., 2011).

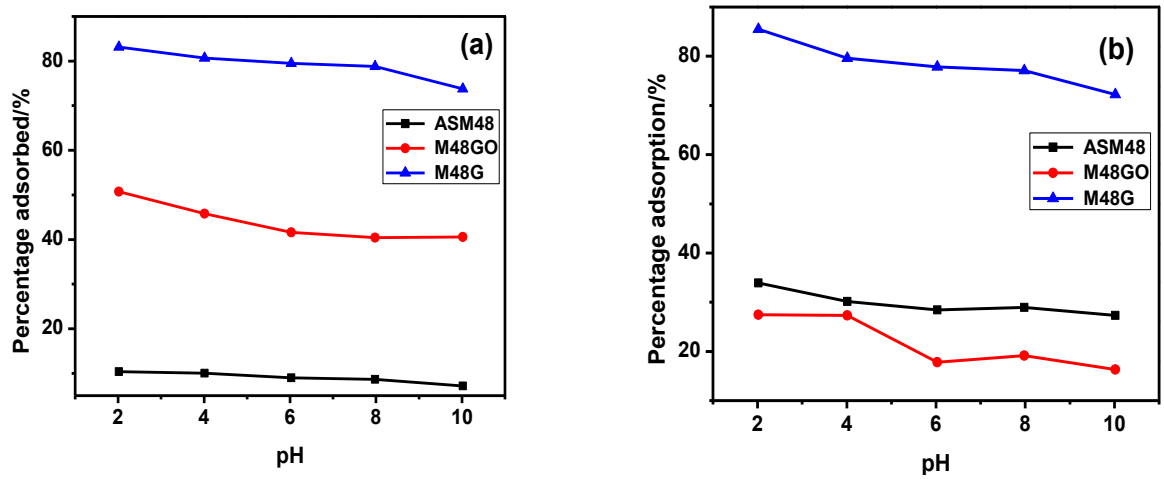

Figure 9.8 (a) Effect of pH on sorption of CAF and (b) Effect of pH on the sorption of PHE on the adsorbents (Conditions: 15 mL of 12.5 ppm Acet and Asp, equilibration time 180 mins, adsorbent dose 40 mg, temperature 25 °C.

9.8.2 Effect of adsorbent dose

The quantity of adsorbent added to the adsorbate is very important in the determination of the adsorption capacity of the adsorbent for a given concentration of the adsorbate. The effect of adsorbent dose was studied using 10 – 60 mg of the adsorbents (Figure 9.9). In the adsorption of CAF, there was a linear increase from 10 to 40 mg with percentage adsorptions of 8.38, 37.3 and 79.4 % for ASM48, M48GO and M48G, respectively. Increased adsorbent dosage after 40 mg resulted in negligible increases in percentage adsorption. This initial increased adsorption is due to an increase in the available sites for adsorption with an increase in mass of adsorbent. In the adsorption of PHE, a similar trend to that of CAF was observed. The optimal dose occurred at 40 mg with percentage adsorption of 28.9, 15.7 and 77.2 %, respectively for ASM48, M48GO and M48G.

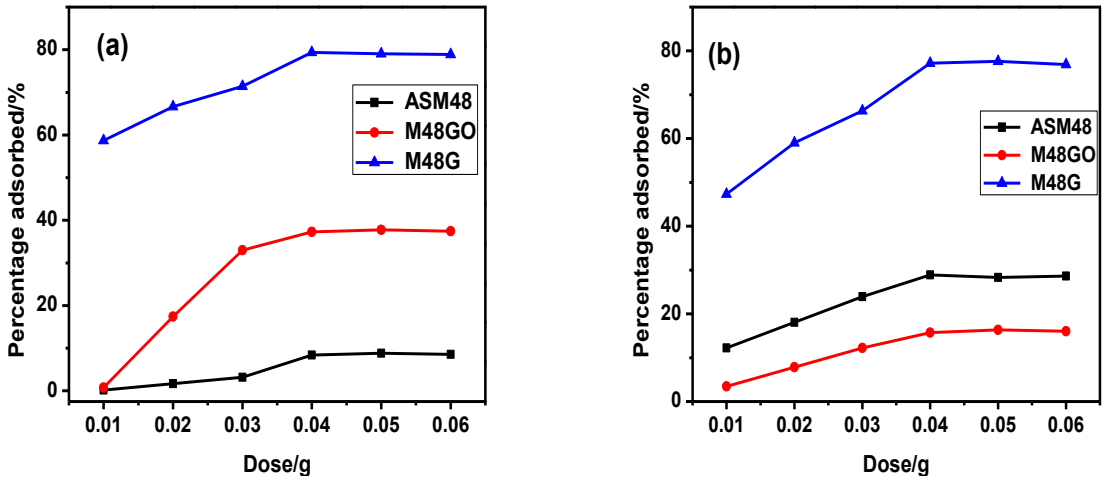

Figure 9.9 (a) Effect of dose on sorption of CAF and (b) Effect of dose on the sorption of PHE on the adsorbents (Conditions: 15 mL of 12.5 ppm Acet and Asp, equilibration time 180 mins, pH 4 temperature 25 °C.

9.8.3 Effect of temperature

The effect of temperature helps in understanding the physical or chemical nature of the adsorption process. The effect of temperature was carried out over a temperature range of 298 – 318 K (Figure 9.10). The results showed that for all adsorbents, an increase in temperature caused a decrease in adsorption capacity. This may be attributed to a decrease in surface activity between the adsorbate and adsorbents implying that the process was exothermic. An increase in temperature caused a reduction in the attractive forces between the adsorbents and adsorbate, thereby causing the adsorbate molecules to escape from the solid phase (adsorbent) into the liquid phase (pharmaceutical solution) (Sen et al., 2012) which resulted in a decrease in adsorption. The changes in entropy ($\Delta S°$), enthalpy ($\Delta H°$) and Gibbs free energy ($\Delta G°$) were determined using the Van't Hoff's equation (Table 9.2). A physisorption process has free energy in the range of -20 – 0 kJ/mol and is -80 – 400 kJ/mol for chemisorptions. The negative $\Delta G°$ values obtained indicated that adsorption was a spontaneous physical process. The $\Delta S°$ values obtained were negative and this indicated a decrease in randomness at the solid/liquid interface as well as indicated that the adsorbents did not undergo any significant changes (Vimonses et al., 2009). The increase in negative $\Delta G°$ values with an increase in temperature suggested that higher temperatures did not fa-

vour the adsorption process in this study. The negative ΔH° values obtained implied that adsorption was exothermic (Arias and Sen, 2009).

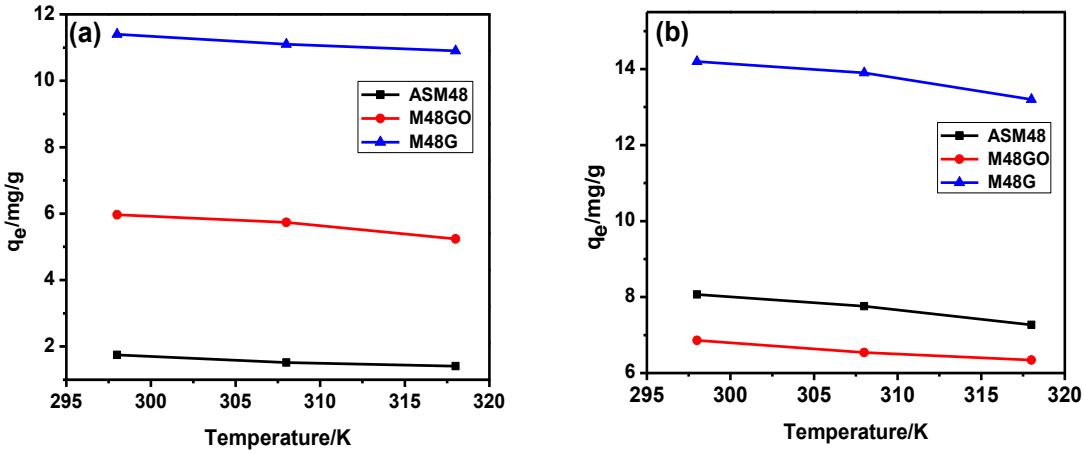

Figure 9.10 (a) Effect of temperature on the adsorption of CAF and (b) Effect of temperature on the adsorption of PHE (Conditions: 200 mL of 25 ppm, equilibration time 180 mins, pH 4)

Table 9.2 Thermodynamic parameters for the adsorption of PHE and CAF onto adsorbents

Adsorbent	Temperature/ K	ΔG°/kJ/mol	ΔH°/kJ/mol	ΔS°/kJ/mol
		Phenacetin		
ASM48	293	-0.302	-0.4105	-1.012
	303	-0.312		
	313	-0.322		
M48GO	293	-0.269	-0.3401	-0.9021
	303	-0.278		
	313	-0.287		
M48G	293	-0.464	-0.964	-0.5531
	303	-0.479		
	313	-0.495		
		Caffeine		
ASM48	293	-0.959	-1.052	-6.794
	303	-1.025		
	313	-3.195		
M48GO	293	-0.266	-0.7342	-4.024
	303	-0.239		
	313	-0.244		
M48G	293	-0.387	-0.643	-1.297
	303	-0.400		
	313	-0.413		

9.8.4 Effect of contact time and adsorbate concentration on kinetics

The effect of contact time on the adsorption of the pharmaceuticals was investigated between 2 – 1440 minutes (Figure 9.11). Adsorption of the pharmaceuticals rapidly increased in the first 30 minutes and thereafter reached equilibrium. The initial rapid removal rate of the pharmaceuticals is due to the increasing number of available sites on the adsorbent surface but thereafter the adsorption rate became slower due to agglomeration of CAF and PHE on the active sites of the ad-

sorbents. This rapid equilibrium is confirmation that this adsorption is probably a physical process (Özdemir et al., 2007, Sen et al., 2012). The kinetic experiments suggest that the adsorption was a 2 step process, firstly, a rapid phase and secondly, a slow intraparticle diffusion. The rapid kinetics is of great importance because it helps in designing small reactor volumes with higher economic efficiency (Sen et al., 2012).

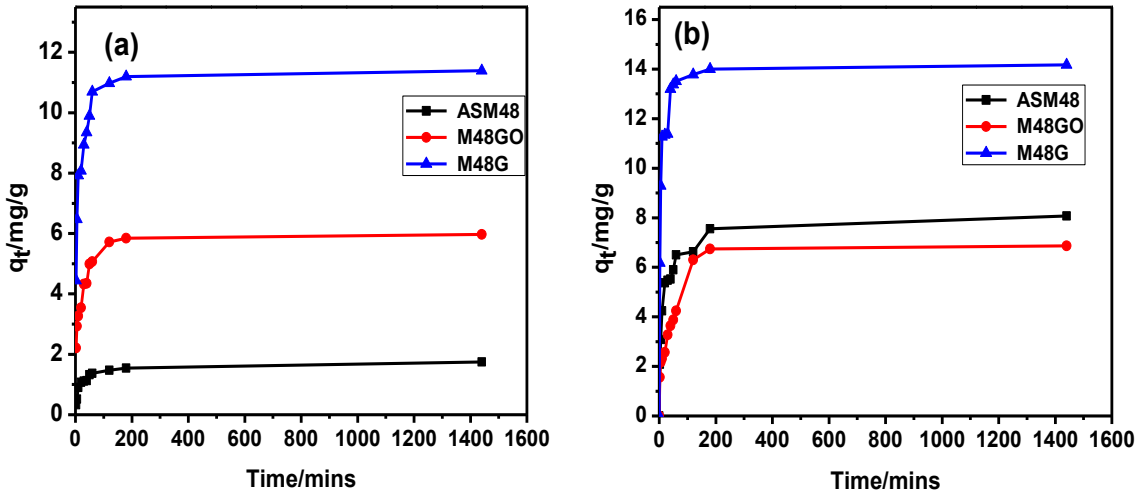

Figure 9.11 Effect of contact time on sorption of (a) CAF and (b) PHE on the adsorbents (Conditions: 200 mL of 25 ppm CAF and PHE, equilibration time 1440 mins, adsorbent dose 150 mg, temperature 25 °C, pH 4).

9.8.5 Adsorption kinetics

Three models were applied to determine the physical or chemical nature of the adsorbents, namely: PFO (equation 9.6), PSO (equation 9.7) and IPD (equation 9.8) models. The adsorption kinetic data were fitted into these three models (Table 9.3). The PSO model was the best fit for all adsorbents because of the high regression correlation (R^2) greater than 0.9999 and there was no significant difference in the value of maximum equilibrium adsorption obtained to that obtained from the experimental q_e value. This indicated that the PSO model was well suited for the description of the adsorption kinetics. The PFO model was not the best fit based on the low regression correlation values obtained and also, there was a significant difference between the low maximum equilibrium adsorption and the experimental q_e values obtained. Therefore, the PSO model best described the adsorption behaviour of CAF and PHE on ASM48, M48GO and

M48G. For intraparticle diffusion, the adsorption process occurred in 2 steps (i) rapid equilibrium is reached as a result of the external surface of the adsorbent adsorbing the adsorbate (ii) slow intraparticle internal diffusion to diffusion to the internal surface of the adsorbent from the bulk solution. The solid adsorbent and liquid adsorbent adsorption process may either be as a result of mass transfer or intraparticle diffusion or a combination of both sorption processes. The pharmaceutical adsorption mechanism from the solution comprises the following steps (Sen et al., 2012, Ma et al., 2012):

a. The movement of CAF and PHE molecules from the bulk solution to the surface of the adsorbents
b. The diffusion of CAF and PHE *via* a boundary layer to the surface of the adsorbents
c. The adsorption of CAF and PHE at the surface active site on the adsorbents
d. Slow intraparticle diffusion of CAF and PHE after the initial rapid adsorption to the internal surface of the adsorbents

The slowest step is usually the controlling step for the rate of sorption and this step may be a combination of external mechanisms and intraparticle diffusion. An IPD plot was obtained by plotting q_t (mg/g) which is weight of sorbent *vs*. square root of time ($t^{0.5}$). The plots appeared as two separate linear regions (external mass transfer of CAF and PHE to the surface of the adsorbents and intraparticle diffusion to the pores of the adsorbents) and this validated that the adsorption process was as a result of several processes. None of the plots had origins of zero and this could be attributed to a variation in the rate of mass transfer in the preliminary and the last adsorption stages. This is indicative that IPD was not the only rate controlling step but it is the rate-limiting step (Sen et al., 2012).

Table 9.3 Kinetic parameters for the adsorption of CAF and PHE from aqueous solution

Model	Parameter	ASM48	M48GO	M48G
		Caffeine		
Pseudo-first order	k_1/min^{-1}	0.0101	0.0194	0.0193
	q_e, eq/mg/g	0.20	1.17	1.51
	R^2	0.8379	0.9791	0.9224
$q_{e,\ exp}$	mg/g	1.75	5.97	11.4
Pseudo-second order	k_2/min^{-1}	9.3512	1.3616	0.5080
	q_e /mg/g	1.76	6.00	11.4
	R^2	0.9998	0.9999	0.9999
Intraparticle diffusion	*K*i/mg/g min$^{-0.5}$	0.0155	0.0165	0.1506
	C/mg/g	1.35	4.54	6.49
	R^2	0.5484	0.3877	0.5288
		Phenacetin		
Pseudo-first order	k_1/min^{-1}	0.0117	0.021	0.508
	q_e, eq/mg/g	1.46	1.35	1.89
	R^2	0.8983	0.9718	0.9724
$q_{e,\ exp}$	mg/g	8.07	6.86	14.2
Pseudo-second order	k_2/min^{-1}	1.74	3.49	0.25
	q_e /mg/g	8.14	6.98	14.2
	R^2	0.9998	0.9990	0.9999
Intraparticle diffusion	*K*i/mg/g min$^{-0.5}$	0.128	0.144	0.134
	C/mg/g	4.32	2.65	10.7
	R^2	0.5309	0.6018	0.3102

9.8.6 Adsorption isotherms

The isotherm models were calculated from the experimental data obtained from the non-linear regression analysis of Freundlich and Langmuir equation isotherm models (Table 9.4). From the correlation coefficient (R^2) obtained, values > 0.99, showed that the Freundlich isotherm was the best fit for the adsorption data when compared to the Langmuir isotherm. The Freundlich con-

stant K_F (adsorption capacity) and N were also calculated. The K_F value for M48G appeared higher in the adsorption of both CAF and PHE which implied that the adsorption was highest for M48G. The values of N obtained, indicated that the adsorption was favourable (Shao et al., 2014). The highest q_m values obtained in the adsorption of CAF and PHE was with M48G which correlated with the K_F value from the Freudlich isotherm

Table 9.4 Isotherm parameters for the adsorption of CAF and PHE onto the adsorbents

Isotherm	Parameters	ASM48	M48GO	M48G
		Caffeine		
Langmuir	q_m/ mg/g	14.9	48.8	153.8
	b/ L/mg	13.9	3.14	0.0065
	R^2	0.7156	0.9901	0.9839
Freundlich	K_F	3.26	10.6	25.4
	N	1.03	1.31	1.37
	R^2	0.999	0.998	0.9985
Temkin	B	708	292	131
	b/ J/mol	3.50	8.50	18.9
	A/ L/g	9.73	20.5	43.1
	R^2	0.9575	0.9829	0.9778
		Phenacetin		
Langmuir	q_m/ mg/g	122	75.2	212.7
	b/ L/mg	2.17	2.51	0.91
	R^2	0.9524	0.8967	0.9755
Freundlich	K_F	10.2	5.24	31.7
	N	1.08	1.213	1.385
	R^2	0.9999	0.9927	0.9984
Temkin	B	164	232	104
	b/ J/mol	15.1	10.7	24.2
	A/ L/g	36.9	25.2	51.0
	R^2	0.9745	0.9753	0.9777

9.8.7 Desorption studies

Desorption studies were carried out using acidic ethanol (pH 2). High desorption efficiencies of 83 and 76% for M48GO, 45 and 42% for M48G, and 45 and 30% for ASM48, were obtained for PHE and CAF, respectively. Similar results were obtained in a study by Bui et al. (2013).

9.9 Conclusion

This study showed the effectiveness of as-synthesised MCM-48 (ASM48), and graphene oxide (M48GO) and graphene (M48G) encapsulated MCM-48 as suitable adsorbents for the removal of pharmaceuticals (CAF and PHE) from aqueous solution. The amount of CAF and PHE adsorbed by the adsorbent was found to increase with an increase in initial concentration of the adsorbate, amount of adsorbent and contact time. Adsorption of the pharmaceuticals from aqueous solution was pH dependent and the maximum adsorption capacity of CAF was 153.8 and PHE was 212.7 mg/g for M48G at a temperature of 25 °C. The adsorption kinetics revealed that the adsorption process was mostly a 2 step process because of the rapid equilibrium and the slow almost stagnant intraparticle diffusion. The experimental data best fitted the pseudo second order model and the Langmuir isotherm model best described the adsorption. Thermodynamic studies revealed the adsorption process as spontaneous and exothermic in nature.

9.10 Acknowledgements

We gratefully acknowledge the School of Chemistry and Physics, University of KwaZulu-Natal, South Africa, for providing the laboratory facilities and instrumentation used in this research and also to the AAU small grant for financial assistance.

References

Al-Khateeb, L. A., Almotiry, S. & Salam, M. A. 2014. Adsorption of pharmaceutical pollutants onto graphene nanoplatelets. *Chemical Engineering Journal,* 248**,** 191-199.

Arias, F. & Sen, T. K. 2009. Removal of zinc metal ion (Zn 2+) from its aqueous solution by kaolin clay mineral: a kinetic and equilibrium study. *Colloids and Surfaces A: Physicochemical and Engineering Aspects,* 348**,** 100-108.

Beck, J., Vartuli, J., Roth, W., Leonowicz, M., Kresge, C., Schmitt, K., Chu, C., Olson, D. H. & Sheppard, E. 1992. A new family of mesoporous molecular sieves prepared with liquid crystal templates. *Journal of the American Chemical Society,* 114**,** 10834-10843.

Bui, T. X. & Choi, H. 2009. Adsorptive removal of selected pharmaceuticals by mesoporous silica SBA-15. *Journal of Hazardous Materials,* 168**,** 602-608.

Bui, T. X., Kang, S.-Y., Lee, S.-H. & Choi, H. 2011. Organically functionalized mesoporous SBA-15 as sorbents for removal of selected pharmaceuticals from water. *Journal of Hazardous Materials,* 193**,** 156-163.

Bui, T. X., Pham, V. H., Le, S. T. & Choi, H. 2013. Adsorption of pharmaceuticals onto trimethylsilylated mesoporous SBA-15. *Journal of Hazardous Materials,* 254**,** 345-353.

Castiglioni, S., Bagnati, R., Fanelli, R., Pomati, F., Calamari, D. & Zuccato, E. 2006. Removal of pharmaceuticals in sewage treatment plants in Italy. *Environmental Science & Technology,* 40**,** 357-363.

Chen, P.-K., Lai, N.-C., Ho, C.-H., Hu, Y.-W., Lee, J.-F. & Yang, C.-M. 2013. New synthesis of MCM-48 nanospheres and facile replication to mesoporous platinum nanospheres as highly active electrocatalysts for the oxygen reduction reaction. *Chemistry of Materials,* 25**,** 4269-4277.

Dubach, U. C., Rosner, B. & Stürmer, T. 1991. An epidemiologic study of abuse of analgesic drugs: effects of phenacetin and salicylate on mortality and cardiovascular morbidity (1968 to 1987). *New England Journal of Medicine,* 324**,** 155-160.

Freundlich, H. 1906. Over the adsorption in solution. *Journal of Physical Chemistry,* 57**,** 385-470.

Gibson, L. 2014. Mesosilica materials and organic pollutant adsorption: part B removal from aqueous solution. *Chemical Society Reviews,* 43**,** 5173-5182.

Ho, K. Y., Mckay, G. & Yeung, K. L. 2003. Selective adsorbents from ordered mesoporous silica. *Langmuir,* 19**,** 3019-3024.

Ho, Y.-S. & Mckay, G. 1998. Sorption of dye from aqueous solution by peat. *Chemical Engineering Journal,* 70**,** 115-124.

Jones, O. A., Lester, J. N. & Voulvoulis, N. 2005. Pharmaceuticals: a threat to drinking water? *TRENDS in Biotechnology,* 23**,** 163-167.

Khetan, S. K. & Collins, T. J. 2007. Human pharmaceuticals in the aquatic environment: a challenge to green chemistry. *Chemical Reviews,* 107**,** 2319-2364.

Kushwaha, A. K., Gupta, N. & Chattopadhyaya, M. 2014. Enhanced adsorption of methylene blue on modified silica gel: equilibrium, kinetic, and thermodynamic studies. *Desalination and Water Treatment,* 52**,** 4527-4537.

Langmuir, I. 1918. The adsorption of gases on plane surfaces of glass, mica and platinum. *Journal of the American Chemical Society,* 40**,** 1361-1403.

Larsson, D. J., De Pedro, C. & Paxeus, N. 2007. Effluent from drug manufactures contains extremely high levels of pharmaceuticals. *Journal of Hazardous Materials,* 148**,** 751-755.

Li, X., Wang, Z., Li, Q., Ma, J. & Zhu, M. 2015. Preparation, characterization, and application of mesoporous silica-grafted graphene oxide for highly selective lead adsorption. *Chemical Engineering Journal,* 273**,** 630-637.

Liu, X., Zhang, H., Ma, Y., Wu, X., Meng, L., Guo, Y., Yu, G. & Liu, Y. 2013. Graphene-coated silica as a highly efficient sorbent for residual organophosphorus pesticides in water. *Journal of Materials Chemistry A,* 1**,** 1875-1884.

Luo, Y.-B., Zhu, G.-T., Li, X.-S., Yuan, B.-F. & Feng, Y.-Q. 2013. Facile fabrication of reduced graphene oxide-encapsulated silica: A sorbent for solid-phase extraction. *Journal of Chromatography A,* 1299**,** 10-17.

Ma, J., Yu, F., Zhou, L., Jin, L., Yang, M., Luan, J., Tang, Y., Fan, H., Yuan, Z. & Chen, J. 2012. Enhanced adsorptive removal of methyl orange and methylene blue from aqueous solution by alkali-activated multiwalled carbon nanotubes. *ACS Applied Materials & Interfaces,* 4**,** 5749-5760.

Mangrulkar, P. A., Kamble, S. P., Meshram, J. & Rayalu, S. S. 2008. Adsorption of phenol and o-chlorophenol by mesoporous MCM-41. *Journal of Hazardous Materials,* 160**,** 414-421.

Marcano, D. C., Kosynkin, D. V., Berlin, J. M., Sinitskii, A., Sun, Z., Slesarev, A., Alemany, L. B., Lu, W. & Tour, J. M. 2010. Improved synthesis of graphene oxide. *ACS Nano,* 4**,** 4806-4814.

Martínez, J. L. 2008. Antibiotics and antibiotic resistance genes in natural environments. *Science,* 321**,** 365-367.

Martucci, A., Pasti, L., Marchetti, N., Cavazzini, A., Dondi, F. & Alberti, A. 2012. Adsorption of pharmaceuticals from aqueous solutions on synthetic zeolites. *Microporous and Mesoporous Materials,* 148**,** 174-183.

Meng, H., Li, Z., Ma, F., Wang, X., Zhou, W. & Zhang, L. 2015. Synthesis and characterization of surface ion-imprinted polymer based on SiO 2-coated graphene oxide for selective adsorption of uranium (vi). *RSC Advances,* 5**,** 67662-67668.

Nam, S.-W., Jung, C., Li, H., Yu, M., Flora, J. R., Boateng, L. K., Her, N., Zoh, K.-D. & Yoon, Y. 2015. Adsorption characteristics of diclofenac and sulfamethoxazole to graphene oxide in aqueous solution. *Chemosphere,* 136**,** 20-26.

Özdemir, O., Çınar, M., Sabah, E., Arslan, F. & Çelik, M. S. 2007. Adsorption of anionic surfactants onto sepiolite. *Journal of Hazardous Materials,* 147**,** 625-632.

Peng, R., Zhao, D., Dimitrijevic, N. M., Rajh, T. & Koodali, R. T. 2011. Room temperature synthesis of Ti–MCM-48 and Ti–MCM-41 mesoporous materials and their performance on photocatalytic splitting of water. *The Journal of Physical Chemistry C,* 116**,** 1605-1613.

Sen, T. K., Thi, M. T., Afroze, S., Phan, C. & Ang, M. 2012. Removal of anionic surfactant sodium dodecyl sulphate from aqueous solution by adsorption onto pine cone biomass of Pinus Radiate: equilibrium, thermodynamic, kinetics, mechanism and process design. *Desalination and Water Treatment,* 45**,** 263-275.

Shao, Y., Wang, X., Kang, Y., Shu, Y., Sun, Q. & Li, L. 2014. Application of Mn/MCM-41 as an adsorbent to remove methyl blue from aqueous solution. *Journal of Colloid and Interface Science,* 429**,** 25-33.

Snyder, S. A., Adham, S., Redding, A. M., Cannon, F. S., Decarolis, J., Oppenheimer, J., Wert, E. C. & Yoon, Y. 2007. Role of membranes and activated carbon in the removal of endocrine disruptors and pharmaceuticals. *Desalination,* 202**,** 156-181.

Thuc, C. N. H. & Thuc, H. H. 2013. Synthesis of silica nanoparticles from Vietnamese rice husk by sol–gel method. *Nanoscale Research Letters,* 8**,** 1-10.

Vimonses, V., Lei, S., Jin, B., Chow, C. W. & Saint, C. 2009. Kinetic study and equilibrium isotherm analysis of Congo Red adsorption by clay materials. *Chemical Engineering Journal,* 148**,** 354-364.

Wang, J., Chen, Z. & Chen, B. 2014. Adsorption of polycyclic aromatic hydrocarbons by graphene and graphene oxide nanosheets. *Environmental Science & Technology,* 48**,** 4817-4825.

Weber, W. J. & Morris, J. C. 1963. Kinetics of adsorption on carbon from solution. *Journal of the Sanitary Engineering Division,* 89**,** 31-60.

Yang, K., Chen, B. & Zhu, L. 2015. Graphene-coated materials using silica particles as a framework for highly efficient removal of aromatic pollutants in water. *Scientific Reports,* 5**,** 11641-11653.

Zhao, Y., Ding, M. & Chen, D. 2005. Adsorption properties of mesoporous silicas for organic pollutants in water. *Analytica chimica acta,* 542**,** 193-198.

10.0 CHAPTER 10: CONCLUSION AND RECOMMENDATIONS

Mesoporous materials are materials with pore diameters between 2 - 50 nm, according to IUPAC classification. Mesoporous silica are characterised by high surface area and very large pores. They have an extensive network of –OH groups which can be functionalised (manipulated) for a host of applications. Siliceous materials can be modified with different functional groups and applied as adsorbents in adsorption of a wide variety of contaminants from the environment.

This study synthesised three silica/ordered mesoporous silica from TEOS and agrowaste and investigated its application as adsorbents of two dyes and five phamaceuticals in aqueous media. Synthesised SNT and SNP were applied in batch adsorption studies of MB and MR. The effects of contact time, pH, adsorbent dose, initial concentration of adsorbate and temperature were determined in the adsorption process. Also, the adsorption parameters were investigated in the adsorption of MB on to MCM-41 and citric acid grafted MCM-41, sulfamethoxazole on to graphene oxide/graphene encapsulated SNT, acetaminophen and aspirin on to ASM41, MCM-41, graphene oxide and graphene coated MCM-41 and caffeine and phenacetin on to AS-M48, MCM-48 coated with graphene oxide and graphene.

From the results obtained, the following were concluded:

1. The synthesis of SNT and SNP was carried out and their structures were confirmed by FTIR, SEM and TEM analysis. SNP and SNT were applied in the adsorption of methylene blue (MB) and methylene red (MR) dyes from aqueous solution. Optimum adsorption of MR and MB onto SNT and SNP occurred at optimum conditions of pH 10, and a dose of 5 mg for MR and 20 mg for MB at room temperature. SNP performed marginally better as compared to SNT, in the adsorption of MR and MB from aqueous solutions. This may be because of a slightly better surface area. The Langmuir adsorption isotherm provided the best fit to the experimental data for both dyes onto both adsorbents. The adsorption kinetics best fitted the pseudo-second-order kinetics. The study proved that mesoporous silica from elephant grass is a good adsorbent for the removal of MR and MB from aqueous solution.

2. The synthesis of MCM-41 from TEOS and its grafting with citric acid was carried out and their structures were confirmed using FTIR, SS-NMR, EA, textural analysis, SEM and TEM techniques. A decrease in surface area of citric acid grafted MCM-41, an increase in percentage carbon (from EA) and the introduction of carboxylic functional groups was observed in citric acid grafted MCM-41. The new properties of the modified material showed that it can be used for the adsorption of cationic dye from wastewater. The modified adsorbent (0.6SCA-MCM-41) had an improved maximum adsorption capacity of MB dye (204.08 mg/g) as compared to unmodified MCM-41 (89.3 mg/g) because of the presence of the carboxyl groups. The equilibrium adsorption data obtained fitted into the Temkin, Freundlich and Langmuir isotherms suggesting the material is a favourable adsorbent. The adsorption process involved intraparticle diffusions and was exothermic and spontaneous. An increase in temperature decreased the adsorption of MB. The optimum pH for adsorption was 10 and lower temperatures resulted in higher adsorption capacities.
3. MCM-41 was synthesized using agrowaste as a precursor and citric acid was grafted on it. Its structure was determined from FTIR, low and wide angle XRD analysis, SEM and TEM image analysis and textural analysis. The presence of the carboxylic acid functional group proved that the grafting with citric acid had indeed occurred. The modified adsorbent (SCA-MCM-41) had an improved adsorptive capacity of MB dye (28.8 mg/g) as compared to unmodified MCM-41 (20.8 mg/g) because of the presence of the carbonyl groups from the CA. The equilibrium adsorption data obtained fitted the Freundlich isotherms. The data obtained fitted the pseudo-second order model with a high correlation value ($R^2 > 0.99$). The adsorption process involved intraparticle diffusions and was exothermic and spontaneous. An increase in temperature decreased the adsorption of MB. The optimum pH for adsorption was 8 and optimum temperature was 25 ^{o}C.
4. The encapsulation of previously synthesised SNT with GO and G was confirmed with SEM and TEM analysis as well as a variety of other techniques. The encapsulation of SNT with GO and G resulted in increased hydrophobicity and led to increased adsorption of sulfamethoxazole. Batch adsorption studies were carried out to determine the adsorption behaviour of SMZ on SNTGO and SNTG. The adsorbents were effective in the removal of SMZ from aqueous solutions with a q_m of 125 and 248 mg/g obtained for SNTGO and SNTG, respectively. An ionic strength of 20 mM NaCl, temperature of 25 ^{o}C and pH 2 provided the optimum conditions for adsorption. The

adsorption kinetics followed the pseudo-second order model and the experimental data best fitted the Freundlich isotherm model. The adsorbents were effective in the treatment of real environmental samples showing that it can be used in the treatment of industrial effluents polluted with SMZ. The adsorbents were regenerated and were still efficient after 2 cycles, thus showing that they can be recycled.

5. Previously synthesized MCM-41 from TEOS was encapsulated with graphene oxide/graphene and as-synthesised MCM-41 was synthesised. The structures of the synthesised adsorbents were confirmed by a number of analytical methods. The surface properties showed an increase in its hydrophobicity and the adsorption studies showed improved adsorption of acetaminophen and aspirin. Batch adsorption studies were carried out to study the adsorption behaviour of acetaminophen and aspirin on MCM-41, ASM41, MCM-41-GO and MCM-41-G. The least adsorption for acetaminophen and aspirin was recorded with MCM-41 because of its highly hydrophilic nature. All the adsorbents were effective in the removal of acetaminophen and aspirin from aqueous solution but ASM41 was the best adsorbent for aspirin at a pH of 2, adsorbent dose of 40 mg and a temperature of 25 °C. MCM-41-G was the best adsorbent for acetaminophen at pH 2, adsorbent dose of 40 mg and a temperature of 25 °C. The adsorption kinetics fitted the pseudo-second order model and the best fit isotherm was the Freundlich model. The adsorbents were also effective in the treatment of real environmental samples. The adsorbents showed they were still efficient after 2 cycles of regeneration.
6. As-synthesised MCM-48, and MCM-48 encapsulated with graphene oxide/graphene were synthesised and their strucutres confirmed with a host of characterization techniques. Low angle XRD and HRTEM revealed a cubic mesophase, FTIR analysis showed increased oxygen and carbon functionalities, EA revealed that there was increased carbon content in the modified materials. These properties makes these adsorbents excellent for the adsorption of caffeine and phenacetin. The amount of caffeine and phenacetin adsorbed by the adsorbent was found to increase with an increase in initial concentration, amount of adsorbent and contact time. Adsorption of the pharmaceutical from aqueous solution was optimum as a pH of 2 and the maximum adsorption capacity of caffeine was 153.8 and phenacetin was 212.7 mg/g for M48GO at a temperature of 25 °C. The adsorption kinetics revealed that the adsorption process was mostly a 2 step process because of the rapid equilibrium and the slow almost stagnant intraparticle diffusion afterwards. The experimental data best fitted the pseudo second order model and the Langmuir isotherm

model was best suited. Thermodynamic studies revealed the adsorption process as spontaneous and exothermic in nature

This study showed that although silica is strongly hydrophilic, a manipulation of functionalities can lead to improved properties for the adsorption of various classes of pollutants. Mesoporous silica and ordered mesoporous silica synthesized from agrowaste had properties that were very comparable to those synthesized from commercial precursors such as TEOS.

10.1 Future Recommendations

- More ordered mesoporous materials such as SBA-15, MCM-48 should be synthesized from agrowastes and modified for the adsorption of (organic) pollutants
- These materials should be applied in the adsorption of a broader range of pollutants (such as heavy metals and polycyclic aromatic hydrocarbons)
- Adsorbent materials with a photocatalyst (e.g titania) that degrades and mineralizes the pollutant to unharmful substances should also be investigated as a means of completely degrading the pollutant through adsorption.
- Other functional groups should be used in the modification of silica surface for specific target analytes

APPENDIX A

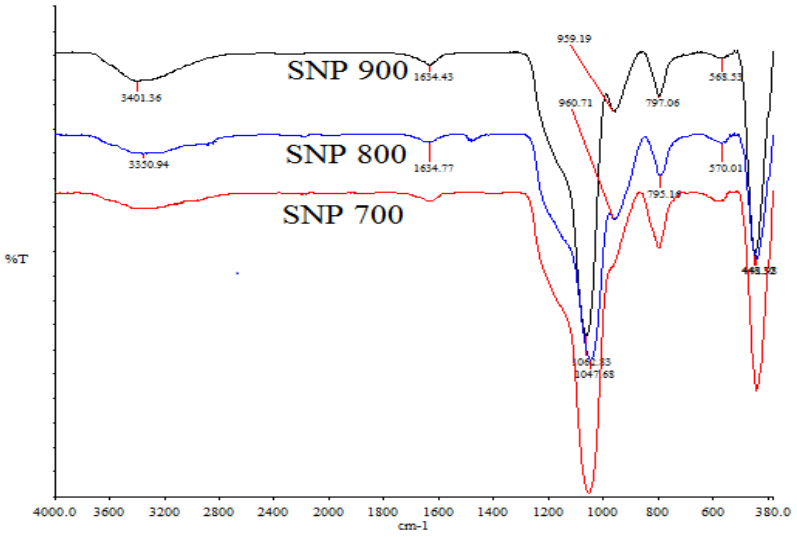

Appendix A 1.1: FTIR spectra of SNP 700, SNP 800 and SNP 900

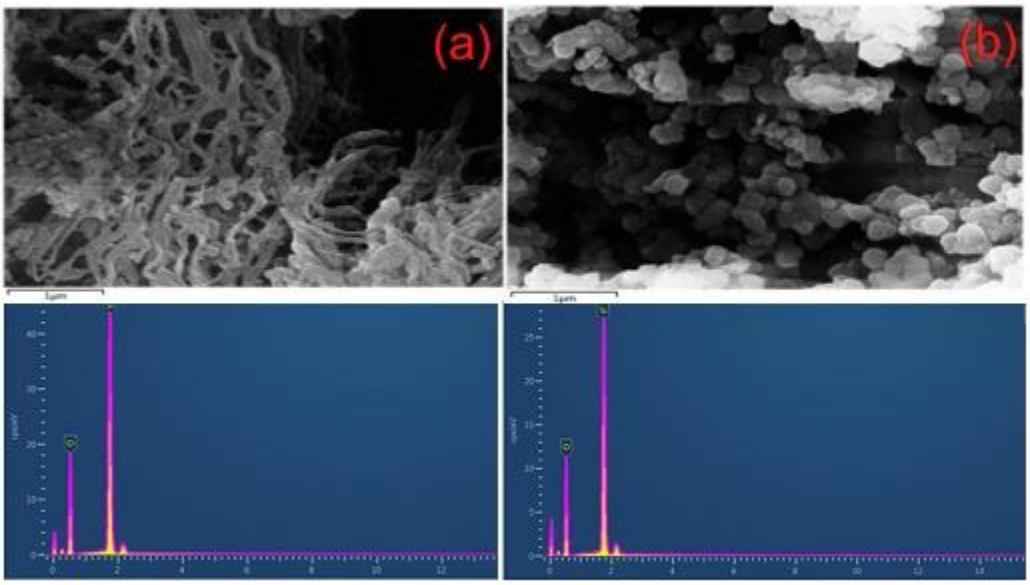

Appendix A 1.2: EDX spectra of a) SNT and b) SNP

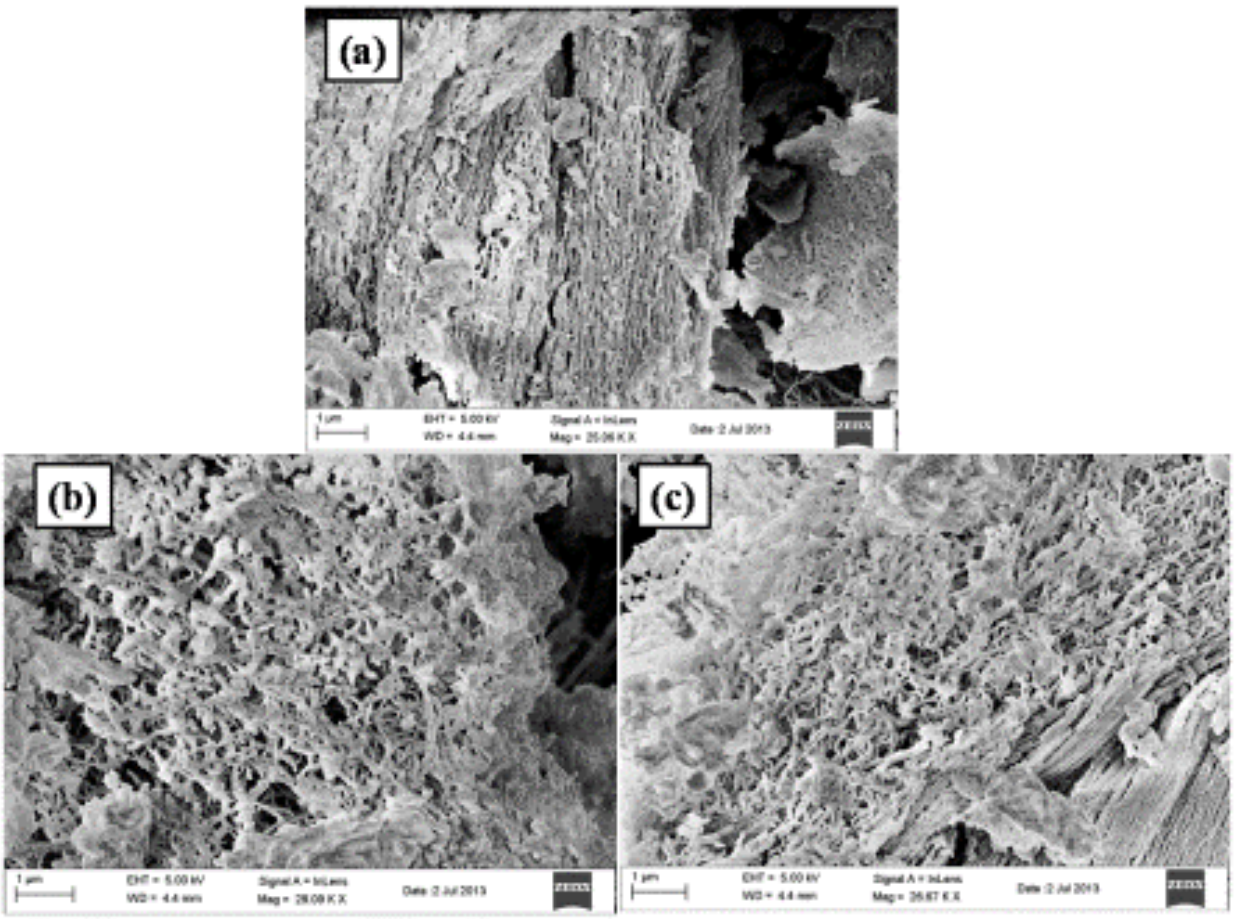

Appendix A 1.3: SEM images of (a) SNP 700 (b) SNP 800 (c) SNP 900

APPENDIX B

Table 1: Values showing PZC results for SNT and SNP

SNT		SNP	
ph Final	pH Initial	ph Final	pH Initial
2.04	0.01	2.05	0.01
4.15	-0.37	3.93	-0.22
6.54	-2.38	4.47	-2.07
7.09	-2.29	5.4945	-1.5955
7.61	-1.09	6.68	-0.93
10.21	-0.22	10.03	-0.18

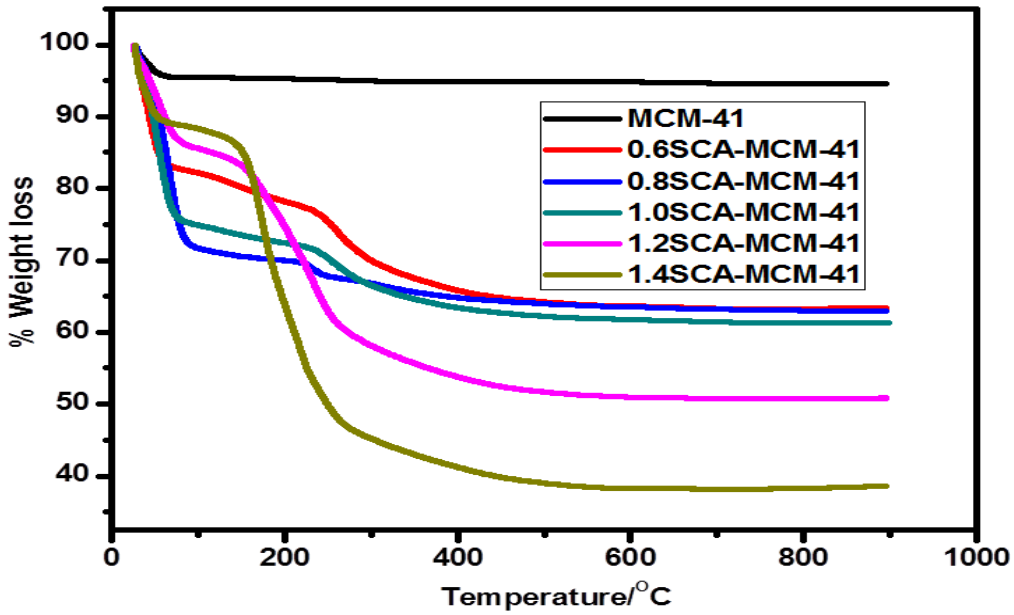

Appendix B 1.1: TGA profiles of MCM-41, 0.6SCA-MCM-41, 0.8SCA-MCM-41, 1.0SCA-MCM-41, 1.2SCA-MCM-41, 1.4SCA-MCM-41

APPENDIX C

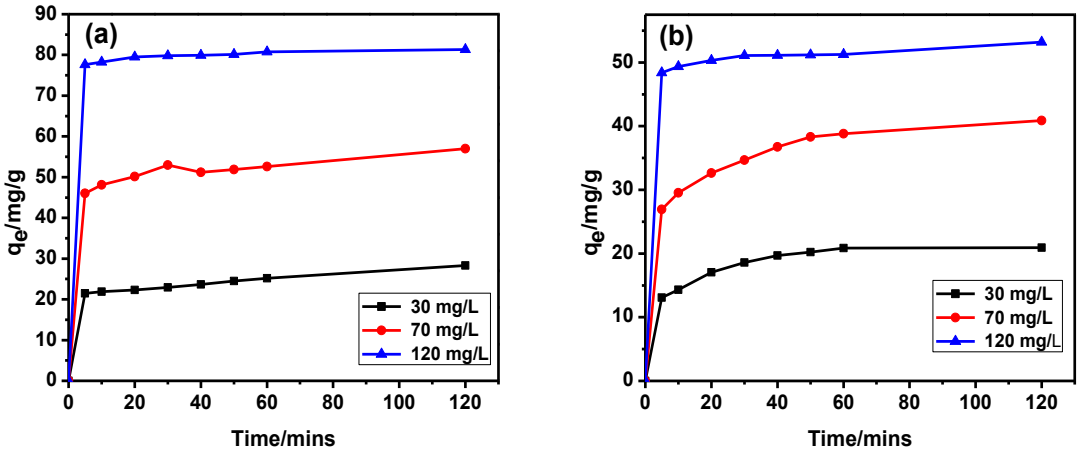

Appendix C 1.1: Effect of contact time on MB adsorption on (a) SCA-MCM-41 and (b) MCM-41